QUANTUM-CONFINED CdS NANOPARTICLES ON DNA TEMPLATES

DISSERTATION

Presented to the Graduate Council of The

University of North Texas in Partial

Fulfillment of the Requirements

For the Degree of

DOCTOR OF PHILOSOPHY

By

Young Gyu Rho, B.S., M.S.

Denton, Texas

May, 1998

Rho, Young Gyu, Quantum-Confined CdS Nanoparticles on DNA Templates. Doctor of Philosophy (Physics), May, 1998, 218 pp., 6 tables, 62 illustrations, bibliography, 126 titles.

As electronic devices became smaller, interest in quantum-confined semiconductor nanostructures increased. Self-assembled mesoscale semiconductor structures of II-VI nanocrystals are an especially exciting subject because of their controllable band gap and unique photophysical properties. Several preparative methods to synthesize and control the sizes of the individual nanocrystallites and the electronic and optical properties have been intensively studied. Fabrication of patterned nanostructures composed of quantum-confined nanoparticles is the next step toward practical applications.

We have developed an innovative method to fabricate diverse nanostructures which relies on the size and a shape of a chosen deoxyribonucleic acid (DNA) template. DNA has anionic atoms which can bind transition metal ions such as Zn^{2+}, Cd^{2+} and Hg^{2+}. The DNA can thus control the location of nanoparticles synthesis. Therefore, diverse nanoscale structures composed of arrays of quantum-confined nanocrystallite can be fabricated on DNA fixed to solid substrates without using complicated and expensive photolithography.

Mesoscale arrays of Q-CdS nanostructures were fabricated on pUCLeu4 plasmid and ϕX 174 RF II DNA. These DNAs are double-stranded and in A-form are

The samples were prepared either by dropping Cd^{2+}/DNA complexes on carbon-coated TEM grids or by floating the grids on Cd^{2+}/DNA or DNA only solutions. The grids with DNA only were reacted with Cd^{2+} by dipping the grids into a cadmium solution. The grids were exposed to H_2S gas to form the Q-CdS nanoparticle arrays. Various ratios and concentrations of Cd^{2+}/DNA were examined.

Conventional, analytical and high resolution transmission electron microscopy were used to characterize the Q-CdS nanostructures. Absorption and photoluminescence spectroscopies were used for optical characterization.

The experimental results demonstrate the feasibility of fabricating self-assembled semiconductor structures of Q-SC using DNA templates.

QUANTUM-CONFINED CdS NANOPARTICLES ON DNA TEMPLATES

DISSERTATION

Presented to the Graduate Council of The

University of North Texas in Partial

Fulfillment of the Requirements

For the Degree of

DOCTOR OF PHILOSOPHY

By

Young Gyu Rho, B.S., M.S.

Denton, Texas

May, 1998

ACKNOWLEDGMENTS

I thank God who has lead me to this point and I would like to turn in all this glory to Him.

I would like to specifically thank my advising Professor, Dr. Russell F. Pinizzotto, for his invaluable guidance and teaching, and for his financial support throughout my graduate studies at UNT. Without his support I could not have this glorious moment.

I would like to thank Dr. Jeffery L. Coffer, Dr. Robert M. Pirtle, Dr. Irma L. Pirtle and Mrs. Xin Li for their collaborative research efforts, valuable advice and kindness. I thank Dr. Elizabeth G. Jacobs, Dr. Harry Mallela, and Mr. David C. Garrett for their valuable time to teach and help me with all the technical steps to be an electron microscopist during my early stage in this electron microscopy group. I also want to thank all the members in Professor Pinizzotto's group, Dr. Hong Yang, Dr. Yujing Wu, Dr. Patrick Diehl, Dr. Tejpal K. Hooghan, Mrs. DaXue Xu, Mr. Yandong Chen, Mrs. Piedad Pena and Miss. Dawn Flanders for their help and encouragement.

Finally, I would like to thank my parents for their endless love and sacrifices which have provided the opportunities for me to be what I am today. I also thank my brothers, sister and my wife for their support and encouragement.

This research has been partially supported by the National Science Foundation through the Small Grants for Exploratory Research Program, and the University of North Texas Faculty Research Program.

TABLE OF CONTENTS

LIST OF TABLES

LIST OF ILLUSTRATIONS

CHAPTER 1

INTRODUCTION

1.1 Introduction

Since the early 1980s, quantum-confined semiconductors (Q-SC) have been of great interest to physicists, chemists and materials scientists because of their unique photophysical properties. When the sizes of crystallites are comparable to or less than their bulk Bohr exciton diameters, the quantum mechanical wave functions of electrons and holes are confined inside of the crystals, similar to the "particle in a box" of elementary quantum mechanics.[1] As a result, the band gap energies of nanometer size crystallites are increased by up to a few electron volts compared to bulk materials.[1-7] For example, for quantum-confined CdS (Q-CdS), the band gap energy can be tuned between 2.5 and 4.5 eV.[1] Nanocrystalline semiconductors in this size regimen are called "quantum dots," "zero-dimensional (0D)," or quantum-confined semiconductors.

Group II-VI nanocrystalline compound semiconductors have a variety of energy band gaps at room temperature: HgTe (0.14 eV), CdTe (1.50 eV), CdSe (1.74 eV), CdS (2.42 eV), ZeSe (2.67 eV) and ZnS (3.68 eV).[3,8] In addition, these II-VI materials can be fabricated with relatively less effort and expense compared to other quantum-dot fabrication methods such as vapor phase crystal growth and photolithography. Several preparative methods to synthesize and control the crystallite size for desired photophysical properties have been reported in the literature.[9-16] Also, the electronic and

optical properties of many quantum-confined semiconductors have been intensively studied.[4] Direct gap semiconductors with a relatively large band gap energy, such as Q-CdS, are especially interesting nanocrystalline materials because of their high photoluminescence efficiency and possible applications in high-speed (approximately picosecond) opto-electronic devices, detector devices, light emitting diodes, lasers, and solar energy conversion devices.[5,8,17-18]

However, nanocrystallites can be used in real devices only when they are ordered into patterns with one, two, or three dimensions. Characterization of the physical behavior of long-range ordered nanocrystallites is necessary to learn how to use the materials in actual devices. Thus, fabrication of patterned structures of Q-SC is an important objective for future optoelectronic device applications and nanocircuit technology.[19] A few methods of assembling nanocrystalline semiconductors into ordered structures have been introduced, such as the Langmuir-Blodgett thin film fabrication method[20] and self-organization of nanocrystallites into two or three dimensional structures using volumetric restriction techniques,[21] but these methods result in continuous sheets or films, not in specifically defined mesoscale structures.

In 1996, Coffer, Pinizzotto, and Pirtle suggested an innovative method of fabricating self-assembled mesoscale semiconductor structures using deoxyribonucleic acid (DNA) molecules as templates.[23-24] This dissertation describes these fabrication methods and the initial results of the self-assembly of arrays of quantum-confined CdS nanoparticle structures using well-defined polynucleotides as structural templates.

As described in detail in Chapter 2, DNA molecules are composed of the four

monomers deoxyadenylate, deoxyguanylate, deoxycytidylate, and deoxythymidylate. Each of these monomers is comprised of a phosphate, a sugar, and one of four nitrogenous bases. The monomers are covalently linked to each other through sugar-phosphate bonds to form a polynucleotide. Since DNA molecules have anionic sites such as the oxygen atoms of the phosphate groups and sugar hydroxyl groups, divalent transition metal ions such as Zn^{2+}, Cd^{2+}, and Hg^{2+} can bind to these negatively charged sites.[24-27] Thus, by binding the metal, DNA might stabilize the formation of quantum-confined nanocrystallites and control the formation of the nanoparticles. If true, the shapes and sizes of the semiconductor nanostructures could be dictated by the size and shape of the DNA chosen as the template.

For example, different sizes of "quantum wires" and "quantum rings" can be fabricated on different sizes of linear and circular DNA, respectively. "Quantum dots" can be fabricated on small DNA fragments. Other structures like a "quantum cross" can be assembled on singly- or multiply-branched DNA (Figure 1.1). Based on these elements, more complex nanostructures can be fabricated.

Different types of nanocrystallites can be fabricated by the same method, such as HgTe, CdTe, CdSe, CdS, PbS, PbSe, ZeSe and ZnS. Different solid substrates such as silicon dioxide/silicon, sapphire, mica, glass, and carbon thin films can be used. Diverse sizes and shapes, and different types of semiconductor quantum structures can be assembled on the different substrates without the use of photolithography.

In the experiments reported in this dissertation, Q-CdS was chosen to demonstrate the fabrication of self-assembled nanoparticle structures. A Circular plasmid DNA

designated pUCLeu4 (3455 base pairs), in the undigested form (called circular DNA in this dissertation), in the linearized form, and in the relaxed circular form (called relaxed DNA in this dissertation), and ϕX 174 RF II DNA (5386 base pairs) were selected as templates because of their known B-form lengths of 1.17 μm and 1.83 μm, respectively. Using templates with known microstructures, the Q-CdS/DNA nanostructures could be detected and unambiguously identified by transmission electron microscopy.

The general preparative methodology for fabrication of II-VI semiconductor nanostructures on DNA templates is divided into five steps (Figure 1.2).

1) Formation of a cationic surface on the substrate. The substrate is coated with a surfactant such as benzalkonium chloride or polylysine to form a thin film (near monolayer) of cationic charge. This modified substrate enhances DNA adsorption through the interaction of the anionic atoms of the phosphate and the cationic surfactant.

2) Deposition of DNA on the substrate. An aqueous solution of DNA is deposited on the substrate by spin-coating for uniform deposition of the DNA.

3) Exposure of the substrate to Cd^{2+} ions. The DNA attached to the substrate is exposed to Cd^{2+} solution either by dropping the Cd^{2+} solution on the substrate or by dipping the substrate into the cadmium solution. The cadmium ions bind to the anionic sites on the polynucleotides.

4) Removal of non-DNA bound cadmium. The cadmium ions on the non-nucleotide regions of the substrate are removed by a gentle wash with a polar nonaqueous solvent such as ethanol.

5) Addition of chalcogenide source. The semiconductor nanostructures are synthesized when the Cd^{2+}/polynucleotide/substrate is exposed to a gaseous chalcogenide source, such as hydrogen sulfide (H_2S). The H_2S reacts with the cadmium to form CdS.

Most of the samples synthesized for this dissertation were made on thin amorphous carbon films to make the TEM sample preparation easy and simple.

Fabrication and processing of the samples used for this dissertation followed one of two specific methods.

First method (Chapter 4)

1) formation of Cd^{2+}/DNA complexes by mixing DNA and cadmium solutions;
2) deposition of Cd^{2+}/DNA complexes onto carbon/Cu TEM grids;
3) reaction of the adsorbed Cd^{2+}/DNA complexes by exposing the grid to H_2S gas to form the desired nanocrystalline arrays.

Second method (Chapter 6)

1) deposition of DNA onto a carbon/Cu TEM grid;
2) formation of the Cd^{2+}/DNA complexes by dipping the grid into cadmium solution;
3) reaction of the Cd^{2+}/DNA complexes by exposure to H_2S gas.

After fabrication of the nanoparticles on the DNA, photophysical characterization, (absorption and photoluminescence spectroscopies) of the Q-CdS/DNA was carried out using an HP 8452A diode array spectrophotometer and a Spex Fluorolog-2 0.22 m double spectrometer with UV/visible excitation (λ_{ex} = 375 nm). Nanostructural characterization was performed using conventional transmission electron microscopy (CTEM, bright field and dark field), analytical electron microscopy (AEM), x-ray energy dispersive spectroscopy (XEDS), and selected area electron diffraction patterns (SADP). High resolution electron microscopy (HREM) was performed to study the lattices of the quantum-confined CdS nanoparticles.

This research project has been performed by collaboration of three groups: the isolation and purification of the pUCLeu4 plasmid DNA (circular, linear and relaxed) was carried out by Dr. Robert M. Pirtle's research group at UNT; CdS synthesis and optical characterization were performed by Dr. Jeffery L. Coffer's research group at Texas Christian University; and structural characterization was performed by Dr. Russell F. Pinizzotto's research group at UNT.

In this dissertation, demonstration of the self-assembly of mesoscale semiconductor structures fabricated on pUCLeu4 plasmid and ϕX 174 RF II DNA templates is presented, along with the structural and photophysical characterization of the Q-CdS nanostructures. Chapter 2 summarizes the basic theory of quantum-confined semiconductors (Q-SC), DNA structure and synthesis, and DNA - metal ion interactions. In Chapter 3, the results of previous experiments on the formation of Q-CdS stabilized by calf thymus DNA (carried out by Hong Yang and Shelli R. Bigham, former graduate

students of Dr. Pinizzotto and Dr. Coffer) are presented. Structural and optical characterization of Q-CdS nanoparticles formed on calf thymus DNA in solution are described in detail. The size distribution of the Q-CdS nanoparticles formed on calf thymus DNA is also reported. In Chapter 4, details of the experimental method used to form Q-CdS nanostructures on solid substrates are presented. Typical Q-CdS/DNA nanostructures formed by this technique are described, along with other unidentified microstructures. In Chapter 5, DNA microstructures observed using the Kleinschmidt imaging method are described, and the sizes of circular and linear pUCLeu4, and circular and linear ϕX 174 RF II DNA (A-form vs B-form DNA) are compared. In Chapter 6, the results of different DNA deposition methods are described. The results of using various concentrations of cadmium and DNA, and different DNA: cadmium ratios are presented, as well. The size distribution of hexagonal CdS particles is compared to the size distribution of diamond cubic phase nanoparticles. Chapter 7 summarizes the experimental results.

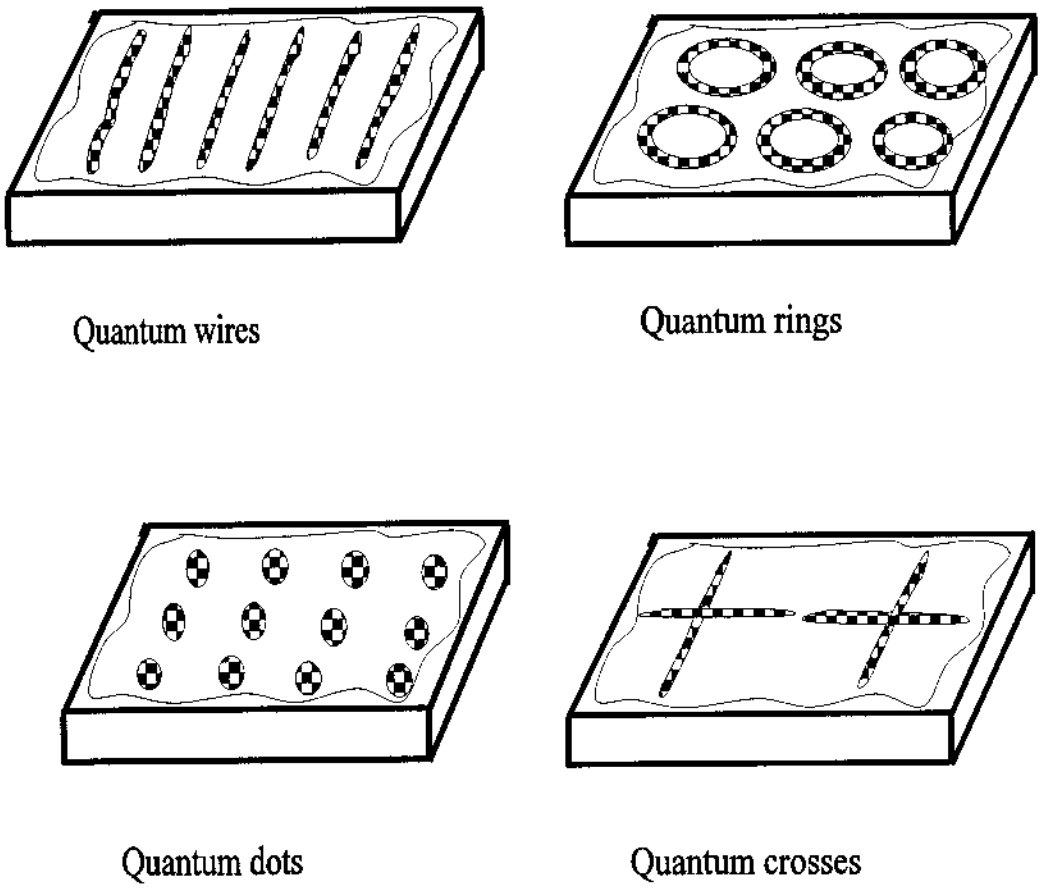

Figure 1.1 Possible semiconductor nanostructures formed on linear, circular, short, and branched DNA templates.

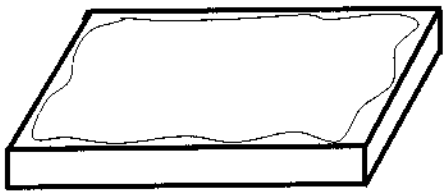

1. Formation of a cationic surface on the substrate

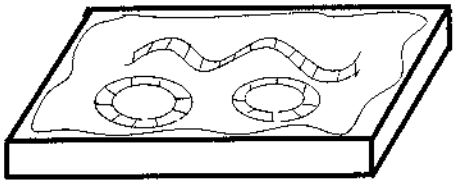

2. Deposition of DNA on the substrate

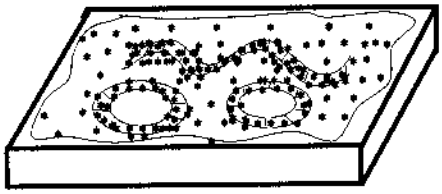

3. Exposure of the substrate to cadmium ions

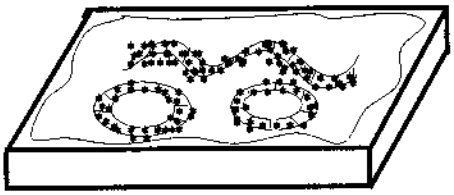

4. Removal of non-DNA bound cadmium

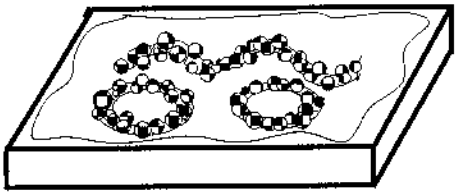

5. Addition of chalcogenide source and conversion into II-VI semiconductor nanoparticles

Figure 1.2 General preparative methodology for fabrication of II-VI semiconductor nanostructures on DNA templates.

REFERENCES

1. A. P. Alivisatos, Science **27**, 933 (1996).

2. B. O. Dabbousi, M. G. Bawendi, O. Onitsuka and M. F. Rubner, Appl. Phys. Lett. **66**, 11 (1995).

3. N. Peyghambarian, S. W. Koch and A. Mysyrowicz, *Introduction to Semiconductor Optics* (Prentice Hall, Englewood Cliffs, New Jersey, 1993), pp. 7-8.

4. J. Kuczynski and K. Thomas, J. of Phys. Chem. **89**, 2720-2722 (1985).

5. S. A. Empedicles, D. J. Norris and M. G. Bawendi, Phys. Rev. Lett. **77**, 3873 (1996).

6. E. S. Smotkin, C. Lee, A. J. Bard, A. Campion, M. A. Fox, T. E. Mallouk, S. E. Webber and J. M. White, Chem. Phys. Lett. **152,** 3 (1988).

7. A. N. Goldstein, C. M. Echer and A. P. Alivisatos, Science **256**, 5 (1992).

8. A. D. Yoffe, in *Advances in Physics*, edited by D. Sherrington (Taylor & Francis, London and Washington, DC., 1993), Vol. 42, p. 252.

9. A. I. Ekimov and A. A. Onushchenko, JETP Lett. **34**, 345 (1982).

10. R. Rossetti, S. Nakahara and L. E. Brus, J. of Chem. Phys. **79**, 2 (1983).

11. A. I. Ekimov, and A. A. Onushchenko, JETP Lett. **40**, 1136 (1984).

12. Y. Wang and W. Mahler, Optics Commun. **61**, 233 (1987).

13. Y. Wang, N. Herron, W. Mahler and A. Suna, J. Opt. Soc. Am. B **6**, 808 (1989).

14. J. L. Coffer, S. R. Bigham, R. F. Pinizzotto and H. Yang, Nanotechnology **3**, 69-76 (1992).

15. Y. Wang, A. Suna, W. Mahler and R. Kasowski, J. Chem. Phys. **87**, 12 (1987).

16. A. Fojtik, H. Weller, U. Koch and A. Henglein, Ber. Bunsengers. Phys. Chem. **88**, 969-977 (1984).

17. A. G. Cullis, P. W. Smith, P. J. Parbrook, B. Cockayne, P. J. Wright and G. M. Williams, Appl. Phys. Lett. **55**, 20 (1989).

18. A. A. Guzelian, U. Banin, A. V. Kadavanich, X. Peng and A. P. Alivisatos, Appl. Phys. Lett. **69**, 10 (1996).

19. A. P. Alivisatos, K. P. Johnson, X. Peng, T. E. Wilson, C. J. Loweth, M. P. Bruchez, Jr. and P. G. Schultz, Nature **382**, 6592 (1996).

20. J. H. Fendler, "Membrane-Mimetic Approach to Advanced Materials," in *Advances in Polymer Science* (Springer-Verlag, Berlin, Heidelberg, New York, 1994), pp. 27-29.

21. C. B. Murray, C. R. Kagan and M. G. Bawendi, Science **262**, 218 (1994).

22. R. F. Pinizzotto, Y. G. Rho, Y. Chen, R. M. Pirtle, I. L. Pirtle, J. L. Coffer and X. Li, Mater. Res. Soc. Symp. Proc. **452,** 591 (1997).

23. J. L. Coffer, S. R. Bigham, R. F. Pinizzotto, Y. G. Rho, R. M. Pirtle and I. L. Pirtle, Appl. Phys. Lett. **69**, 3851 (1996).

24. V. A. Bloomfield, D. M. Crothers and I. Tinooco, Jr., *Physical Chemistry of Nucleic Acids* (Harper & Row, New York, 1974), pp. 420-427.

25. J. K. Barton and S. J. Lippard, "Nucleid Acid-Metal Ion Interactions" in *Metal Ions in Biology,* edited by Thomas G. Spiro, (John Wiley & Sons, Inc., New York, 1980), Vol. I, Chap. 2, pp. 33-81.

26. W. Saenger, *Principles of Nucleic Acid Structure* (Springer-Verlag, New York, (1984), pp. 201-203.

27. B. Norden, P. Lincoln, B.Akerman and E. Tuite, in *Metal Ions In Biological Systems*, edited by A. Sigel and H. Sigel, (Marcel Dekker, Inc., New York, 1996), Vol. 33, Chap.7, pp. 177-208.

CHAPTER 2

THEORY

2.1 Basic Theories of Quantum-Confined Semiconductors

2. 1. 1 Quantum-Confined Semiconductors (Q-SC)

Semiconductor crystallites whose sizes are comparable to or smaller than their bulk Bohr exciton radius ($R \leq a_B$) are called nanocrystallites or quantum-dot semiconductors.[1-4] These spatially limited small semiconductor particles confine charge carriers, and the kinetic energies of these confined carriers are increased and quantized. As the result, the band gap energy of the semiconductors is increased and the optical properties of the semiconductors are changed. The changes in material properties due to spatial restriction of the electron-hole pairs are called quantum-confinement effects or size quantization effects. Quantum-confinement also arises as a result of changes in the density of electronic states. Because the small nanocrystals have only one or a few electron-hole pairs in each particle, the energy states of these pairs become more discrete (Figure 2.1)[4,5]

The physical size needed to form a quantum-dot depends on the physical properties of the semiconductor such as band gap, effective mass and exciton binding energy.[6,7] For example, a semiconductor with a large effective mass and a large exciton binding energy has a small Bohr exciton radius, and the onset of quantum-confinement occurs at a much smaller particle diameter than semiconductors with a small effective

mass, small exciton binding energy and a larger Bohr excition radius.[6]

An "exciton" is an electron-hole pair that moves together under a Coulombic potential with a finite separation distance forming a structure analogous to a hydrogen atom.[7] The Bohr exciton radius is the distance between the electron and the hole. The binding energy of the exciton is inversely proportional to the Bohr exciton radius. The exciton binding energy is very small and the exciton radius is vary large compared to that of a hydrogen atom.[5] The exciton diameter is inversely proportional to the effective masses of the electron and the hole. The energy of the electron in an exciton is slightly below the edge of the conduction band.[8]

Effective mass is an experimentally determined property of an electron or a hole in a solid. It is inversely proportional to the curvature of the parabolic energy band structures ($E = \hbar^2k^2/2m$). The effective mass depends on the band structure. For example, the effective electron mass can be as low as 1% of the free electron mass at the center or near the boundary of a Brillouin zone.[9]

Nanocrystalline semiconductors consist of several tens to several thousand atoms and are 10 to 200 Å[2,10-15] in diameter with the same unit cell as the bulk material. Efros and Efros divided quantum-size effects into three cases according to the radius, R, of the semiconductor cluster[16]: (1) weak confinement region ($R>a_e$ and $R>a_h$), (2) medium confinement ($a_h<R<a_e$), and (3) strong confinement ($R<a_e,a_h$), where $a_e = \hbar^2\varepsilon_2/m^*_e e^2$ and $a_h = \hbar^2\varepsilon_2/m^*_h e^2$ are the electron and hole Bohr radius, and ε_2 is dielectric constant of the nanocrystalline semiconductor.[16]

Quantum-confined semiconductors can be prepared by a number of methods.[16-38] The most common methods are epitaxial crystal growth and photolithography, and chemical synthesis, under development since 1970[17] and 1981,[18] respectively.

Using advanced crystal growth techniques such as molecular beam epitaxy (MBE), metal organic chemical vapor deposition (MOCVD), and sophisticated electron-beam or x-ray lithography and etching techniques, it is possible to fabricate one-, two- or three-dimensional carrier-confined nanoscale structures. These small structures with sizes comparable to the Bohr exciton radius, are commonly called quantum wells, quantum wires, and quantum dots or zero-dimension semiconductors.[15,39-40] With the synthetic methods, diverse types of binary quantum-sized compound semiconductors can be prepared in stabilizing media which are required to initiate particle growth of crystallites. Ekimov and Onushchenko prepared CuCl nanocrystalline material on glass in 1982.[18] Many different binary compound semiconductors have been prepared on a variety of media since that time. Quantum-confined colloidal CdS clusters were synthesized by Rossetti and co-workers in 1983,[34] on glass by Ekimov and Onushchenko in 1984,[35] in both polymer and zeolite by Wang in 1987[36] and 1989,[37] and using calf thymus DNA in solution by Coffer and Pinizzotto in 1992.[38]

Since quantum-confined CdS stabilized by DNA templates is the subject of this dissertation, the synthetic method of Q-SC fabrication is discussed in this Chapter.

The first observation of the quantum-confinement effect, observed as changing colors of semiconductor clusters during the synthesis of colloidal particles, was reported 100 years ago by M. Lucas.[12] Quantum-size effects in colloidal CdS and AgI

semiconductor clusters were experimentally observed and correctly explained by Berry for the first time in 1967.[41] In 1981, Ekimov and Onushchenko observed blue-shifted optical absorption from CuCl microcrystallites in a silicate glass, and they claimed that this occurred due to carrier confinement.[18] Their experimental observation was theoretically explained using the effective mass approximation with a particle-in-a-sphere model by Efros and Efros in 1982.[16] Additional systematic studies of quantum-size effects in small semiconductor particles have been performed by Brus and others.[7,42-51]

2.1.2 Theoretical Models of the Energy Band Structure of Q-SC

Theoretical models for calculating energy band structures of Q-SC have been developed using different approaches by different researchers.[7,16,42-51] Efros and Efros first developed a theory using an effective mass approximation (EMA) model.[16] They considered the surfaces of spherical microcrystallites as infinite potential barriers for the charge carriers, and excluded the Coulombic interaction of electron-hole pairs. They also ignored the effect of the dielectric constant of the background materials, the stabilizing media. In 1983, Brus extended this effective-mass approximation method by including the Coulombic interaction and the effect of the dielectric constant of background matrix materials.[7,42-43]

Here I will describe a few fundamental steps needed to find the energy states of a single electron-hole pair in a spherically shaped semiconductor nanoparticle, and explain how quantum-confinement is related to the size of the crystal. The calculation is based on the EMA methods developed by Efros and Efros, [16] and Brus.[7,44]

The calculation is simplified using the following assumptions[39-40]:

First, it is assumed that the Q-SC maintains the same atomic structure as the bulk material. This allows us to use Bloch wavefunctions to describe the motion of the electrons and the holes in the lattice. A Bloch wavefunction is a product of the periodicity of the lattice and a plane wave[39-40,42]

$$\Psi_{\lambda,k}(\mathbf{r}) = e^{i\mathbf{k}\cdot\mathbf{r}}\, u_{\lambda,k}(\mathbf{r}) \tag{1}$$

$$\text{where } u_{\lambda,k}(\mathbf{r}) = u_{\lambda,k}(\mathbf{r}+\mathbf{n}) \tag{2}$$

Here $e^{i\mathbf{k}\cdot\mathbf{r}}$ is the plane wave and $u_{\lambda,k}(\mathbf{r}) = u_{\lambda,k}(\mathbf{r}+\mathbf{n})$ is the periodicity of the lattice the lattice vector $\mathbf{n}$, which also called the Bloch function. The general Hamiltonian that governs the envelope function for electrons and holes in the effective-mass approximation[52] is

$$\hat{H} = -\frac{\hbar^2}{2m_e^*}\nabla_e^2 - \frac{\hbar^2}{2m_h^*}\nabla_h^2 + V(r_e) + V(r_h) - \frac{e^2}{\varepsilon_2|r_e - r_h|} \tag{3}$$

where m_e^* and m_h^* are the electron and the hole effective masses, respectively, and ε_2 is the dielectric constant of the semiconductor. $V(r_e)$ and $V(r_h)$ are the potential energies experienced by the localized electron and hole, and r_e and r_h are the position coordinates of the electron and hole in the solid.

Second, it is assumed that the potential energy is zero inside the particles, and infinity at the surface of the particles. Therefore, the wavefunctions of the electrons and holes vanish on the surface of a sphere.

Third, the Coulombic interaction term can be ignored because the kinetic energies

of the confined electron and hole are large compared to the potential energy of the electron-hole pairs.

With these assumptions, the Schrödinger equation of a single electron - hole pair in spherical coordinates is:[40,49]

$$\left[-\frac{\hbar^2}{2m_e^*} \nabla_e^2 - \frac{\hbar^2}{2m_h^*} \nabla_h^2 \right] \Psi_{eh}(r,\Theta,\Phi) = (E-E_g)\ \Psi_{eh}(r,\Theta,\Phi) \qquad (4)$$

E_g is the band gap energy of the bulk semiconductor. Since there is no coupling term between the electron and the hole, the total wavefunction can be separated into two independent wavefunctions: one depends only on the motion of the electron, and the other depends only on the motion of the hole:

$$\Psi_{eh}(r, \Theta, \Phi) = \Psi_e(r, \Theta, \Phi)\, \Psi_h(r, \Theta, \Phi) \qquad (5)$$

Because the wavefunctions are independent, the Schrödinger equation also can be separated:[40]

$$-\frac{\hbar^2}{2m_e^*} \nabla_e^2\ \Psi_e(r,\Theta,\Phi) = (E_e-E_g)\ \Psi_e(r,\Theta,\Phi) \qquad (6a)$$

$$-\frac{\hbar^2}{2m_h^*} \nabla_h^2\ \Psi_h(r,\Theta,\Phi) = E_h\ \Psi_h(r,\Theta,\Phi) \qquad (6b)$$

E_e and E_g are the electron and hole energies states in the conduction band and valence band, respectively. These Schrödinger equations are for a single particle-in-a-sphere, a problem discussed in most Quantum Mechanics, Mathematical Physics, and other

semiconductor textbooks.[39-40,53-54] Equation 6a is for the motion of a single electron in the conduction band, and Eq. 6b is for the motion of a single hole in the valence band. The wavefunction for a single particle in an infinite potential well using the effective-mass approximation in spherical coordinates[40,49] is:

$$\psi_{e,h}(r,\Theta,\Phi) = \sqrt{\frac{2}{R^3}}\,\frac{j_l(\alpha_{n,l}\, r/R)}{j_{l+1}(\alpha_{n,l})}\, Y_{l,m}(\Theta,\Phi) \tag{7}$$

were j_l is the spherical Bessel function of order of l, α_{nl} is the nth root of the spherical Bessel function of lth order with quantum numbers $n = 1, 2, 3, \cdots \infty$ and $l = 0, 1, 2, 3, \cdots \infty$, and R is the radius of the crystal. $Y_{l,m}(\Theta,\Phi)$ is a spherical harmonic. The boundary conditions are satisfied if $j_l(\alpha_{nl}) = 0$, for $n = 1, 2, 3 \cdots \infty$. If we substitute eigenfunction (7) into Schrödinger equations (6a) and (6b), then the eigenenergies of the electron in the conduction band and the hole in the valence band are:

$$E_e = E_g + \frac{\hbar^2}{2m_e^*}\,\frac{\alpha_{nl}^2}{R^2} \tag{8a}$$

$$E_h = \frac{\hbar^2}{2m_h^*}\,\frac{\alpha_{nl}^2}{R^2} \tag{8b}$$

The energy of a non-interacting single electron-hole pair in a small quantum-confined semiconductor cluster is found by adding the eigenenergies of the electron and the hole.[16,55]

$$E_{eh} = E_g + \frac{\hbar^2}{2m_e^*}\frac{\alpha_{nl}^2}{R^2} + \frac{\hbar^2}{2m_h^*}\frac{\alpha_{nl}^2}{R^2} = E_g + \frac{\hbar^2}{2\mu R^2}\alpha_{nl}^2 \qquad (9)$$

where μ is the reduced mass ($\mu = 1/(m^{*}_{e}{}^{-1} + m^{*}_{h}{}^{-1})$). The first few roots of the spherical Bessel function[39-40,33] are $\alpha_{10} = \pi$, $\alpha_{11} = 4.4934$, $\alpha_{12} = 5.7635$, ···. Therefore, the lowest energy state of a non-interacting electron-hole-pair is

$$\hbar\omega_{1,0} = E_g + \frac{\hbar^2\pi^2}{2\mu R^2} \qquad (10)$$

The second term on the right hand side of equation (10) is the energy increase due to quantum confinement. This equation also shows that the total energy increases as the cluster size, *R*, decreases.

Thus, we have developed a simple model for calculating the energy levels of a charge carrier in a quantum-dot semiconductor without considering Coulombic interaction or dielectric constant of the background materials. This simple model may be acceptable for the small quantum-confined semiconductors (strong confinement), since the kinetic energy, which is proportional to $1/R^2$, dominates the Coulombic potential energy, which is proportional to $1/R$. Also, most inorganic semiconductors have a large dielectric constant, in the range of 5-12. Thus, the Coulombic interaction is heavily screened and the calculated energy is essentially the same as the energy of the localized electron kinetic energy.[7] However, the Coulombic potential term of the electron-hole pair becomes more important as the quantum-dot size increases. Furthermore, the dielectric constant of the background material must be included because the Coulombic interaction

is affected by the matrix.[7,43] Thus, the Coulombic interaction term combined with dielectric polarization must be used to accurately calculate energy states.

The potential energy of an electron-hole pair in a quantum-dot semiconductor matrix can be written as[7]

$$V(r_e,r_h) = -\frac{e^2}{\varepsilon_2|r_e-r_h|} + \sum_{n=1}^{\infty} \alpha_n \frac{(r_e^{2n}+r_h^{2n})}{R^{2n+1}} \frac{e^2}{2} \tag{11}$$

$$\textit{where} \quad \sum_{n=1}^{\infty} \alpha_n \frac{(r_e^{2n}+r_h^{2n})}{R^{2n+1}} \frac{e^2}{2} \quad \textit{is the polarization term}$$

$$\textit{with} \quad \alpha_n = \frac{(\varepsilon_2-\varepsilon_1)(n+1)}{\varepsilon_2(\varepsilon_2 n+\varepsilon_1 n+\varepsilon_1)}$$

ε_2 and ε_i are the dielectric constants of the semiconductor crystal and the background medium, respectively, and n = 1, 2, 3, $\cdots \infty$. Again, it is assumed that the potential energy of the electron and the hole inside of the particles is zero, and the potential energy is infinity at the surface of the particles. By combining equations (3) and (11), we have a new Hamiltonian with a polarization term.

$$\hat{H} = -\frac{\hbar^2}{2m_e^*}\nabla_e^2 - \frac{\hbar^2}{2m_h^*}\nabla_h^2 - \frac{e^2}{\varepsilon_2|r_e-r_h|} + \sum_{n=1}^{\infty} \alpha_n \frac{(r_e^{2n}+r_h^{2n})}{R^{2n+1}} \frac{e^2}{2} \tag{12}$$

Thus, the lowest excited state energy for an electron-hole pair estimated by Brus[7] is

$$E_{eh} = E_g + \frac{\hbar^2\pi^2}{2R^2}\left[\frac{1}{m_e^*} + \frac{1}{m_h^*}\right] - \frac{1.8e^2}{\varepsilon_2 R} + \frac{e^2}{R}\overline{\sum_{n=1}^{\infty} \alpha_n \left(\frac{r_e + e_h}{R}\right)^{2n}} \qquad (13)$$

The bar over the last term indicates an average of the lowest energy of a single electron or hole wavefunction. The first term is the band gap energy, the second term is the kinetic energy of the localized electron and hole, the third term is the Coulomb interaction energy, and the fourth term is the dielectric polarization energy.

The effective-mass approximation method is a reasonable guide and obtains reasonable agreement with experimental results.[55] Kayanuma and Hu extended Brus's EMA model using a variational calculation method. Both infinite[45-46] and finite[47-49] potential barriers at the surface of particles were used for the crystal size range 10 to 20 Å. For the finite potential barrier case, the carrier confinement was lowered due to the wavefunction penetrating into the host matrix, and the results had better agreement with experimental data.

The energy of the lowest excited electronic state for a CdS nanoparticle as a function of the size, as calculated by Brus, is illustrated in Figure 2.2.[7]

2.1.3 Band Structure of Q-SC

Generally, a bulk crystal contains approximately 10^{23} atoms and 10^{24} electrons per unit volume.[39] The electrons in each individual atom have discrete energy levels filled from the lowest energy states according to the Pauli principle. As atoms are brought together to form a solid, the discrete energy levels of each atom interact with each other.

This interaction causes a splitting of the energy levels into approximately 10^{23} sublevels a few eV in width. Therefore, the spacing between the sublevels is so close that they appear to be a countinuous band of energy. These band-like energy levels can be divided into two: a completely filled valence band, that is, a group of ground state electrons; and an empty conduction band, that is, a group of excited state electrons (Figure 2.3a). This is similar to the energy separation in a molecule between the highest occupied molecular orbital (HOMO) and the lowest unoccupied molecular orbital (LUMO).[43-44] The energy region between the valence band and conduction band is the energy gap, and no other energy levels are allowed within this energy gap. This energy gap is called the band gap, E_g, and is defined as the energy necessary to create and separate an electron and a hole far enough apart so that their Coulomb interaction is negligible.[7]

In the quantum-dot semiconductor case, as described in the previous sections, the energy bands become discrete and quantized due to the low density of states.[4,5,10] The band gap energy increases because of the confinement effect on the exciton (Figure 2.3b).

Semiconductors can be divided into two categories based on the band gap structure. If the lowest energy of the conduction band and the highest energy of the valence band are at the same point in $\boldsymbol{k}$ space (at the center of the first Brillouin zone), it is called a direct band gap semiconductor. If they occur at different points in $\boldsymbol{k}$ space, it is called an indirect band gap semiconductor (Figure 2.4).[39] The transition of electrons between the valence band and the conduction band for a direct gap semiconductor can occur with the absorption of only photon energy. The electron transition for indirect gap semiconductors cannot occur without the assistance of phonon energy to a larger $\boldsymbol{k}$-space

energy. As a result, the transition rate in indirect gap semiconductors is very small. From conservation of energy, $\hbar\omega = E_f - E_i$ for a direct gap semiconductor, and $\hbar\omega = E_f - E_i \pm \hbar\Omega$ for an indirect gap semiconductor.[56] Here, $\hbar\omega$ is the photon energy, E_f and E_i are the final and initial energy states of the electron, and $\hbar\Omega$ is the phonon energy (the plus and minus signs indicate the phonon energy for emission and absorption, respectively). The efficiency of the optical transition in semiconductors mainly depends on the energy band gap structure of the semiconductor.

2.1.4 Quantum-Confined CdS (Q-CdS)

CdS is one of the group II-VI compound semiconductors with a direct band gap. CdS has two crystal structures, hexagonal-close packed (wurtzite) and face-centered cubic (zincblend).[5,39,57] According to Horst Weller,[5] most of the nanometer-size colloidal CdS crystals are the zinc-blende cubic phase, while most macrocrystallites are the hexagonal phase. Using high resolution electron microscopy and SADP, Coffer and Pinizzotto also showed that CdS nanocrystals with an average diameter of 5.6 nm are the zincblende cubic phase.[38]

The bulk band gap energy of CdS at room temperature is 2.42 eV with a corresponding absorption edge wavelength of approximately 515 nm.[5,8,28,55,57] Quantum confinement effects for CdS particles start at a diameter of approximately 6 nm.[7] When the CdS nanoparticle size becomes less than 4 nm, the absorption edge is shifted approximately 0.9 eV to shorter wavelengths (approximately 373 nm).[9] The exciton radius for CdS is approximately 3 nm and the binding energy of the excition is only

0.05 eV, compared to 0.053 nm and 13.51 eV, respectively, for the hydrogen atom.[5,58]

2.1.5 Absorption and Photoluminescence Spectroscopies of Q-SC

When semiconductors absorb photons with energies equal to or larger than the band gap energy, the bound electrons in the valence band are promoted to the conduction band with the creation of a hole in the valence band.[40] The excited electron in the conduction band can relax back to the ground state with emission of a photon with an energy corresponding to the band gap energy. Photon absorption and emission via these electronic transition processes can be measured using absorption and photoluminescence spectroscopy which yield valuable information about the optical and electronic properties of the semiconductor. Quantum-confinement effects, such as the increase in band gap energy with decreasing particle size, can be easily observed using UV-visible light.[5,34,42]

Photon emission in semiconductors occurs through the two relaxation processes, radiative and the non-radiative. If the energy of an excited electron in the conduction band is converted into a photon by recombining the electron with a hole in the valence band, this is the radiative process. However, there are many other possible ways for an electron to lose energy without the emission of a photon, such as electron-phonon interaction, carrier-carrier interaction, surface effects, etc.[8,19]

The photophysical properties of a quantum-confined semiconductor are strongly influenced by the surface states of the nanoparticles, because as the size of the nanocrystallite gets smaller, the surface atom percentage of the nanocrystallite gets larger.[5,6,19,42,58-59] Therefore, excited electrons in quantum-dot semiconductors can become

localized on surface defect sites such as interstitial atoms, impurities, dislocations, vacancies, etc.[5-6,59] The energies of the excited electrons may be close to the conduction band (shallow traps) or within the band gap (deep traps), as shown in Figure 2.5, and produce photoluminescence at longer wavelengths (lower energies). The charge carriers can also recombine with defect sites nonradiatively.[8] Because of these deep and shallow traps, Q-CdS often exhibits broad photoluminescence in the lower energy red region near 660-nm.[8,19]

2.2 Basic Theories of DNA

2.2.1 Deoxyribonucleic Acid and Its Structure

Deoxyribonucleic acid (DNA), first discovered in white blood cells by Friedrich Miescher in 1869, is the major genetic material in the chromosomes of almost all organisms.[60] DNA molecules are composed of the four basic monomers: deoxyadenylate, deoxyguanylate, deoxycytidylate, and deoxythymidylate (Figure 2.6). All nucleotides are comprised of a phosphate, a sugar (2'-deoxy-D-ribose), and one of four nitrogenous bases (also called heterocyclic rings, composed of carbon and nitrogen atoms). The four nitrogenous bases, adenine (A), guanine (G), cytosine (C), and thymine (T) are shown in Figure 2.6.[60-61] Adenine and guanine are purine bases (with six and five-membered heterocyclic rings), and cytosine and thymine (only in DNA)/uracil (only in RNA) are pyrimidine bases (with six-membered heterocyclic rings). Each base, without its phosphate groups, is connected to a sugar group through the C -1' of 2'-deoxyribose by an *N*-glycosidic bond (*N*-9 for purines and *N*-1 for pyrimidines) and is called a nucleoside

(deoxyadenosine, deoxyguanosine, deoxycytidine, and deoxythymidine). The nucleotides thus can be called phosphorylated nucleosides. The carbon atom position in the sugar ring is marked with a prime to distinguish it from the carbon in the base. For example, in a nucleoside, C-2 indicates the second carbon atom position of one of the four bases, and C-2' indicates the second carbon atom position of that sugar ring.

The nucleotides are covalently linked to each other through regularly repeating sugar - phosphate bonds; a phosphate group on C-5' of a sugar (above the pentose ring) connected to the other phosphate group on C-3' (below the pentose ring) of the same sugar to make a long polynucleotide chain (Figure 2.7).[60] These bonds are called 5'-3' phosphodiester bonds (this is also called the positive direction) and the entire polynucleotide chain will have the same orientation. The alternating sugar and phosphate residues form the "backbone" of the molecule, and the purine and pyrimidine bases are attached to the backbone via the C-1' position of the deoxyribose (sugar ring). If a DNA molecule has one phosphate - sugar backbone, it is called single-stranded DNA. If it has two phosphate - sugar backbones, it is called double-stranded DNA (most DNA is double-stranded, while most RNA is single-stranded).

According to Watson and Crick, for double-stranded DNA, the two DNA chains are wound around each other outside of the bases in a right handed helix form, and the phosphate - sugar backbones run in opposite directions (antiparallel) (Figure 2.8).[60,63-64] The bases in the middle, the purines and pyrimidines, are connected to each other as pairs by weak, noncovalent hydrogen bonds.[60-64] The hydrogen bonds are the interactions between the positively charged H atoms (due to the attachment of hydrogen to nitrogen or

oxygen atoms; the hydrogen atoms are called donors) and the negatively charged atoms (called acceptors) such as carbonyl oxygen (-C=O) or the lone pair electrons on nitrogen (N:).[60,63] As shown in Figure 2.9,[60] two hydrogen bonds are separated by 2.85-2.9 Å in an A-T base pair and three hydrogen bonds are separated by 2.83-2.86 Å in a C-G base pair.[60] The distance between the two sugar-phosphate backbones in a A-T area is 1.11 nm and that distance in a C-G area is 1.08 nm. According to the Chargaff study, because of the chemical structures of the bases, only adenine can pair with thymine, and guanine with cytosine; that is, a purine base (adenine or guanine) of one strand of DNA can combine with a pyrimidine base (cytosine or thymine) of an opposite DNA strand.[60-61,63-65] Chargaff found that the number of moles of adenine equaled that of thymine, and that the number of moles of guanine equaled that of cytosine. The amount of adenine + guanine also equaled the amount of cytosine + thymine in every DNA. The adenine - thymine (AT) and guanine - cytosine (GC) pairs are parallel to one another and perpendicular to the helical axis.[63-64]

There are several different DNA conformations (A, B, C, D, T, and Z-forms).[60,63-65] The DNA conformation is controlled by the relative humidity and the amount of salt each DNA contains. The conformations differ in number of base pairs per turn, tilt angle between the bases, direction of the helix, etc.[60,63,65] According to X-ray crystallographic studies, A, B, and Z DNA are the common forms. B-DNA, discovered by Watson and Crick, is the most common conformation among the diverse DNA structures.[60,63-65] B-DNA has its double helix in the right-handed direction, and when this DNA has 92% relative humidity, the pitch of the helix is 34 Å with approximately 10.4

base pairs for one full turn.[60,65] The separation distance between nucleotides is 3.4 Å and the rotation angle of each nucleotide is 34.6°.[60]

A noticeable feature of B-form DNA is the presence of two distinct grooves, called the major groove (12 Å wide) and the minor groove (6 Å wide)[61] These grooves are present because the glycosidic bonds of a base pair are not diametrically opposite each other.[60] The main differences between A-form and B-form DNAs are the relative humidity and the salt they contain, and the sugar pucker position, i.e. the displacement of the C-2' and C-3' carbon atoms. If the displacement of carbon atom C-2' or C-3' is on the same side as the C-5' atom, it is called the *endo* conformation, and if it is the opposite side of the C-5' atom, it is called the *exo* conformation.[63-65] For example, if the C-2' atom is displaced to the same side as C-5', it is called C-2' *endo,* as shown in Figure 2.10.[63,65]

When B-form DNA dries to approximately 75% relative humidity, the conformation changes to A-form. The pitch of A-form DNA is 24.6 Å with approximately 11 base pairs for a single turn and a rotation angle of 32.7° for each nucleotide.[60,65] The sugar pucker of the A-form is C-3' *endo* while that of the B-form is C-2' *endo.*[63,65] The diameters of the B and A-forms of DNA are approximately 23.7 Å and 25.5 Å, respectively.[61]

Z-DNA, discovered by Alexander Rich, is a left-handed helix. The phosphates in the backbone zigzag due to the dinucleotide rather than a mononucleotide.[60-61,63-65] Z-form DNA has only one deep helical groove and the pitch of the double helix is 45.6 Å with 12 base pairs for a full turn.[60] The double helix diameter of Z-DNA is 18.4 Å.[60]

The sizes of naturally occurring DNA molecules are diverse, from 1 kilobase (kb)

(0.33 μm, plasmid DNA) to 10,000 kb (4 cm, chromosomes in mammals) in living organisms.[61,66] Much smaller polynucleotides, as small as 10 to 15 base pairs (32 Å to 49 Å), can be routinely synthesized in the laboratory. The shapes of DNA are either circular or linear, with no branches. Most of the natural circular DNAs are supercoiled (highly twisted). Circular DNAs can be supercoiled either negatively (underwound) or positively (overwound) and can be relaxed by cleaving and closing a phosphodiester bond in one or both of the strands using enzymes called DNA topoisomerases.[60] The length, diameter, and twist angle of DNA also depend on the degree of twisting.[60]

2.2.2 pUCLeu4 Plasmid DNA and Its Synthesis

Plasmids are naturally occurring small, circular, double-stranded DNA molecules which can replicate independently of the host chromosome in bacteria and unicellular eukaryotes such as yeasts.[66-67,69] These extrachromosomal genetic elements found in most bacteria have their own origin of replication and hence can replicate autonomously. Most plasmid DNAs are supercoiled and the molecular weights vary from 10^6 to 10^8. Plasmid DNAs can be classified into two major categories, transmissible and nontransmissible, depending on the ability of cell-to-cell contact transfer for their replication. Three kinds of plasmid DNA are known: F plasmid (a group of plasmid which has self-transmissibility for replication, also called sex plasmid), R plasmid (a group of plasmids carrying genes for antibiotic resistance), and *Col* plasmid (a group of plasmids producing colicins which kill or inhibit the growth of other bacteria).[68-69] These relatively small plasmid DNA molecules are easy to synthesize, isolate and handle (ranging in size from 1

kilobase to over 200 kilobases) and are widely used in genetic engineering as cloning vectors.[67,70-71]

Molecular cloning is a method used to produce a large amount of the same kind of recombinant DNA by inserting a desired DNA fragment into an appropriate vector. Cloned DNA can be amplified by putting the recombinant DNA back into a suitable host cell (called transformation).[67] The steps for synthesizing DNA by genetic engineering procedures are as follows. First, both types of DNA, the cloning vector and the DNA to be inserted (also called the foreign DNA), are extracted from each organism and purified by one of several known methods. Using certain restriction enzymes (also called restriction endonucleases, for example, *EcoRI*), appropriate sized insert DNA fragments can be isolated by cutting specific sites of the original DNA molecule. The desired cloning site of the vector DNA can be cleaved by treating it with the same kind of restriction enzyme which was used for the foreign DNA.[60,67,70] The size of the insert DNA fragment can be selected to generate a desired length of the hybrid molecules by agarose gel electrophoresis. By ligating these two different DNAs by DNA ligase, each end of the insert DNA molecule is covalently joined to the opened ends of the vector DNA through the C-3' hydroxyl and C-5' phosphate groups. Thus, circular chimeric plasmids are regenerated.[70] In this way, almost any foreign DNA can be inserted into a cloning vector without disrupting any essential function of the vector.[70] By putting the chimeric DNA back into a host cell such as *Escherichia coli* (*E. coli*), the chimeric DNA is replicated in large amounts just like the original plasmid DNA.[60,67-70]

pUCLeu4 DNA is a recombinant DNA molecule which was generated by

inserting a human DNA fragment (a 781-basepair *Kpn*I-*Sst*I fragment) encompassing a leucine $tRNA_{AAG}$ gene as a foreign DNA into the plasmid cloning vector pUC19 (Figure 2.11)[72] and transforming it using *E. coli.*[72] pUC19 is small plasmid vector DNA with 2686 base pairs and a high copy number.[71,73]

2.2.3 ϕX174 RF II DNA and Its Synthesis

ϕX174 RF II (Replicative Form II) DNA is double-stranded circular DNA, produced from RF I (Replicative Form I) during the replication of ϕX174 DNA.[74,75] ϕX174 is a small icosahedral virus (called a bacteriophage or phage) containing a single-stranded circular DNA molecule with 5386 nucleotides. It is approximately 1.83 μm in circumference.[74] The replication of ϕX174 DNA starts by injecting this single-stranded DNA (called a "plus" strand) into a suitable host cell such as *E. coli.*, and coating this injected plus strand with single-stranded DNA-binding proteins (SSBs).[74] Since all DNA replication is performed in double-stranded form, the injected original "plus" molecule is used as a template to synthesize a complementary "minus" strand molecule. Then, by combining a primase with the preprimosome (six proteins : *dnaB*, *dnaC*, *dnaT*(i), *PriA*(n'), *PriB*(n), and *PriC*(n")), a mobile primosome is assembled on the ϕX174 DNA.[74] Subsequently, RNA primer, a short RNA chain, is synthesized on the DNA template by this primosome, and the respective minus strand DNA molecule is polymerized by DNA polymerase using the RNA primer. The RNA primer is removed by DNA polymerase I and the small gap between C-5' and C-3' is filled by DNA ligase. In this way, the circular, single-stranded DNA chromosome is converted into the duplex (plus/minus) replicative

form. This form, ready for replication, the supercoiled double helical DNA, is called ϕX174 RF I.[74] As the next step, a nicking enzyme (also called an endonuclease), gene A proteins (*gpA*), cleaves a specific phosphodiester bond (the base between 4305 and 4306) of the plus-strand of the supercoiled ϕX174 RF I to introduce the nick which generates the replication origin. ϕX174 RF I DNA with a small gap at the point of origin of the plus strand is called ϕX174 RF II DNA, which is the middle step of the whole replication cycle. The nicking enzyme *gpA* is bound covalently at the C-5' end of the nicked DNA and is detached to generate a new round of rolling circle synthesis. When the newly made free C-5' end is linked onto the new C-3' end, a new circular plus single strand progeny is produced. By repeating these steps, more copies of DNA are produced for making progeny. This type of DNA replication is called the rolling-circle replication mechanism.[74]

2.3 Basic Theories of Metal Ion - DNA Interactions

2.3.1 Historical Background

The study of DNA - metal ion interactions originated in the discovery of the antibacterial (anticancer) activity of some platinum group metals by F. P. Dwyer and his co-workers in 1953.[76] It was found that the activity was caused by the metal complexes attacking the DNA of the bacteria. It was also found that many other di-cation metal ions like the transition metal ions had the same property.[78] Metal-DNA interactions, especially with heavy metals such as uranium, have also been applied to electron microscopy (TEM and STM) for studying the microstructures of biological samples.[76-77,79-80]

Divalent metal ions, such as transition metal ions, have unique electronic properties and specific reactions with biological molecules. Therefore, metal ions have been used to probe the physical and chemical structures of nucleic acids and proteins.[78] It is now recognized that metal ions are essential to life, and nucleic acids cannot perform their biological functions such as replication, transcription, and translation without their participation.[76-78]

Since the early 1990s, metal binding to DNA molecules has also been of interest to chemists, physicists and material scientists for stabilizing colloidal quantum-dot semiconductors.[38,81-82] In 1996, Stem and Barton considered double helical-DNA bound with metal complexes as an ideal medium which might be used as a long-range charge transferring wire ("DNA wire") because of the highly ordered stack of electronically coupled bases.[83] Our research group demonstrated nanoscale fabrication of Q-SC by combining transition metal ions, such as Cd^{2+} with a double-helical DNA template, also in 1996.[84-85]

DNA has many metal ion binding sites, such as the oxygen atoms of phosphate groups, sugar hydroxyl groups, base keto groups, and nitrogen atoms.[76-77] There are a diverse number of metal ions which interact with nucleic acids, such as alkali (Li, Na, K, Rb, and Cs), alkaline earth (Mg, Ca, Sr, Ba), and transition metals (Mn^{2+}, Ru^{3+}, Co^{2+}, Co^{3+}, Ni^{2+}, Pd^{2+}, Pt^{2+}, Cu^{2+}, Ag^{+}, Au^{3+}, Zn^{2+}, Cd^{2+}, and Hg^{2+}).[65,76-77,87] Different metal ions have different preferred binding sites.[77] DNA-metal binding reactivity depends on the pH and pK level,[76-77] and on the tautomeric states of the nucleotides.[76-77] Metal-DNA interactions have been studied using NMR, Raman spectroscopy, x-ray crystallography,

and UV absorption spectroscopy.[65,76-77]

Since 1953, thousands of articles about metal - DNA interactions have been published. The specific binding sites for specific metal ions are now well-known from the biochemical point of view. The fundamentals of metal-DNA binding are briefly described in the following section.

2.3.2 Metal - DNA Binding Sites and Modes

The double-stranded deoxyribonucleotides which consist of a pair of phosphate units, deoxy-ribose sugar rings, and one pair of four heterocyclic purine or pyrimidine bases, offer a rich variety of sites for metal reactivity. Metal binding to the DNA molecules is closely related to pH and pK (ionization constant) values.[60,77] When the pH level of the solution is low, the excess H^+ ions can bind to the negatively charged oxygen atoms of the phosphate groups (protonation), and as result, the anionic phosphate oxygen atoms become neutralized.[77] On the other hand, when the pH level of the solution is high, NH and OH of the bases and the sugar ring lose H^+ ions (deprotonation) and thus negatively charged oxygen and nitrogen atoms are available for metal ion interaction.[77] The protonation and deprotonation of bases occurs at pH values of 3.5 and 10.5, respectively. At pH 7, nucleotides exist mainly as anions due to negative charges on the phosphate groups.[77]

Protons on the sugar and bases of nucleotides can shift from one nitrogen or oxygen atom to another (tautomerization reactions) depending on the pK of the hetero atoms, and on the dielectric constant of the solvent.[60,77] For example, the amino ($C\text{-}NH_2$)

form (donor) attached to C-6 of adenine and to C-4 of cytosine can be changed to the imino (C = NH) form (acceptor), and the keto (C = O) form (acceptor) attached to C-6 of guanine and C-4 of thymine can be changed to the enol (C-OH) form (donor) (Figure 2.12). However, under normal physiological conditions the equilibria of the tautomerization reactions lie strongly in favor of the amino and keto forms.[60] Therefore, metal ions primarily attack nitrogen atoms and keto oxygen atoms of the base rings.

The phosphate groups of DNA are well recognized as binding sites for all kinds of metal ions. Each DNA nucleotide has one negatively charged phosphate oxygen atom which can have electrostatic interactions with high affinity for metal ions.[76-78]

The hydroxyl group of the pentose sugar ring is a poor ligand for metal coordination.[76] The ribose oxygen atoms interact preferentially with alkali and alkaline earth ions, but not with transition metal ions, except for Cd^{2+}.[76,88] Cd^{2+}, Cu^{2+}, and Zn^{2+} were examined by Goodgame and co-workers, but only Cd^{2+} was found to bind ribose oxygen atoms of DNA.[87] However, when the pH level is increased to 8.5 to 10, a binding site for transition metal ions, such as Cu^{2+}, is generated by deprotonation of the C-3' hydroxyl group.[76]

The bases in DNA have the greatest number of sites for metal ion interactions. The heterocyclic nitrogen bases are good ligands for transition metals, alkali, and alkaline earth metal ions. The primary metal binding sites the of purine bases in order of affinity are $N_7 >> N_1$, N_3 for adenine and $N_7 >> N_1$, N_3, O_6 for guanine, and for the pyrimidine bases, $N_3 > O_2$ for cytosine and $O_2 > O_4$ (base keto) for thymine[76-77,88] (Figure 2.13). The keto oxygen O_6 of guanine does not interact directly with metal ions

because N_7 is a better ligand, and metal binding to both O_6 and N_7 are not geometrically favored.[77] The base amino groups of both adenine and cytosine do not directly interact with metal ions. However, under strong alkaline conditions, the amino groups are deprotonated and become good reaction sites for transition metal ions.[77]

Metal interactions with DNA can be divided into two main modes: a surface or groove interaction in the minor groove area of the helix, and an intercalative interaction in the major groove area of the helix.[89] In the minor groove, the anionic phosphate groups are much closer to each other than in the major groove, so electrostatic attraction to metal ions are much more favorable. Also in the minor groove area, because of the geometrical positions of the atoms and the affinity between cations and base atoms, the electrostatic binding of metal ions is more favorable for A-T sequences than for C-G sequences.[76,89] In the major groove, the anionic phosphate groups are separated farther from each other, so the metal ions can access the base atoms such as O_6 (or N_6) in the purine rings and O_4 (or N_4) in the pyrimidine rings.[76]

Metal-DNA interactions affect the overall stability of the double-helical DNA structure.[76-77,86] Without metal binding, DNA itself is unstable because the anions of the phosphate groups repel each other.[86] After metal binding to the phosphate groups, the electrostatic repulsions between neighboring nucleotides is decreased and the DNA is stabilized in an ordered structure.[76,86] However, if metal ions interact with the bases, they disrupt the hydrogen bonding and destabilize the helix, which makes the DNA structure weak.[76-77,86]

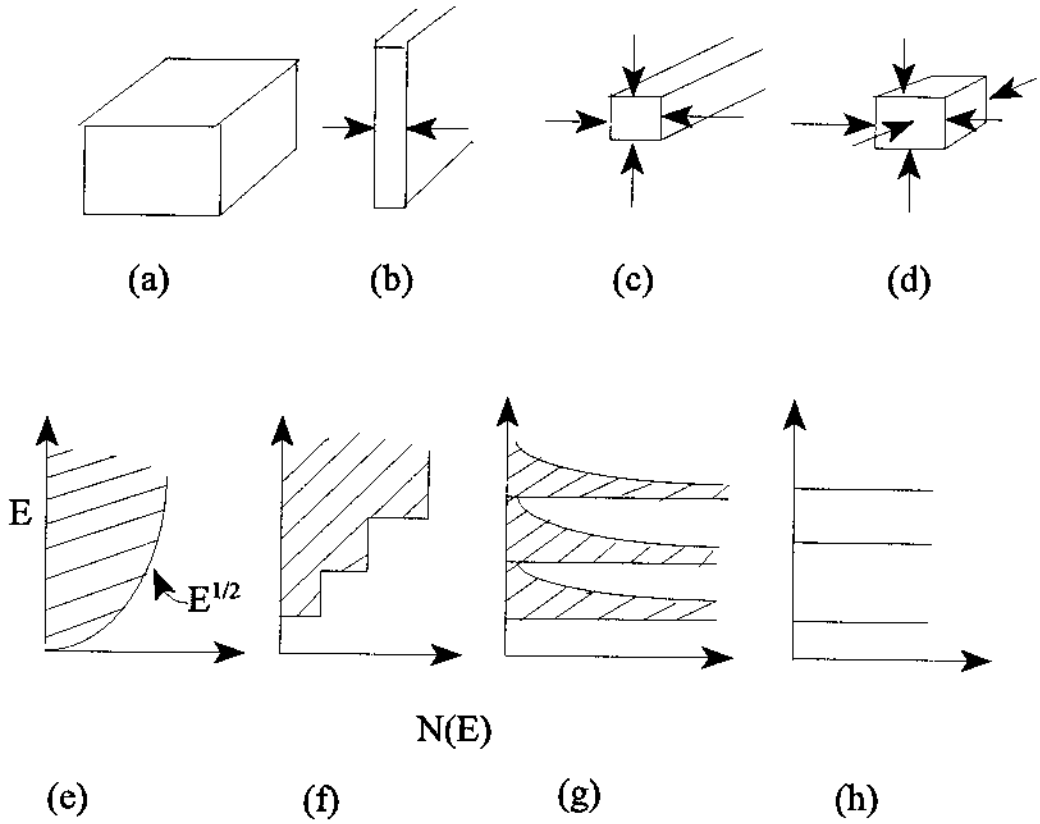

Figure 2.1 Illustrations of confining dimensions and corresponding densities of electron states. As the dimensions of the semiconductor are spatially restricted, such as (a) bulk semiconductor, (b) quantum well, (c) quantum wire, and (d) quantum-dot, the densities of states are reduced and become more discrete as illustrated in (e) through (h): (e) 3-D, (f) 2-D, (g) 1-D, and (h) 0-D.

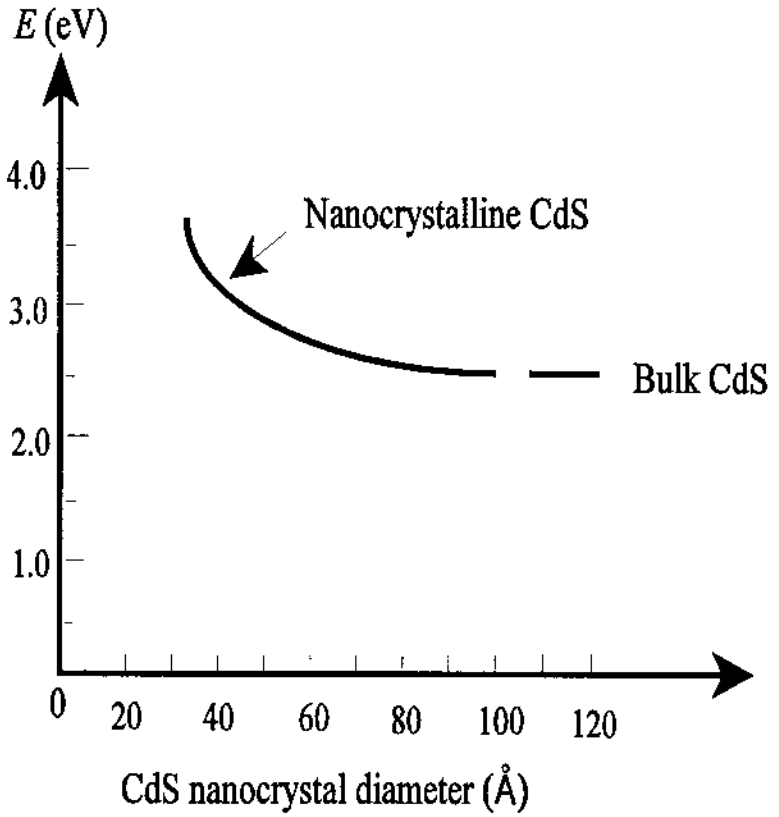

Figure 2.2 Energy of the lowest excited electronic state as a function of diameter for CdS nanoparticles. The short horizontal solid line indicates the bulk band gap energy of CdS.

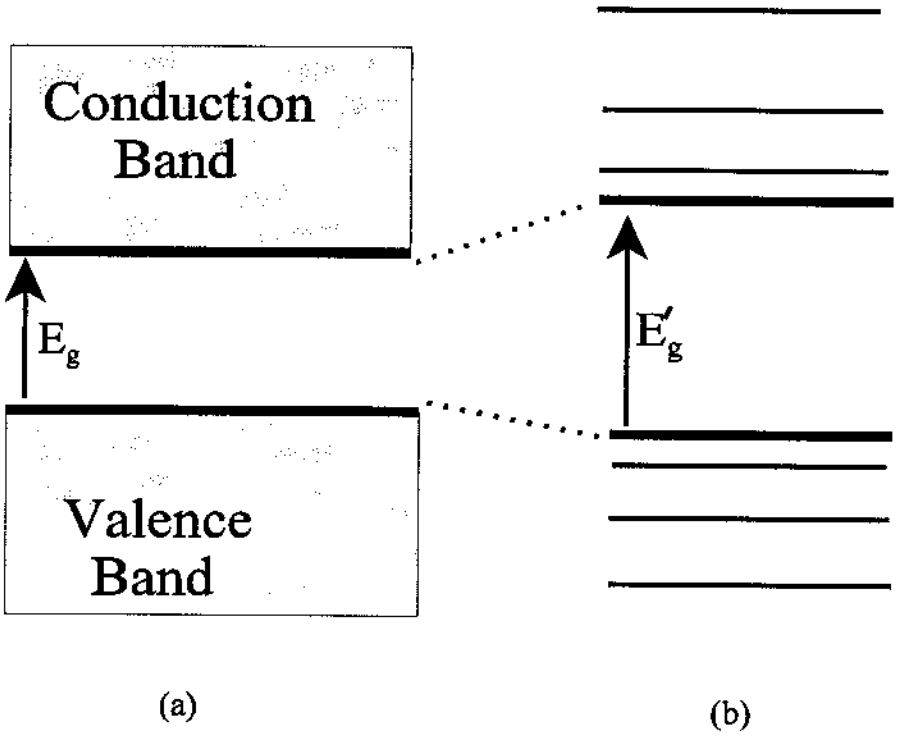

Figure 2.3 Band structure for (a) bulk semiconductor, and (b) quantum-dot semiconductor.

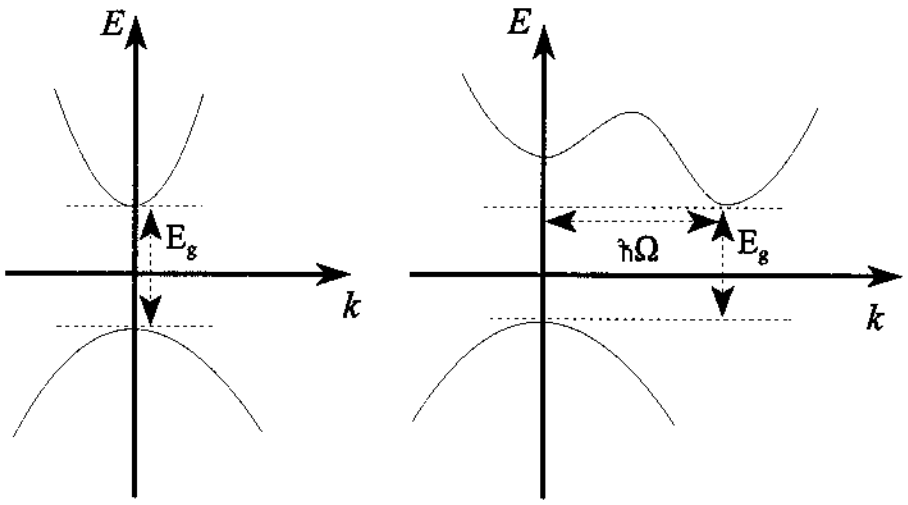

(a) (b)

Figure 2.4 Band gap structures of semiconductors: (a) direct gap, and (b) indirect gap.

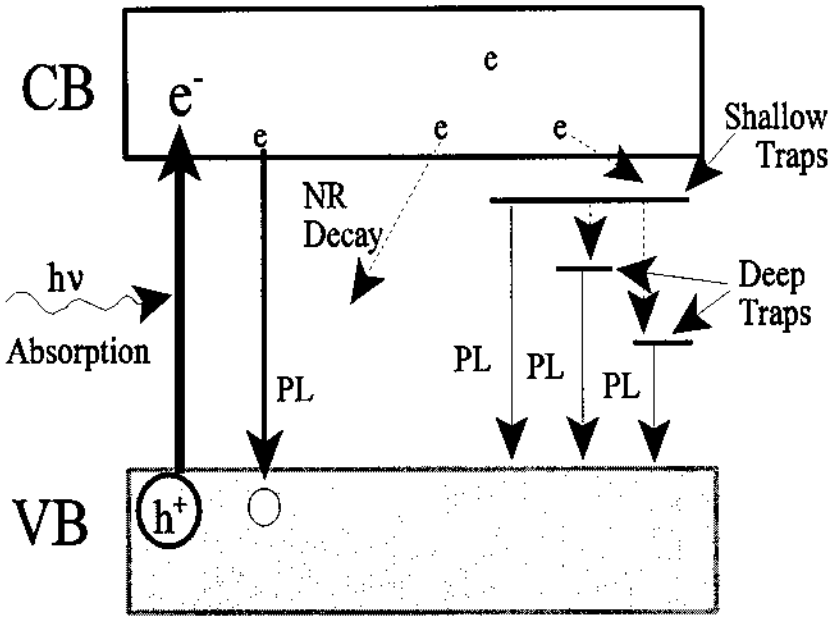

Figure 2.5 Electron transition diagram for quantum-confined semiconductors. (PL = photoluminescence)

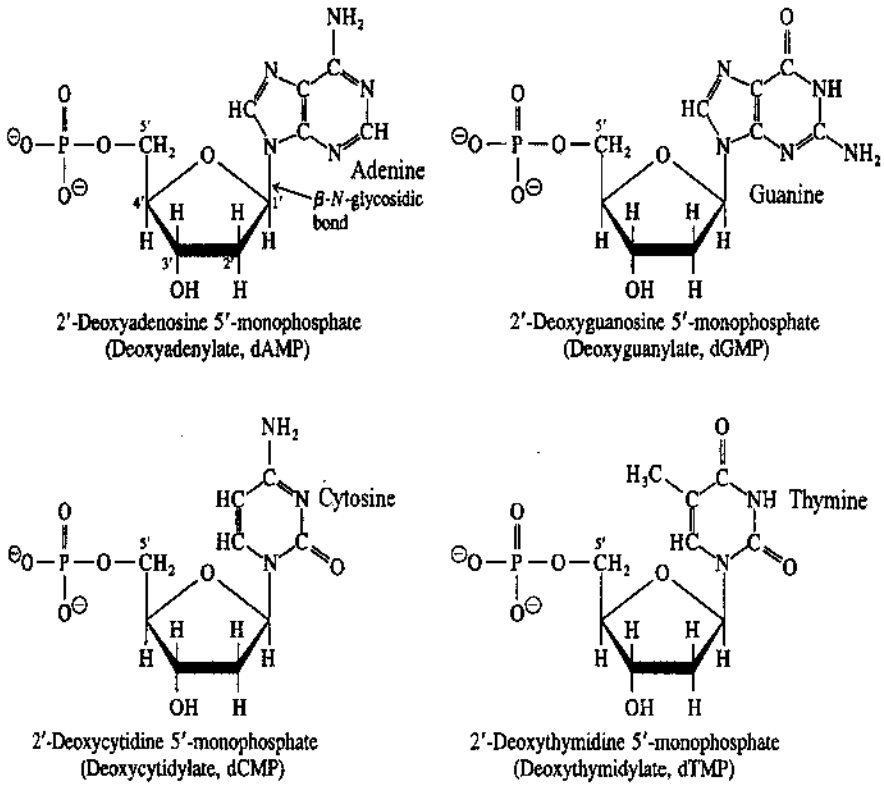

Figure 2.6 Chemical structures of the four deoxyribonucleotides in DNA [Reprinted from J. D. Rawn, *Biochemistry*,[60] with permission].

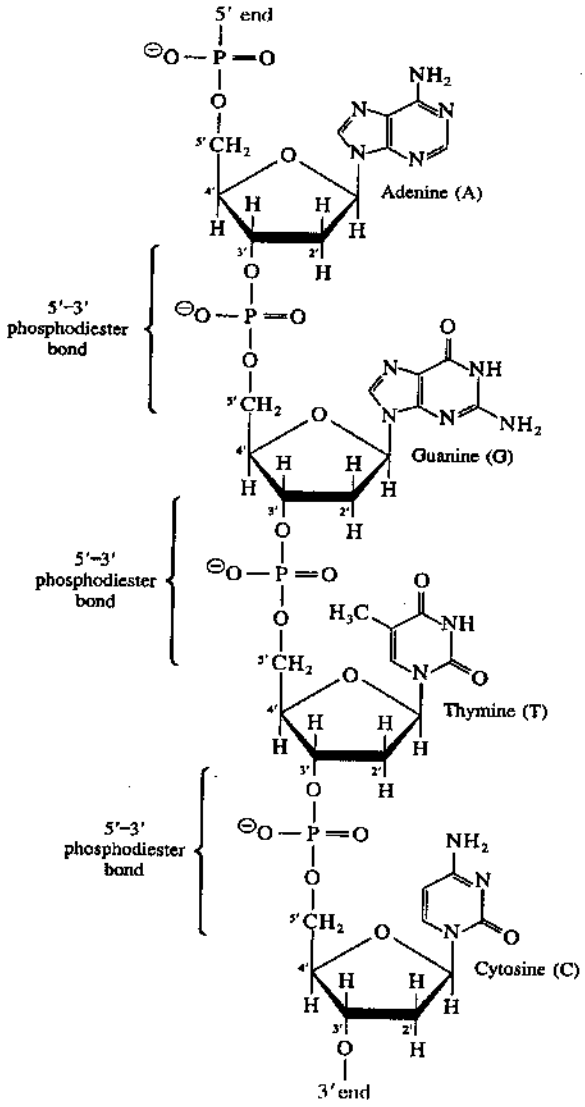

Figure 2.7 Covalently linked polynucleotide chain of DNA [Reprinted from J. D. Rawn, *Biochemistry*,[60] with permission].

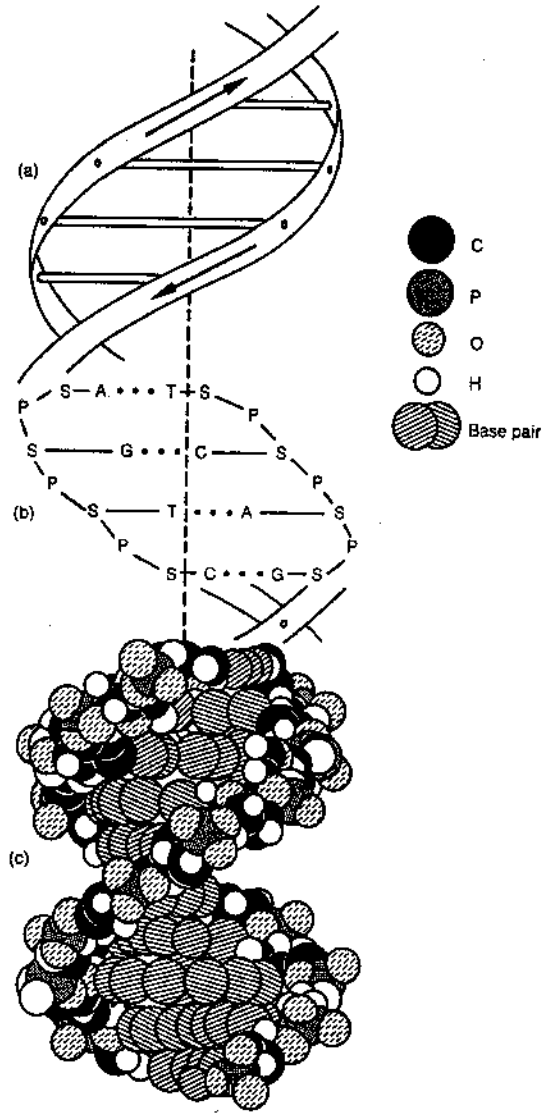

Figure 2.8 Right-handed helix form of the-double stranded DNA structure: (a) sugar-phosphate backbone, (b) interactions between the four base pairs, and (c) three dimensional structure of the polynucleotides [Reprinted from W. Guschlbauer, *Nucleic Acid Structure*,[63] with permission].

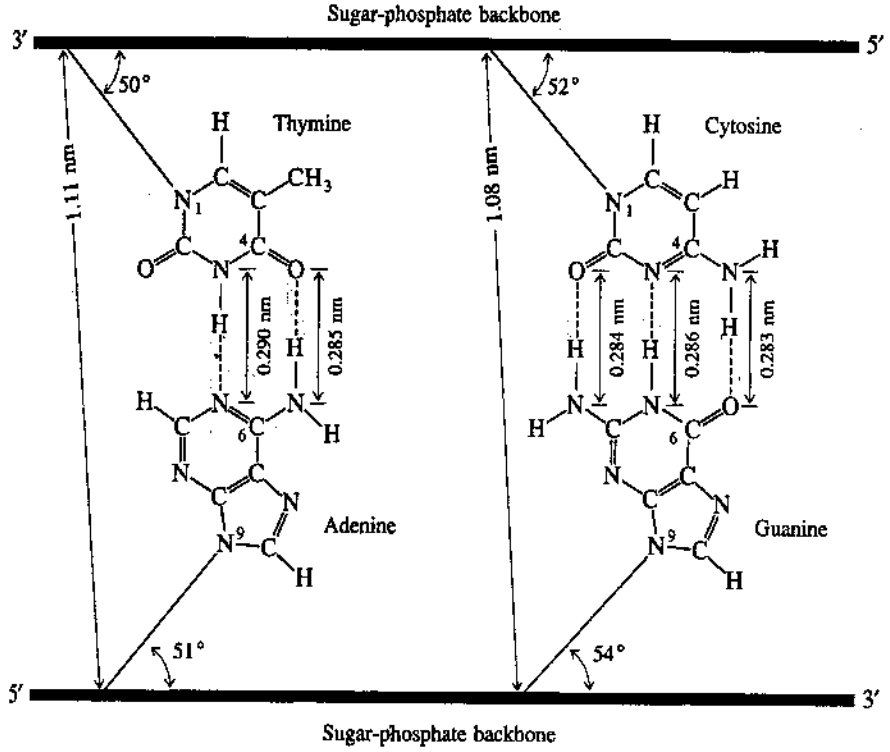

Figure 2.9 The hydrogen bonds between thymine and adenine, and between cytosine and guanine [Reprinted from J. D. Rawn, *Biochemistry*,[60] with permission].

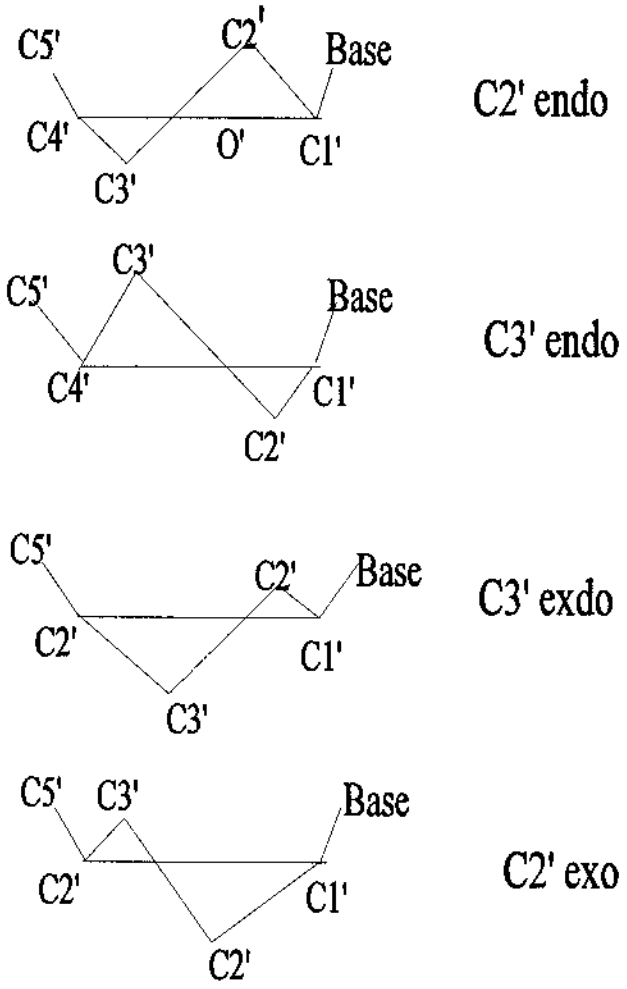

Figure 2.10 Illustration of the different sugar pucker conformations.

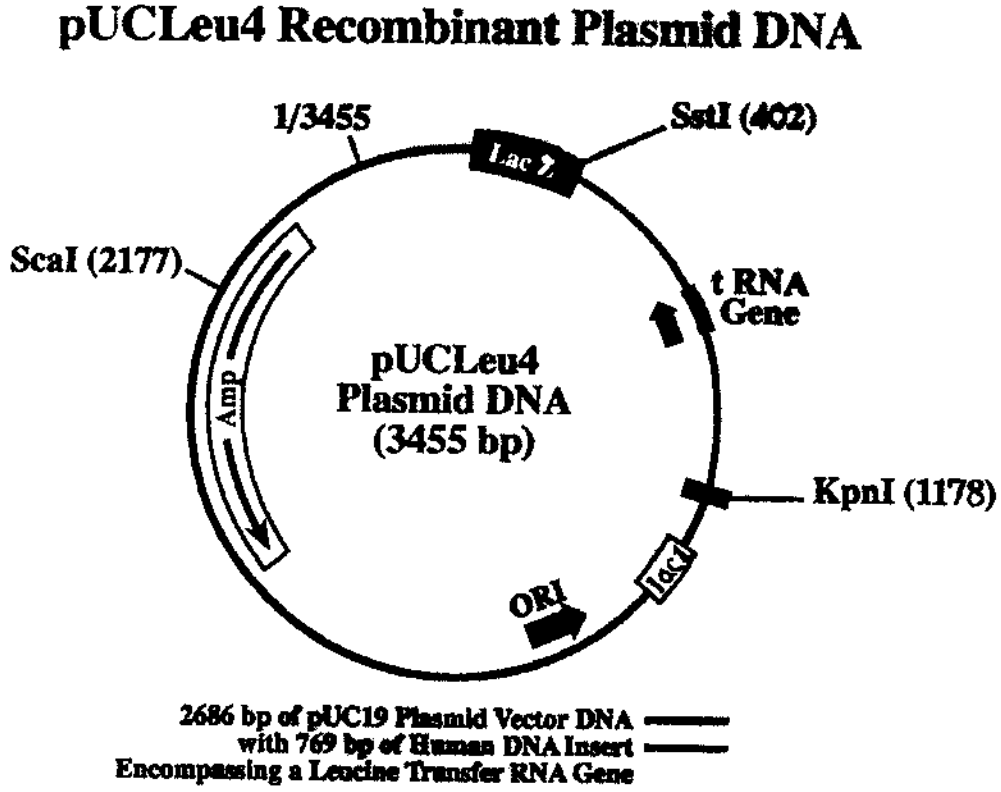

Figure 2.11 Map of pUCLeu4 plasmid DNA.

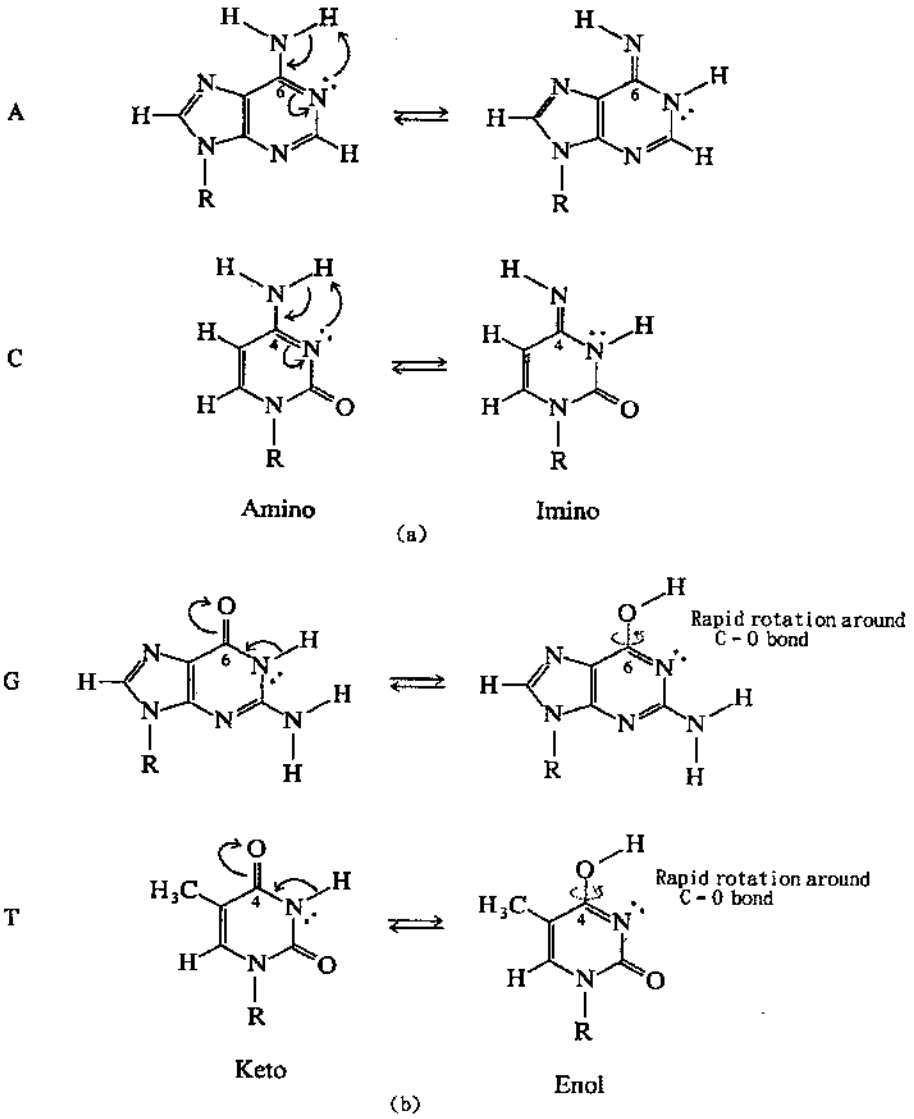

Figure 2.12 Tautomerization: (a) from amino to imino and (b) from keto to enol [Reprinted from J. D. Rawn, *Biochemistry*,[60] with permission].

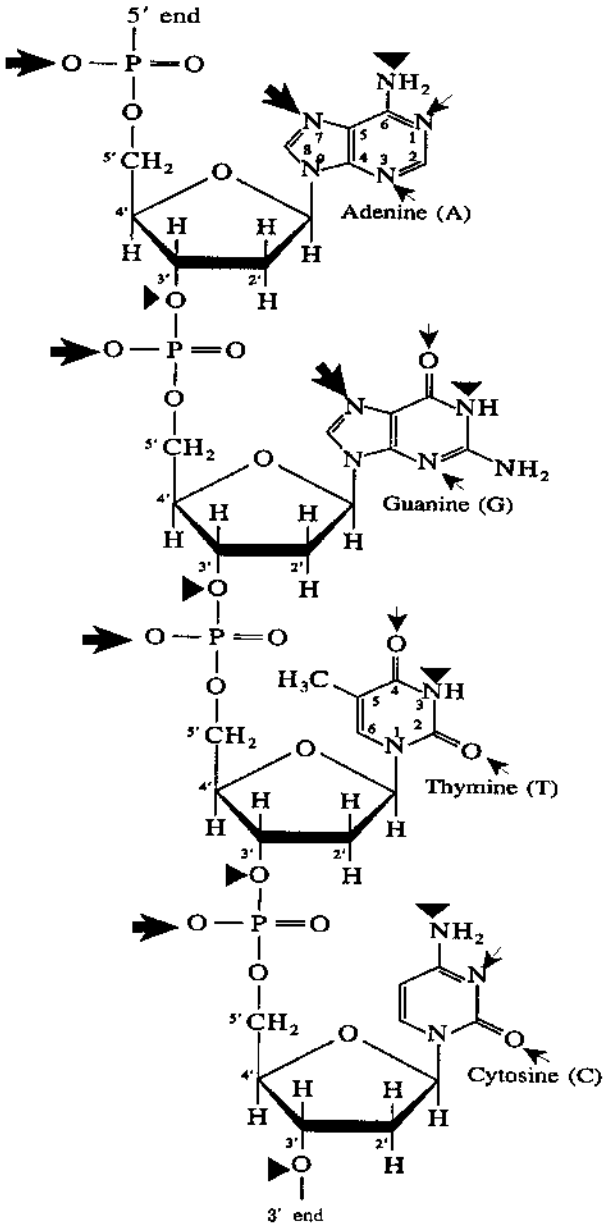

Figure 2.13 Illustrations of possible metal-polynucleotide binding sites. The large and small arrows indicate strong and weak binding sites with high and low affinities, respectively, at normal pH. The trangles indicate poor binding sites or possible binding sites at high pH [Modified from J. D. Rawn, *Biochemistry*,[60] with permission].

REFERENCES

1. B. O. Dabbousi, M. G. Bawendi, O. Onitsuka and M. F. Rubner, Appl. Phys. Lett. **66,** 11 (1995).

2. L. Brus, Appl. Phys. A **53**, 465-474 (1991).

3. S. A. Empedocles, D. J. Norris and M. G. Bawendi, Phys. Rev. Lett. 77, 18 (1996).

4. A. P. Alivisatos, Science **27**, 933 (1996).

5. H. Weller, Angew. Chem. International Ed. Engl. **32**, 41-53 (1993).

6. M. O'Neil, J. Marohn and G. McLendon, J. of Phys. Chem. **94**, 4356-4363 (1990).

7. L. E. Brus, J. Chem. Phys. **80**, 9 (1984).

8. A. Fojtik, H. Weller, U. Koch and A. Henglein, Ber. Bunsengers. Phys. Chem. **88**, 969-977 (1984).

9. R. E. Hummel, *Electronic Properties of Materials* (Springer-Verlag, New York, 1985), p. 60.

10. A. J. Nozik, F. Williams, M. T. Nenadovic, T. Rajh and O. I. Micic, J. of Phys. Chem. **89**, 397-399 (1985).

11. P. E. Lippens and M. Lannoo, Phys. Rev. B **39**, 15 (1989).

12. Y. Wang, A. Suna, W. Mahler and R. Kasowski, J. Chem. Phys. **87**, 12 (1987).

13. N. Chestnoy, T. D. Harris, R. Hull and L. E. Brus, J. of Phys. Chem. **90**, 15 (1986).

14. R. R. Chandler and J. L. Coffer, J. of Phys. Chem. **95**, 4 (1991).

15. A. N. Goldstein, C. M. Echer and A. P. Alivisatos, Science **256**, 5 (1992).

16. A. L. Efros and A. L. Efros, Sov. Phys. Semicond. **16**, 7 (1982).

17. L. Esaki, IBM J. Res. **14**, 61 (1970).

18. A. I. Ekimov and A. A. Onushchenko, JETP Lett. **34**, 345 (1982).

19. Y.Wang and N. Herrin, J. of Phys. Chem. **92**, 4988-4994 (1988).

20. J. J. Ramsden, S. E. Webber and M. Grätzel, J. of Phys. Chem. **89**, 2740-2743 (1985).

21. J. L. Coffer, R. R. Chandler, C. D. Gutsche, I. Alam, R. F. Pinizzotto and H. Yang, J. of Phys. Chem. **97**, 3 (1993).

22. N. Herron, J. C. Calabrese, W. E. Farneth and Y. Wang, Science **259**, 1426 (1993).

23. E. S. Smotkin, R. M. Brown, Jr., L. K. Rabenberg, K. Salomon, A. J. Bard, A. Campion, M. A. Fox, T. E. Mallouk, S. E. Webber and J. M. White, J. of Phys. Chem. **94**, 19 (1990).

24. C. H. Fischer and A. Henglein, J. of Phys. Chem. **93**, 14 (1989).

25. C. Petit and M. P. Pileni, J. of Phys. Chem. **92**, 2282-2286 (1988).

26. E. S. Smotkin, C. Lee, A. J. Bard, A. Campion and M. A. Fox, Chem. Phys. Lett. **152**, 3 (1988).

27. N. Herron, Y. Wang, and H. Eckert, J. Am. Chem. Soc. **112**, 4 (1990).

28. J. Kuczynski and J. K. Thomas, J. of Phys. Chem. **89**, 2720-2722 (1985).

29. C. B. Murray, C. R. Kagan and M. G. Bawendi, Science **270,** 1335 (1995).

30. E. M. Clausen, H. G. Craighead, J. M. Worlock, J. P. Harbison and L. M. Schiavone, Appl. Phys. Lett. **55**, 1427 (1989).

31. L. T. Canham, Appl. Phys. Lett. **57**, 1046 (1990).

32. L. Brus, Advanced Materials **5**, 4 (1983).

33. K. A. Littau, P. J. Szajowski, A. J. Muller, A. R. Krotan and L. E. Brus, J. of Phys. Chem. **97**, 1224-1230 (1993).

34. R. Rossetti, S. Nakahara and L. E. Brus, J. of Chem. Phys. **79**, 2 (1983).

35. A. I. Ekimov and A. A. Onushchenko, JETP Lett. **40**, 1136 (1984).

36. Y. Wang and W. Mahler, Optics Commun. **61**, 233 (1987).

37. Y. Wang, N. Herron, W. Mahler and A. Suna, J. Opt. Soc. Am. B **6**, 808 (1989).

38. J. L. Coffer, S. R. Bigham, R. F. Pinizzotto and H. Yang, Nanotechnology **3**, 69-76 (1992).

39. N. Peyghambarian, S. W. Kzoch and A. Mysyrowicz, *Introduction to Semiconductor Optics* (Prentice Hall, Englewood Cliffs, New Jersey, 1993), pp. 23-36, 110-114, 245-249 and 253.

40. H. Haug and Stephan W. Koch, *Quantum Theory of the Optical and Electronic Properties of Semiconductors* (World Scientific, Teaneck, New Jersey,1990), pp. 27-44, 324-332 and 333-340.

41. C. R. Berry, Phys. Rev. **161**, 848 (1967).

42. L. Brus, J. of Phys. Chem. **90**, 2555-2560 (1986).

43. L. Brus, IEEE J. of Quantum Electron. **QE-22**, 9 (1986).

44. M. G. Bawendi, M. L. Steigerwald and L. E. Brus, Ann. Rev. of Phys. Chem. **41**, 77-96 (1990).

45. Y. Kayanuma, Solid State Comm. **59**, 405 (1986).

46. Y. Kayanuma, Phys. Rev. B **38**, 9797 (1988).

47. Y. Kayanuma and H. Momiji, Phys. Rev. B **41**, 14 (1990).

48. Y. Z. Hu, S. W. Koch, M. Lindberg, N. Peyghambarian, E. L. Pollock and F. F. Abraham, Phys. Rev. Lett. **64**, 15 (1990).

49. Y. Z. Hu, M. Lindberg and S. W. Koch, Phys. Rev. B **42**, 3 (1990).

50. P. E. Lippens and M. Lannoo, Phys. Rev. B **39**, 15 (1989).

51. Y. Wang and N. Herron, Phys. Rev. B **42**, 11 (1990).

52. N. F. Borrelli, D. W. Hall, H. J. Holland and D. W. Smith, J. Appl. Phys. **61,** 12 (1987).

53. G. Arfken, *Mathematical Methods for Physicists,* 3rd ed. (Academic Press, Harcourt Brace Jovanovich Publishers, New York, 1985), pp. 622-630.

54. C. Cohen-Tannoudji, B. Diu and F. Laloë, *Quantum Mechanics,* Vol. II (Chongno Book Center, South Korea, 1977), pp. 924-931.

55. A. D. Yoffe, in *Advances in Physics*, edited by D. Sherrington (Taylor & Francis, London and Washington, DC, 1993), **42**, pp. 173-266.

56. S. Perkowitz, *Optical Characterization of Semiconductors*: *Infrared, Raman, and Photoluminescence Spectroscopy* (Academic Press Limited, University Printing House, Cambridge, 1993), p 27.

57. A. G. Cullis, P. W. Smith, P. J. Parbrook, B. Cockayne, P. J. Wright and G. M. Williams, Appl. Phys. Lett. **55**, 20 (1989).

58. L. E. Brus, Ann. Rev. of Phys. Chem. **41**, 477-496 (1990).

59. H. Wang and N. Herron, J. of Phys. Chem. **95**, 525 (1991).

60. J. D. Rawn, *Biochemistry* (Carolina Biological Supply Company, Neil Patterson Publishers, 1989), pp. 665-673.

61. L. Stryer, *Biochemistry* (W. H. Freeman and Company, New York, 1988), pp. 83, 649-656.

62. J. D. Watson, *Molecular Biology of the Gene,* 3rd ed. (W. A. Benjamin, Inc. Menlo Park, California, 1976), p. 52.

63. W. Guschlbauer, *Nucleic Acid Structure* (Springer-Verlag, New York, 1976), pp.15-18.

64. F. H. C. Crick, in *Nucleic Acid Research Future Development,* edited by K. Mizobuchi, I. Watanabe and J. D. Watson (Academic Press, New York, 1983), Chap. 1, pp.11-13; R. E. Dickerson, B. N. Conner, M. L. Kopka and H. R. Drew, Chap. 2, pp.35-40.

65. V. A. Bloomfield, D. M. Crothers and I. Tinoco, Jr. *Physical Chemistry of Nucleic Acids* (Harper & Row, Publishers, New York, Evanston and San Francisco, 1974), pp. 10-19 and 420-427.

66. P. Broda, *Plasmids* (W. H. Freeman and Company, Oxford and San Francisco, 1979), pp. 1-15.

67. R. E. Glass, *Gene Function, E. coli and Its Heritable Elements* (University of California Press, Berkeley and Los Angeles, 1982), pp. 14 and 159-163.

68. B. Lewin, *Genes IV,* 4th ed. (Oxford University Press and Cell Press, New York, 1990), pp. 451-456.

69. B. Lewin, *Gene Expression, Volume 3, Plasmids and Phages* (John Wiley & Sons, New York, 1977), pp. 97, 160-168 and 261-268.

70. T. M. Fritsch, *Molecular Cloning, A Laboratory Manual,* 2cd ed. (Cold Spring Harbor Laboratory Press, New York, 1989), pp. 1.2 and 1.13-1.24.

71. R. Schleif, *Genetics and Molecular Biology,* 2cd ed. (The Johns Hopkins University Press, London Ltd., 1993), pp. 265-274.

72. Y. N. Chang, I. L. Pirtle and R. M. Pirtle, Gene **48**, 165-174 (1986).

73. *Product Catalog and Reference Guide* (New England Biolabs, Inc.1996), p. 206.

74. J. D. Watson, *Molecular Biology of the Gene,* 4th ed. (The Benjamin/Cummings Publishing Company, Inc., Menlo Park, California, 1987), pp. 302-334.

75. M. W. Strickberger, *Genetics* (Macmillan Publishing Co. Inc., New York, 1976), pp. 90-92.

76. B. Rosenberg, "Nucleic Acid-Metal Ion Interactions" in *Metal Ions in Biology,* edited by T. G. Spiro, (John Wiley & Sons, Inc., New York, 1980), Vol. I, Chap. 1, pp.3-13; J. K. Barton and S. J. Lippard, Chap. 2, pp. 33-81; L. G. Marzilli, T. J. Kistenmacher and G. L. Eichhorn, Chap. 5, pp. 181-199 and 227-236.

77. W. Saenger, *Principles of Nucleic Acid Structure* (Springer-Verlag, New York, 1984), pp. 105-114 and 201-211.

78. J. Kozelka, in *Metal Ions In Biological Systems,* edited by A. Sigel and H. Sigel, (Marcel Dekker, Inc., New York, 1996), Vol. 33, pp.1-23.

79. A. K. Kleinschmidt and R. K. Zahn, "Über Desoxyribonucleinsäure-Molekeln" in Pritein-Mischfilmen. Z. Naturforsch. B **14**, 770-775 (1959).

80. A. K. Kleinschmidt, Methods Enzymol. **12** (B), 361 (1968).

81. S. R. Bigham and J. L. Coffer, Colloids and Surfaces A: Physicochem. Eng. Aspects **95**, 211-219 (1995).

82. J. L. Coffer and R. R. Chandler, Mat. Res. Soc. Symp. Proc. **206,** 257 (1991).

83. E. D. A. Stemp and J. K. Barton, in *Metal Ions In Biological Systems*, edited by A. Sigel and H. Sigel, (Marcel Dekker, Inc., New York, 1996), Vol. 33, pp. 325-452.

84. J. L. Coffer, S. R. Bigham, R. F. Pinizzotto, Y. G. Rho, R. M. Pirtle and I. L. Pirtle, Appl. Phys. Lett. **69**, 3851 (1996).

85. R. F. Pinizzotto, Y. G. Rho, Y. Chen, R. M. Pirtle, I. L. Pirtle, J. L. Coffer and X. Li, Mat. Res. Soc. Symp. Proc. **452,** 591(1997).

86. M. Sabat and B. Lippert, in *Metal Ions In Biological Systems*, edited by A. Sigel and H. Sigel, (Marcel Dekker, Inc., New York, 1996), Vol. 33, pp. 143-168.

87. D. M. L. Goodgame, I. Jeeves, C. D. Reynolds and A. C. Skapski, Nucleic Acids Research **2**, 8 (1975).

88. V. G. Bregadze, J. G. Chkhaberidze and I. G. Khutsishvili, in *Metal Ions In Biological Systems,* edited by A. Sigel and H. Sigel, (Marcel Dekker, Inc., New York, 1996), Vol. 33, pp. 253-265.

89. B. Norden, P. Lincoln, B. Akerman and E. Tuite, in *Metal Ions In Biological Systems*, edited by A. Sigel and H. Sigel, (Marcel Dekker, Inc., New York, 1996), Vol. 33, pp. 177-208.

CHAPTER 3

CdS/CALF THYMUS DNA

3.1 Introduction

The photophysical properties of group II-VI quantum-confined semiconductor (Q-SC) nanoparticles can be controlled by controlling size and surface structures during synthesis.[1-2] As mentioned in Chapter 2, there are several ways to prepare Q-SC materials using stabilizing media. It is known that transition metal ions such as Cd^{2+} can bind to the anionic sites of nucleic acids, such as oxygen atoms of phosphate and hydroxyl groups, and to nitrogen atoms of the purine and pyrimidine bases.[3-4] Therefore, calf thymus deoxyribonucleic acid (DNA) was employed as a stabilizer in this experiment. This research was focused on the influence of polynucleotide stabilizers on the formation and the photophysical properties of quantum-confined cadmium sulfide (Q-CdS) semiconductor nanocrystallines.

Q-CdS particles stabilized by calf thymus DNA are easily prepared in solution at room temperature.[5] Q-CdS/calf thymus DNA was prepared in aqueous solution by initially adding metal ions to DNA in solution, followed by reaction with sulfide. Therefore, the Cd^{2+} could bind to all possible spatial regions of the DNA which had an affinity for metal ions.

The Q-CdS crystals were characterized using high resolution transmission electron microscopy (HREM), UV/visible absorption spectroscopy, and steady-state

photoluminescence (PL) spectroscopy.

3.2 Experimental

3.2.1 Preparation of Q-CdS in Calf Thymus DNA in Solution

In this experiment, approximately 15 mg of deoxyribonucleic acid (calf thymus DNA obtained from Sigma Chemical Company and used as received)[6] was dissolved in 5.0 mL of distilled, deionized H_2O in a 50 mL round-bottom flask. The flask with nucleotide solution in it was allowed to stand for approximately thirty minutes to allow the DNA to be dissolved slowly. To make a homogeneous solution, the nucleotide was mixed thoroughly with a Pasteur pipet by drawing up a small portion and allowing it to run back down the side of the flask. The relative molar nucleotide concentration was determined spectrophotometrically by employing an ε value of 6600 M^{-1} cm^{-1} for DNA at an absorption wavelength of 260 nm.[7] After dilution to 12 mL, the final molar nucleotide concentration was approximately 2.5×10^{-3} M. The flask which contained the DNA solution was fitted with a rubber septum and purged very slowly with nitrogen for approximately twenty minutes. In a separate flask, 5.0 μL of a freshly prepared 1 M $Cd(ClO_4)_2 \cdot 6H_2O$ solution, prepared from the solid (Johnson-Matthey, electronic grade)[8], was diluted to 2 mL and purged thoroughly with nitrogen for approximately 20 minutes. The final Cd^{2+} concentration was 4×10^{-4} M. In a third flask, 5.0 μL of a fresh 1 M $Na_2S \cdot 9H_2O$ solution, prepared from the solid (98%, Aldrich)[9], was diluted to 5 mL and also purged thoroughly with nitrogen. The final S^{2-} concentration was 4×10^{-4} M.

The formation of Q-CdS particles was performed in two steps. First, 2 mL of the Cd^{2+} solution was added to the DNA flask and the mixture was purged with nitrogen for approximately 5 minutes. Second, 5 mL of the S^{2-} solution was transferred to the reaction flask containing the DNA and Cd^{2+} under a nitrogen atmosphere via syringe. A yellow color was observed near-instantaneously from the flask containing the DNA, Cd^{2+} and S^{2-}. Before the characterization experiments were carried out, synthesis of CdS/DNA clusters was allowed for at least twenty minutes.

3.2.2 TEM Sample Preparation and Microscopy

A Hitachi H-9000 high resolution transmission electron microscope (HREM) operating at 300 kV was used to characterize the samples. TEM samples were prepared by concentrating the CdS/DNA samples in an ultracentrifuge by spinning at 4200 × g for 20 min. 1-2 drops of the dense CdS/DNA material collected from the bottom of the tube used for the spin were dropped on amorphous carbon films supported by standard copper TEM grids, and allowed to dry in air for about 30 minutes. The largest objective lens aperture of the HREM which allowed all diffracted beams with a d-spacing larger than the <400> (0.1453 nm) of CdS, was used to obtain Q-CdS lattice images. Interplanar spacings were determined using selected area electron diffraction pattern (SADP) data. The particle size distribution was determined by measurement of the diameters of several hundred individual particles using a Houston Instruments Digitizing Tablet interfaced to an IBM-PC. The BASIC program developed by Dr. Russell F. Pinizzotto at UNT was used to calculate average particle size, standard deviation, and size distribution using both

normal and log-normal distribution statistics and histograms.

3.2.3 Steady-State Spectroscopy

Absorption spectroscopy was performed using 1 cm quartz cuvettes on either a HP 8452A diode array spectrophotometer or a Varian Cary 3 double beam instrument. A Spex Fluorolog-2 0.22-m double spectrometer was used to record the steady-state photoluminescence (PL) spectra. Constant excitation with a typical excitation wavelength of 375 nm was provided via light from a 450 W Xe lamp focused into a single 0.22 m monochromator.

3.3 Results and Discussion

3.3.1 Q-CdS Synthesis

In these experiments, Q-CdS nanocrystallites were stabilized by calf thymus deoxyribonucleic acid (DNA). The synthesis of nanophase particles was straightforward and was carried out in two steps: (1) a sub-millimolar (10^{-4} M) solution of aqueous cadmium ions was added to a solution of DNA about 10^{-3} M in nucleotide concentration; (2) after thorough ebullition (bubbling at room temperature to reduce the oxygen) with nitrogen, the CdS nanoclusters were made in solution by adding 10^{-4} M of sulfide ions to this mixture. The reactions are

$$Cd^{2+}/DNA \xrightarrow[S^{2-}\ (Na_2S \text{ or } H_2S)]{N_2} Q\text{-}CdS/DNA$$

The formation of quantum-confined cadmium sulfide nanoparticles can be clearly identified by the intense yellow color.

3.3.2 TEM Characterization

A typical transmission electron micrograph of a Q-CdS nanoparticle is presented in Figure 3.1. Numerous nanometer size particles with lattice spacings consistent with the diamond cubic phase (Hawleyite) of cadmium sulfide are observed. Statistical particle size distribution analysis is presented in Table 3.1. The average particle size is 5.6 nm, with a maximum of 12 nm and minimum of 2.3 nm. In some cases, as shown in Figure 3.2, the lattice image contrast is different in the center compared to the periphery of the particle. It is usually possible to continuously image the lattice planes of the particle by defocusing the objective lens. Approximately 15 % of the particles have this microstructure which may be due to particles that are shaped like hollow spheres. The basic mechanisms of CdS particle nucleation and growth on DNA are not known, but this microstructure may provide some clues to understand it. Since sulfide ions are added later, there may be steric restriction for forming CdS clusters by the limited volume for S^{2-} and Cd^{2+} ions in the inner base pair region. The particles may nucleate and grow while

still attached to the DNA molecule, or the nucleated particle may detach from the DNA and then grow.

Statistical particle size analysis data are shown in Table 3.1. The average particle size measured using more than 300 CdS nanoparticles synthesized on calf thymus DNA is 5.6 nm. The standard deviation is 1.83 nm and the largest and smallest particle sizes are 12.1 nm and 2.4 nm, respectively. The histograms for the particle size measurements are presented in both normal and log-normal form in Figure 3.3. From the shape of the distributions it is apparent that the particle size distribution is best fit to a Guassian-type distribution using log-normal statistics. This statistical analysis results in high-quality, reliable data since the sizes of a large number of nanocrystallites were measured.

Figure 3.4 is a typical SADP of Q-CdS particles stabilized using calf thymus DNA. The measured d-spacings match those of zinc-blende cubic CdS. The experimental d-spacings are compared with the literature values for the diamond cubic (zincblende) structure, wurtzite structure and graphite as published in the JCPDS files in Table 3.2. The experimental d-spacings were compared to graphite to show that the nanoparticles are not from small graphitic inclusions in the amorphous carbon support films. The lattice structures of CdS/calf thymus DNA nanoparticles observed in HREM are also completely different from the graphite lattice structures. The graphite structures have very long, curved lattice planes. The lattice parameter of diamond cubic CdS is 0.572 nm

3.3.3 Steady-State Spectroscopy

The photoluminescence (PL) emission and absorption spectra of Q-CdS with 4×10^{-4} M Cd^{2+} and S^{2-} and 2.5×10^{-3} M nucleotide are shown in Figure 3.5. A complete graph is not shown in Figure 3.5, but the PL emission spectrum revealed that the trap emission range is broad from 480-720 nm, with a peak near 620 nm. According to earlier studies of Q-CdS, the emission in the 500-600 nm region is related to cadmium vacancies (V^0_{Cd})[10] while the emission at greater than 600 nm is related to sulfur vacancies (V_s^+).[11] In comparison, Q-CdS stabilized by the inverse micelle method with a 1:1 cadmium-to-sulfur ratio typically yields very weak emission.[12] Therefore, the observation of strong emission for 1:1 Cd/S prepared in the presence of calf thymus DNA is significant.

The threshold of the absorption spectrum is at approximately 480 nm which is blue-shifted compared to bulk CdS (515 nm). These data confirm that the CdS particles stabilized on calf thymus DNA are quantum-confined.[13]

3.3.4 Variation of Cadmium or Sulfide Concentrations During Particle Synthesis

To probe the chemical origin of the defects responsible for trap PL, the effects of varying cadmium or sulfide ion concentration during particle formation were examined. As shown in Figure 3.6, the absorption spectra of varying cadmium concentration (Figure 3.6A) are similar to the absorption spectra of varying sulfide concentration (Figure 3.6B). The emission intensity shows an overall increase as the cadmium ion concentration is increased, with maximum intensity near 620 nm. The emission intensity decreases in the 500-600 nm region as sulfide ion concentration is increased. The peak is considerably

sharper for excess sulfide than for excess cadmium. During cluster formation, the excess sulfide ions may interact with the Cd atoms responsible for the 550 nm emission. Similar phenomenon, quenching of 580 nm emission, was observed by adding excess H_2S to Q-CdS/zeolites.[14]

3.3.5 Aging

The Q-CdS nanoparticles are stable from flocculation for at least two weeks when stored in air at room temperature. If they are stored in closed vials at 5 °C, the nanoparticles are stable for more than two years. Previous experiments using monomeric nucleotides such as adenosine triphosphate (ATP) or adenosine monophosphate (AMP) with identical concentrations/conditions to the calf thymus DNA experiments resulted in CdS particles which flocculated within 12 to 24 hours regardless of storage conditions (N_2 atmosphere, temperatures ranging from 5 °C to -60 °C). This result suggests that a polymeric nucleotide is required for nanocluster stability.

The emission intensity grows with time for both samples: excess cadmium or excess sulfide. The Q-CdS particles prepared with excess sulfide have a narrow emission linewidth after aging for 6 weeks in a closed vial at 5 °C (FWHM shrinks by 35% in 5.5 weeks), suggesting that under these particular conditions the semiconductor surface reconstructs to yield a range of defect sites (traps) with slightly narrower energies (Figure 3.7).

3.4 Summary and Conclusions

Calf thymus DNA was used to stabilize the formation of Q-CdS nanoparticles (prepared at a concentration of 4×10^{-4} M Cd^{2+} and S^{2-} and 2.5×10^{-3} M DNA). High resolution transmission electron microscopy was used to characterize the microstructures of the Q-CdS nanoparticles. The average nanoparticle size is 5.6 nm with a standard deviation of 1.83 nm. The largest and the smallest crystallites are 12 nm and 2.3 nm, respectively. Selected area electron diffraction pattern data confirms that Q-CdS nanoparticles stabilized by calf thymus DNA have the zincblende cubic structure. The absorption threshold of Q-CdS/calf thymus DNA is at approximately 480 nm, blue-shifted from that of bulk CdS (515 nm) and consistent with quantum-confinement. The PL emission spectrum of the Q-CdS particles has a maximum intensity near 620 nm with broad trap emission ranging from 480-720 nm. Additional PL spectroscopy performed with varying cadmium and sulfide concentrations reveals that the overall emission intensity increases as the concentration of the cadmium is increased and decreases as the sulfide concentration is increased. The Q-CdS semiconductor nanoparticles stabilized on calf thymus DNA are very stable from flocculation when stored in closed vials at 5 °C.

Table 3.1 Particle size distribution analysis.

Normal Distribution Analysis		Log Normal Distribution Analysis	
Avg. Particle Size	5.55 nm	Avg. Log Particle Size	0.72
Std. Deviation	1.83 nm	Log Std. Deviation	0.014
% Std. Deviation	30.98 %		
Max. Particle Size	12.1 nm	Log Max. Particle Size	1.08
Min. Particle Size	2.4 nm	Log Min. Particle Size	0.37

Table 3.2 Comparison of measured d-spacings of Q-CdS/calf thymus DNA nanoparticles with values for zinc-blende (ZB) CdS, wurtzite (W) CdS and graphite (nm).[15]

Experimental d-spacings of CdS/DNA	ZB-CdS	W-CdS	Graphite
0.330	0.330	x	0.335
	x	0.306	x
0.283	0.286	x	x
	x	0.265	x
	x	x	0.213
0.1.9	0.202	x	0.203
	x	0.187	x
0.171	0.172	x	0.180
0.165	0.165	0.160	0.168
0.142	0.143	x	x
	0.131	0.133	x
0.126	0.128	x	x
	x	0.122	0.123
0.115	0.117	0.119	0.116

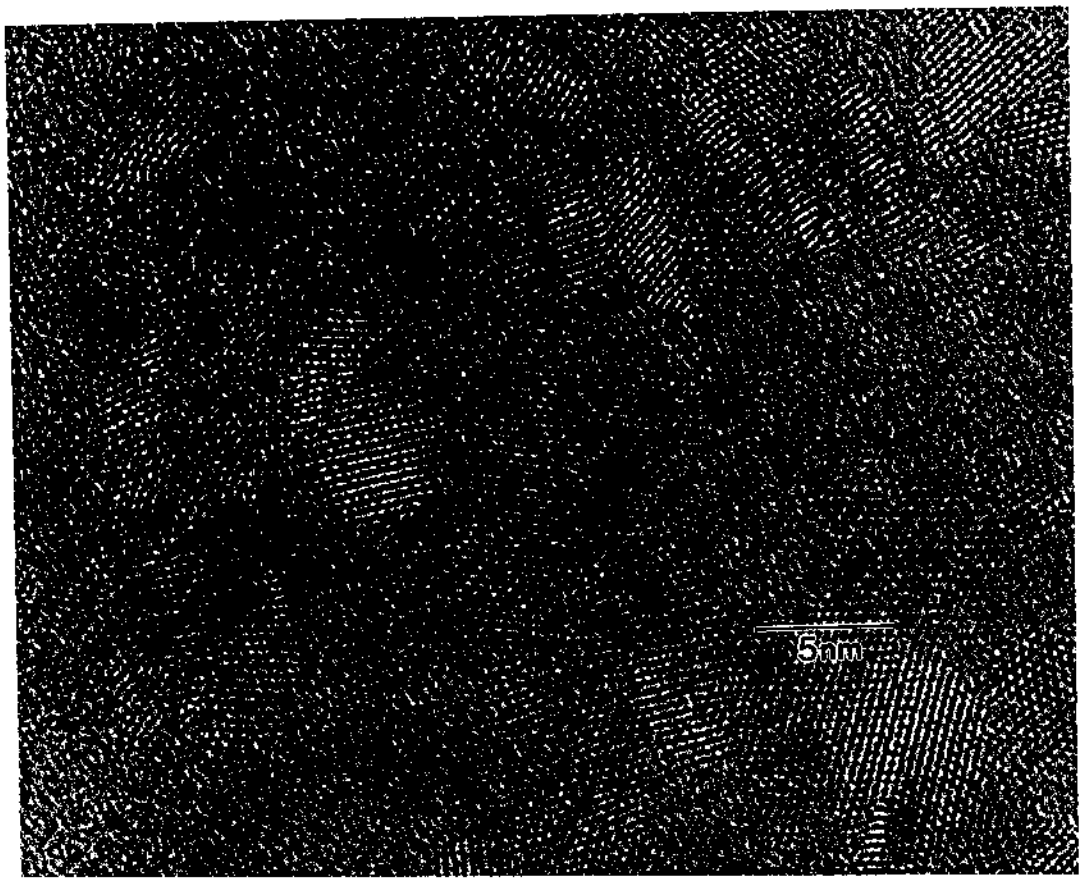

Figure 3.1 A typical high-resolution TEM image of Q-CdS prepared in the presence of calf thymus DNA.

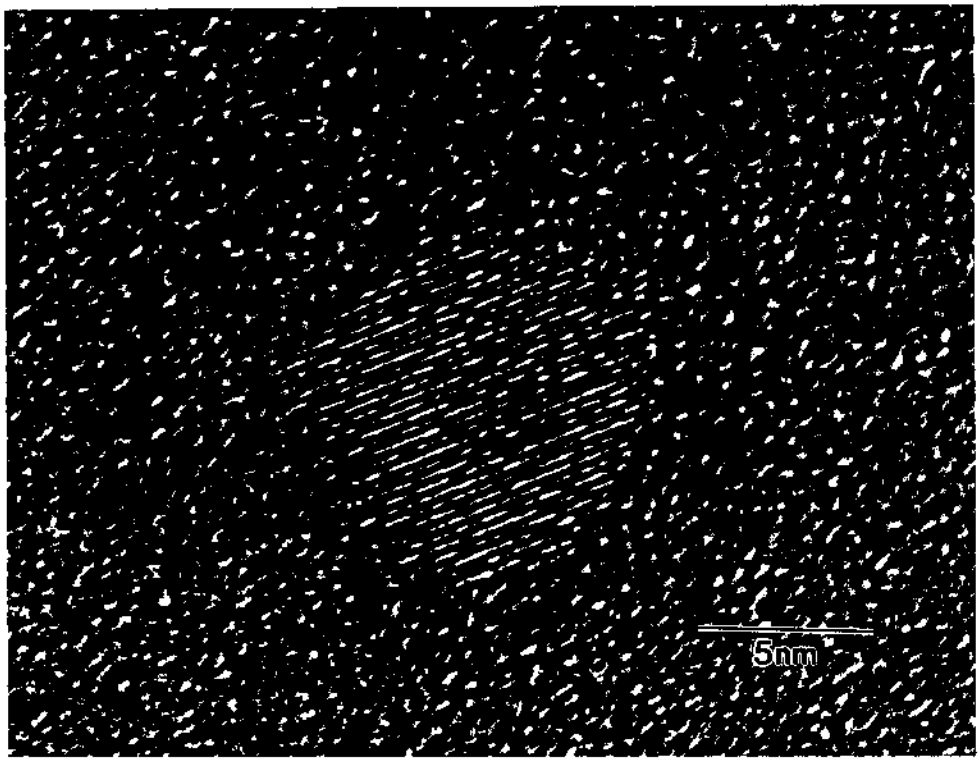

Figure 3.2 The unique HREM microstructure observed for approximately 15 % of the Q-CdS particles. The center of the particles have different contrast than the periphery.

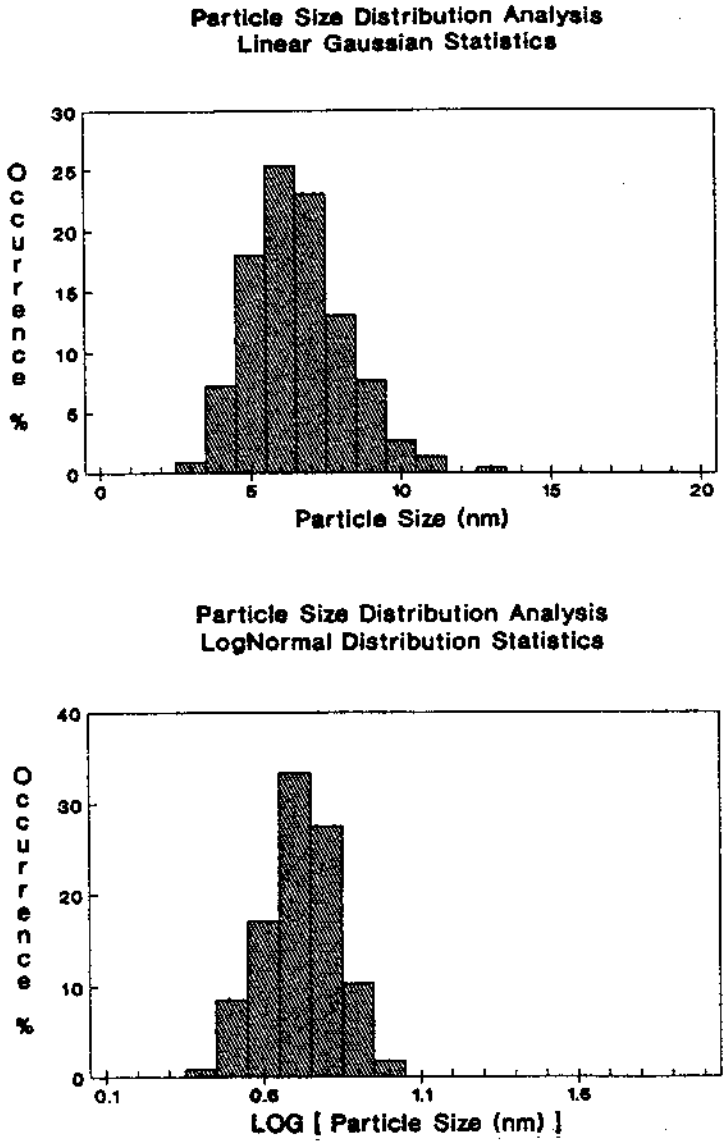

Figure 3.3 Normal and log-normal particle size distribution for Q-CdS stabilized by calf thymus DNA

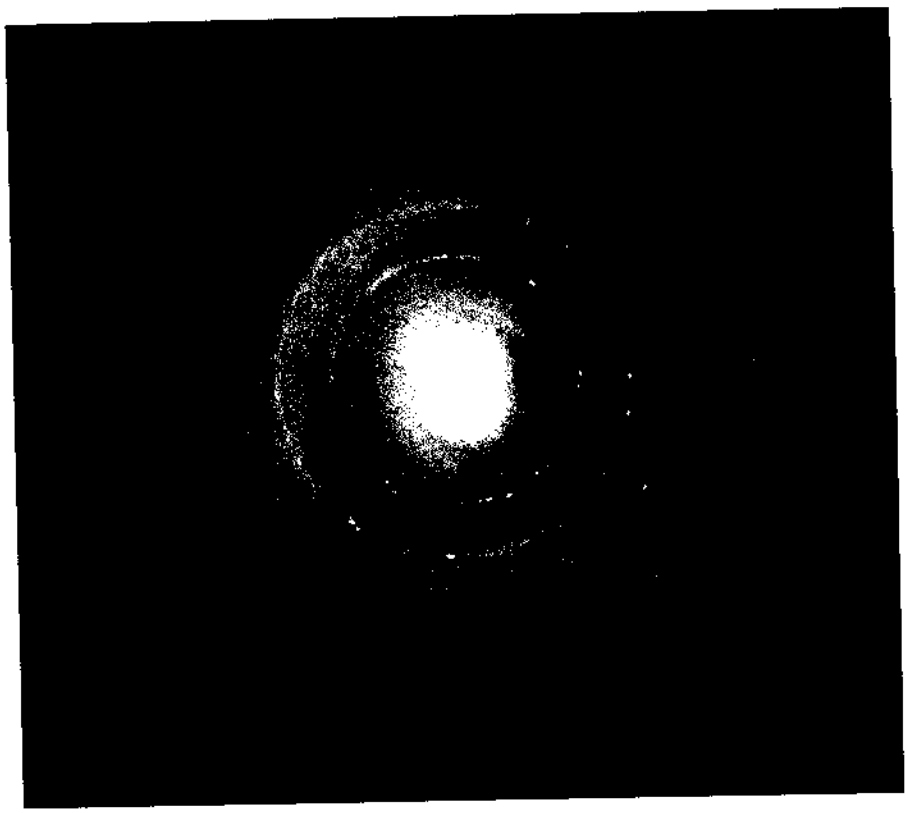

Figure 3.4 SADP of Q-CdS particles stabilized by calf thymus DNA.

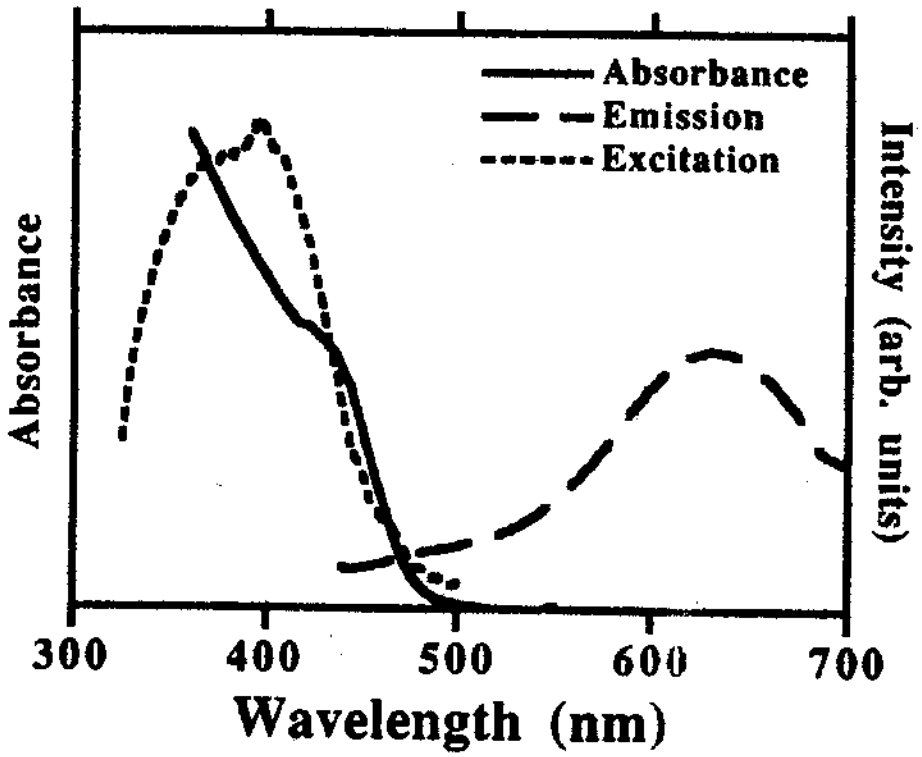

Figure 3.5 Photoluminescence and absorption spectra of Q-CdS prepared at a concentration of 4.2×10^{-4} M Cd^{2+} and S^{2-}, and 2.5×10^{-3} M nucleotide. Excitation wavelength is 375 nm.

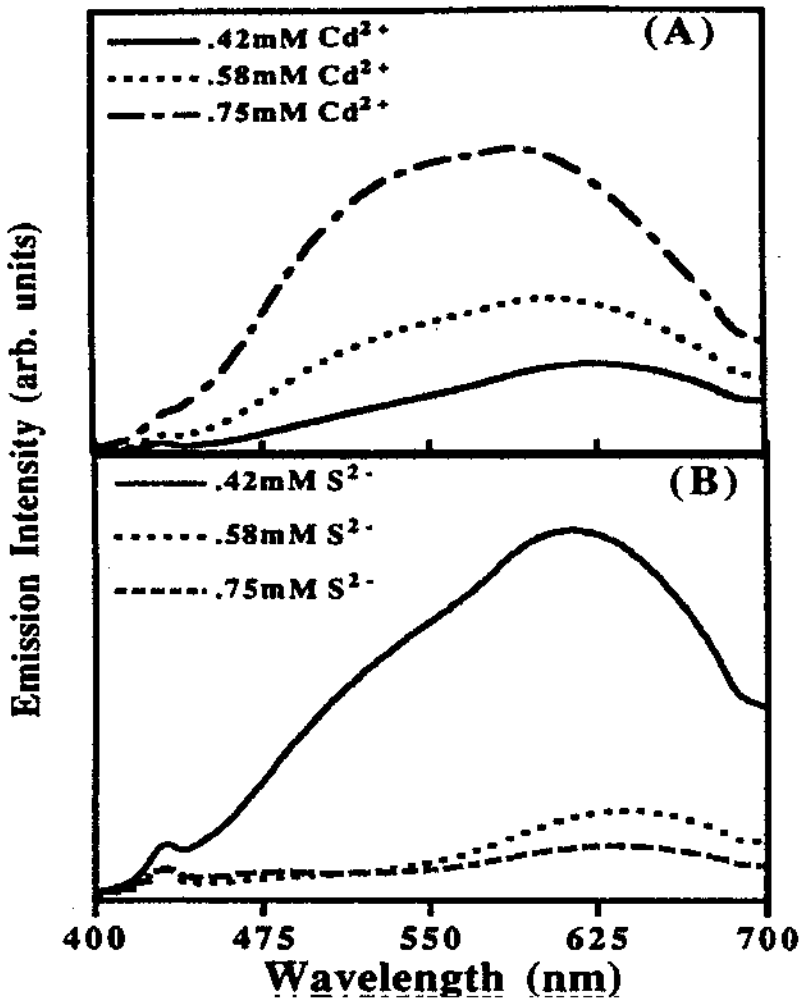

Figure 3.6 Emission spectra of Q-CdS solutions stabilized by 2.5 x 10^{-3} M calf thymus DNA, demonstrating (A) the effect of varying [Cd^{2+}] while holding [S^{2-}] constant at 4.2 x 10^{-4} M; (B) the effect of varying [S^{2-}] while holding [Cd^{2+}] constant at 4.2 x 10^{-4} M.

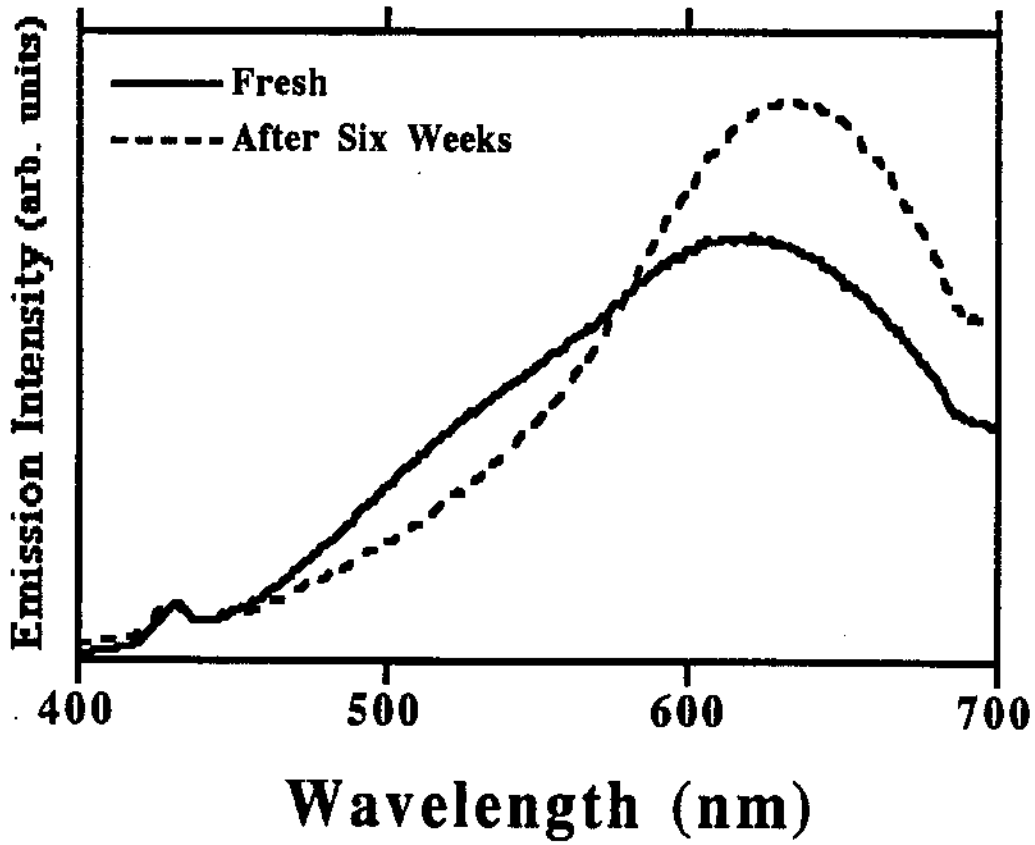

Figure 3.7 PL spectra of Q-CdS/DNA, both freshly prepared and aged for 6 weeks in a closed vial at 5°C.

REFERENCES

1. L. E. Brus, J. of Phys. Chem. **90**, 2555 (1986).

2. Y. Wang and N. Herron, J. of Phys. Chem. **95**, 525 (1991).

3. J. K. Barton and S. J. Lippard, "Nucleid Acid-Metal Ion Interactions" in *Metal Ions in Biology,* edited by T. G. Spiro, (John Wiley & Sons, Inc., New York, 1980), Vol. I, Chap. 2, pp. 33-81.

4. W. Saenger, *Principles of Nucleic Acid Structure* (Springer-Verlag, New York, 1984), pp. 105-114 and 201-211.

5. R. R. Chandler, S. R. Bigham and J. L. Coffer, J. Chem. Ed. 70, A7 (1993).

6. *Biochemicals and Reagents for Life Science Research,* Cat. # D 1501 (Product Catalog, Sigma, St. Louis, MO, 1997), p. 348.

7. *CRC Handbook of Biochemistry and Molecular Biology, Vol. I, Nucleic Acids,* 3rd ed. edited by G. D. Fasman, (Chemical Rubber Company, Cleveland, OH, 1975) pp. 589-90.

8. *Research Chemicals, Metals and Materials,* Cat. # 12936 (Product Catalog, Alfa Aesar, A Johnson-Matthey Company, Ward Hill, MA, 1997), p. 119.

9. *Catalog Handbook of Fine Chemicals,* Cat. # 20804-3 (Product Catalog, Aldrich Chemical Company, Inc., Milwaukee, WI, 1994), p. 1273.

10. Y.Wang and N. Herron, J. of Phys. Chem. **92**, 4988-4994 (1988).

11. J. J. Ramsden, S. E. Webber and M. Grätzel, J. of Phys. Chem. **89**, 2740-2743 (1985).

12. P. Llanos and J. K. Thomas, Chem. Phys. Lett. **123**, 299 (1986).

13. M. Steigerwald and L. E. Brus, Acc. Chem. Res. **23**, 183 (1990).

14. Y. Wang, and N. Herron, J. of Phys. Chem. **91**, 257 (1987).

15. *Elemental and Interplanar Spacing Index* (U.S. Department of Commerce, National Institute of Standards and Technology, JCPDS-International Centre for Diffraction Data, 1601 Park Lane, Swarthmore, PA, 19081, 1989), CDF # 102622, 09100, PDF # 34-0567, p. 250.

CHAPTER 4

CdS/pUCLeu4 PLASMID DNA

4.1 Introduction

As mentioned in Chapter 1, quantum-confined semiconductor (Q-SC) nanoparticles such as Q-CdS may be useful materials for optoelectronic and detector devices.[1] However, it is practically impossible to apply these materials to actual devices because of the lack of control of long-range assembly and patterning. This is a major limiting factor in developing a new semiconductor technology based on group II-VI quantum-confined semiconductor materials.

Since 1983, biomimetic stabilizers such as reverse micelles, microemulsions, vesicles, etc. have been applied to synthesize Q-SC materials into organized nanoscale structures. These methods have recently received more attention by chemists, physicists, and materials scientists,[2-3] but they only stabilize Q-SC nanoparticles and do not result in long-range ordered structures.

Other approaches, such as molecular beam epitaxy (MBE) and metal organic chemical vapor deposition (MOCVD), are currently used to build quantum structures such as quantum wires and quantum dots. However, these techniques also have fabrication problems and are too expensive to be used for commercial devices.

Since early 1996,[2] Coffer and Pinizzotto have been developing an innovative method for fabricating self-assembled mesoscale semiconductor structures of Q-SC using

biological macromolecules such as deoxyriboncleic acid (DNA) as templates. The structure of DNA is well-known (Chapter 2). DNA varies in length, depending on the specific DNA chosen. Also, since the early 1960s, it has been known that DNA has an ordered phosphate backbone and a number of other sites such as phosphate groups, hydroxyl groups, and purine and pyrimidine bases, which can interact with transition metals such as Cd, Cu, Zn, Pt, Mn, Co, Mg, etc.[4] Based on this knowledge, calf thymus DNA was employed as a stabilizer to fabricate quantum-confined semiconductor particles in solution.[5] As mentioned in Chapter 3, CdS nanoparticles approximately 5.6 nm in diameter were synthesized in solution using calf thymus DNA.

As soon as it was shown that DNA stabilized colloidal CdS nanoparticles, the idea of fabricating predesigned nanoscopic semiconductor structures on solid substrates using the specific size and shape of DNA as a template was proposed.[2,6] In this way, an array of mesoscale self-assembled semiconductor structures matching the shapes of the biopolymer stabilizers might be fabricated without expensive and complicated photolithography.

In the early experiments (Chapter 3), all of the processing steps for fabricating Q-CdS particles on DNA were carried out in solution without supporting the DNA on a solid substrate.[5] As a result, because of the flexibility of the DNA stabilizer in solution, it was impossible to control the formation of predesigned nanostructures. After extensive studies by Jervis and Pettit,[7] and Rhodes and Klug,[8] it was shown that aminoalkyl-derivatized glass slides and freshly cleaved mica have an affinity for DNA. If the DNA binds to a solid substrate, the overall shape of the self-assembled nanostructure is dictated

by the shape of the DNA bound to it. In later experiments, Cd^{2+}/DNA complexes were first bound onto a solid substrate, and then H_2S gas was added to form pre-designed CdS nanoscale semiconductor structures. Since the Q-CdS particles are initially formed by combination of metal ions like Cd^{2+} on anionic DNA sites, the bound DNA controls the location of nanoparticle synthesis. Based on this simple self-assembly process, various quantum structures such as quantum wires, quantum rings, quantum dots, etc. can be fabricated using linear DNA, circular DNA, and small DNA fragments, respectively. Furthermore, because many other transition metals can be bound to DNA, different semiconductor materials can be fabricated using the same technique.

The original plan for fabricating mesoscale semiconductor structures on solid substrates is as follows:

(1) DNA/Cd^{2+} complexes are formed in solution. The solution is placed on polylysine derivatized solid substrates such as glass slides, SiO_2 on silicon, sapphire, or mica. The Cd^{2+}/DNA/solid substrate assemblies are spun to form a uniform coating and the samples are air dried.

(2) The dried Cd^{2+}/DNA/substrates are rinsed in a polar nonaqueous solvent such as ethanol or in deionized water to remove excess cadmium, and they are air dried again.

(3) The substrates are exposed to H_2S gas to form Q-CdS nanoparticles in the desired configuration.

To simplify TEM sample preparation, thin amorphous carbon films supported by copper TEM grids were used as the substrates for the initial experiments.

Compared to other methods, the use of biopolymer stabilizers to fabricate

mesoscale semiconductor structures composed of an array of Q-SC has many advantages. First, many semiconductors can be synthesized, such as CdS, CdSe, CdTe, ZnS, HgTe, etc. Second, different types of substrates can be used, as mentioned above. Third, various substrate surface morphologies may be used, from native to polished surfaces, to anchor the biopolymer onto the substrates. Fourth, a diverse range of DNA of different size, shape, structure, and length can be used for templates. Fifth, post-synthesis modification of the nanostructure is possible using enzyme chemistry.

In the first experiments, pUCLeu4 DNA in several forms (circular, linear, and relaxed) was used due to its known size (1.17 μm with 3455 base pairs) and shape (circular and linear), so that the mesoscale structures could be readily detected and unambiguously identified using transmission electron microscopy.

The goals of this research were to fabricate mesoscale semiconductor structures of Q-CdS using circular and linear DNA molecules anchored to a solid substrate, and to characterize the nanoparticles and mesoscale semiconductor structures. These Q-CdS nanoparticles and mesoscale structures were studied by AEM and HREM. UV/visible absorption spectroscopy and steady-state photoluminescence (PL) spectroscopy were used to characterize the optical properties of the Q-CdS particles on DNA. Fabrication and characterization of the thin carbon films, which were the major substrate used for TEM analysis, were also part of this research.

4.2 Experimental

4.2.1 Synthesis and Purification of the pUCLeu4 DNA Templates

Synthesis and Purification of the pUCLeu4 DNA was carried out in Dr. Robert M. Pirtle's laboratory at UNT.[9] As described in Chapter 2, the pUCLeu4 DNA was generated by cloning a human DNA fragment (781-base pairs *Kpn*I-*Sst*I) encompassing a leucine $tRNA_{AAG}$ gene as a foreign DNA into pUC19 vector DNA. A large amount of pUCLeu4 plasmid DNA, produced by *E. coli,* was extracted from the bacterial cells by an alkaline procedure, and treated with RNases A and T_1 to degrade the bacterial RNA. The bacterial RNA was extracted with phenol:chloroform (1:1) and chloroform:isoamyl alcohol (24:1), and precipitated with cold ethanol. The chromosomal bacterial DNA and degraded RNA were removed from the pUCLeu4 plasmid DNA by HPLC on an anion exchange column using a NaCl gradient.[10]

According to an assay pythagarase gel electrophoresis, approximately 70% of the undigested pUCLeu4 plasmid DNA synthesized with this method was supercoiled. The supercoiled pUCLeu4 plasmid DNA molecules were treated to generate either the relaxed circular or linear form for use as DNA templates. Relaxed circular DNA was generated by cutting and rejoining one of the 3' or 5' phosphodiester bonds using DNA topoisomerase I enzyme. Linear DNA was made by cutting both phosphodiester bonds using a restriction endonuclease II.

4.2.2 Fabrication and Preparation of Carbon Support Films on Cu TEM Grids

1. Carbon substrate fabrication. The thin carbon films which were the primary substrates used for these experiments were fabricated using a JEOL JEE-4X evaporator. Because carbon film is physically rigid and stable in the electron beam, and because carbon film has an amorphous structure which can be easily distinguished from the samples being examined in the electron microscope, it is widely used as a support film for both biological and inorganic samples.[11]

Since the Q-CdS/DNA structures are on the nanometer scale, a very fine and flat surface is necessary to distinguish the CdS/DNA semiconductor structures from the structures of the carbon film. Also, the carbon film must be spectroscopically pure to be used for chemical analysis in electron microscopy. Therefore, the carbon films used for these experiments were made with extreme care.

To generate a high quality carbon film which satisfies these conditions, the evaporator was thoroughly cleaned with acetone and metal polishing paste. The evaporation was performed under very low vacuum (as low as 2×10^{-6} Torr). To achieve a high quality vacuum, the evaporator was turned on approximately 5 hours before use to allow the vacuum to reach lower than 2×10^{-6} Torr.

One side of a carbon rod was sharpened to approximately 1 mm diameter for a length of about 6-8 mm using a fine file. Carbon evaporation is achieved by resistively heating the contact area of two sharpened carbon rods, so the thin carbon tip makes it easier to control the evaporation process. If the diameter of the tip is too large or the tip is sharpened into a conical shape without making it long enough, the thin tip area may be

burnt off before achieving the required film thickness. The carbon rods used were spectroscopically pure with an impurity level less than 2 ppm. The sharpened carbon rods were mounted on a spring loaded holder which controlled the lateral movement so that the rods contact each other until the desired film thickness is achieved. The carbon rods were positioned about 10 to 15 cm above the specimen stage. Freshly cleaved mica, fresh side upward, was placed on the specimen stage (underneath the carbon rods) using tweezers. A piece of white paper was placed on the mica to check the film thickness during deposition. When preparations were complete, the bell jar was covered and the work-chamber was evacuated for an hour to reduce the vacuum level to lower than 2×10^{-6} Torr. When high vacuum was achieved, the mica substrate was covered with a shutter and the heating current increased slowly until the tip of the carbon rod glowed red. After a few seconds, the particles which were generated during the sharpening of the carbon rod were removed. The shutter was then opened and the heating current increased to evaporate the carbon. The current was increased as slowly as possible until the tips of the carbon rods glowed white so that the carbon films were deposited by evaporation and not by arcing, which produces many carbon fragments. Depending on the height of the carbon rods, but after 2 or 3 evaporation cycles with each being approximately 20 to 30 seconds long, carbon film deposition was complete. The film thickness can be estimated by experience and can also be checked by the color change of the white paper.

2. Preparation of carbon substrate on Cu TEM grids. The carbon films were placed on acetone-cleaned 400 mesh Cu TEM grids. The grids were placed shiny side up on a wire mesh which was in steam-sterilized distilled water contained in a Buchner

funnel or a dish that could be drained. The carbon film was separated from the mica substrate by dipping the mica into water and floating off the carbon film. The TEM grids were coated by aligning the separated carbon film on top of the TEM grids and then draining the water. The wire mesh was picked up using tweezers and placed on filter paper to remove the water remaining on both the wire mesh and the TEM grids. The carbon coated grids were used within 30 minutes, before they were completely dry, or after complete drying, depend on the types of experiments carried out. For example, wet carbon films were used when the DNA was deposited using the dropping method, and dry carbon substrates were used when the DNA was deposited by floating the grids on the DNA or Cd^{2+}/DNA solutions.

4.2.3 Preparation Q-CdS/pUCLeu4 DNA Samples

The fabrication of quantum-confined cadmium sulfide nanoparticles on DNA templates was performed in three steps. Three types of pUCLeu4 plasmid DNA, circular (undigested pUCLeu4 plasmid DNA), linearized, and relaxed circular, were used as templates.

1. Preparation of DNA and Cd^{2+} in solution. In a typical experiment, approximately 2 ml of 2 mM DNA (the amount of DNA is defined on a per nucleotide basis) was prepared from the original concentration of about 2 mg/ml in mass concentration. To prepare the molar nucleotide concentration of 2 mM DNA solution, the original DNA concentration of 2 mg/ml was first converted into a molar concentration. 10 μl of 2mg/ml DNA was taken with a microliter syringe and diluted

with 10 ml of distilled deionized water in a 50 ml round-bottom flask. The DNA solution was throughly mixed by shaking it manually for approximately 10 minutes. The concentration of the diluted solution was measured using a UV/visible spectrophotometer (an ε value of 6600 M^{-1} cm^{-1} was employed at an absorption wavelength of 260 nm).[12] After the original DNA concentration was determined, the desired concentration, 2 mM, could be easily prepared.

In a separate beaker, 100 mM Cd $(ClO_4)_2 \cdot 6H_2O$ solution was freshly prepared from the solid (Johnson-Matthey, electronic grade)[13] which was dissolved slowly by shaking for approximately 10 minutes. To make 2 ml of 2 mM cadmium ion solution from the 100 mM Cd^{2+} solution, 40 µl of the 100 mM solution was diluted in 1.96 ml of distilled deionized water.

2. Mixing Cd^{2+} and DNA in solution. Formation of cadmium metal ion/DNA complexes was carried out by mixing the two previously prepared solutions, 2 mM Cd^{2+} and 2 mM DNA, in a 1:1 ratio in a 10 ml beaker. The mixed solution was stirred with a pipette by squeezing the solution in and out of it for two to three minutes to mix the Cd^{2+} and DNA homogeneously. The beaker was shaken slowly for approximately 10 minutes to maximize the interaction between the cadmium ions and the DNA.

3. Deposition of the Cd/DNA complexes on substrates and reaction of Cd^{2+} with S^{2-}. In a typical experiment, 1 to 5 µl of the Cd^{2+}/pUCLeu4 DNA solution was deposited onto the substrate in air. When solid substrates were used, the substrates were coated with polylysine to enhance DNA adhesion. The substrates were rotated at approximately 100 rpm for approximately 5 minutes for uniform deposition of the

complexes.

The formation of Q-CdS nanoparticles on DNA was carried out by exposing the air-dried substrates to excess H_2S gas in a sealed chamber for approximately one hour.

4.2.4 TEM Sample Preparation.

TEM samples were prepared on thin amorphous carbon films to make the sample preparation simple and easy (Figure 4.1). As described in step 3 of Section 4.2.3, two to three drops of one or two μL of 2 mM Cd^{2+}/DNA (at 1:1 DNA to Cd^{2+} ratio) were dropped onto carbon film/copper TEM grids using a microliter syringe. Excess solution was blotted from the side or bottom of the grid with a sharp corner of a piece of filter paper. Because of the hydrophobic nature of the carbon film and the surface tension of the water drop, the deposition of the Cd^{2+}/DNA complexes onto the carbon-coated TEM grids was very difficult. The carbon films usually broke due to these effects. It was later learned that breakage was reduced by using wet carbon films. The carbon coated TEM grids were prepared as described in Section 4.2.2 and used within 30 minutes, before the carbon films were completely dry. After drying in air, the samples were placed on anti-static Lint Guard polyshield paper and placed in a vial which could be sealed with a rubber septum. The samples were exposed to H_2S gas by adding H_2S gas into the vial using a gas-tight microliter syringe. The reaction was allowed to proceed for approximately 30 minutes to one hour to form Q-CdS particles on DNA.

The samples described above were examined before and after metal shadowing. Low angle metal shadowing of the samples was performed using a JEOL JEE-4X

evaporator with 80:20 platinum:palladium as described next.

4. 2.5 Electron Microscopy (BF, DF, XEDS, SADP and HREM)

1. TEM sample preparation and characterization of carbon substrates.

Since the scale of the Q-CdS/DNA semiconductor structures is in the nanometer size range, very fine and flat substrate surfaces are necessary for TEM analysis. Microstructural characterization of the carbon films was started because commercial carbon films (purchased from ACF-Metals)[14] have many artefacts. Some of these microstructures, formed during film fabrication, are similar in size and shape to the microstructure of Q-CdS/linear DNA. In the initial stages of our experiments, these microstructures were similar enough to be misleading. Therefore, the carbon films used for TEM substrates were fabricated in our laboratory and always examined before use.

The carbon films were characterized by direct observation using bright field conventional transmission electron microscopy (BF TEM). In BF TEM, the specimens are imaged by subtractive contrast induced by elastic and inelastic interaction between the electron beam and the specimen atoms.[15] Image formation, especially for an amorphous material like the carbon film, depends on the atomic mass and thickness variations of the specimen. Therefore, to enhance contrast, the carbon films used for this TEM analysis were prepared by low angle (approximately 5-7 °) heavy metal shadowing.

Metal wire (0.08 inch in diameter) with a composition of 80:20 platinum:palladium was used as a source of evaporation material. Metal evaporation was done as follows:

(1) a 5 mm diameter carbon rod is sharpened to approximately 1 to 1.2 mm diameter for a length of 10 mm. The thin tip of the carbon rod is required to reduce the contact area between the tips to increase the resistance of the circuit, which generates more heat. Otherwise, the maximum allowed operating current may be exceeded before evaporation is complete; (2) metal wire is wound closely on the sharpened tip, otherwise not only metal, but also carbon is evaporated; (3) metal shadowing is carried out with as low an operating current as possible. The operating current is increased very slowly to avoid abrupt current changes due to changes in the contact area between the tips of the carbon rods. (The carbon rods are held in contact during evaporation by a spring-loaded holder. As the carbon rod is evaporated, the contact area changes continuously). The evaporation was performed in as low a vacuum as possible (approximately 2×10^{-6} Torr) to reduce indirect deposition due to collisions between the evaporated metal source atoms and residual gas molecules in the deposition chamber.

Two kinds of carbon films, commercial or fabricated in our laboratory, were examined by TEM with and without metal shadowing. A JEOL 100 CX operating at 100 kV was used. Bright field transmission electron microscopy was the prime method used to characterize the surface structures of the carbon substrates. The image contrast can be increased by filtering out electrons scattered at large angles, hence the smallest available objective aperture was used to maximize contrast.

2. **Transmission Electron Microscopy of Q-CdS/DNA.** Both analytical transmission electron microscopy (AEM) and high resolution electron microscopy (HREM) were used for microstrustural characterization of the Q-CdS/DNA mesostructures. The basic principles and alignment procedures for AEM and HREM used in our laboratory were described in the Ph.D. dissertations of Dr. Hong Yang[16] and Dr. Tejpal Kaur Hooghan.[17] The mesoscale semiconductor structures were imaged using a combination of bright field, dark field, and high resolution electron microscopy. Analytical electron microscopy, X-ray energy dispersive spectroscopy (XEDS) for elemental chemical analysis and selected area electron diffraction (SADP) for phase identification were performed using both a JEOL 100 CX and a JEOL 200 CX operating at 100 kV and 200 kV, respectively. Lattice imaging of Q-CdS particles on DNA was performed using a Hitachi H-9000 HREM with a demonstrated lattice resolution of 1 Å operating at an accelerating voltage of 300 kV. Q-CdS nanoparticle sizes and size distributions were determined using HREM micrographs. The samples were examined both with and without metal shadowing.

4.2.5 Absorption and Photoluminescence Spectroscopy

Absorption and photoluminescence spectroscopy of two different concentrations of CdS/plasmid DNA complexes, 50 and 150 nanomoles (the ratio of Cd^{2+} to DNA was 1:1), were performed by Dr. Coffer's group at TCU using an HP 8452A diode array spectrophotometer and a Spex Fluorolog-2 0.22m double spectrometer, respectively. The experimental procedures for preparing the Cd^{2+}/DNA complexes in solution were

described in Section 4.2.3. One drop of each concentration of CdS/DNA was placed on a polylysine-coated glass slide and allowed to dry in air for several hours to overnight. To prevent dust from settling onto the samples, the glass slides were covered while drying. The samples were then exposed to hydrogen sulfide gas for approximately one hour.

Absorption spectroscopy is based on the measurement of the intensity before and after light passes through an absorbing medium. Absorption can often be described by the Lambert-Beer Law, $A = \log I_o/I = c\varepsilon$, where A is the absorbency of the sample, ε is the absorption coefficient, and I_o and I are the intensities of the incident and transmitted beams.[18] Since materials only absorb photons with energies equal to or larger than the band gap energy, the band gap of a semiconductor can be measured by noting the absorption onset. Photoluminescence spectroscopy is based on the measurement of the photon intensity emitted by the radiative recombination process of the electron-hole pairs in semiconductors. The wavelengths of the photons produced by recombination depend on the band gap energy and the energies of traps within the band gap.[19] Quantum-confinement in semiconductors is depends on the size of the nanocrystallites. Hence, the average size of the nanoparticles can be estimated with absorption and PL measurements.[20]

4.3 **Results and Discussion**

4.3.1 Surface Structures of Carbon Substrates

Bright field (BF) TEM micrographs of surface structures of the two carbon

substrates, without and with metal shadowing, are shown in Figures 4.2 and 4.3, respectively. Figures 4.2a and 4.3a show typical surface structures of carbon films made in our laboratory, and Figures 4.2b and 4.3b show typical surface structures of commercial carbon films. The micrographs of the commercial carbon films reveal many kinds of nanoscale features. Since we are at the initial stage of using DNA templates, the linear microstructures shown in Figure 4.3b are similar enough to the expected DNA structures to be confusing. The surface structure of the carbon film made in our laboratory is very fine and smooth. The dark objects in Figure 4.2a were used to focus the image and were intentionally photographed to show the presence of the carbon film. The microstructures observed on the commercial carbon films were carefully examined using electron diffraction to identify the presence of any crystallites, which could also be misleading. No diffraction patterns were obtained from those microstructures. These results demonstrated that commercial carbon films were unusable for our work. Hence, all of our experiments were performed using carbon films made in our own laboratory.

4.3.2 AEM and HREM Characterization of Q-CdS/DNA

1. Conventional TEM of Q-CdS/pUCLeu4 plasmid DNA. The bright field and dark field (DF) TEM micrographs shown in Figures 4.4a and 4.4b are typical Q-CdS/pUCLeu4 plasmid DNA mesostructures on carbon substrates. The dark ring shown in Figure 4.4a is an assembly of CdS nanoparticles on a circular pUCLeu4 template. Since DNA molecules are biopolymers with low electron density, the DNA molecule itself cannot be observed in the TEM. CdS nanoparticles form not only on the

DNA, but also on the carbon film because excess Cd^{2+} ions may not have been completely removed from the carbon substrate. However, as described previously, if polylysine derivatized substrates such as mica or silicon are used, it may be possible to wash off the excess Cd^{2+} before exposure to H_2S gas preventing extraneous CdS nanoparticle formation. The contrast of the Q-CdS/DNA is greater than the contrast of CdS particles alone on the carbon substrates. This may imply that more Q-CdS nanoparticles are formed on the DNA than on the carbon substrate due to the numerous binding sites on DNA molecules, as mentioned in Chapter 2.

The dark field image in Figure 4.4b, shows the same Q-CdS/DNA area as in Figure 4.4a. The individual CdS nanocrystallites on the DNA template are clearly visible. The dark field image was obtained using the smallest diameter diffraction ring, corresponding to the [111] planes of CdS. The Q-CdS structure shown in Figure 4.4a is approximately 10 nm thick and 0.7 μm long.

2. HREM Characterization of Q-CdS/plasmid DNA. Figure 4.5 is a typical HREM lattice image of quantum-confined CdS nanocrystallites on a pUCLeu4 plasmid DNA template. This HREM micrograph is from a Q-CdS/DNA structure similar to the one shown in Figure 4.4a. It shows only a part of the circular structure. The individual nanocrystallites have no particular orientation relationship with each other, with the DNA or with the carbon substrate. The average diameter of the nanocrystallites is approximately 5 nm. According to the HREM data, diverse sizes of CdS nanoparticles are closely packed on the DNA and only a few Q-CdS particles are scattered on the substrate. This implies that most of the Cd^{2+} ions interact with the anionic atoms of the

DNA when the DNA and cadmium ion solutions are mixed together. The CdS nanoparticles nucleate on the DNA and grow when exposed to H_2S gas, as expected. In Chapter 3, two nucleation and growth mechanisms for CdS nanocrystallites were discussed. The mechanisms assume that the CdS particles nucleate on the binding sites of the DNA and grow either: (1) attached to the DNA, or (2) after the particles detach from the DNA. Here, it does not matter whether they are attached to the DNA or not, because the CdS nanocrystallites are formed after the Cd^{2+}/DNA molecules are deposited and fixed on the substrates.

The BF and HREM data presented in Figures 4.4a and Figure 4.5 demonstrate the feasibility of fabricating self-assembled mesoscale semiconductor structures of Q-SC using DNA templates. The data also implies that different shapes and sizes can be formed using different DNA templates.

3. SADP data of the Q-CdS/DNA. Figure 4.6 shows a typical selected area electron diffraction pattern for a Q-CdS/DNA nanostructure. The lattice spacings measured from the electron diffraction patterns of the nanocrystallites stabilized on the DNA are identified as the diamond cubic phase of CdS. As mentioned in Chapter 2, there are two possible CdS crystal structures: the zincblende diamond cubic phase (Hawleyite), which is common in small nanocrystallites, and the hexagonal-close packed phase (wurtzite) which is common in larger crystallites.[21] Some of the lattice spacings, for example, the [111] of the cubic phase and the [002] of the hexagonal phase, are similar. This may make it difficult to determine which crystal structure is present (Table 4.1). However, the phases can be clearly identified using the intensities of the diffraction rings.

For example, for cubic CdS, the first ring (0.336 nm) due to the [111] planes is the strongest (100%), the second ring (0.206 nm) from the [220] planes is the next strongest (80%), and the third ring (0.175 nm) from the [311] planes is the third strongest (60%). These relative intensities match our experimental data (Table 4.1).[22] For hexagonal CdS, the intensity of the ring diameters for the 0.359 nm [100] planes and the 0.316 nm [101] planes are 62% and 100%, respectively. These rings were not observed in our electron diffraction patterns. Thus, the SADP data prove that the nanoparticles are the zincblende diamond cubic (Hawleyite) phase of CdS.

The diffraction pattern in Figure 4.6 shows only three rings due to the [111], [220] and [311] lattice planes clearly, but three additional rings due to the [331], [511] and [531] lattice planes are visible in the negative. Some electron diffraction rings are always weak or invisible. Diffraction rings with low relative intensities cannot be observed. The TEM microstructures and SADP data for the cubic phase and hexagonal phase are compared in more detail when the results of the CdS only samples are discussed in Chapter 6.

4. XEDS spectrum of Q-CdS particles. The chemical composition of the nanoparticles as determined by X-ray energy dispersive spectromety (XEDS) shows that the nanocrystallites consist of cadmium and sulfur (Figure 4.7). The small silicon K_α peak shown in the spectrum came from the silicon-lithium detector. This silicon peak occurs when long counting times or high counting rates are used.[23] The large copper peaks in the spectrum are from the TEM grid which supports the carbon substrate.

5. CdS/DNA Sizes. pUCLeu4 plasmid DNA was used for these experiments

because of its known size, 1.17 μm, which can be identified unambiguously in the electron microscope. However, the sizes of the CdS/DNA structures observed by TEM varied from approximately 0.7 μm to 1.2 μm. In most cases, the actual size was smaller than the calculated length of 1.17 μm. The shrinking of the DNA was caused by dehydration when the TEM samples were prepared. When DNA size measurements were made using the Kleinschmidt imaging method, it was found that the DNA contracted approximately 21% (circular) to 26% (linear) when the samples were examined in the TEM because of the dehydration (Chapter 5). Micro-folding or molecular overlapping due to Cd^{2+} interactions may be another possible explanation. Binding of metal ions to DNA can lead either to a highly coiled structure or to an extended flexible shape.[24] The folded DNA structures cannot be directly observed by TEM, but the thickness variations observed along the CdS/DNA visible in both BF and HREM micrographs (Figures 4.4a and 4.5) may due to folding or overlapping. Some of the CdS/DNA structures were approximately 60% of the original DNA size; this may be due to both dehydration and folding of the DNA molecules. A detailed discussion of the experimental DNA size data is presented in Chapter 5.

4.3.3. Supercoiled Circular DNA Structures

Only a few of the expected mesoscale semiconductor structures of Q-CdS/pUCLeu4 circular plasmid DNA were observed by TEM. Considering the number of DNA molecules used for each experiment, it was curious that so few of the structures were found. At times, Q-CdS particles on plain-carbon substrates were not

observed for several repeated experiments. It is possible that DNA was on the samples, but just not observable without CdS nanoparticle decoration. These results suggested that we needed to find the DNA on the samples. Therefore, low angle metal shadowing was performed.

As shown in Figure 4.8a, large numbers of supertwisted DNA structures were found in the undigested circular DNA. These microstructures were not observed before metal shadowing. This BF image shows the DNA alone, before the formation of CdS. Selected area diffraction pattern data for this sample did not indicate the presence of Q-CdS particles. The supercoiled DNA molecules might become visible if they were decorated with CdS nanoparticles.

The reason why Q-CdS nanoparticles were not observed in previous experiments was unknown. Therefore, another experiment was performed to determine why the CdS nanocrystals were not observed.

Before metal shadowing, the results were similar to previous experiments. After metal shadowing, nanostructures similar to supercoiled DNA were observed (Figure 4.8b). The first two rings of the SADP from these areas (Figure 4.8b) are visible and match cubic CdS (Figure 4.8c). The shapes seen in Figure 4.8b are similar to the shapes seen in Figure 4.8a, but the DNA in Figure 4.8b is slightly larger than the DNA in Figure 4.8a. This is due to the attachment of small CdS nanoparticles to the DNA.

Since the microstructures were observed after metal shadowing, the CdS particles on the supercoiled DNA could not be distinguished from the metal shadowing. However, the presence of CdS was detected by SADP. Only weak electron diffraction patterns were

observed (Figure 4.8c) probably because the numbers and sizes of the CdS particles were small. These results indicated that many circular Q-CdS nanoscale semiconductor structures might be observable if relaxed circular DNA was used as a template.

The inhomogeneous distribution of supercoiled DNA observed in one large area is probably due to the sample preparation method used. As described in Sections 4.2.3 and 4.2.4, the samples were prepared by dropping a few 1-2 microliter drops of Cd^{2+}/DNA complexes on carbon-coated copper TEM grids. Because of the surface tension of the water and the hydrophobic nature of the carbon films, the drops remain as spherical drops on the carbon film until they are dry. Thus, all of the Cd^{2+}/DNA is deposited in one area, the last contact area of the drop.[25] When large drops were placed on the carbon-coated TEM grids, the excess solution was blotted from the bottom of the grid with a sharp corner of a piece of filter paper. Therefore, most of the Cd^{2+}/DNA was deposited at the area contacted by the filter paper.

4.3.4 Other TEM Microstructures of Q-CdS/DNA

1. Network-like structures. Besides the circular and supercoiled Q-CdS/DNA microstructures, many other unidentified microstructures were observed. One of the most common was a high concentration of network-like material, as shown in Figures 4.9a, 4.9b, and 4.9c. These were typical microstructures observed for the three types of samples, CdS/circular, CdS/linear, and CdS/relaxed DNA. The microstructure shown in Figure 4.9a is from CdS/circular DNA before metal shadowing. The microstructures shown in Figures 4.9b and 4.9c are from the CdS/linear and the CdS/relaxed DNA,

respectively, after metal shadowing. SADPs from these areas show only typical amorphous carbon patterns (Figure 4.9d) which implies that Q-CdS nanoparticles are not present in these materials. After metal shadowing more detailed net-like microstructures were repeatedly observed. These microstructures might come from the high DNA concentration probably caused by the dropping deposition method.

However, if these net-like microstructures are only composed of densely packed DNA, they should not be observed in TEM without heavy metal shadowing. This implies that there must be some other materials that enhance the images in the TEM. Even though Q-CdS nanoparticles were not detected with SADP, the 2 mM cadmium might be bound to the DNA. Insufficient cadmium may be available to form CdS nanocrystallites big enough to be detected by SADP, but enough cadmium is available to interact with most of the binding sites of the DNA for contrast in the TEM. We assume this because the microstructures of the Cd^{2+}/DNA samples without exposure to H_2S gas which were made from the same Cd^{2+}/DNA solution at the same time with the same method show similar results (compare Figure 4.10 to Figure 4.9). Figure 4.10a shows the microstructure of Cd^{2+}/circular DNA without metal shadowing and Figure 4.10b shows the same sample with metal shadowing. It is likely that the microstructure shown in Figure 4.10a was observable because of the contrast due to cadmium.

2. Low Density DNA-Like Microstructures. Low density DNA-like microstructures were also observed in the three samples. Figures 4.11a, 4.11b, and 4.11c are the CdS/circular, CdS/linearized and CdS/relaxed DNA, respectively. The DNA molecules found in the circular and relaxed DNA samples (Figures 4.11a and 4.11c) are

DNA (Figure 4.11b) is the relaxed form of the plasmid DNA. However, individual DNA molecules could not be identified by their shapes and sizes because the molecules overlap and are connected together. CdS nanoparticles were not observed by BF TEM or by SADP in these microstructures.

Compared to the microstructures of the DNA only samples (to be described in Chapter 5), the DNA molecules observed here are connected together to form net-work like structures. This implies that the cadmium may induce DNA interconnection when the DNA is mixed with the cadmium in solution.

3. Other unidentified microstructures. Figure 4.12 shows other unidentified microstructures observed these experiments. Figure 4.12a was before metal shadowing and Figure 4.12b was after metal shadowing. These microstructures were occasionally observed in all three samples. The SADP of the microstructure in Figure 4.12a shows the cubic CdS pattern. The microstructure shown in Figure 4.12b may be the same material shown in Figures 4.9a and 4.9c. SADP from the area shown Figure 4.12b did not detect the presence of CdS nanoparticles.

The overall results of the experiments described in this chapter suggest the following three conclusions: (1) the amount of cadmium used (one cadmium ion per nucleotide) may be insufficient to produce numerous CdS/DNA nanostructures, explaining why only a few nanostructures were observed in each experiment even though large number of DNA molecules were presented; (2) not only cadmium ions but also crystalline cadmium perchlorate ($Cd(ClO_4)_2 \cdot 6H_2O$) may bind to DNA. Otherwise, there may be insufficient cadmium to form an array of 5 nm particles since there are only 3-4

binding sites on each nucleotide; and (3) it is not necessary that all of the Cd atoms interact with all of the DNA in the Cd^{2+}/DNA solution. There may be excess Cd to bind to some sites either as Cd ions or cadmium perchlorate crystals. This may explain the presence of CdS/DNA nanostructures or isolated nanoparticles on blank carbon in the 1:1 DNA to Cd experiments.

4.3.5 Absorption and Photoluminescence Spectroscopy

Figure 4.13 shows the results of optical characterization of the Q-CdS nanoparticles formed on pUCLeu4 plasmid DNA on polylysine glass slides. These are typical absorption and photoluminescenc spectra for a Q-CdS/DNA thin film. The data illustrate the effect of the varying the amount of Cd^{2+}/DNA on the absorption spectrum. Two different concentrations, 50 nmoles and 150 nmoles of Cd^{2+}/DNA at 1:1 ratio of Cd^{2+} to DNA, were examined. The dashed line shows the absorption edge of the 50 nmole sample and the solid line shows the data for the 150 nmole sample. Both spectra have similar absorption edges, and both are shifted to the higher energy, the blue region with a wavelength near 450 nm, compared to bulk CdS which has its absorption edge near 515 nm. Comparing the spectrum of the 150 nmole sample to that of the 50 nmole sample, the absorption curve increases in intensity, but the absorption edge does not shift. This suggests that the increased concentration does not affect the size of the CdS particles, but only affects the number of particles.

The peak of the corresponding photoluminescence spectrum of these CdS nanoparticles is observed near 530 nm, which is in the green region.

These absorption and photoluminescence spectra confirm that the CdS nanoparticles formed on pUCLeu4 plasmid DNA exhibit quantum-confinement effects. It should be noted that the PL maximum of the Q-CdS prepared with DNA templates bound to a solid substrate is different than the Q-CdS prepared using mobile DNA in solution (described in Section 3.3.5). The PL maximum for the CdS nanoparticles synthesized on solid substrates is shifted to higher energy compared to the CdS nanoparticles synthesized in solution. This may mean that the nanoparticles formed on DNA on a solid substrate are slightly smaller.

4.3 Summary and Conclusions

Self-assembled mesoscale quantum-confined CdS semiconductor structures were fabricated on pUCLeu4 plasmid DNA templates. Three different types of DNA, undigested circular, linearized, and relaxed circular DNA, were used as templates. The nanostructures were fabricated using the following three steps:

(1) 2 mM Cd^{2+} solution was mixed with 2 mM nucleotide solution to form Cd^{2+}/DNA complexes.

(2) the complex solution was dropped on amorphous carbon films supported by Cu TEM grids.

(3) air-dried grids were exposed to H_2S gas to form Q-CdS nanoparticle arrays in the shape of the DNA template.

Microstructural characterization of the Q-CdS/DNA mesoscale semiconductor structures was performed using conventional TEM and HREM. Analytical transmission

electron microcopy, SADP and XEDS were used for phase identification and elemental chemical analysis. BF and DF images show circular structures composed of an assembly of CdS nanocrystallites. HREM of a part of the ring shows diverse sizes of CdS particles packed onto the DNA without any particular orientation relationships among the Q-CdS crystallites, the DNA, or substrate. The average diameter of the Q-CdS is approximately 5 nm. The lattice spacings measured by electron diffraction match the diamond cubic phase of CdS. Chemical analysis by XEDS indicates that the nanocrystallites contain only Cd and S. The CdS/DNA nanostructure sizes observed by TEM varied from approximately 0.7 μm to 1.2 μm.

These BF, DF, SADP and HREM data prove that the Q-CdS semiconductor particles are formed on the DNA templates, and demonstrate the possibility of fabrication of varying sizes and shapes of mesoscale semiconductor structures using different sizes and shapes of DNA templates.

After metal shadowing, large numbers of supercoiled DNA structures were found in the undigested CdS/plasmid DNA samples. Highly concentrated network-like structures were frequently found in the all three samples: CdS/circular DNA, CdS/linearized DNA, and CdS/relaxed DNA. The network-like structures were found with and without metal shadowing, and most did not contain CdS nanoparticles. Low density DNA-like and other unidentified microstructures were also found in all three samples.

Table 4.1 Comparison of the observed selected area diffraction data of the Q-CdS/plasmid DNA particles with the ICDD values for cubic and hexagonal CdS.[22] The values of the d-spacings are in nanometers (nm).

Experimental Values		Cubic CdS		Hexagonal CdS	
d-spacing	Intensity Order	d-spacing	Intensity	d-spacing	Intensity
				0.359	62
0.337	1	0.336	100	0.336	91
		0.290	40	0.316	100
				0.245	29
0.207	2	0.206	80	0.207	48
				0.190	50
				0.179	8
0.176	3	0.175	60	0.176	31
				0.173	15
		0.168	10	0.168	5
		0.145	20	0.140	15
		0.134	30	0.139	15
0.134	4	0.134	30	0.133	8
0.120	6	0.119	30	0.120	9
0.113	5	0.112	30	0.113	7

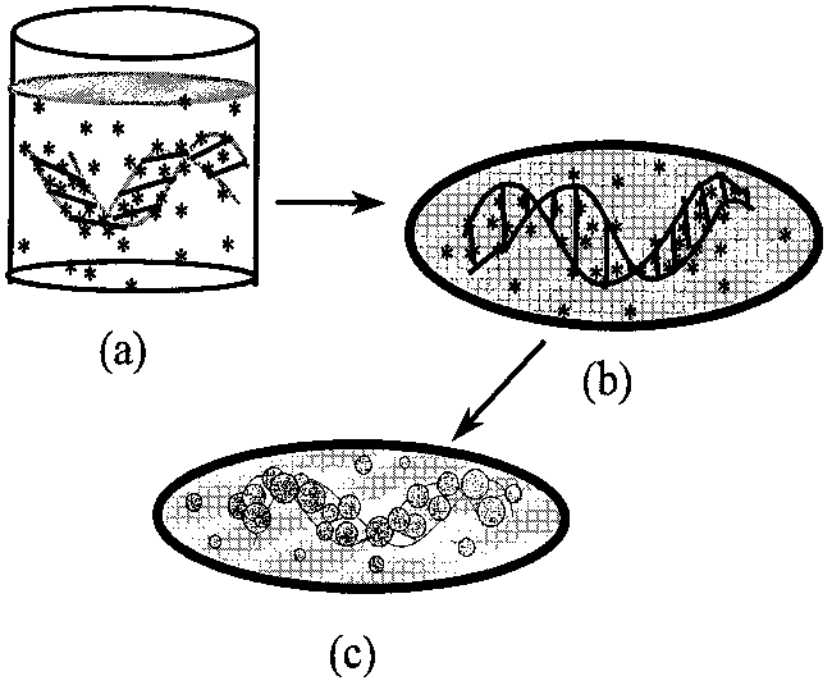

Figure 4.1 Illustration of Q-CdS/DNA nanostructure fabrication on a carbon-coated TEM grid. (a) 1:1 ratio of 2 mM Cd^{2+} to 2 mM DNA solution is prepared. (b) Cd^{2+}/DNA complexes are dropped onto carbon film/copper TEM grids. (c) Grids are exposed to H_2S gas to form Q-CdS nanoparticles on the DNA template.

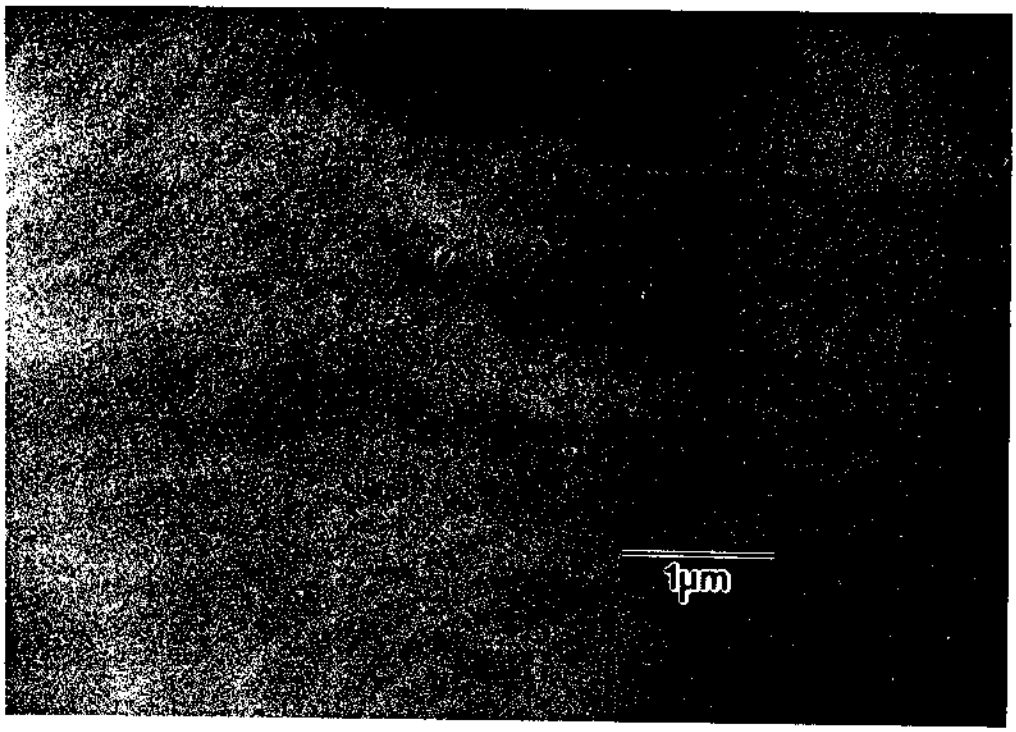

(a)

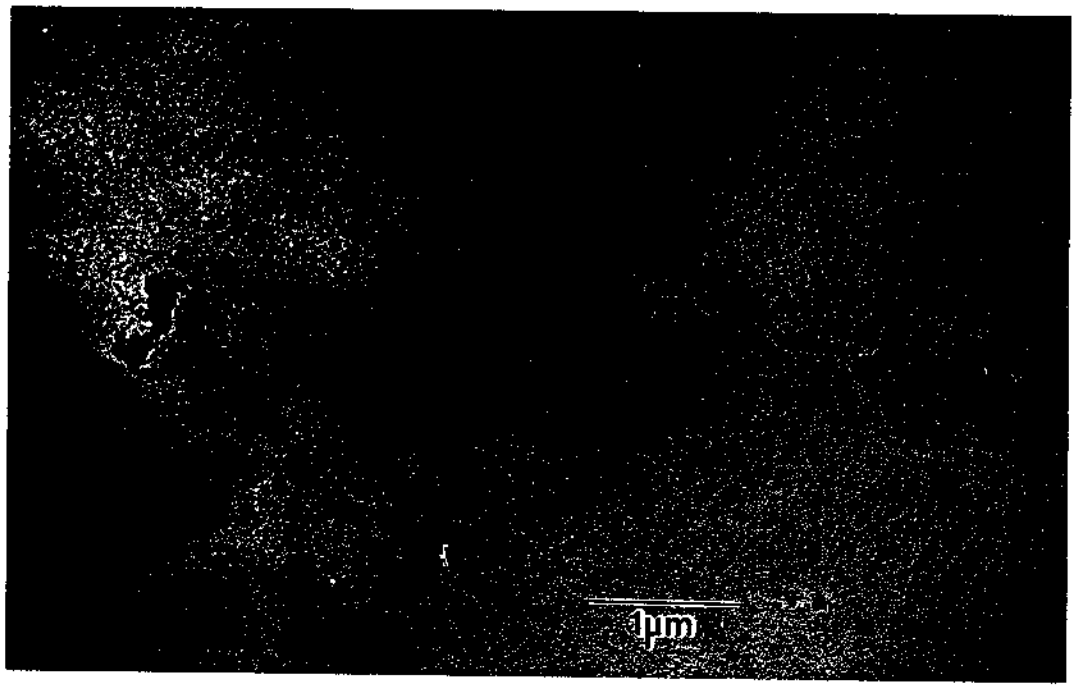

(b)

Figure 4.2 Surface structures of carbon substrates before metal shadowing: (a) made in our laboratory; (b) commercial carbon film.

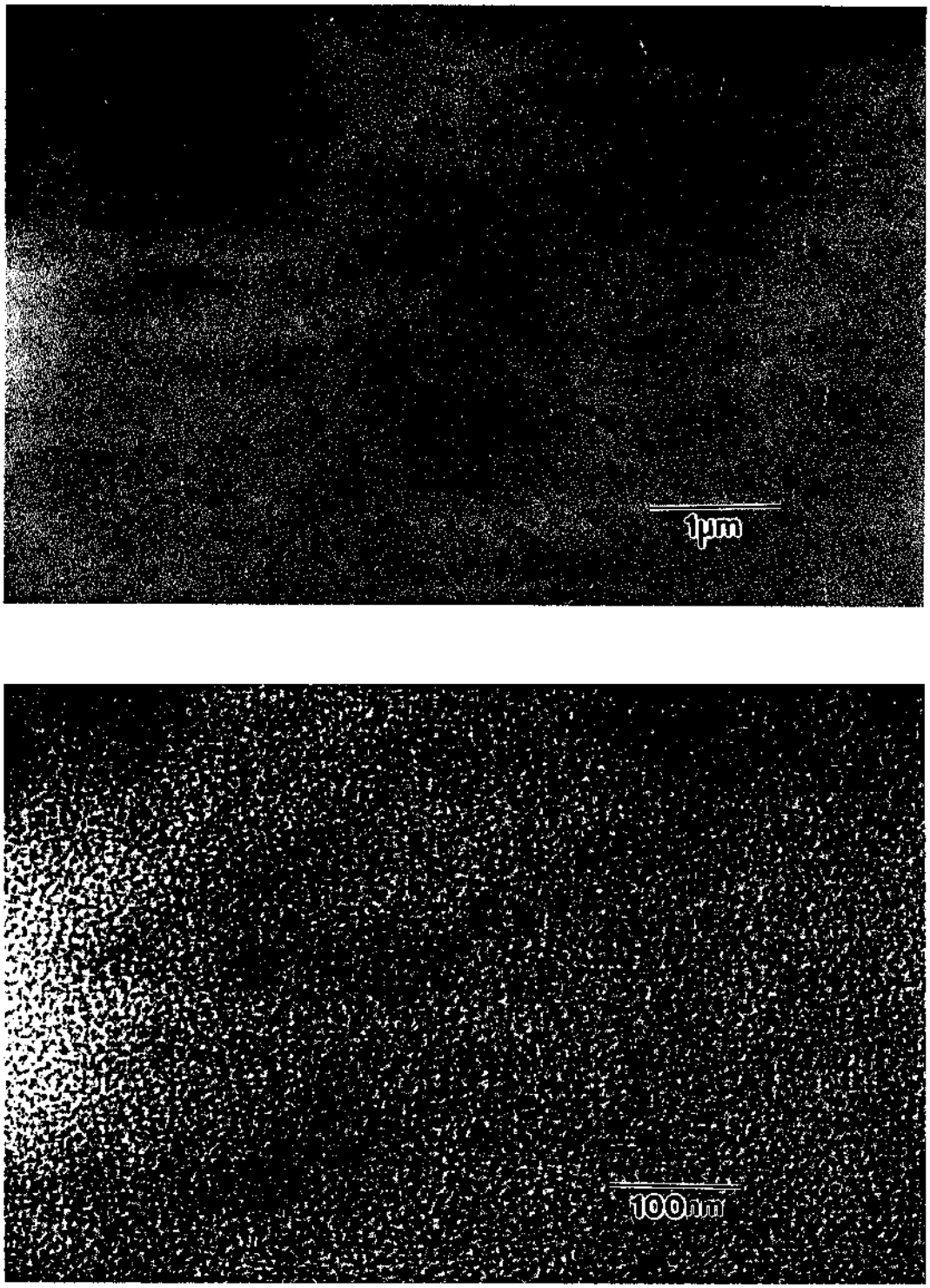

(a)

Figure 4.3 Surface structures of carbon substrates after metal shadowing: (a) made in our laboratory; (b) commercial carbon film.

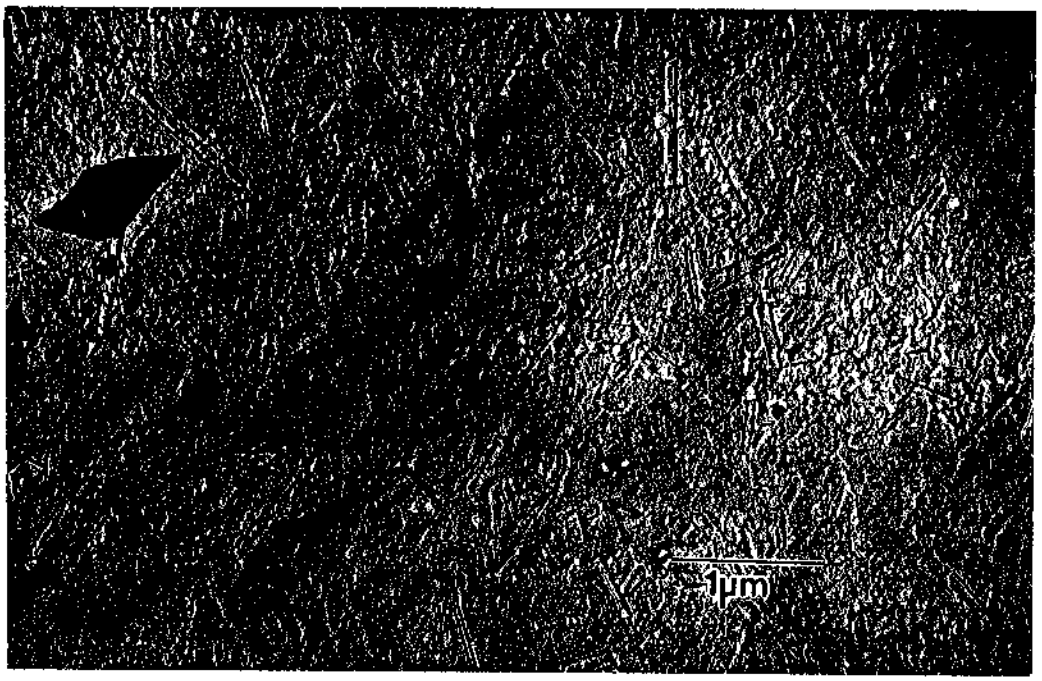

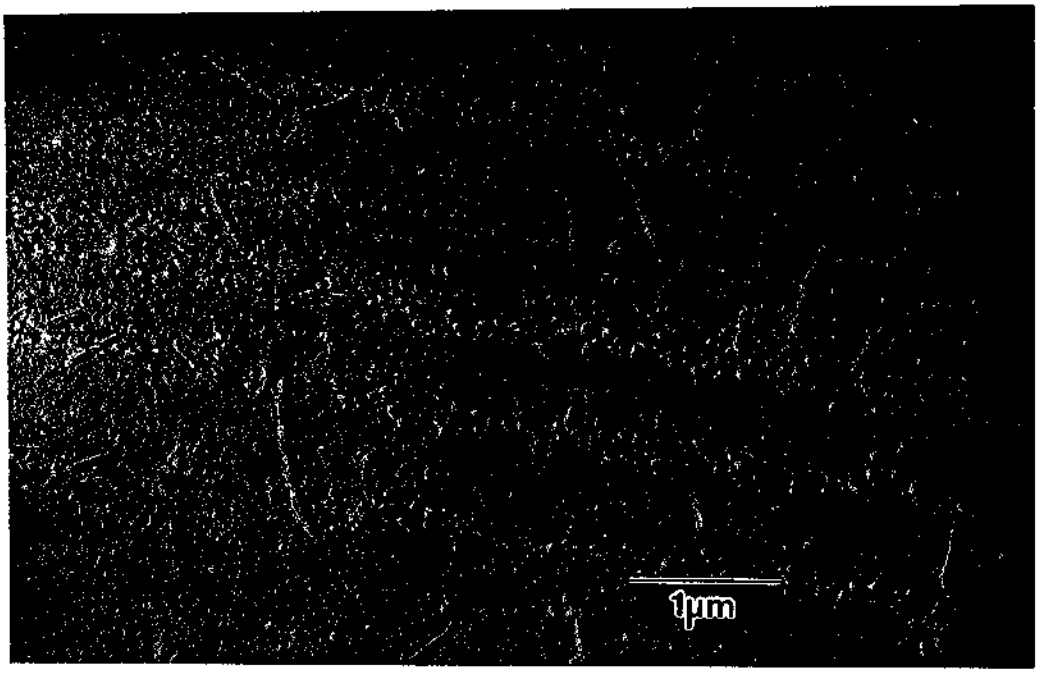

(b)

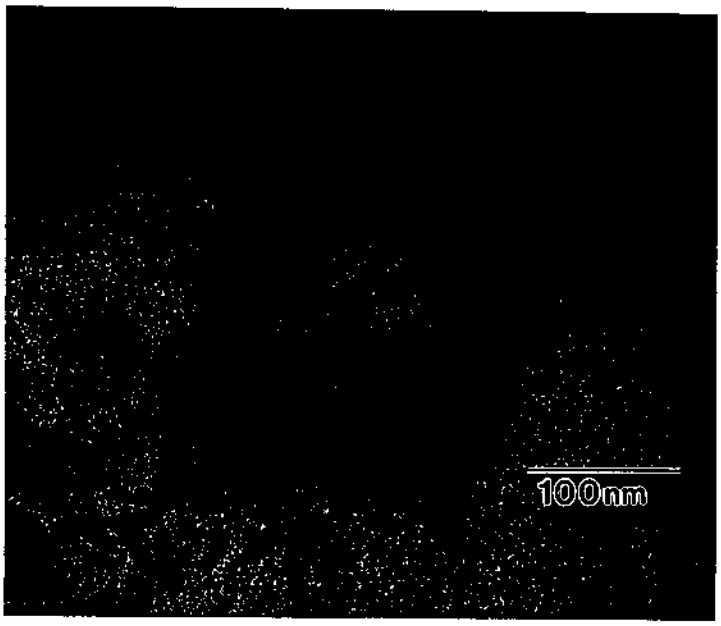

(a)

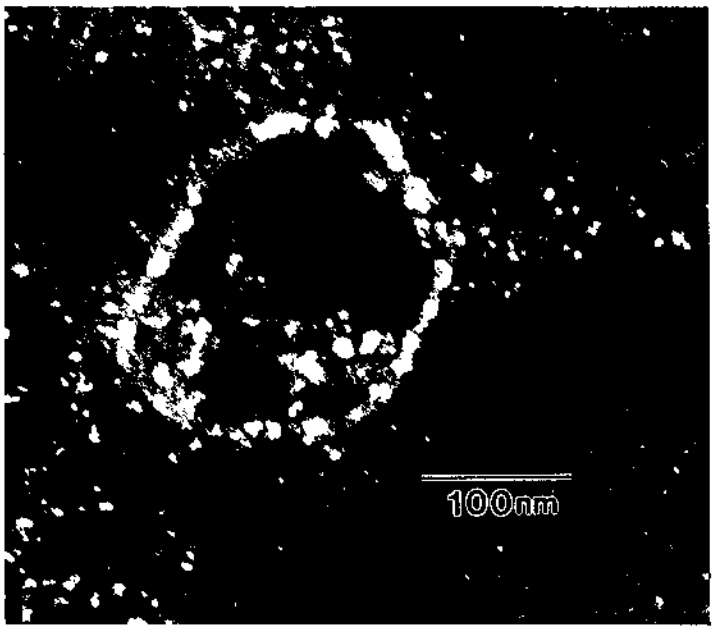

(b)

Figure 4.4 Q-CdS semiconductor structure on pUCLeu4 plasmid DNA: (a) bright field image; (b) dark field image.

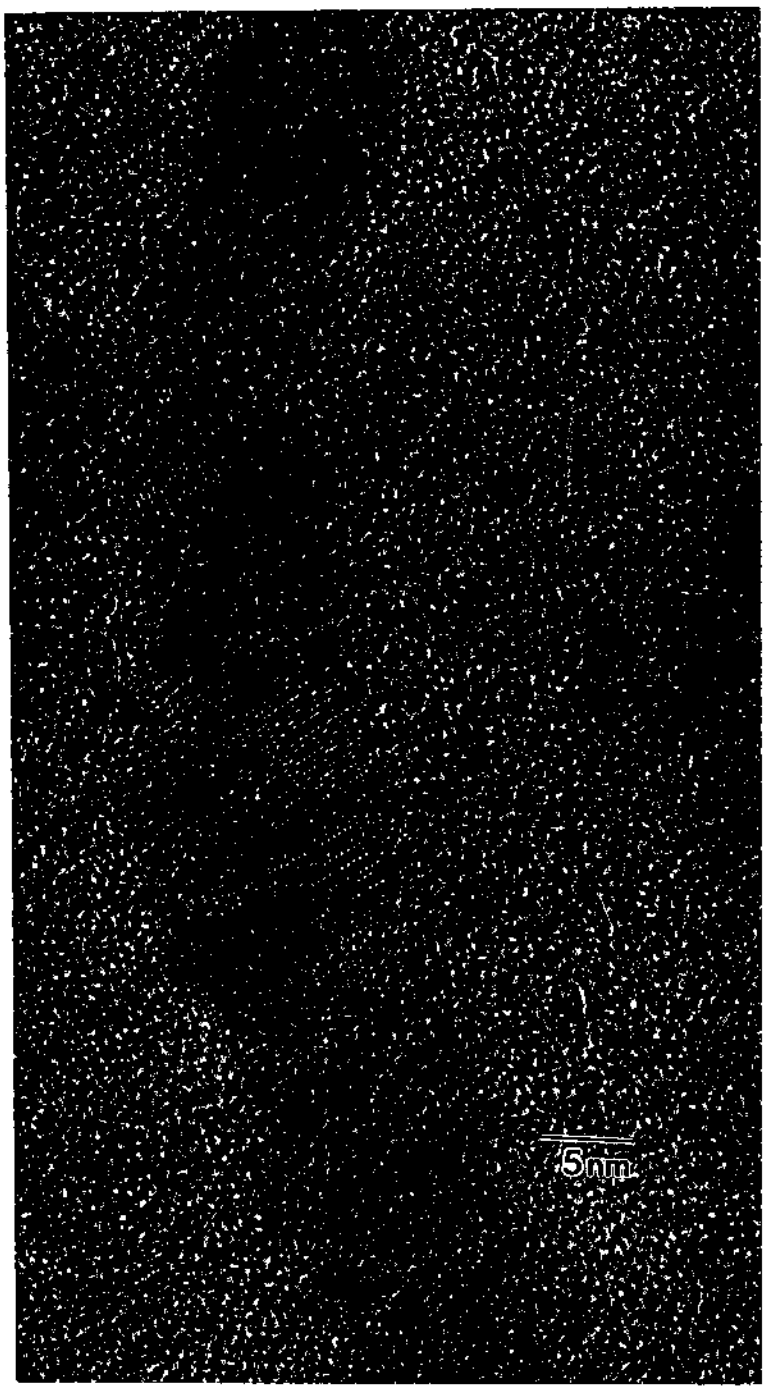

Figure 4.5 A typical HREM lattice image of a Q-CdS/plasmid DNA nanostructure.

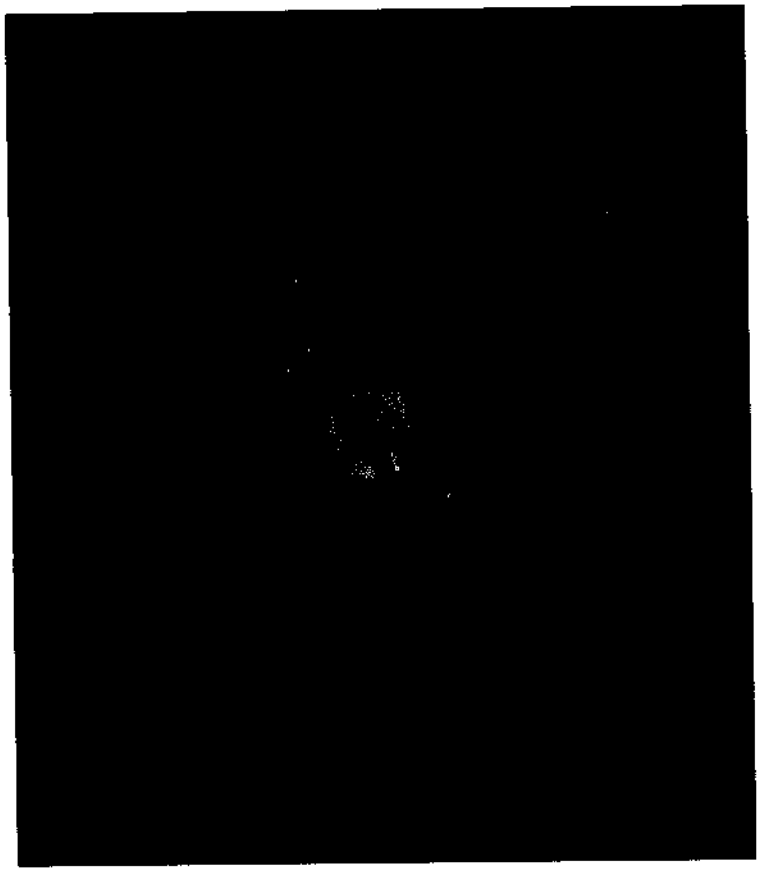

Figure 4.6 Selected area electron diffraction pattern of the Q-CdS/DNA nanostructure shown in Figure 4.4

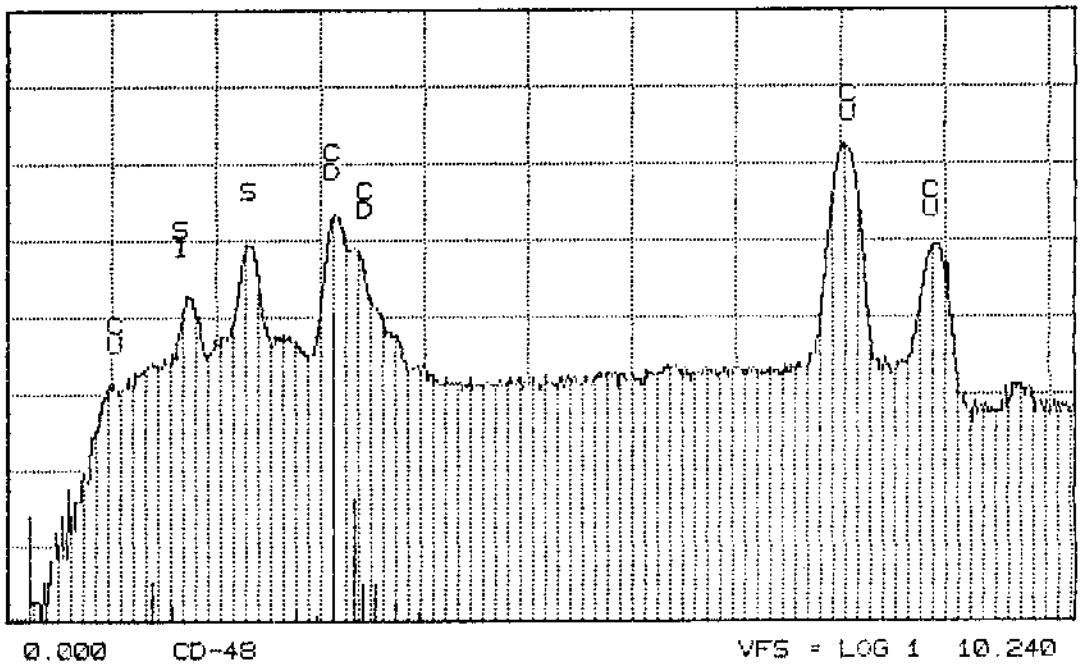

Figure 4.7 XEDS spectrum of CdS nanoparticles synthesized in this experiment.

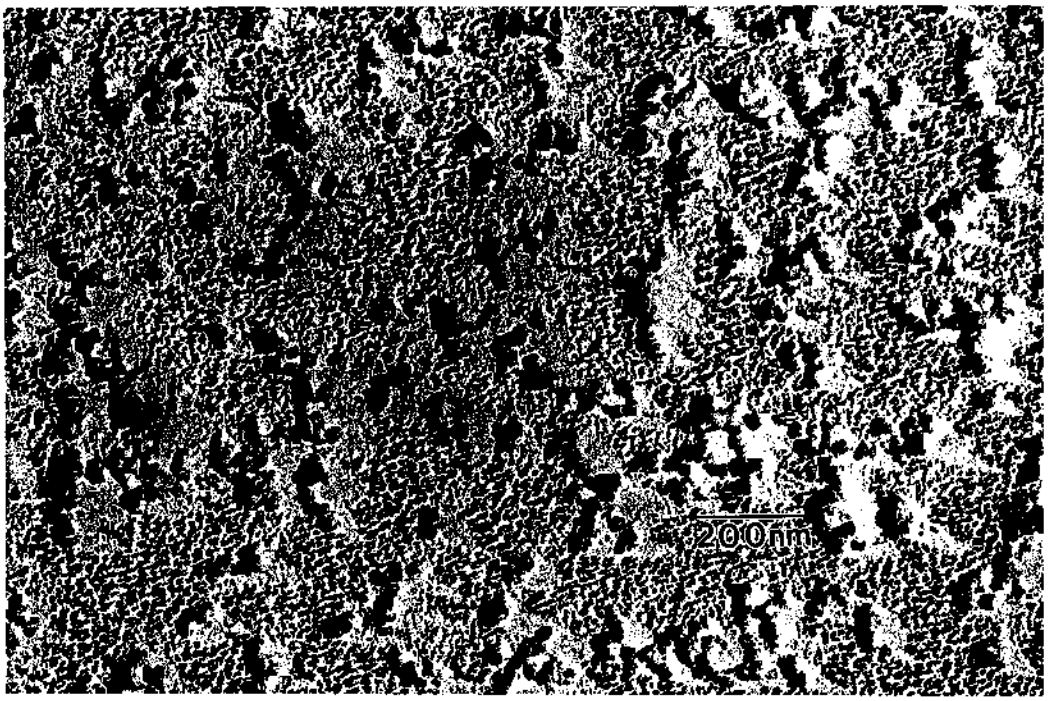

(a)

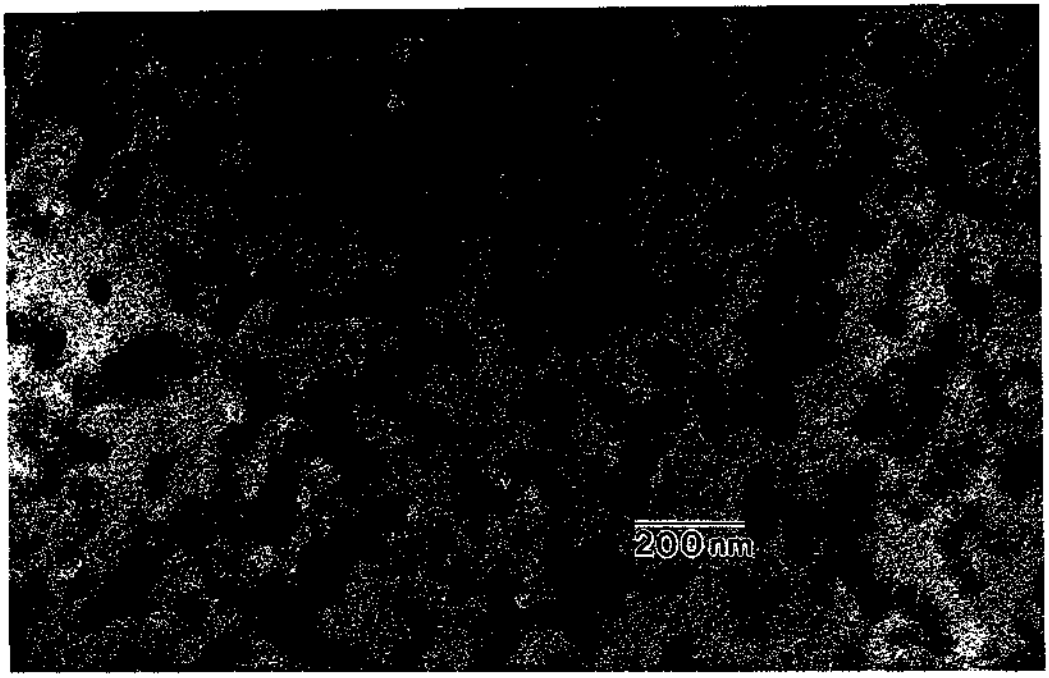

(b)

Figure 4.8 Supercoiled DNA microstructures in: (a) undigested, circular DNA; (b) undigested, circular DNA with CdS nanoparticles; (c) SADP from (b).

(c)

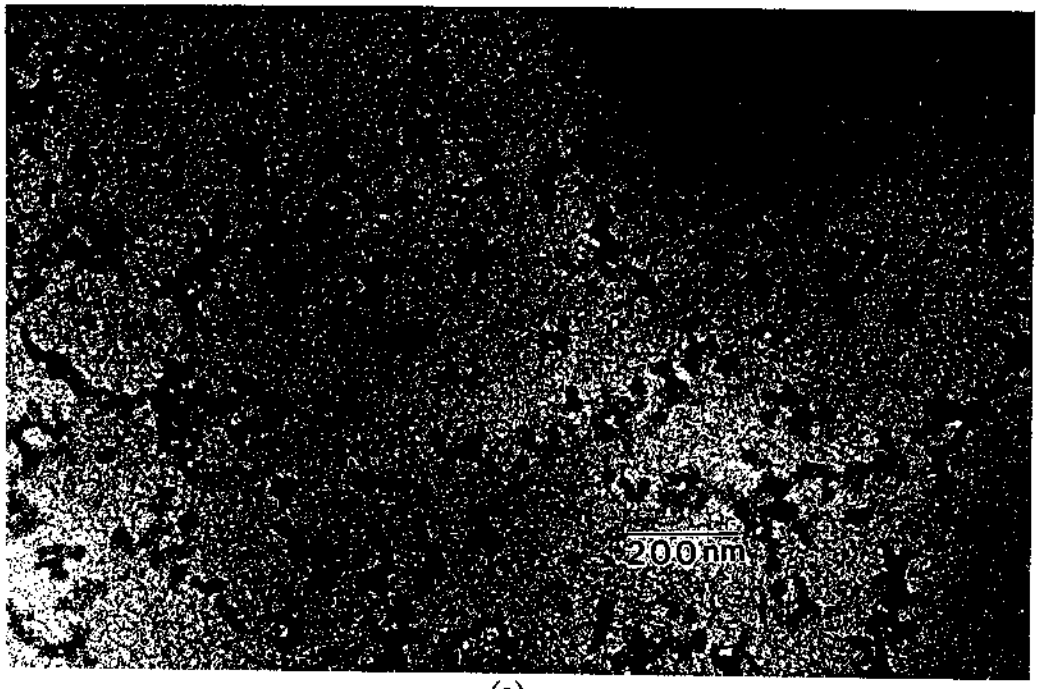

(a)

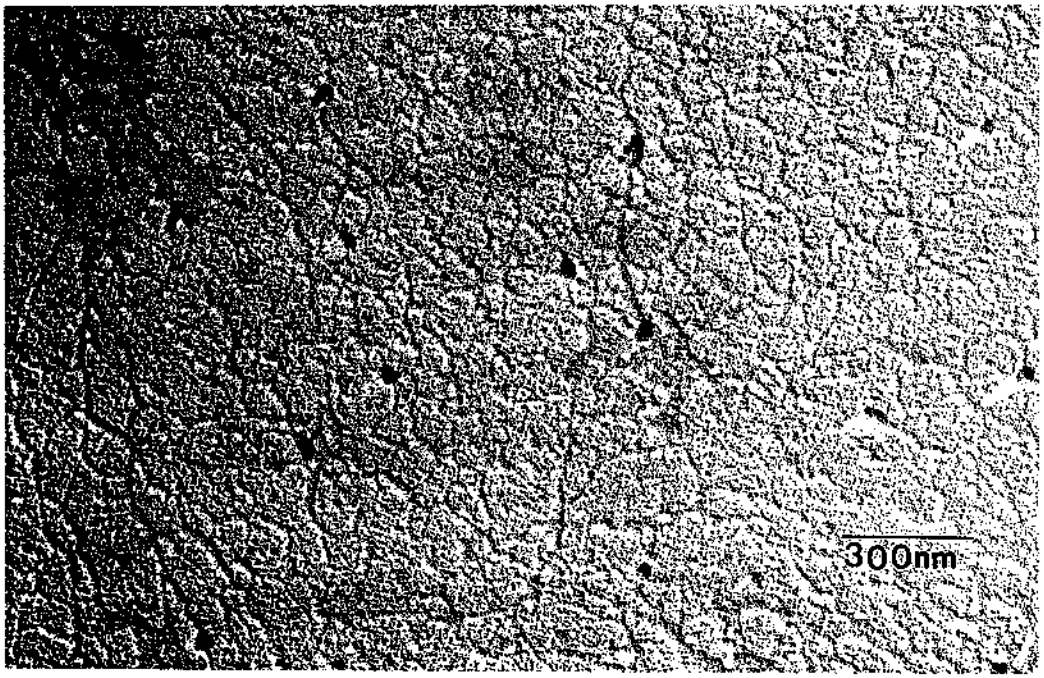

(b)

Figure 4.9 Network-like microstructures observed for: (a) CdS/circular DNA without metal shadowing; (b) CdS/linear DNA with metal shadowing; (c) CdS/relaxed circular DNA with metal shadowing; and (d) typical SADP from (a).

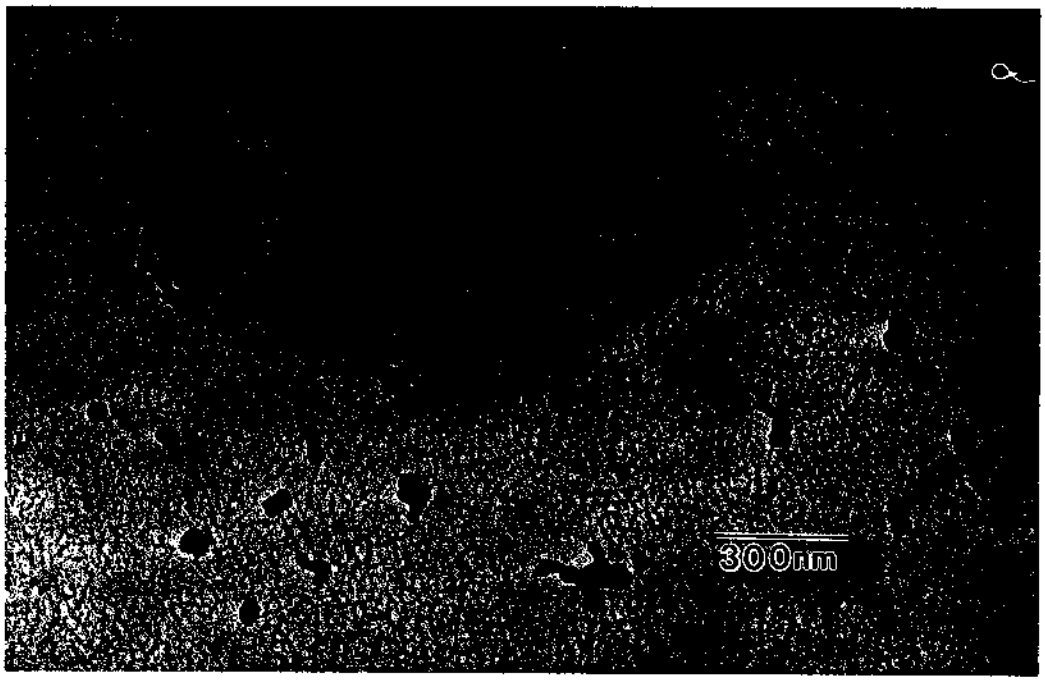

(c)

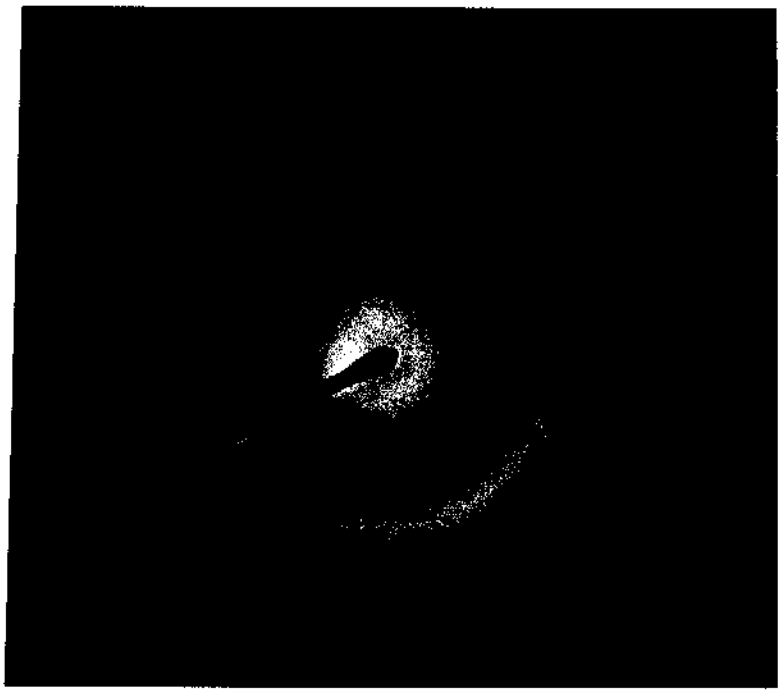

(d)

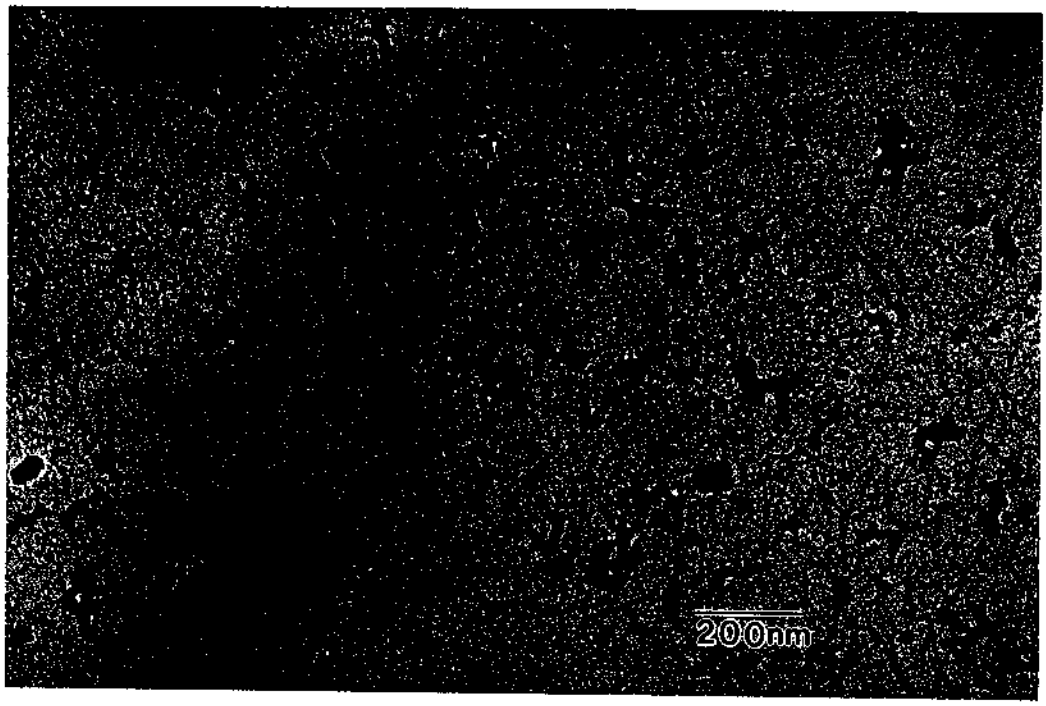

(a)

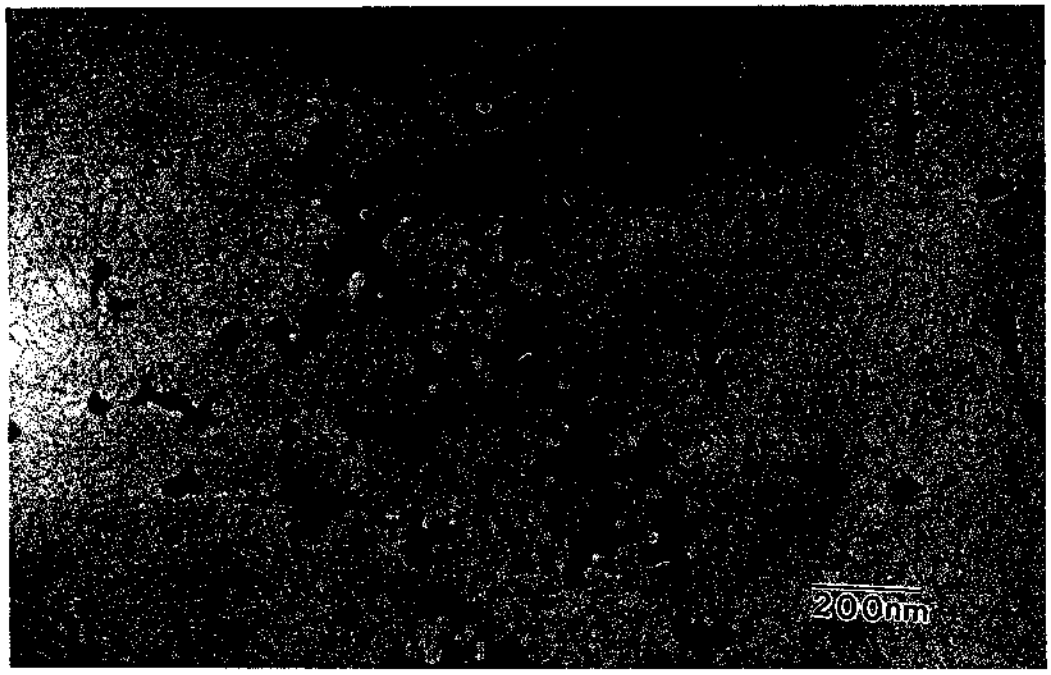

(b)

Figure 4.10 Net-like microstructure of Cd^{2+}/circular DNA sample: (a) before metal shadowing and (b) after metal shadowing.

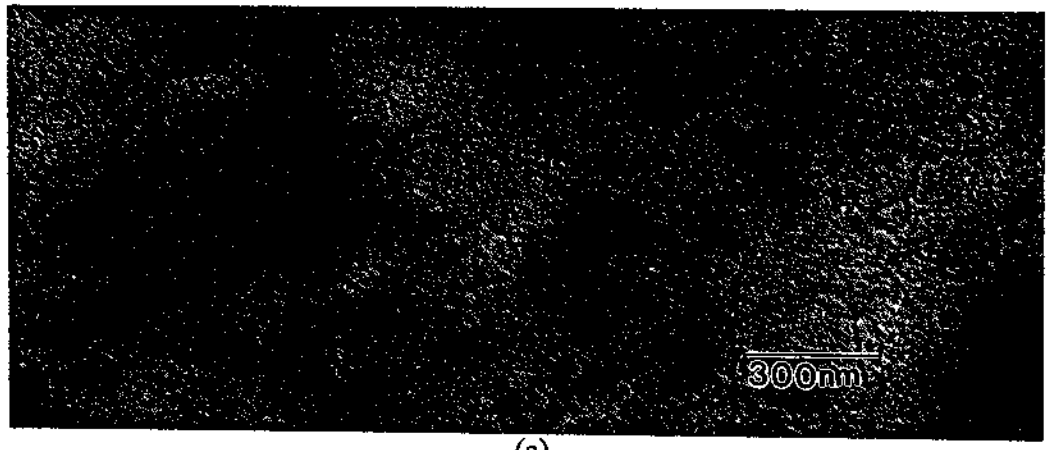

(a)

(b)

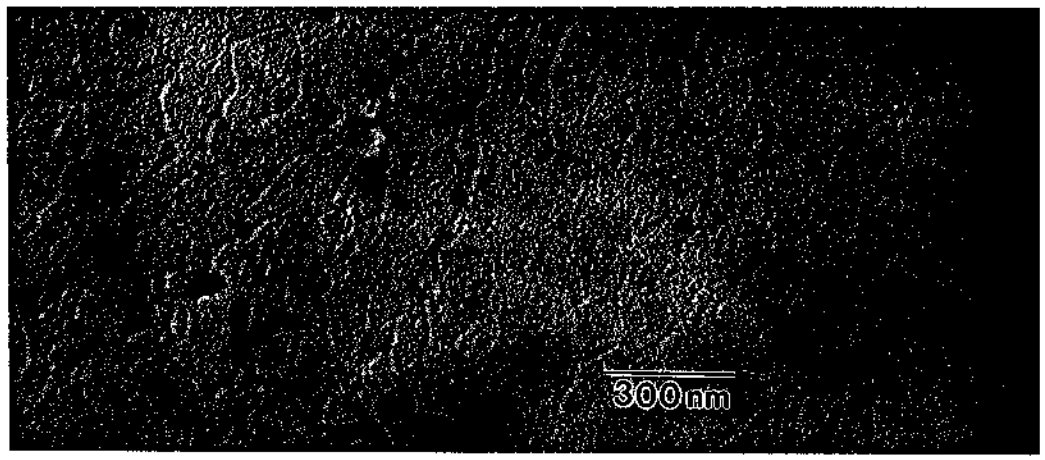

(c)

Figure 4.11 Low density DNA-like microstructures after metal shadowing:
(a) CdS/circular DNA, (b) CdS/linear DNA, and (c) CdS/relaxed DNA.

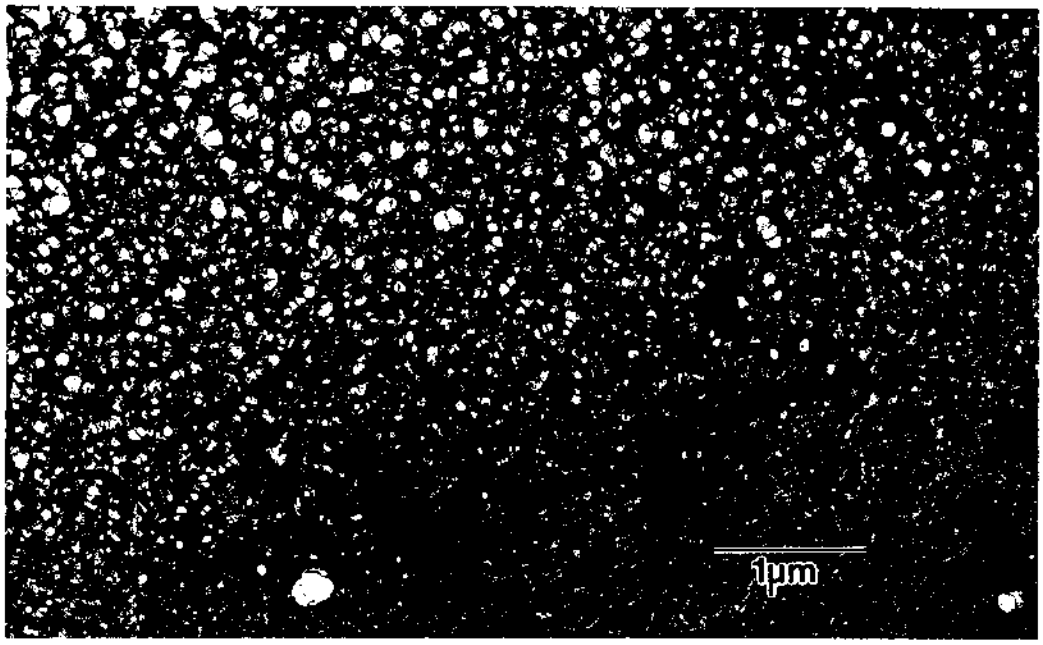

(a)

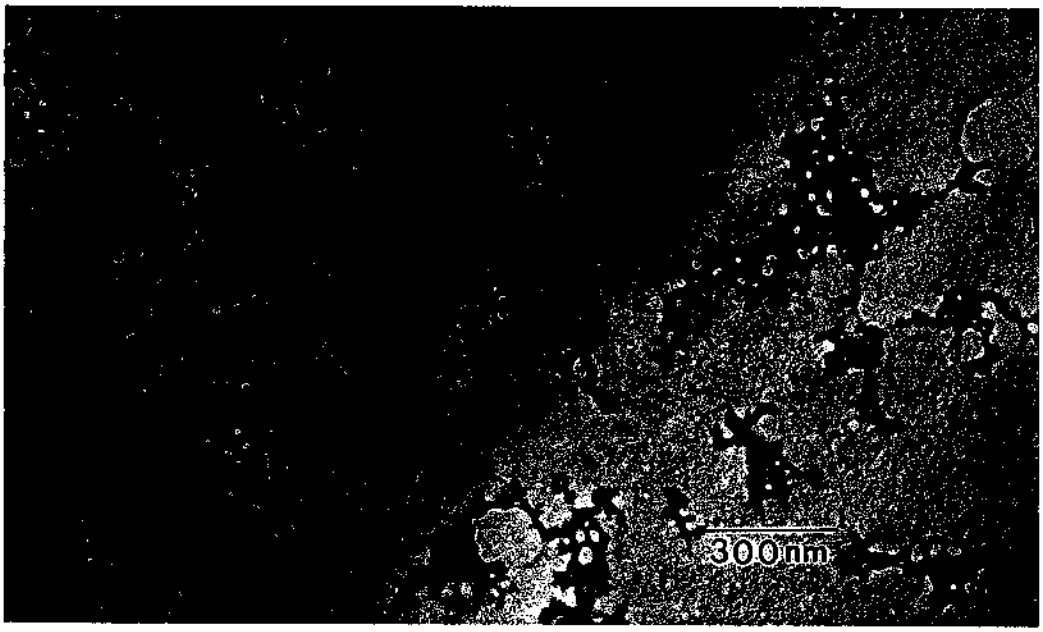

(b)

Figure 4.12 Unidentified microstructures observed in the three samples.
(a) microstructure recorded before metal shadowing in the CdS/circular DNA sample with CdS cubic phase diffraction patterns, and (b) the microstructure recorded after metal shadowing in the CdS/relaxed DNA sample without CdS diffraction patterns.

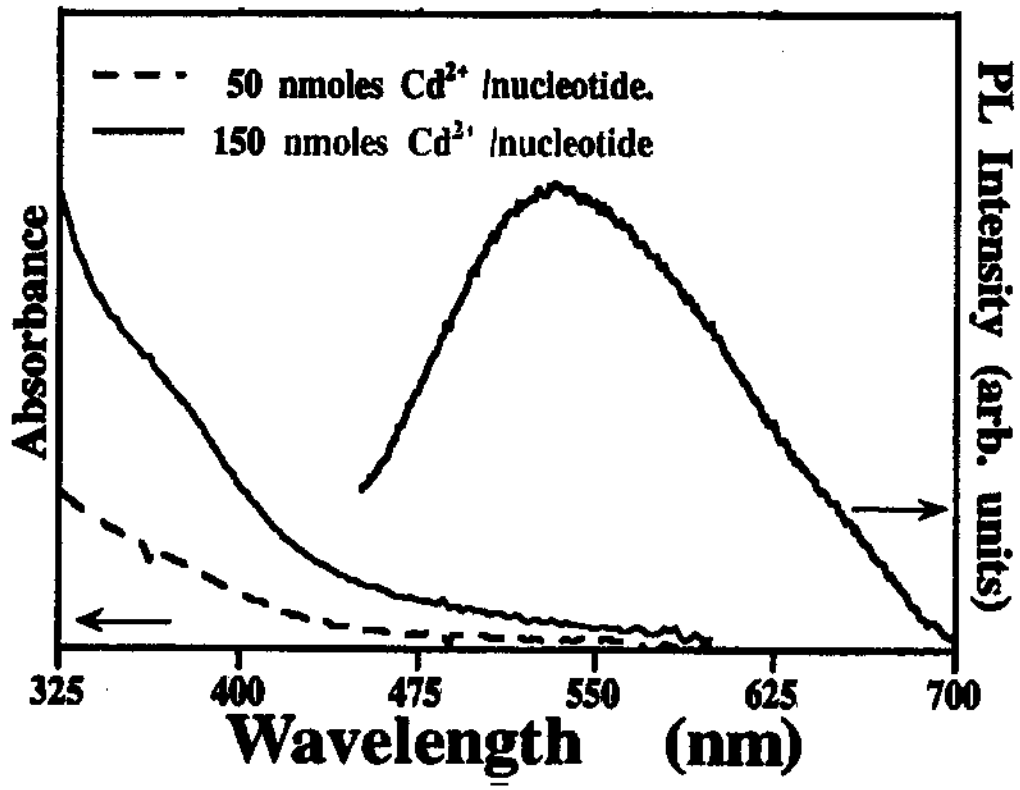

Figure 4.13 UV/visible absorption and photoluminescence spectra of multilayer thin films of CdS/DNA supported on a polylysine-coated glass slide.

REFERENCES

1. N. Peyghambarian, S. W. Kzoch and A. Mysyrowicz, *Introduction to Semiconductor Optics*, (Prentice Hall, Englewood Cliffs, New Jersey, 1993), p.1.

2. J. L Coffer, S. R. Bigham, R. F. Pinizzotto, Y. G. Rho, R. M. Pirtle and I. L. Pirtle, Appl. Phys. Lett. **69**, 3851 (1996).

3. "Advances in Microcrystalline and Nanocrystalline Semiconductors" in *Materials Research Society Symposium Proceeding,* Vol. 452, edited by R. W. Collins, P. M. Fauchet, I. Shimizu, J. C. Vial, T. Shimada and A. P. Alivisatos, (Pittsburgh, Pennsylvania, 1997).

4. W. Saenger, *Principles of Nucleic Acid Structure* (Springer-Verlag, New York, 1984), p. 201.

5. J. L. Coffer, S. R. Bigham, R. F. Pinizzotto and H. Yang, Nanotechnology **3**, 69, (1992).

6. R. F. Pinizzotto, Y. G. Rho, Y. Chen, R. M. Pirtle, I. L. Pirtle, J. L. Coffer and X. Li, Mater. Res. Soc. Symp. Proc. **452** 591 (1997).

7. L. Jervis and N. M. Pettit, J. Chromatogr. **97**, 33 (1974).

8. D. Rhodes and A. Klug, Nature **286**, 573 (1980).

9. Y. N. Chang, I. L. Pirtle and R. M. Pirtle, Gene **48**, 165 (1996).

10. M. Merion and W. Warren, BioTechniques 7, 60 (1989).

11. M. A. Hayat, *Principles and Techniques of Electron Microscopy: Biological Applications, Vol. 1* (Van Nostrand Reinhold Company, New York, 1970), p. 324.

12. *CRC Handbook of Biochemistry and Molecular Biology, Vol. I, Nucleic Acids*, 3rd ed., edited by G. D. Fasman, (Chemical Rubber Company, Cleveland, OH, 1975) pp. 589-90.

13. *Research Chemicals, Metals and Materials,* Cat. # 12936 (Product Catalog, Alfa Aesar, A Johnson-Matthey Company, Ward Hill, MA, 1997), p. 119.

14. ACF - Metals, 2239 E. Kleindale Road, Tucson, AZ.

15. S. L. Flegler, *Scanning and Transmission Electron Microscopy* (W. H. Freeman and Company, New York, 1993), p. 53.

16. H. Yang, Ph.D. Dissertation, University of North Texas, Denton, TX (1993).

17. T. K. Hooghan, Ph.D. Dissertation, University of North Texas, Denton, TX (1997).

18. UV Spectrometry Group, "Techniques in Visible and Ultraviolet Spectrometry" *Standards in Absorption Spectroscopy Vol. I*, edited by C. Burgess and A. Knowles, (Chapman and Hall, London, New York, 1981), p. 3.

19. Z. Sobiesierski, "Linear and Nonlinear Optical Spectroscopy of Surfaces and Interfaces" in *Epioptics,* edited by J. F. McGilp, D. Weaire and C. H. Patterson, (Springer, New York, 1995), pp. 138-140.

20. L. Spanhel, M. Haase, H. Weller and A. Henglein, J. Am. Chem. Soc. **109**, 5649 (1987).

21. H. Weller, Angew. Chem. Interact. Ed. Engl. **32**, 41 (1993).

22. International Centre for Diffraction Data (12 Campus Blvd., Newtown Square, PA) Powder Diffraction File PDF # 10-0454 and 41-1049.

23. D. B. Williams and C. B. Carter, *Transmission Electron Microscopy, Vol. IV* (Plenum Press, New York, 1996), p. 32.

24. J. K. Barton and S. J. Lippard, "Nucleid Acid-Metal Ion Interactions" in *Metal Ions in Biology Vol. 1*, edited by T. G. Spiro, (John Wiley & Sons, Inc., New York, 1980), p. 60.

25. R. D. Deegan and S. R. Nagel, Science News **152**, 298 (1997).

CHAPTER 5

DNA MICROSTRUCTURAL CHARACTERIZATION AND SIZE MEASUREMENT BY THE KLEINSCHMIDT METHOD

5.1 Introduction

In the previous Chapter, three different kinds of pUCLeu4 plasmid DNA, undigested circular, linearized and relaxed circular DNA, were used to fabricate mesoscale Q-CdS semiconductor nanostructures. In each experiment, approximately 2 mM nucleotide was mixed with 2 mM cadmium in solution. The number of pUCLeu4 DNA in a 2 mM nucleotide solution is approximately 1.79×10^{14} per milliliter (there are 6910 nucleotides in pUCLeu4 plasmid DNA). Therefore, two or three 1-2 μl drops of this solution contain approximately 10^{11} pUCLeu4 DNA molecules. However, as reported in Chapter 4, only a few CdS/DNA microstructures were usually observed by TEM. Since so few structures were observed, it was necessary to study the DNA alone, without cadmium or CdS. Also, the sizes of the CdS/DNA mesoscale semiconductor structures were found to vary. Most of the structures were smaller than calculated using the known number of base pairs assuming the B-form of DNA. In Chapter 4, possible causes of DNA shrinkage other than dehydration of DNA were discussed, such as folding or overlapping of some DNA areas due to Cd^{2+} interactions. Comparing the microstructures of DNA without Cd^{2+} to the DNA with Cd^{2+} might explain the microstructural size discrepancy.

The observation of a large number of supercoiled DNA molecules (Chapter 4) was another reason to examine the DNA alone.

According to the gel electrophoresis test, the undigested DNA was composed of approximately 30% relaxed circular DNA, which indicated that a large number of relaxed DNA structures should be observed. We also expected to observe a large number of circular and linear CdS/DNA mesoscale semiconductor structures from both the relaxed and the linearized DNA. However, as noted in Chapter 4, clearly defined CdS/DNA structures were not found in those samples. The observation of the highly concentrated neural-network and other microstructures from all three CdS/DNA samples required us to examine the DNA without Cd^{2+} ions.

Because of the high concentrations of supercoiled DNA and the net-like microstructures observed in previous experiments, the DNA concentration was changed to 5 μg/ml, which is approximately 15.13 μM in nucleotides (1.314×10^{12} DNA molecules per milliliter). This DNA concentration is approximately one thousand times smaller than used in previous experiments. In addition, commercial relaxed DNA, ϕX 174 RF II DNA,[1] was examined for comparison.

In these experiments, three kinds of DNA, undigested circular and linearized pUCLeu4 plasmid DNA, and ϕX 174 RF II DNA, were examined using the Kleinschmidt method. The undigested circular DNA was used because according to gel electrophoresis, approximately 30% of the DNA was not supercoiled. All three DNA samples were made at the same time under the same conditions to compare the results with as few experimental variations as possible.

The basic protein film technique developed by Kleinschmidt and Jahn is a simple and reliable method of preparing nucleic acids for electron microscopy.[2] The negatively charged DNA molecules are mixed with cytochrome c, a basic protein, and are spread into a monolayer on the surface of a dilute salt solution, ammonium acetate. A nucleic acid-protein monolayer surface film is formed by diffusion and the DNA molecules adhere to the surface-denatured protein film. The nucleic acid-protein complex is adsorbed onto a carbon film on a TEM grid. To increase the contrast of the DNA in the electron microscope, the complexes are treated with heavy metals, such as uranyl acetate, to stain them, and the molecules are shadowed with metal at a low angle.

5.2 Experimental

5.2.1 TEM Sample Preparation Using the Kleinschmidt Method

TEM sample preparation using the Kleinschmidt method must be performed in a clean and vibration-free environment. The use of clean apparatus, tools, containers and reagents, and wearing gloves are very important because surface active agents such as detergent, oil and grease can destroy the spreading DNA-protein monolayer film.

TEM sample preparation for imaging DNA molecules using the Kleinschmidt method is described below.

1. Preparation of the spreading solutions. Preparation of the stock solutions for the Kleinschmidt Method such as ammonium acetate, cytochrome c, ethylene diamine tetraacetate (EDTA), and uranyl acetate is well described in most electron microscopy textbooks on biological macromolecules.[2-3] For multiple experiments, stock solutions can

be prepared at one time as follows:

1. 500 ml of 2 M ammonium acetate at pH 7.5

2. 10 ml of 4 mM EDTA at pH 7.5

3. 10 ml of 0.4 mg/ml cytochrome c (store at 4 °C)

4. 50 ml of 50 mM uranyl acetate (store at 4 °C in darkness)

DNA solution was prepared as needed because it degrades during long-term storage. About 1 ml of 5 μg/ml DNA solution was prepared by adding approximately 1 ml of steam-sterilized distilled water to 2.5 μl of 2 mg/ml original DNA solution for the pUCLeu4 plasmid DNA. About 1 ml of 1 μg/ml concentration of ϕX 174 RF II DNA (approximately 3 μM in nucleotide and approximately 1.68×10^{11} DNA per milliliter) was prepared by adding approximately 1 ml of steam-sterilized distilled water to 1 μl of 1 mg/ml original DNA concentration.

2. Mixing the spreading solutions. For each experiment, the solutions were prepared as described below, in three separate containers for the three different types of DNA. The beakers, tweezers, and pipet tips were cleaned throughly or exchanged for new ones to prevent mixing of DNA types.

First, approximately 100 ml hypophase solution of 0.25 M ammonium acetate of pH 7.5 was prepared from the 2 M stock solution by diluting it with steam-sterilized distilled water in a Petri dish. The level of the solution was kept just below the edge of the dish. Graphite powder was evenly sprinkled on the solution so that when the DNA-protein spreading mixture was dropped onto it, the graphite powder indicated the position of the edge of the film.

Second, in a small vial, 100 μl of the hyperphase spreading solution was made by mixing 25 μl of 4 mM EDTA (pH 7.5), 25 μl of cytochrome c of 0.4 mg/ml, 25 μl of 2 M ammonium acetate (pH 7.5), and 50 μl of 5 μg/ml pUCLeu4 plasmid DNA or 1 μg/ml ϕX 174 RF II DNA. The spreading solution was stirred with a pipet to form a homogeneous solution by repeatedly drawing up a small portion and allowing it to run back down for one minute. For the best results, this solution should be used within one hour of mixing.[3]

Third, approximately 5 ml of stain was prepared by diluting at 1:100 ratio the stock solution of uranyl acetate and 90% ethanol. The uranyl acetate solution should be used within 30 min after exposing it to light.[2] Approximately 10 ml of a rinsing solution of 90% ethanol was prepared. Filter paper is used absorb the excess solution from the samples.

3. Spreading the mixtures and making TEM samples. First, a glass slide was lifted by its edge taking care not to touch the side of the slide which was going to be immersed into the solution. The glass slide was rinsed with hypophase ammonium acetate solution. The glass side was carefully placed in a Petri dish with the immersed end resting on the bottom edge and the other side resting on the rim of the dish, as shown in Figure 5.1. This was done with care so as to not disturb the graphite powder. Excess graphite powder was rinsed from the slide with a few drops of ammonium acetate. One must wait for approximately one minute for the movement of the hypophase ammonium acetate solution both in the beaker and on the glass slide to stop.

Second, the spreading solution was dropped on the inclined slide from a position

about 1 cm above the level of the ammonium acetate solution so that the solution runs down the slide slowly. The DNA-protein film is allowed to stop spreading. Approximately 1 minute later, the DNA film area was distinguishable by the position of the edge of the graphite powder.

Third, carbon-coated TEM grids were placed on top of the middle area of the DNA-protein film with the carbon-coated side down. Approximately 30 to 60 seconds later the grids were lifted straight upward by tweezers and the drop of liquid held by the film was removed by touching the edge of the grids with filter paper. In this step, one edge of the grids was bent upwards to be able to put the grid on the DNA-protein film parallel to the surface to not break the DNA-protein film and to make it easier to handle the grids. To bend the grid, the grid was placed on clean filter paper with the carbon-coated side down and a side of the grid was pressed with a razor blade until it bent approximately 20 to 30 degrees.

Fourth, the TEM sample was stained by dipping it into dilute uranyl acetate solution for approximately 30 seconds. The grid was rinsed by immersing it into 90% ethanol for approximately 15 seconds. The grid was then put on filter paper to remove excess liquid. About 5 grids were made for each type of DNA. They were dried in air for approximately 30 minutes before continuing.

4. Metal shadowing. The dried grids were metal shadowed at approximately a 5-7 degree angle with Pt:Pd using a JEOL JEE-4X high vacuum evaporator. All three types of samples were shadowed at the same time and under the same conditions for direct comparison. The samples were attached to a glass slide with double-sided tape to

prevent moving and mixing of the samples during handling. Each sample was labeled with a permanent marker on the back side of the slide. The basic principles and methods of metal shadowing were described in Chapter 4.

5.2.2 Transmission Election Microscopy and DNA Size Measurement

A JEOL 100 CX TEM operating at 100 kV was used to image the DNA microstructures. Conventional bright field imaging was the main method used for these experiments. Microstructures were recorded with the smallest objective aperture to maximize contrast in the images. The length of each DNA molecule was measured using a digitizing tablet interfaced to an IBM-PC with a computerized quantitative microscopy analysis system called Sigma Scan.[4] Each DNA length was measured by tracing each DNA molecule in the micrograph. Approximately 30 to 65 DNA molecules were measured for each type of sample.

5.3 Results and Discussion

5.3.1 DNA Microstructures

Figure 5.2 shows the general DNA microstructures observed when the Kleinschmidt method of sample preparation was used for (a) circular and (b) linear pUCLeu4 plasmid DNA, and (c) ϕX 174 RF II DNA. As shown in the micrographs, the DNA molecules are in irregular chain-like shapes. Closed but fully relaxed DNA molecules were observed for both undigested circular DNA and linearized DNA. Completely unwound and linear DNA was also observed in both types of DNA samples.

DNA molecules wound only a few times, like twisted rubber bands, were also observed. Large numbers of tightly coiled DNA molecules were found in both samples. A large number of opened, linear DNA molecules were observed in the ϕX 174 RF II DNA, with only a few percent closed and tightly wound. Various sizes of dot-like structures were observed in all three samples. Using higher magnification, the dot-like structures appeared to be densely coiled DNA molecules or small DNA fragments (Figure 5.3). As shown in Figure 5.2a, the undigested circular DNA had approximately 20% relaxed DNA and over 5% opened DNA. Not shown in Figure 5.2, the remainder, other than the dot-like structures, was tightly coiled DNA. Figure 5.4 shows typical supercoiled DNA microstructures from both the undigested circular and linearized pUCLeu4 plasmid DNA. Micrograph 5.4a shows a high concentration of supercoiled DNA and 5.4b shows a high magnification view of the supercoiled DNA. These figures also show structures consisting of a few DNA molecules tangled together. It is not known whether the tangled structures arise from the interactions between DNA molecules or simply from the superposition of DNA over the same area. The observed percentage of supertwisted DNA in the circular DNA samples was approximately 75%.

Approximately 30% opened DNA and approximately 10% relaxed circular DNA were found in the linearized DNA samples (Figure 5.2b). The rest of the linearized DNA, approximately 60%, is supercoiled. It was difficult to illustrate these percentages in one micrograph because the distribution of the various forms is inhomogeneous. However, it should be noted that the reported percentage distributions are based on direct TEM observations. The large percentage of supercoiled DNA was anticipated from the gel

electrophoresis test. However, approximately 5% of the opened DNA found in the undigested circular DNA samples seemed broken by handling during the sample preparation. The observation of the relaxed circular molecules and the supercoiled DNA molecules in the linearized samples indicates that not all of the DNA was digested by the topoisomerase II enzyme.

Figure 5.2c is a typical microstructure of the ϕX 174 RF II DNA. Approximately 90% of the ϕX 174 RF II DNA is linear and less than 5% is relaxed and closed DNA, and only a few percent is supercoiled. The ϕX 174 RF II was supposed to be in the relaxed and closed form, but most was observed to be open, as seen in Figure 5.2c.

Even though the concentration of the DNA is sometimes high (Figure 5.5), the DNA molecules are generally not tangled with each other. This may be due to the repulsive forces of the anion atoms or the oxygen atoms of the phosphate groups, as mentioned in Chapter 2.[5]

Figure 5.6 shows selected microstructures of the circular and linear DNA that can be used as templates for the fabrication of predesigned mesoscale Q-SC structures. As shown in Figures 5.6 (b) and (c), the linear form of DNA was often found in the opened DNA, but no perfect circular DNA molecules were found.

5.3.2 DNA Size Measurements and Size Distributions

The experimentally determined DNA lengths were compared to the lengths calculated using the known number of base pairs (Table 5.1). Fully relaxed DNA molecules of each of the three types were chosen for measurement. The average DNA

lengths, as measured directly from TEM micrographs, were 0.89 μm, 0.84 μm, and 1.25 μm for the circular, linear and ϕX 174 RF II DNA, respectively. As shown in Table 5.1, the A-form is approximately 72% of the length of the B-form. The average lengths of the three DNA samples were close to those calculated for the A-forms of DNA.

The measured DNA size varied from 0.57 μm to 1.06 μm which is approximately 50% to 90% of A-form DNA for both circular and linear pUCLeu4 DNA, and varied from 1.01 μm to 1.62 μm which is approximately 57% to 88% of the ϕX 174 RF II DNA A-form (Figure 5.7). According to the size distribution measurements, most of the pUCLeu4 (circular and linear) DNA is between 0.75 μm and 0.95 μm with relatively little between 0.6 μm and 0.7 μm. However, for the opened ϕX 174 RF II DNA case, more of the DNA is smaller in size. These results suggest that the DNA might be cleaved when treated with restriction enzyme.

As described in Chapter 2, the A-form DNA is shorter than the B-form due to dehydration. **Therefore, when DNA is used as structural templates for assembling mesoscale semiconductor structures, A-form DNA lengths should be assumed.**

5.3.3 Unidentified Microstructures

The micrographs shown in Figure 5.8 are unidentified microstructures found in the linearized pUCLeu4 samples. Except for Figures 5.8e and 5.8f, the microstructures were imaged after metal shadowing. These microstructures were not commonly observed, except for that shown in Figure 5.8f.

Figure 5.8a shows a large number of linear structures in one area. The lengths of

these structures are approximately 50% of pUCLeu4 plasmid DNA, but the thickness of the structures is about double that of pUCLeu4 (Figure 5.1). The microstructures in Figures 5.8b, 5.8c, and 5.8d are similar to those shown in Section 4.3.4, the highly concentrated net-like microstructures, but are not as dense. Selected area diffraction did not detect any crystallinity. The microstructure shown in Figure 5.8f was often found in both circular and linear pUCLeu4 DNA samples. It may be the same material shown in Figure 4.14a, again with less density. SADP did not detect any crystallinity in this area, either.

5.4 Summary and Conclusions

pUCLeu4 plasmid DNA, both undigested circular and linearized, and ϕX 174 RF II DNA were imaged using BF TEM. The samples were prepared using the Kleinschmidt method. Concentrations of 5 μg/ml for the circular and linear pUCLeu4 DNA, and 1 μg/ml for ϕX 174 RF II DNA were used for the experiments. Approximately 30 to 65 individual DNA lengths were measured for each type of DNA using a quantitative microscopy analysis system.

The DNA microstructures observed were irregular chain-like shapes or sometimes like twisted rubber bands.

Approximately 20% of the undigested circular DNA and approximately 10% of the linearized DNA were observed as closed and relaxed DNA circles. Approximately 5% of the undigested circular DNA and approximately 30% of the linear DNA were observed as open and unwound DNA. The remainder of the samples, approximately 75%

of the undigested circular DNA and 60% of the linear DNA, were observed in supercoiled form.

For the ϕX 174 RF II DNA, approximately 90% was open and less than 5% was closed and relaxed, and only a few percent was supercoiled.

From observations of highly concentrated DNA, there are no ionic interactions between the DNA molecules which may induce tangles.

The average sizes of the circular, linear and ϕX 174 RF II DNA are 0.89 μm, 0.84 μm, and 1.25 μm respectively, close to lengths expected for the A-form.

When DNA is used as structural templates for assembling mesoscale semiconductor structures, A-form DNA lengths should be assumed.

Table 5.1 Comparison of measured DNA sizes with calculated values.

DNA	Calculated Length of B-form Pitch = 0.34 nm/bp	Calculated Length of A-form Pitch = 0.246 nm/bp	Experimental Measured length (average)
pUCLeu4 plasmid (circular, 3455 bp)	1.17 μm	0.85 μm	0.89 μm
pUCLeu4 plasmid (linear, 3455 bp)	1.17 μm	0.85 μm	0.84 μm
ϕX 174 RF II DNA (relaxed circular, 5386 bp)	1.83 μm	1.32 μm	1.25 μm

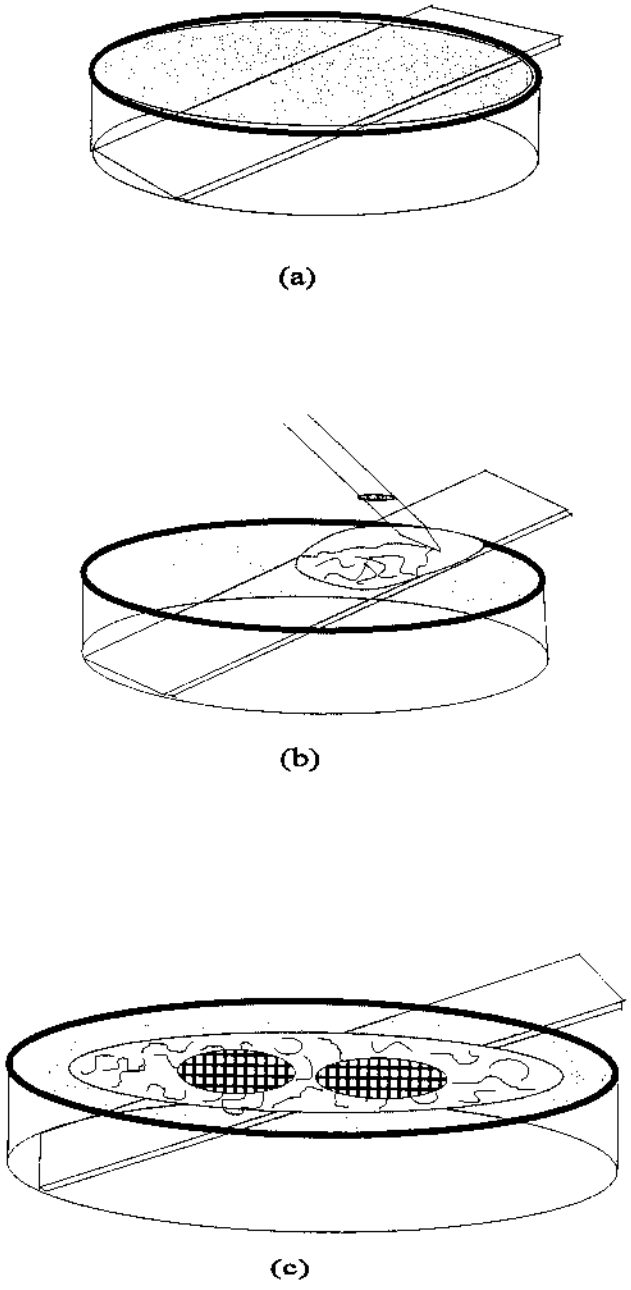

Figure 5.1 DNA-protein spreading apparatus illustrating the spreading processes of the Kleinschmidt method. (a) 0.25 M hypophase ammonium acetate with graphite powder, (b) dropping the spreading solution, and (c) TEM grids on the DNA-protein film.

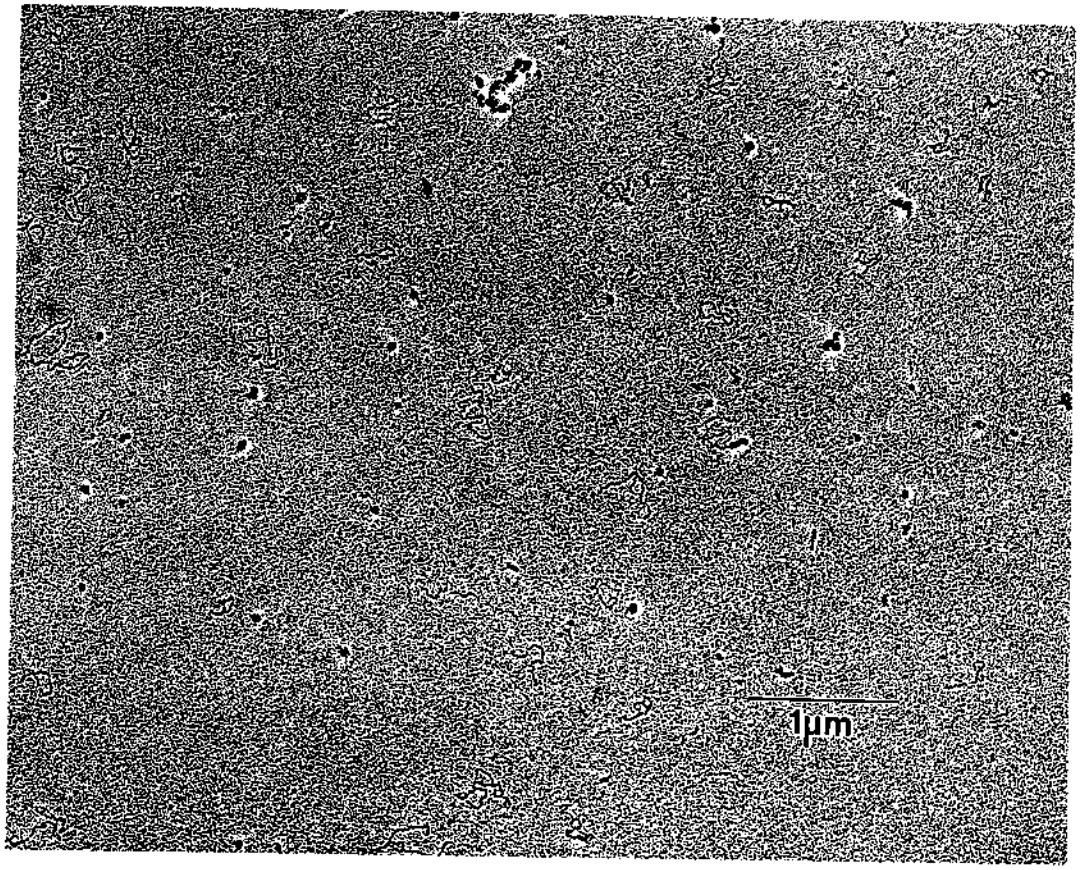

(a)

Figure 5.2 General microstructures of DNA molecules prepared using the Kleinschmidt method: (a) undigested pUCLeu4 plasmid DNA; (b) linearized pUCLeu4 plasmid DNA; and (c) ϕX 174 RF II DNA.

(b)

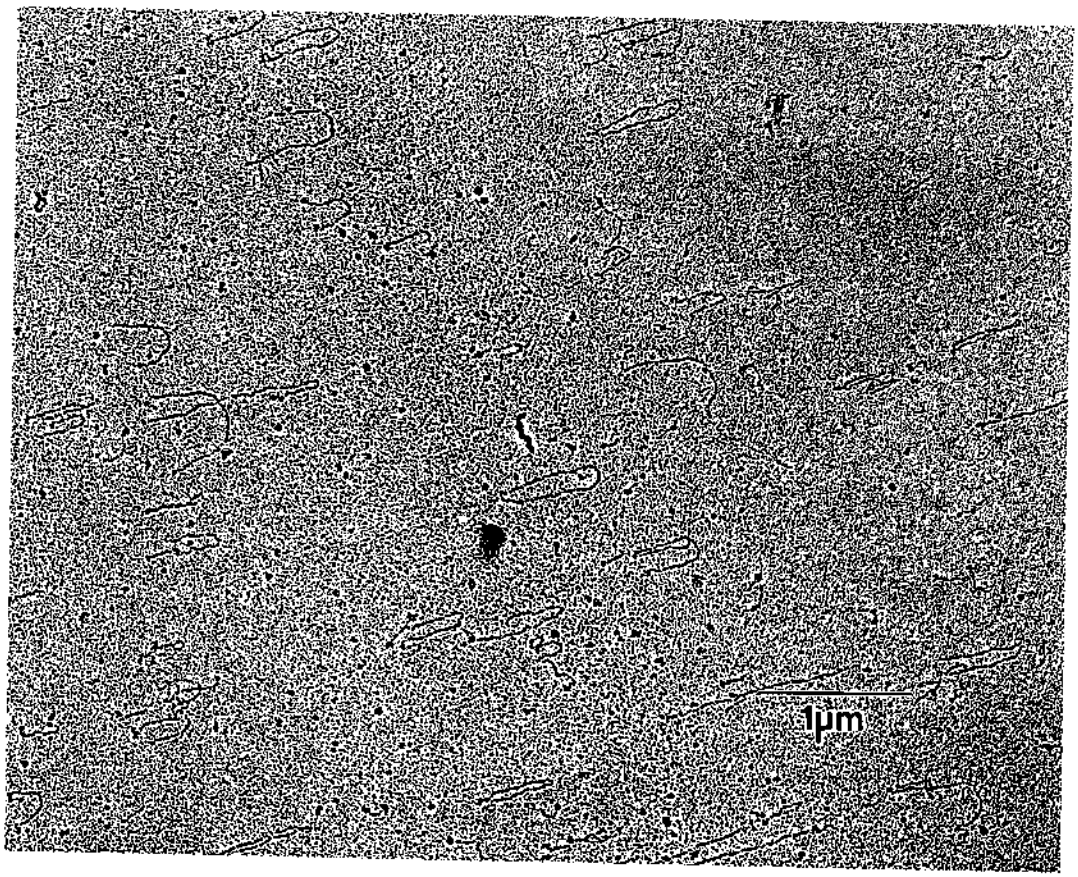

(c)

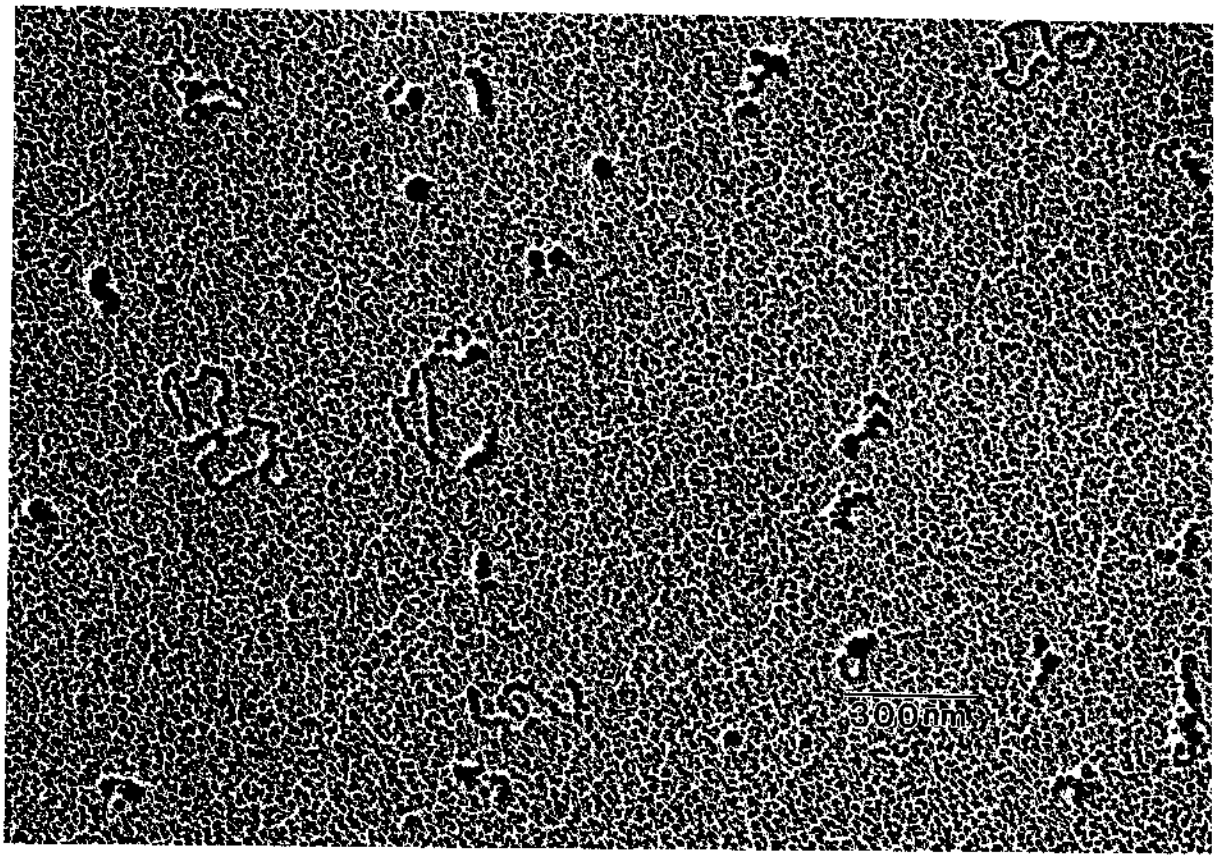

Figure 5.3 Typical dot-like microstructures observed in all three types of DNA samples. This sample is undigested pUCLeu4.

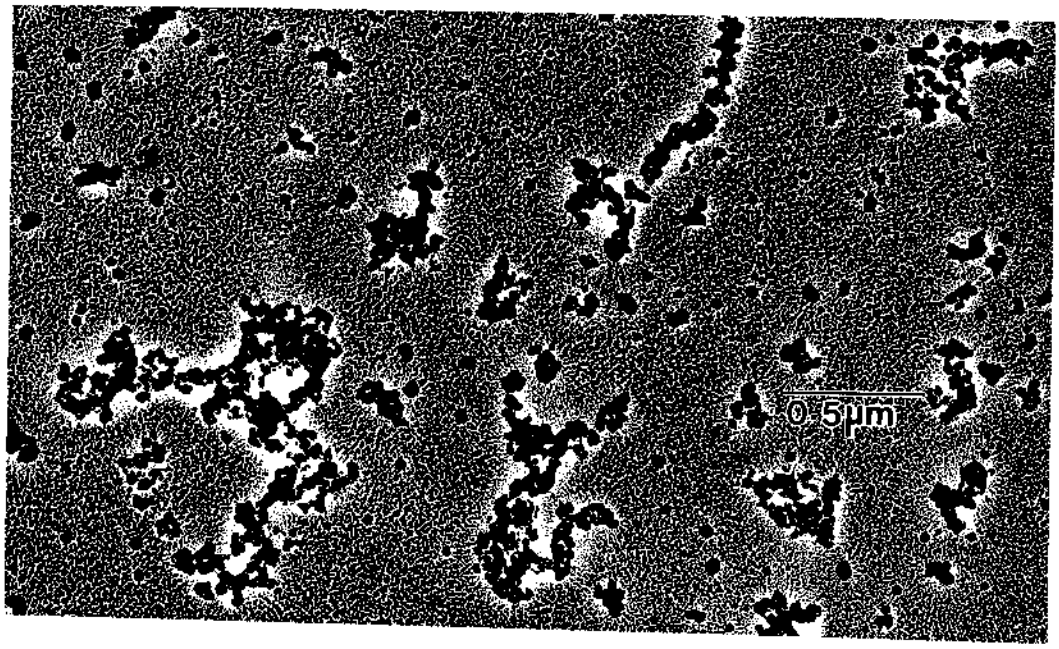

(a)

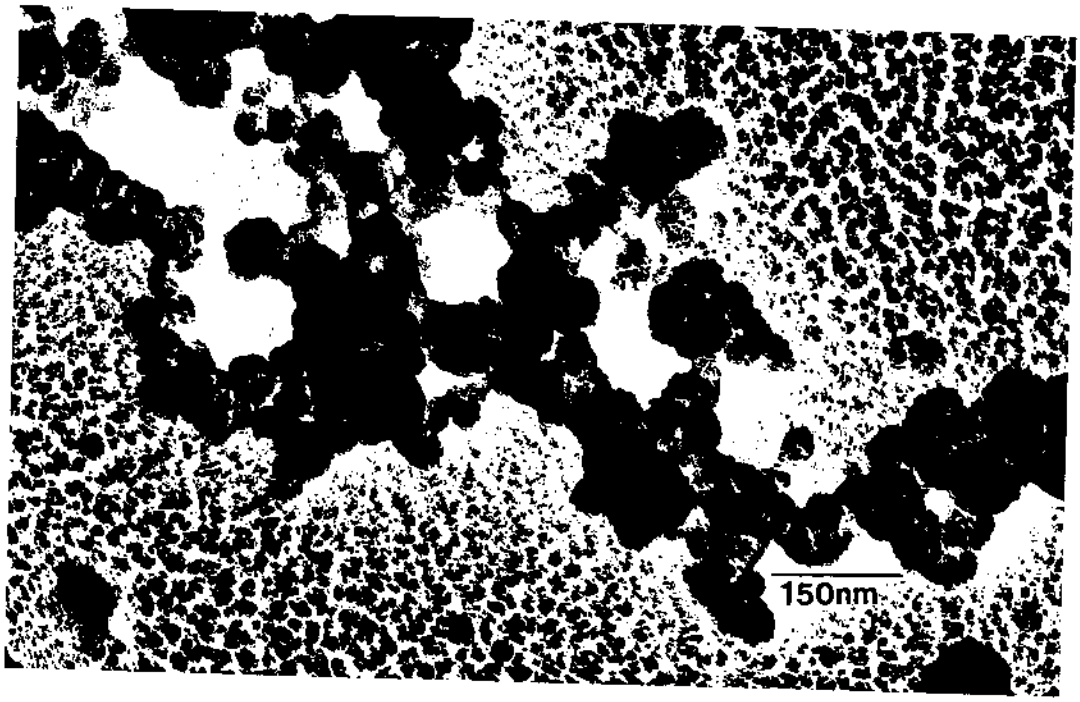

(b)

Figure 5.4 High concentration of supercoiled DNA structures in linearized pUCLeu4 DNA. These are typical microstructures for both undigested DNA and linearized DNA. (a) low magnification, (b) high magnification.

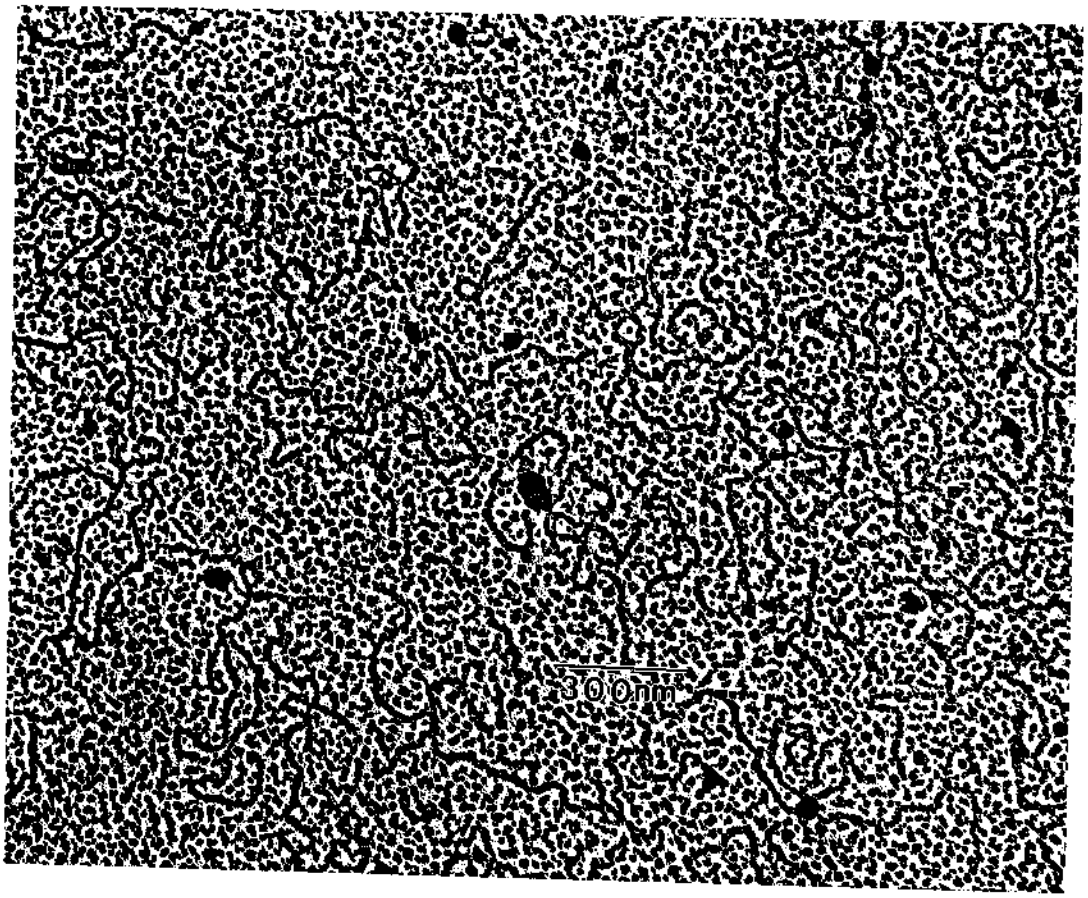

Figure 5.5 High concentration region in the linearized pUCLeu4 sample.

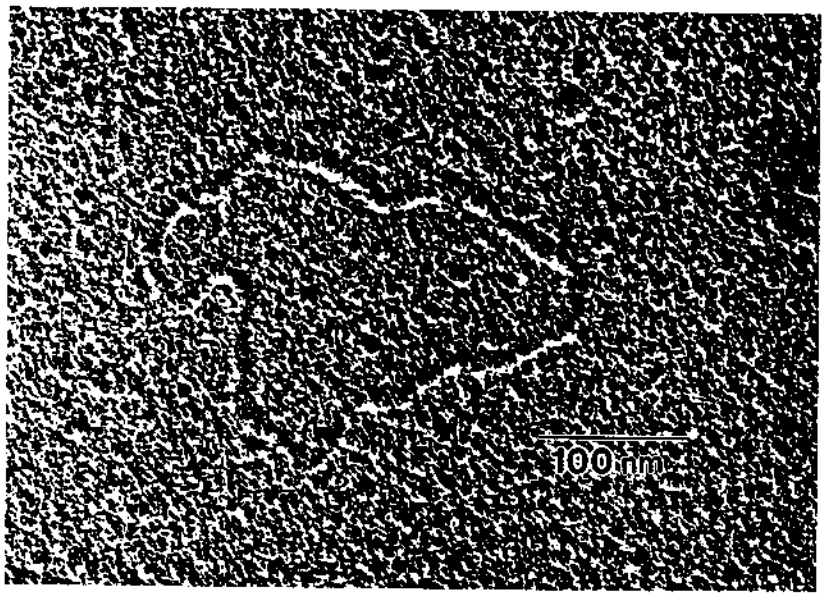

(a)

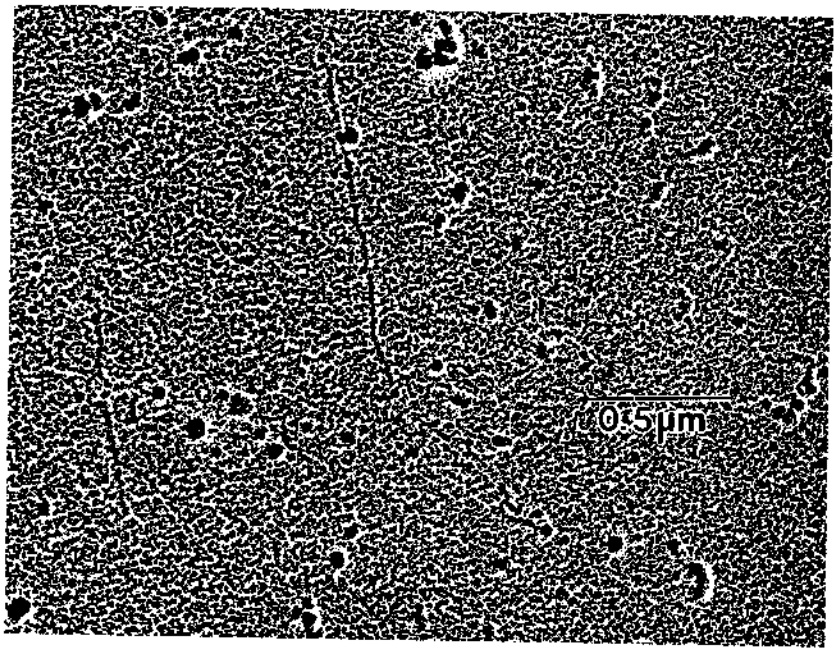

(b)

Figure 5.6 Relaxed circular and linear DNA structures which can be used as DNA templates for fabrication of mesoscale semiconductor structures: (a) undigested circular pUCLeu4 plasmid DNA for quantum rings; (b) linearized pUCLeu4 plasmid DNA; and (c) ϕX 174 RF II DNA, for quantum wires.

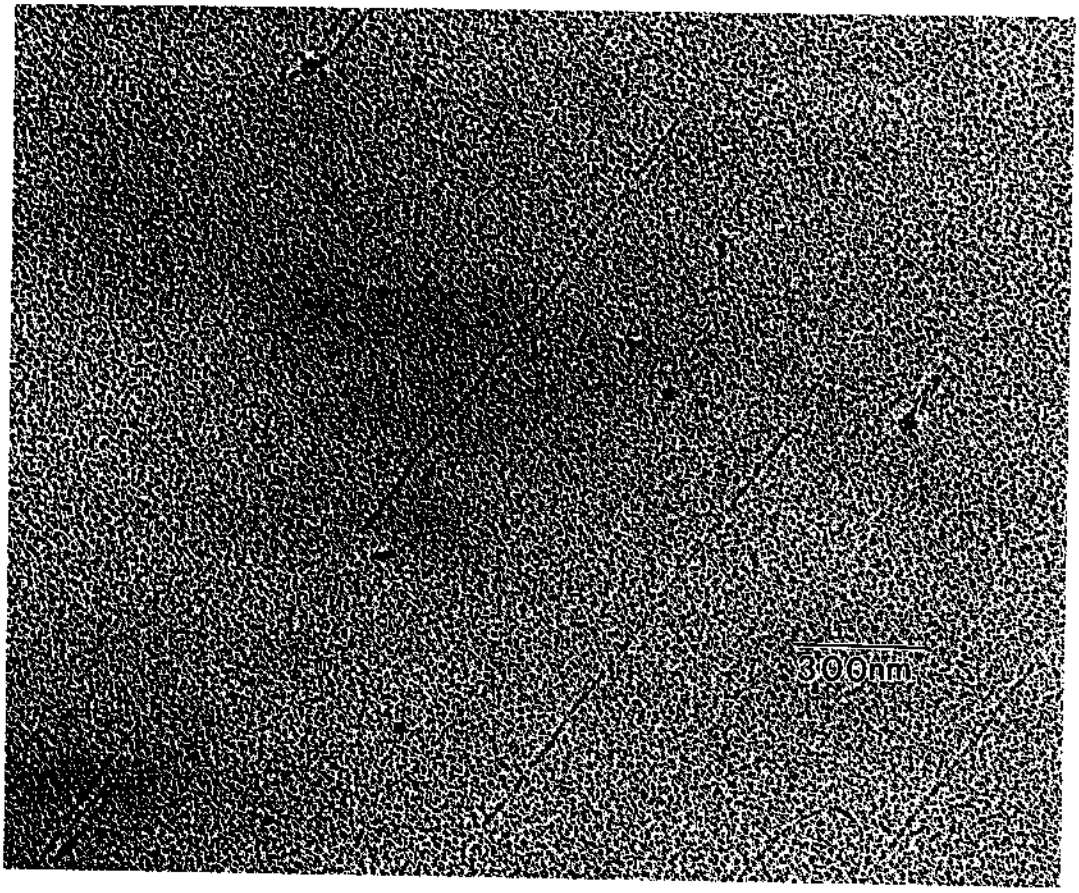

(c)

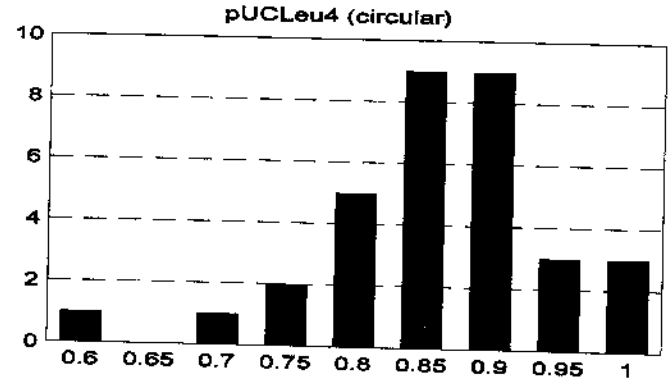

(a)

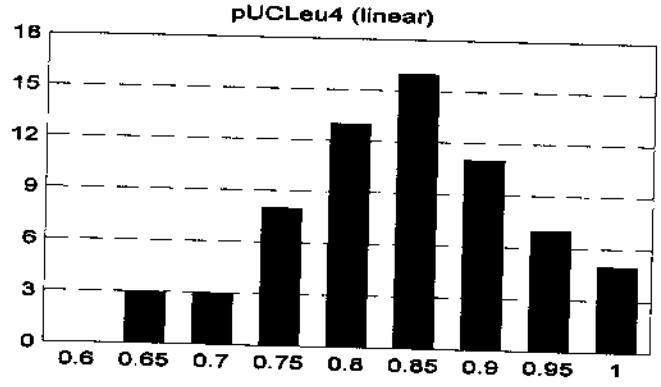

(b)

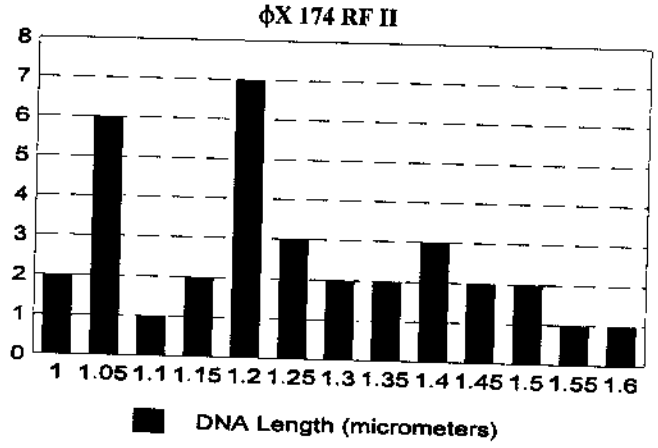

(C)

Figure 5.7 DNA size distribution analysis of (a) circular pUCLeu4, (b) linear pUCLeu4 and (c) ϕX 174 RF II. The average sizes are 0.89 μm, 0.84 μm, and 1.25 μm, respectively.

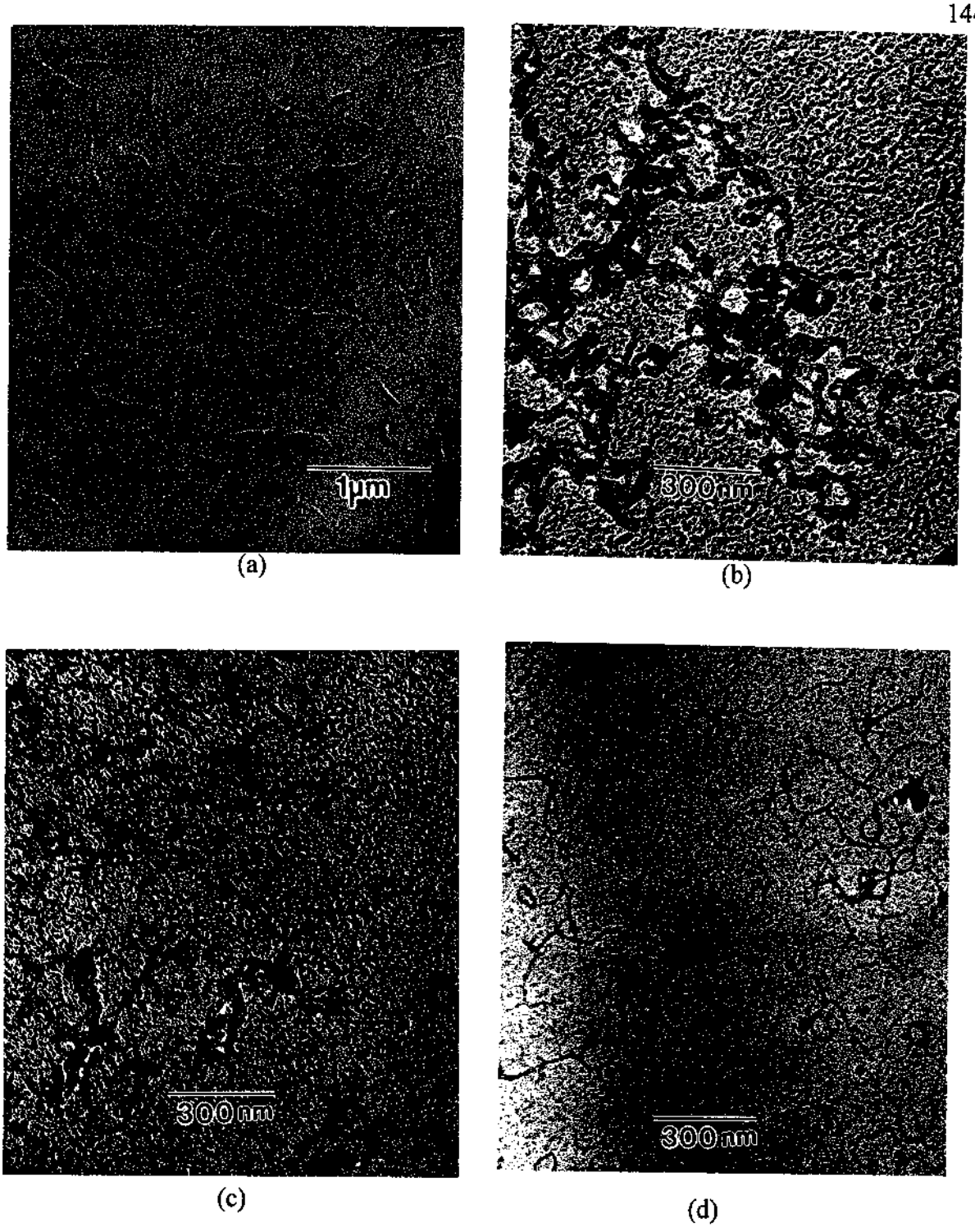

Figure 5.8 Unidentified microstructures observed in the linear pUCLeu4 DNA samples prepared using the Kleinschmidt method. Micrographs (e) and (f) are before metal shadowing. The others are after metal shadowing.

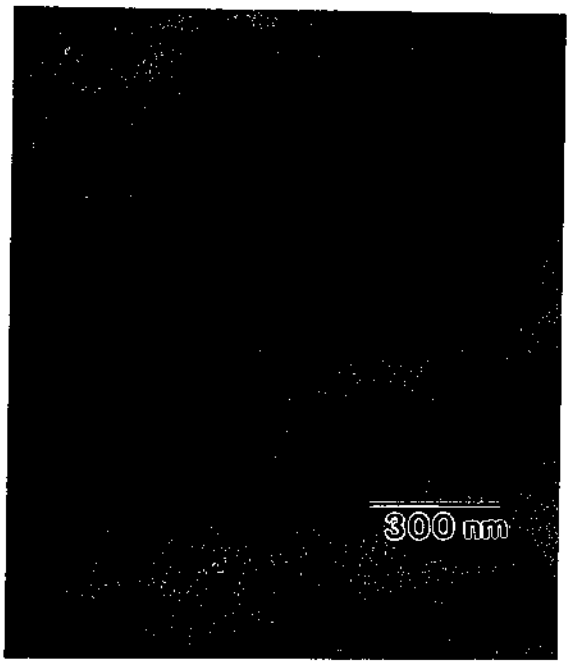

(e)

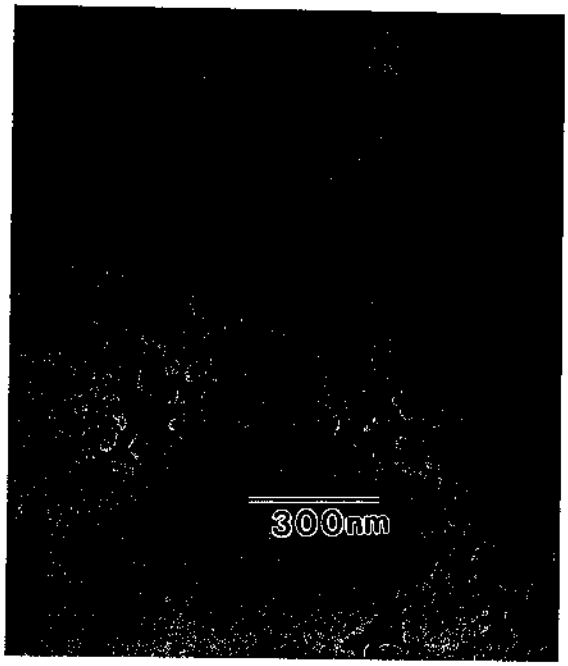

(f)

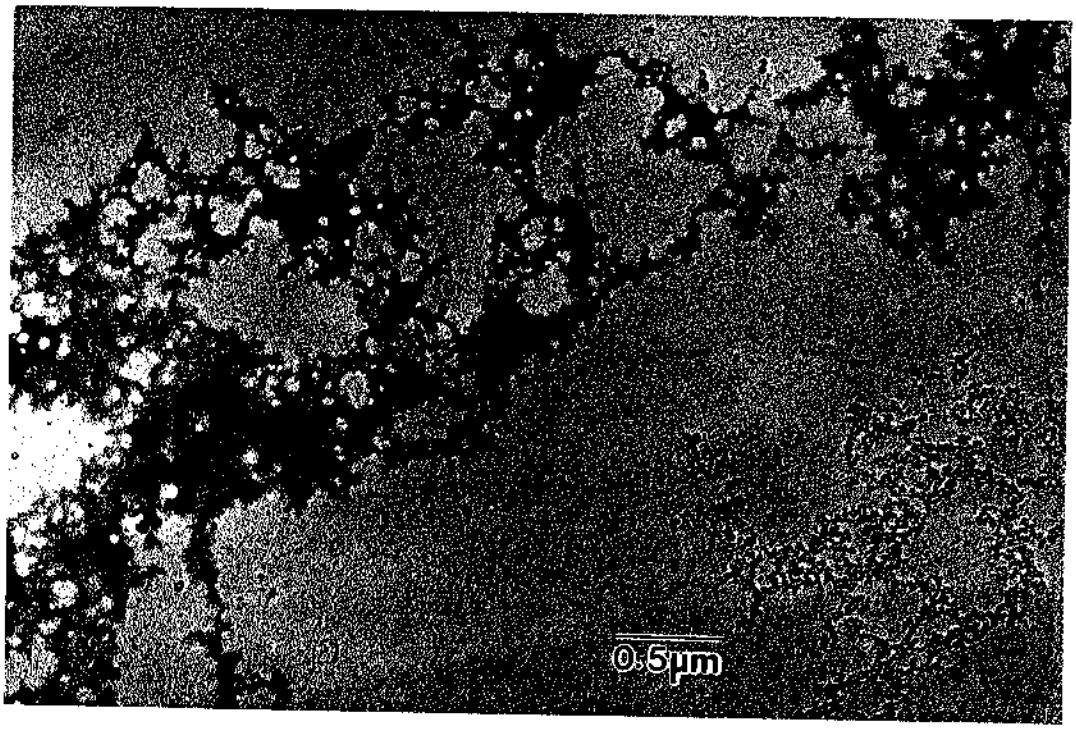

(g)

REFERENCES

1. *Product Catalog and Reference Guide,* Cat. # 302-2s (New England Biolabs, Inc., Beverly, MA, 1996), p. 80.

2. L. W. Coggins, "Preparation of Nucleic Acids for Electron Microscopy" in *Electron Microscopy in Molecular Biology,* edited by J. Sommerville and U. Scheer, (IRL Press, Oxford, England, 1987), pp. 1-14.

3. L. T. Chow and T. R. Broker, "Mapping RNA:DNA Heteroduplexes By Electron Microscopy" in *Electron Microscopy in Biology Vol. I,* edited by J. D. Griffith, (John Wiley and Sons, New York, 1981), pp. 141-156.

4. Video-Based Image Analysis System, MCID M4, Imaging Research, Inc. (St. Catherines, Ontario, Canada, 1992).

5. M. Sabat and B. Lippert, *Metal Ions In Biological Systems,* edited by A. Sigel and H. Sigel, (Marcel Dekker, Inc., New York, 1996), pp. 143-168.

CHAPTER 6

VARIATIONS OF THE EXPERIMENTS

6.1 Introduction

As described in Chapter 4, fabricating nanometer scale Q-CdS structures using DNA templates could not be reliably repeated. Some difficulties were anticipated because there were no previous experiments and because of the molecular scale. However, millions of Q-CdS semiconductors structures should have been observed. Even though the experiments were repeated, the negative results remained basically the same. For the last few experiments, CdS nanoparticles were not observed either. Unidentified microstructures, such as highly concentrated net-like structures, were occasionally found.

To investigate the causes of these negative results, the materials involved in these experiments were examined one at a time. The characterization of the surface structure of the carbon films and the microstructural study of DNA only samples were described in Chapters 4 and 5, respectively. In this Chapter, the other experiments used to investigate the causes of the problems, such as CdS only samples, variations of the cadmium ion and DNA concentrations, and different Cd^{2+}/DNA complex deposition methods, are described.

The experimental variations were based on the results of the previous experiments. A list of experiments with the variations of cadmium and sulfide

concentrations, and different deposition methods is presented in the Table 6.1.

First, as noted before, the CdS nanoparticles which were commonly observed on the blank-carbon film were not observed in several experiments. Therefore, samples with CdS only were examined. The Cd^{2+} concentrations were 1 mM, 2 mM and 4 mM.

Second, after analysis of the DNA only samples studied by the Kleinschmidt method (Chapter 5), we realized that the 2 mM DNA solution used in previous experiments was very large, and the highly concentrated net-like microstructures found in previous experiments might be caused by this high DNA concentration. Therefore, the DNA concentration was changed to 5 μg/ml for pUCLeu4 plasmid DNA and 1 μg/ml for ϕX 174 RF II DNA. Two sets of samples were made with two different concentrations of Cd^{2+} (2 mM and 2 μM) to examine the effect of DNA/Cd^{2+} ratio.

Third, as an alternative deposition method, the Cd^{2+}/DNA complexes were adsorbed onto the carbon coated Cu TEM grid by putting the grid on the Cd^{2+}/DNA solution instead of dropping the complexes onto the TEM grid. This second method might prevent the deposition of highly concentrated Cd^{2+}/DNA complexes at a few local areas, as occurred with the dropping and blotting method.

Fourth, DNA only was adsorbed onto the carbon coated TEM grids, followed by Cd^{2+} reaction with the DNA by dipping the TEM grids into Cd^{2+} solution. With this method, since the DNA interacts with cadmium after the DNA is attached to the carbon film, the shapes of the DNA templates should not be affected by cadmium interactions. This was the original method envisioned for the fabrication of CdS/DNA mesoscale semiconductor structures on solid substrates.

6.2 Experimental

6.2.1 CdS only

The freshly mixed cadmium ion solutions, 4 mM, 2 mM and 1 mM, were prepared according to the method described in Section 4.2.3. One or two drops of each solution were placed on carbon-coated TEM grids. The TEM grids were dried in air for approximately 30 minutes, then exposed to H_2S gas for approximately 30 minutes in the same way as the Q-CdS/DNA samples were prepared (described in Section 4.2.4).

Conventional and analytical transmission electron microscopy, BF, DF, SADP, and XEDS were used to characterize the microstructures, for phase identification, and to determine the chemical composition of the materials. The particle size distribution of the hexagonal phase (wurtzite) CdS was analyzed using a Houston Instruments Digitizing Tablet interfaced to a PC.

6.2.2 Variations of Cadmium Concentration

In these experiments, the methodology used was the same as described in Chapter 4, but the cadmium ion concentration was varied. In the previous experiments, 2 mM DNA (in nucleotide) and 2 mM Cd^{2+} solutions were used. As discussed in Section 4.3.4 the amount of cadmium used (one cadmium ion per nucleotide) may be insufficient to produce numerous CdS/DNA nanostructures. Also, some of the Cd^{2+} should interact with the carbon substrate. Therefore, approximately one hundred times larger Cd^{2+}/DNA ratio was used in this experiment. Two ml of 2 mM cadmium was mixed with 2 ml of 5 μg/ml (approximately 15 μM in nucleotide) pUCLeu4 plasmid

DNA or 2 ml of 1 μg/ml (approximately 3 μM in nucleotide) of the ϕX 174 RF II DNA. In other trials, 2 ml of 2 μM Cd^{2+} was mixed with 2 ml of 5 μg/ml pUCLeu4 plasmid DNA or 1 μg/ml of 2 ml ϕX 174 RF II DNA, close to the 1:1 ratio used in previous experiments, for comparison.

The experimental procedures were the same as those described in Sections 4.2.3 and 4.2.4. Bright field TEM and SADP were the major characterization tools. The samples were examined both with and without metal shadowing.

6.2.3 Cd^{2+}/DNA Deposition by Floating Grids on the Solutions

As discussed in Chapter 4, we believed that the high concentration of supercoiled DNA and the high density of net-like microstructures found over large, localized areas were due to the sample deposition method. In separate experiments, the carbon-coated TEM grid was placed on the Cd^{2+}/DNA complex instead of dropping the mixture onto the TEM grid. In this way, the Cd^{2+}/DNA complexes can be anchored uniformly over the carbon film by adsorption.

Freshly mixed Cd^{2+} and DNA solutions were used because CdS nanoparticles were not observed either with DNA or on the plain-carbon film in earlier experiments. In addition, the numbers of DNA molecules found in previous experiments were far smaller than the numbers found using the Kleinschmidt method described in Chapter 5.

The concentrations and the Cd^{2+}/DNA ratio (2 μM and 2 mM cadmium solutions with either 5 μg/ml pUCLeu4 plasmid DNA or 1 μg/ml ϕX 174 RF II DNA), were the same as described in Section 6.2.2. The preparation and mixing of those solutions were

the same as described in Section 4.2.3.

One or two drops of the well-mixed Cd^{2+}/DNA complexes were dropped on a clean glass slide using a Pasteur pipet. Carbon coated TEM grids were placed on the complex solution with the carbon-coated side down using tweezers. Approximately one or two minutes later the grid was picked up and placed on filter paper with the carbon film side up to remove the excess water. After air drying for approximately 30 minutes, the grids were exposed to H_2S gas as described in Section 4.2.4. With this deposition method, either wet or dry carbon film can be used.

Conventional and analytical transmission electron microscopy (JEOL 100CX and 200CX) and BF, DF, SADP, and XEDS were used to characterize the microstructures, crystallography, and chemical composition of the CdS/DNA and CdS nanoparticles. A high take-off angle x-ray detector with a TN-5500 computer system from Tracor-Northern[1] was used to obtain the XEDS spectra. The samples were characterized without metal shadowing.

6.2.4 DNA Only

Analysis of the previous experiments, floating the TEM grids on the complex solution, revealed bundles of CdS/DNA microstructures in all three types of samples. We believed that these bundled microstructures were formed by the interaction of Cd^{2+} ions and DNA. As will be discussed in Section 6.3.3, the tangled DNA structures could form when the extra cadmium ions combined with the DNA anions pull other DNA molecules to interact with each other. To prevent tangling of the CdS/DNA structures, DNA

molecules were anchored onto the carbon film first, and then the grids with the attached DNA were dipped in Cd^{2+} solution to allow the Cd^{2+} ions to interact with the DNA molecules directly.

From previous experiments, a DNA concentration of 5 μg/ml was known to be too large. Therefore, two different DNA concentrations, 5 μg/ml and 0.5 μg/ml, for both pUCLeu4 plasmid DNA and ϕX 174 RF II DNA were used with 2 mM cadmium solution. The 5 μg/ml DNA was used because we anticipated that many of the DNA molecules attached to the carbon film would be washed away when the grids were dipped into the cadmium solution. A high cadmium concentration, 2 mM, was used to reduce the interaction (dipping) time which might reduce the removal of DNA from the grids.

In addition, DNA only samples were made from the same 5 μg/ml DNA solution using the same deposition method (floating) to compare the concentration and structures of DNA only to those of CdS/DNA. In this way we could examine the percentage of DNA washed away when the grids were dipped into the cadmium solution, and we could examine the microstructures before and after CdS nanoparticle formation.

Two sets of samples with two different DNA concentrations, 5 μg/ml and 0.5 μg/ml, were prepared by dipping them into 2 mM cadmium solution. The DNA and cadmium solutions were prepared as described in Section 4.2.3. One or two drops of DNA solution were dropped onto a clean glass slide with a Pasteur pipet. Carbon-coated TEM grids were placed on the DNA solution, and after one or two minutes the grids were picked up and placed on filter paper to remove the excess water. The samples were air dried for 5 to 10 minutes, then dipped very slowly into cadmium solution one by one,

trying not to disturb the solution to reduce the washing away of the DNA from the grid. After approximately 3 to 5 minutes, the grids were placed on filter paper with the carbon film side up, and were air dried for approximately 30 minutes. The grids were then exposed to H_2S gas for approximately 30 minutes, as described in Section 4.3.4.

Bright field and dark field TEM were used for microstructural characterization. The samples were examined both and without metal shadowing. Some samples were carbon shadowed to enhance the view of the microstructures in the electron microscope. Carbon was used for shadowing because it does not significantly affect the SADP and XEDS data. DNA only samples were also metal shadowed.

6.3 Results and Discussion

6.3.1 CdS Only

1. Diamond cubic phase. Figure 6.1 shows typical microstructures of CdS nanoparticles formed on blank-carbon films deposited by dropping cadmium solution onto the grid as described in Section 4.2.4. The micrographs in Figures 6.1a and 6.1b are BF and DF images of the 1 mM CdS sample, respectively; Figures 6.1c and 6.1d are BF and DF images of the 2 mM sample; Figures 6.1e and 6.1f are BF and DF images of the 4 mM sample. The DF images were recorded from the same areas as the BF images, and the [111] diffraction ring was used. The CdS particle density depended on the cadmium ion concentration used. According to the BF micrographs, the Q-CdS particle size distributions of all three samples are similar to each other and the cadmium concentration does not affect to the CdS particle size. The SADP shown in Figure 6.2 is typical for all

three CdS samples. The measured lattice spacings match the diamond cubic phase (Hawleyite) as shown in Table 6.2. XEDS analysis confirmed that the nanoparticles consisted of cadmium and sulfur.

2. Hexagonal-close packed phase. The hexagonal close-packed phase (wurtzite) of CdS was also found in both the 1 mM and 4 mM cadmium samples. Figures 6.3a and 6.3b are BF and DF images of the hexagonal CdS particles in the 4 mM sample. The DF image is the same area as the BF image. Figure 6.4 is a typical electron diffraction pattern of the hexagonal CdS particles (Table 6.2). The [101] planes were used to form the DF image. The hexagonal CdS crystallites were found in the same sample as the cubic CdS nanoparticles. But, as we can see from the Figures, the two phases are not found together in the same area. The SADP data shown in Figures 6.2 and 6.4 also indicate that the cubic and hexagonal phases do not coexist at the same location. However, this data demonstrates that the two different CdS phases can be grown under the same fabrication conditions.

Figure 6.5 shows a size distribution analysis for 207 hexagonal CdS nanocrystals. The average is 38.4 nm, which is approximately 7 times larger than the diamond cubic phase nanoparticles fabricated using calf thymus DNA (Chapter 3). Size distribution data for cubic CdS in this experiment is not available because we do not have enough HREM data for accurate measurement. However, according to the Figure 6.6a, a HREM micrograph of CdS/circular DNA deposited by the dropping deposition method, the cubic CdS nanoparticles are approximately 4 to 5 nm in diameter. Hexagonal CdS was also found in a previous experiment when the samples were deposited on a derivatized glass

slide by dropping the CdS/pUCLeu4 plasmid DNA complex solution. Figure 6.6b shows the HREM lattice image of hexagonal CdS nanoparticles formed on the pUCLeu4 plasmid DNA on derivatized glass. The hexagonal CdS particles are approximately 10 to 15 nm in diameter which is 2 to 3 times larger than the cubic CdS particles. This data confirms Horst Weller's observation that hexagonal CdS is found only as macrocrystallites.[2] According to Figure 6.3, most of the hexagonal CdS crystals are cubic or rectangular in shape with sharp corners, while the cubic phase crystals observed both in conventional TEM and HREM are nearly spherical.

The cubic and hexagonal CdS crystallite microstructures were inhomogeneously spread over the sample. This suggests that the dropping method of deposition results in CdS formation only in the area contacted by the solution.

3. Microbubble structures. Large numbers of microbubbles were found in the 4 mM CdS only samples. As shown in Figure 6.7a, the sizes and shapes of the microbubbles varied. Many circular bubble structures were examined at high magnification to compare the bubble microstructures with CdS/circular DNA. As shown in Figure 6.7b, the bubbles are clearly distinguishable from the CdS/DNA. For the CdS/DNA, the structures have dark contrast at the location of the CdS/DNA or CdS nanoparticles. On the other hand, the intensity gradually varies from the inside to the outside of the circle for the bubbles. Crystals were not detected using SADP of the microbubbles. XEDS chemical analysis indicated that the main element in the bubbles was chlorine. The bubble-like microstructures were found only with 4 mM cadmium solution. The cadmium solution was prepared from $Cd(ClO_4)_2 \cdot 6H_2O$, so the chlorine

might have been deposited during sample preparation.

6.3.2 Variations of Cadmium Concentration

Before metal shadowing, CdS/DNA structures were not observed for any of the six samples, low-CdS (2 μM Cd^{2+}) and high-CdS (2 mM Cd^{2+}) with circular and linear plasmid DNA, or ϕX 174 RF II DNA. Therefore, the samples were examined after metal shadowing to look for the presence of any DNA or CdS/DNA. After metal shadowing, DNA structures were observed in most samples, but CdS electron diffraction patterns were not observed. The DNA microstructures in Figures 6.8a and 6.8b are from low-CdS/DNA with circular and ϕX 174 RF II DNA, respectively. These two micrographs show high concentrations of DNA microstructures. Figure 6.9 shows the microstructure of a high cadmium CdS/circular DNA sample. This micrograph shows a network in which the DNA molecules are connected to each other. SADP did not detect CdS nanoparticles in this sample either. The DNA shown in Figure 6.9 is similar to the highly concentrated net-like structures shown in Figure 4.11, with a lower density. Many other structures similar to relaxed linear DNA and supertwisted DNA were observed after metal shadowing.

In these experiments, CdS nanoparticles were not found even though the cadmium to DNA concentration ratio was about one hundred to one thousand times that used in previous experiments: 2 mM cadmium to 10^{-5} M or 10^{-6} M DNA. In Chapter 4, we proposed that CdS nanoparticles were not detected by TEM because the cadmium concentration compared to the DNA concentration was too small. However, this

assumption has now been shown to be incorrect.

When repeating experiments, sometimes Q-CdS nanoparticles were found and sometimes they were not. In later experiments, we realized that whenever freshly mixed Cd^{2+} solution was used Q-CdS nanoparticles were found all over the grids, whereas when cadmium stock solution was used, Q-CdS nanoparticles were not found at all. This may be the reason that CdS/DNA nanostructures were not observed before metal shadowing even though it was found that a large number of DNA molecules existed in most samples.

The use of freshly mixed Cd^{2+} solution is an absolute requirement.

6.3.3 Cd^{2+}/DNA Deposition by Floating Grids on the Solutions

Figure 6.10 shows typical CdS/DNA microstructures of the three DNA samples prepared by floating the grids on the Cd^{2+}/DNA complex solution. The samples were made with freshly mixed DNA and cadmium solutions and the microstructures were recorded without metal shadowing. Those microstructures are for 2 mM cadmium/5 μg/ml DNA for the pUCLeu4 DNA, and 2 mM cadmium/1 μg/ml DNA for the ϕX 174 RF II DNA. Figure 6.10a is a bright field image of CdS/circular DNA and Figure 6.10b and 6.10c are dark field images of CdS/linearized and ϕX 174 RF II DNA, respectively. The DF images were recorded using the [111] lattice planes of CdS. These microstructures show bundled DNA with attached CdS nanoparticles. Selected area diffraction patterns (Figure 6.11) of the bundled area are identical to the cubic CdS patterns observed in the previous experiments (Figure 4.6). X-ray energy dispersive spectroscopy (XEDS) in STEM mode was used to analyze the chemical composition of

the material. The XEDS spectrum (Figure 6.12a) was collected for approximately 3 hours using a high take-off angle x-ray detector and a JEOL 200CX. As shown in the XEDS spectrum, the nanoparticles in the bundled DNA contain cadmium and sulfur. The silicon K_α peak is due to fluorescence of the silicon-lithium detector due to the long counting time, as mentioned in Chapter 4.[3] Figure 6.12b is a STEM micrograph showing the area from which the XEDS spectrum was obtained. Figure 6.13 shows a pair of lower magnification BF and DF images of the 2 mM cadmium to 5 μg/ml circular DNA sample. From these Figures we see that the DNA structures are visible due to the presence of CdS nanoparticles. The contrast of the bright field image varies with the number of Q-CdS particles involved. These micrographs also show that 5 μg/ml of DNA is too concentrated to fabricate individual mesoscale semiconductor structures of Q-CdS. These bundled DNA microstructures were observed over large areas at different locations in all three samples. This means that deposition by floating the grid on the solution of CdS/DNA complexes leads to uniform DNA deposition over all of the TEM grid.

From Figures 6.10 and 6.13, we can assume that the bundled DNA structures were formed in solution when the DNA was mixed with aqueous cadmium due to the action of the cadmium ions. As discussed in Chapters 2 and 5, the DNA molecules are generally not tangled together before they are mixed with cadmium. The binding of metal ions to DNA can lead to the formation of crosslinks between nucleic acids.[4] The Figures show that the bundled structures are denser in the middle of the bundles than on the outside, and that the DNA molecules on the outside of the bundles are stretched out. The DNA aggregation can occur when the cadmium ions combined with the anions of the DNA and

interact with other DNA molecules until the cations are neutralized. The DNA molecules on the outside of the bundles may be stretched out due to repulsion between excess cadmium ions, or because there are no other DNA molecules to bind to for cadmium neutralization. If this assumption is correct, the CdS/circular DNA nanostructure should be nearly circular and CdS/linear DNA should be linear. In addition, the high concentration of net-like microstructures found in the previous experiments might due to both the deposition method and the bundling of DNA molecules caused by cadmium.

In Figures 6.10 and 6.13, Q-CdS nanoparticles are found only with DNA, and are not found on the blank-carbon films when DNA is present. Since Q-CdS nanoparticles are found on the blank-carbon substrate when DNA is not present, it is likely that CdS forms preferentially on DNA compared to the amorphous carbon substrates.

Neither Q-CdS/DNA nor Q-CdS nanoparticles were observed in the low cadmium concentration samples with 2 μM Cd^{2+} to 5 μg/ml pUCLeu4 DNA or 1 μg/ml ϕX 174 RF II DNA. This means that 2 μM cadmium is insufficient compared to 5 μg/ml or 1 μg/ml DNA to form Q-CdS easily observable by TEM. As discussed in Chapter 4, this may be the reason why Q-CdS particles were not observed in previous experiments carried out with a 1:1 cadmium: DNA ratio. With a 1:1 ratio, there is enough cadmium to interact with all the binding sites of the DNA, but not enough to form CdS nanoparticles large enough to be detected by TEM. Because of this, as shown in Figures 4.11a and 4.13a, the net-like microstructures were probably formed, but the CdS nanoparticles could not be detected by electron diffraction.

The other possible reason why the CdS/DNA structures were not observed in the

low cadmium samples is the deposition method used. Compare the bundled CdS/DNA structures (Figures 6.10 and 6.13) to the highly concentrated net-like microstructures formed using the dropping method (Figure 4.11). The deposition from the floating method is far less than from the dropping method. As a result, it was difficult to detect by TEM, since the density of the DNA was very low.

6.3.4 DNA Only

1. DNA only samples. The microstructures of the three DNA only samples with 5 μg/ml DNA deposited by floating the grids on the DNA solutions are shown in 6.14a, 6.14b, and 6.14c for circular, linear, and ϕX 174 RF II DNA, respectively. As seen in the Figures, many individual relaxed DNA molecules were observed in all three samples. From the results, it can be assumed that sufficient DNA will be attached to each grid before dipping the grids in cadmium ion solution. Most of the opened DNA molecules in Figure 6.14b are unwound due to the repulsive forces between the neighboring phosphate anions as predicted by theory.[5]

Compared to the Kleinschmidt method, the DNA deposition performed in these experiments was simpler and gave similar results. However, only a few supercoiled DNA molecules were observed. This suggests that DNA deposited on carbon substrates interacts with the carbon film. Few supercoiled DNA molecules were attached to the carbon film here because of insufficient contact area between the DNA and the carbon film.

2. CdS/DNA structures without metal shadowing. The CdS/DNA microstructures for 5 μg/ml circular DNA samples deposited by floating the grids on the DNA solution and dipping the grids into 2 mM cadmium solution followed by reaction with H_2S gas are shown in Figure 6.15. This sample preparation was performed as an alterative method to prevent the aggregation of DNA by the cadmium ions. These are typical microstructures recorded before metal shadowing. In most cases, (Figures 6.15 (a), (b), and (c)), fewer CdS crystallites are formed on the DNA by this dipping method compared to previous experiments. Apparently, the CdS nanoparticles are also smaller than those shown in Figures 4.6a and 6.1. Therefore, it was very difficult to find these structures using TEM, and DF images and diffraction patterns could not be observed. However, for one sample immersed in cadmium solution for 30 minutes, a few CdS/DNA microstructures with more numerous Q-CdS (Figure 6.15d) were found with the SADP of cubic CdS. The length of the CdS/DNA structure is approximately 0.88 μm, which is about the average DNA size measured using the Kleinschmidt method.

Even though SADP and XEDS data for these microstructures are not available, we still believe that these microstructures are Q-CdS/DNA. First, these microstructures are similar to the DNA only structures in Figure 6.14. Second, it is known that DNA alone cannot be observed using TEM, as discussed in Chapter 4. Third, the diameter of the CdS/DNA is about double that of DNA alone. The microstructures shown in Figures 6.15 (a), (b) and (c) are approximately 5 nm thick, while A-form DNA is approximately 2.55 nm thick.[6] This is about the average size of the CdS nanoparticles and about two times larger than the A-form of DNA.

The diameters of the Q-CdS/DNA structures found in these experiments are smaller than found in previous experiments. This may due to the shorter reaction times. Another possibility is the different amount of cadmium deposited on the carbon substrate when using the dropping and the dipping methods. The dropping method deposits not only Cd^{2+}/DNA complex, but also deposits the extra cadmium contained in the solution on the carbon film. Therefore, the extra cadmium deposited on the carbon substrate can be used to form CdS nanoparticles when the grid is exposed to H_2S gas. With the dipping method, the CdS particles are formed with cadmium bound only to DNA molecules with few other ions on the carbon substrate.

3. CdS/DNA microstructures with carbon shadowing. The samples were examined after low-angle carbon shadowing to enhance contrast in the TEM. As mentioned before, finding the CdS/DNA structures was extremely difficult. Often, DNA-like microstructures were detected, but the images displayed only weak contrast.

Figure 6.16 shows typical CdS/DNA structures after carbon shadowing. As expected, the microstructures were observed with little enhancement of image contrast because carbon is a light element. Many isolated and connected DNA structures were observed in each sample. Figures 6.16 (a) and (b) show the microstructures of CdS/5 μg/ml circular DNA and CdS/0.5 μg/ml linear DNA. SADP and DF data could not be observed. Since CdS nanoparticles were not detected on the CdS/DNA structures, a high concentration of CdS nanoparticles formed on bundles of supercoiled DNA molecules was used to obtain an SADP (Figure 6.17). The DF image was recorded using the [111] CdS lattice planes. A relaxed linear DNA structure was found at the same

location as the CdS/supercoiled DNA, and the DF image of the relaxed DNA was recorded simultaneously (Figure 6.17c). The first two rings of the diffraction pattern shown in Figure 6.17c match cubic CdS. The DF image of the DNA microstructure appears bright, as do the CdS/supercoiled DNA structures. This means the nanoparticles on the DNA molecule are also cubic CdS. Using DF mode and the same diffraction conditions, additional CdS/DNA microstructures were found in different samples. Figures 6.18 (a) and (b) are pairs of BF and DF images of low DNA concentration (0.5 μg/ml) CdS/linear and CdS/ϕX 174 RF II DNA, respectively. Since the DNA structures were observed in DF mode, we can assume that the DNA molecules are covered with CdS nanoparticles. However, the individual nanoparticles are not visible.

Evidence of Q-CdS particles formed on DNA can be found by comparing the microstructures of CdS/DNA with those of DNA alone. First, compare the DNA only structures shown in Figure 6.14 with the CdS/DNA structures shown in Figure 6.15 (the magnification is the same). The thicknesses of the CdS/DNA structures are about double the thicknesses of the DNA only structures. Second, the DNA only structures shadowed with metal are continuous with an even thickness while the CdS/DNA structures are discontinuous with varying thickness. Since the CdS/DNA structures are visible in the TEM only due to the presence of CdS nanoparticles, the discontinuities are areas without CdS nanoparticles. The thickness of the structure varies because the CdS particle sizes vary. Third, compare the microstructures of the high concentration of DNA (Figure 6.14b) with those of CdS/DNA (Figures 6.15a and 6.18). The DNA molecules do not interact each other when there is no cadmium. However, when cadmium is present the

DNA molecules are interact and connected to each other.

From the data presented in this section, the DNA anchored by this experimental method remained on the carbon film when the grids were dipped into cadmium solution. Still, even with lowest DNA concentration, 0.5 μg/ml, the DNA was too concentrated to form individual isolated CdS/DNA structures.

4. CdS/DNA structures with metal shadowing. The CdS/DNA microstructures were studied further using heavy metal shadowing. Figure 6.19 shows the microstructures of CdS/DNA with 5 μg/ml circular DNA after metal shadowing. The length of the microstructure shown in Figure 6.19a is approximately 0.9 μm and that shown in Figure 6.19b is approximately 1.17 μm. SADP and DF data were not obtained from these microstructures.

6.4 Summary and Conclusions

In previous experiments, large numbers of CdS/DNA nanoscale structures were expected, but sometimes neither CdS/DNA structures nor Q-CdS particles were found. High concentrations of net-like structures were often found. To investigate the causes of these observations, various concentrations of cadmium (2 mM and 2 μM) and DNA (5 μg/ml, 1 μg/ml, and 0.5 μg/ml), diverse ratios of cadmium to DNA, and different deposition methods were tried. First, various concentrations of CdS only without DNA were examined, since DNA only samples had already been examined as reported in Chapter 5. Second, the samples were prepared using the same dropping method but the DNA concentration was reduced to 5 μg/ml, and two different cadmium

concentrations, 2 mM and 2 μM were used. Third, to prevent the formation of highly concentrated microstructures at localized areas, the samples were prepared by floating the grids on the Cd^{2+}/DNA solution. These samples were made with two different cadmium concentrations (2 mM and 2 μM) to one fixed DNA concentration, 5 μg/ml for the pUCLeu4 and 1 μM for ϕX 174 RF II. Fourth, to inhibit the aggregation of DNA by Cd^{2+}-binding, DNA only was deposited first, then combined with Cd^{2+} by dipping the TEM grids into Cd^{2+} solution. DNA only samples were made from the same DNA solution using the same deposition method to check the percentage of the attached DNA on the grid before and after dipping into cadmium solution and to compare the DNA only structures with CdS/DNA.

Freshly prepared DNA and cadmium solutions were used for the last two sets of experiments. The samples were examined with/without metal shadowing, and with carbon shadowing. Both conventional and analytical transmission electron microscopy were used to characterize the samples.

Two different CdS phases, zincblend diamond cubic (Hawleyite) and hexagonal close packed (wurtzite), were found in the CdS only samples. Even though the two phases were found on the same grid, they were found at different locations. The average crystal size of hexagonal CdS was 38.4 nm, approximately 7 times larger than the cubic phase fabricated on calf thymus DNA in solution (5.6 nm, reported in Chapter 3). The hexagonal CdS particles were cubic or rectangular, while the cubic CdS nanoparticles were nearly spherical.

Large numbers of microbubbles were found in the 4 mM CdS only samples. The

sizes and shapes of the microbubbles varied and the bubbles were easily distinguishable from CdS/DNA.

CdS/DNA structures and CdS nanoparticles were not observed before metal shadowing for all six samples prepared by the dropping method. After metal shadowing, DNA structures without CdS nanoparticles were found in most of the samples. SADP did not indicate the presence of the CdS nanoparticles in the DNA structures. In later experiments, we realized that the CdS/DNA nanostructures were observed only when the freshly mixed Cd^{2+} solution was used. **Therefore, use of freshly mixed Cd^{2+} solution is an absolute requirement.**

Bundled DNA structures with CdS nanoparticles were found in all three 2 mM cadmium to 5 μg/ml plasmid and 1 μg/ml ϕX 174 RF II DNA samples prepared by floating the grids on Cd^{2+}/DNA solution. Selected area diffraction pattern data from aggregated DNA areas identified cubic CdS. Chemical composition analysis by XEDS showed that the nanoparticles on the bundled DNA consist of cadmium and sulfur. The aggregated DNA structures were formed due to cadmium ion interactions when the aqueous cadmium solution was mixed with the DNA solution. Bundled DNA microstructures were observed over large areas and different locations for all three samples. This means that material can be evenly deposited over the grids by floating the grids on the solution.

Neither CdS/DNA nor Q-CdS microstructures were observed for all three low cadmium concentration samples, 2 μM Cd^{2+} to 5 μg/ml plasmid and 1 μg/ml ϕX 174 RF II DNA, respectively. This means that the ratio of 2 μM cadmium to 5 or 1 μg/ml of

DNA is insufficient for Q-CdS nanoparticles formation to be observed using TEM.

Many isolated CdS/DNA microstructures were found after depositing the DNA alone followed by dipping the samples in cadmium solution followed by exposure to H_2S gas. The numbers and sizes of the CdS crystallites formed on the DNA by this method are fewer and smaller than those found in previous experiments. The CdS/DNA microstructures found in this experiment are approximately 5 nm thick. As a result, SADP and DF data could not be obtained.

Isolated and connected CdS/DNA structures were observed after carbon shadowing. DF imaging of the DNA microstructures showed a high density of CdS nanoparticles formed on supercoiled DNA. The DNA structures were visible due to the CdS nanoparticles on the DNA.

Evidence of Q-CdS particles on DNA is found by comparing the thickness variation of the microstructures of CdS/DNA to those of DNA only. The CdS/DNA structures are about twice as thick as DNA only structures. The thickness of the CdS/DNA varies, while it is uniform for the DNA only structures. DNA anchored by this method remained on the carbon film when the grids were dipped into cadmium solution. A DNA concentration of 0.5 μg/ml is still too concentrated for the formation of individual CdS/DNA structures. In the DNA only experiments, we were be able to demonstrate the inhibition of aggregation of DNA induced by Cd^{2+}-binding.

Table 6.1 List of the experiments.

Experiments	Sample Preparation Methods	Variations
CdS only	Deposit Cd^{2+} by dropping the Cd^{2+} solution onto the TEM grids and expose to H_2S gas.	4 mM Cd^{2+}
		2 mM Cd^{2+}
		1 mM Cd^{2+}
Variations of cadmium concentration to fixed DNA concentration (circular, linear and ϕX 174 RF II).	Deposit Cd^{2+}/DNA by dropping the Cd^{2+}/DNA solution onto the grid and expose to H_2S gas.	2 mM Cd^{2+}/5 μg/ml (15 μM) pUCLeu4 DNA
		2 mM Cd^{2+}/3 μg/ml (3 μM) ϕX 174 RF II
		2 μM Cd^{2+}/5 μg/ml (15 μM) pUCLeu4 DNA
		2 μM Cd^{2+}/1 μg/ml (3 μM) ϕX 174 RF II
Circular, linear and ϕX 174 RF II	Deposit Cd^{2+}/DNA by floating grids on Cd^{2+}/DNA solution and expose to H_2S gas.	2 mM Cd^{2+}/5 μg/ml (15 μM) pUCLeu4 DNA
		2 mM Cd^{2+}/1 μg/ml (3 μM) ϕX 174 RF II
		2 μM Cd^{2+}/5 μg/ml (15 μM) pUCLeu4 DNA
		2 μM Cd^{2+}/1 μg/ml (3 μM) ϕX 174 RF II

DNA only deposition (circular, linear and ϕX 174 RF II). The samples were examined without/with metal shadowing, or with carbon shadowing.	Deposit DNA by floating grids on DNA solution. React with cadmium by dipping the grids into cadmium solution. Expose the grids to H_2S gas.	2 mM Cd^{2+}/5 μg/ml (15 μM) pUCLeu4 DNA
		2 mM Cd^{2+}/1 μg/ml (3 μM) ϕX 174 RF II DNA
		2 mM Cd^{2+}/0.5 μg/ml (1.5 μM) pUCLeu4 DNA
		2 mM Cd^{2+}/0.5 μg/ml (1.5 μM) ϕX 174 RF II DNA
DNA only (circular, linear and ϕX 174 RF II). Examined with metal shadowing	Deposit DNA by floating grids on DNA solution.	5 μg/ml (15 μM) circular and linear pUCLeu4 DNA; ϕX 174 RF II DNA 1 μg/ml (3 μM)

Table 6.2 Comparison of experimental d-spacings with cubic and hexagonal CdS. ICDD values.[7]

Diamond cubic CdS				Hexagonal CdS			
Experimental spacing	Intensity Order	Index (nm)	Intensity %	Experimental spacing	Intensity Order	Index (nm)	Intensity %
						0.359	62
0.335	1	0.336	100	0.335	7	0.336	91
		0.290	40	0.315	5	0.316	100
				0.246	1	0.245	29
0.206	2	0.206	80	0.206	3	0.207	48
						0.190	50
0.177	3	0.175	60	0.175	6	0.176	31
		0.168	10			0.173	15
				0.152	2	0.152	3
		0.145	20			0.14	15
0.134	4	0.134	30	0.130	4	0.130	4
						0.116	14
0.120	6	0.119	30	0.125	8	0.126	9
0.112	5	0.112	30			0.116	14
				0.098	9	0.098	6

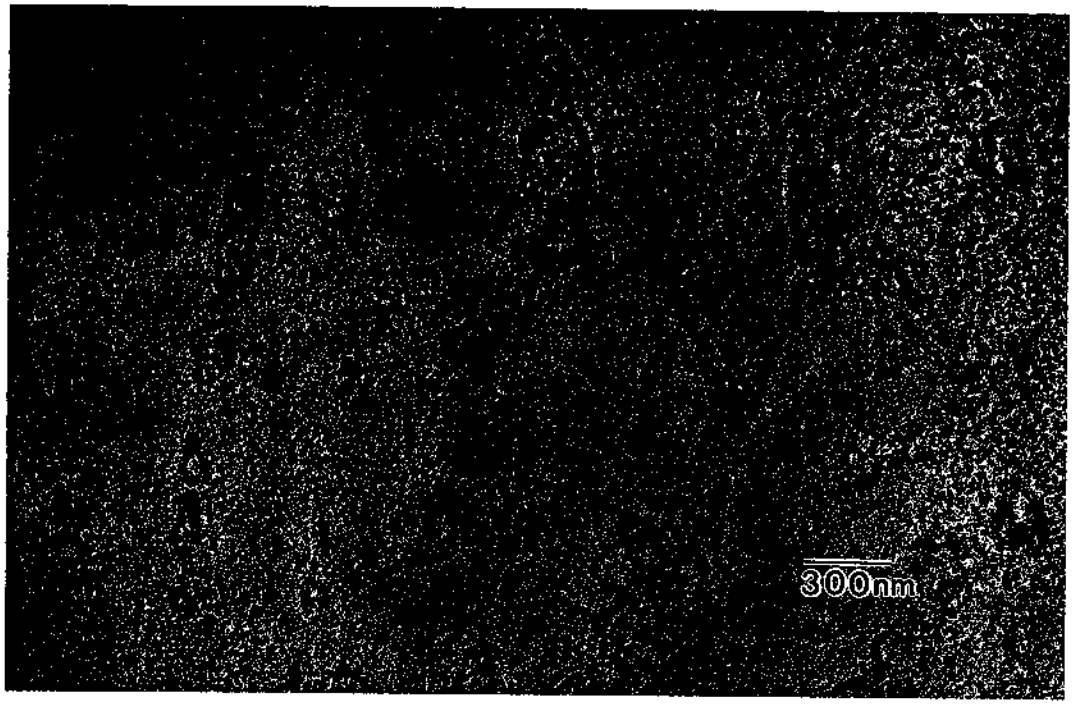

(a)

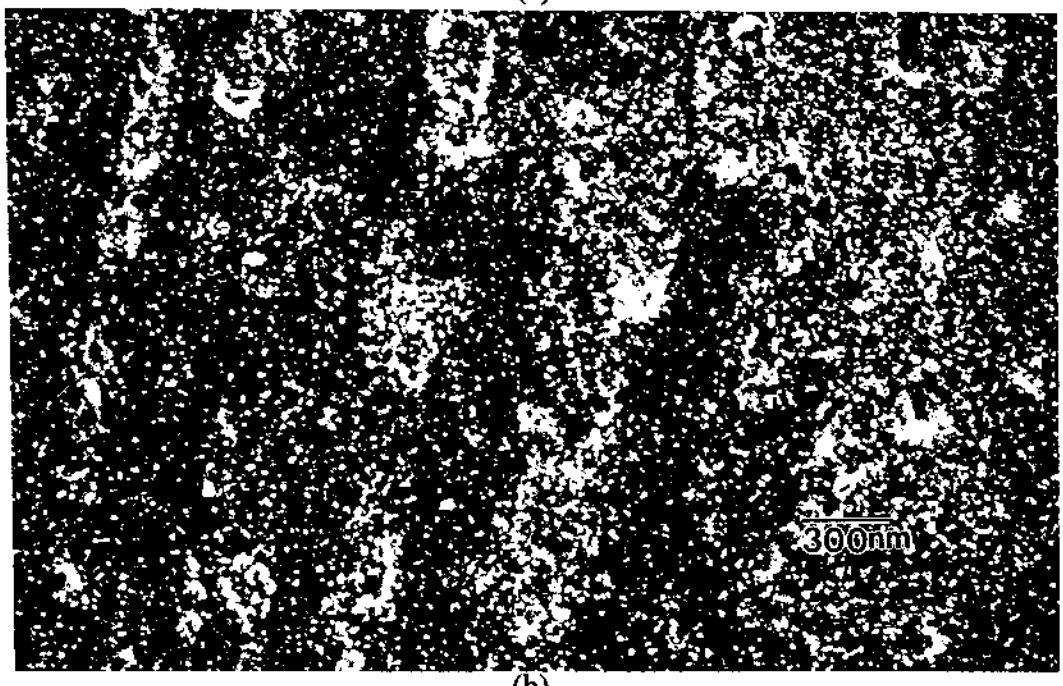

(b)

Figure 6.1 Typical microstructures of diamond cubic CdS nanoparticles formed on a blank-carbon substrate by the dropping deposition method. (a) and (b) are BF and DF images of the 1 mM sample, (c) and (d) are BF and DF images of 2 mM sample, and (e) and (f) are BF and DF images of the 4 mM sample.

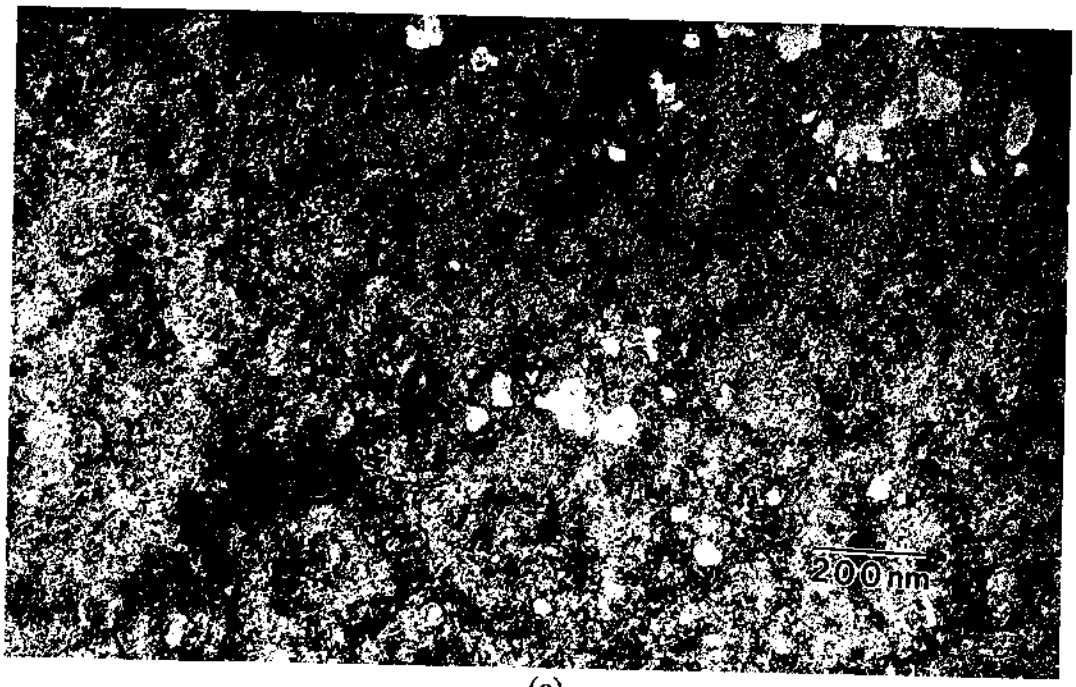

(c)

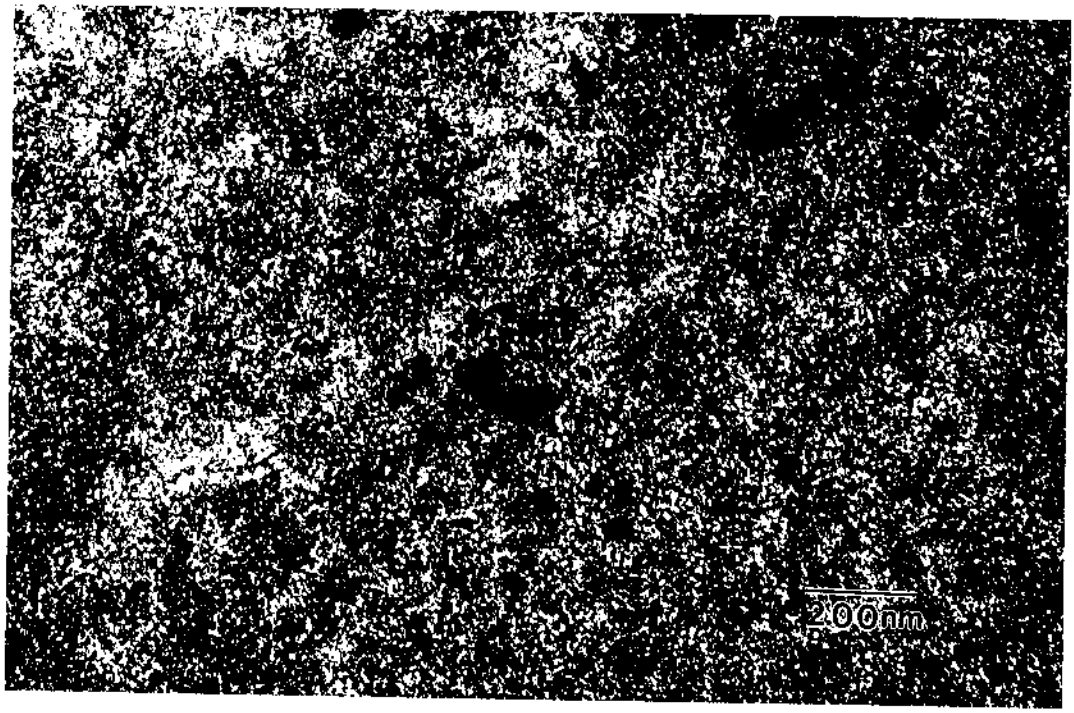

(d)

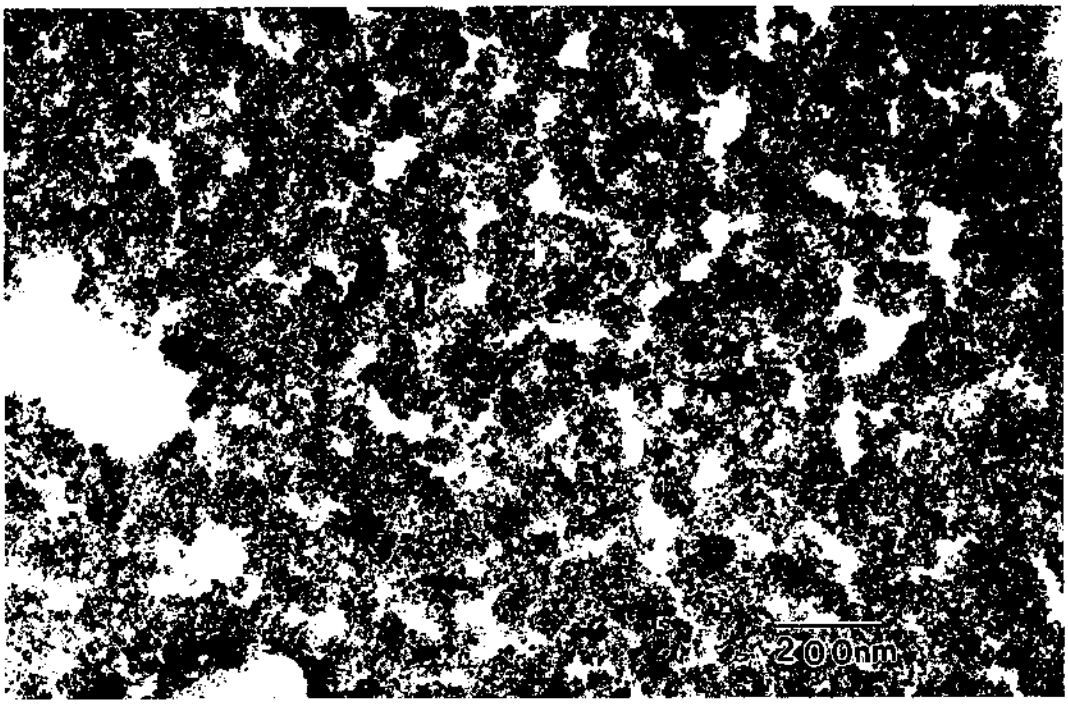

(e)

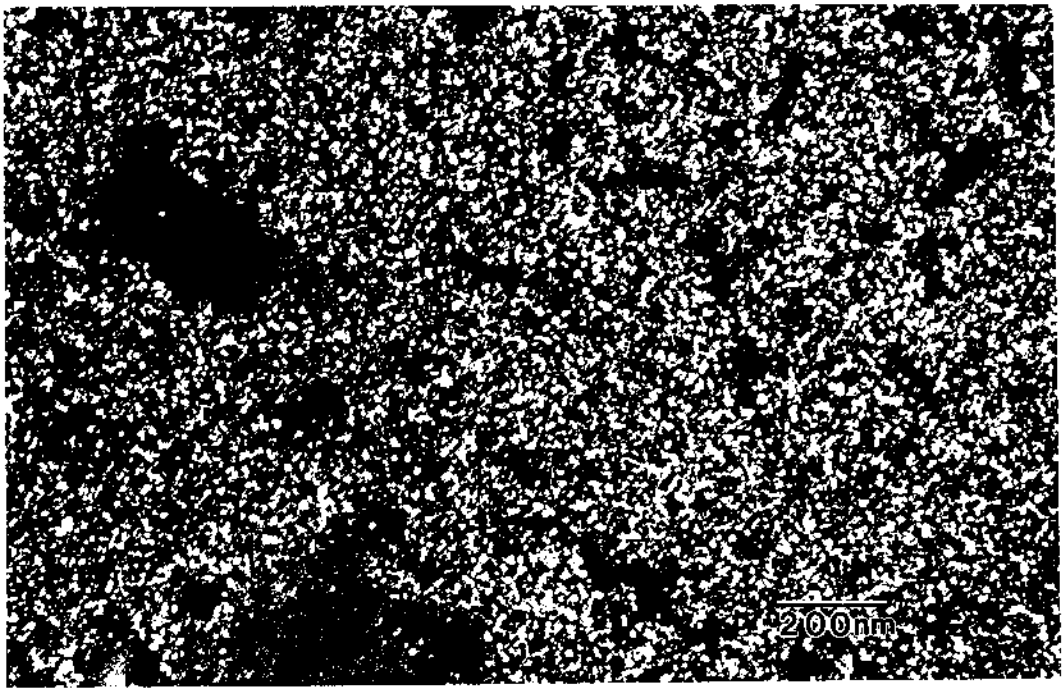

(f)

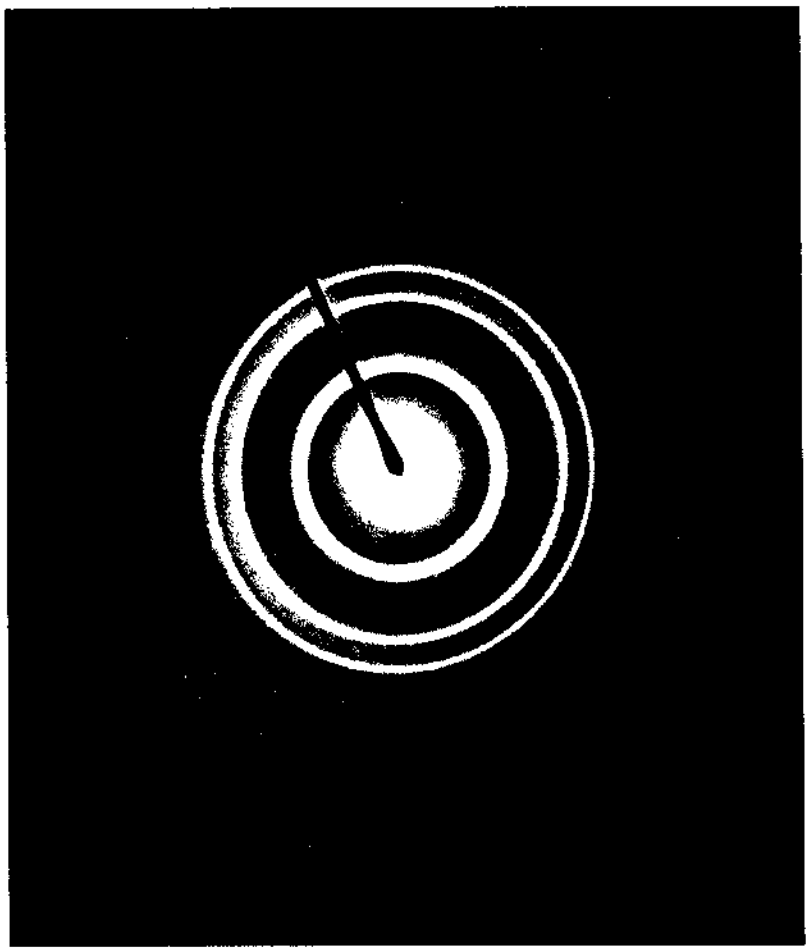

Figure 6.2 A typical selected area electron diffraction pattern obtained from the CdS nanoparticles shown in Figure 6.1. The measured d-spacings match the of zincblend diamond cubic phase of CdS.

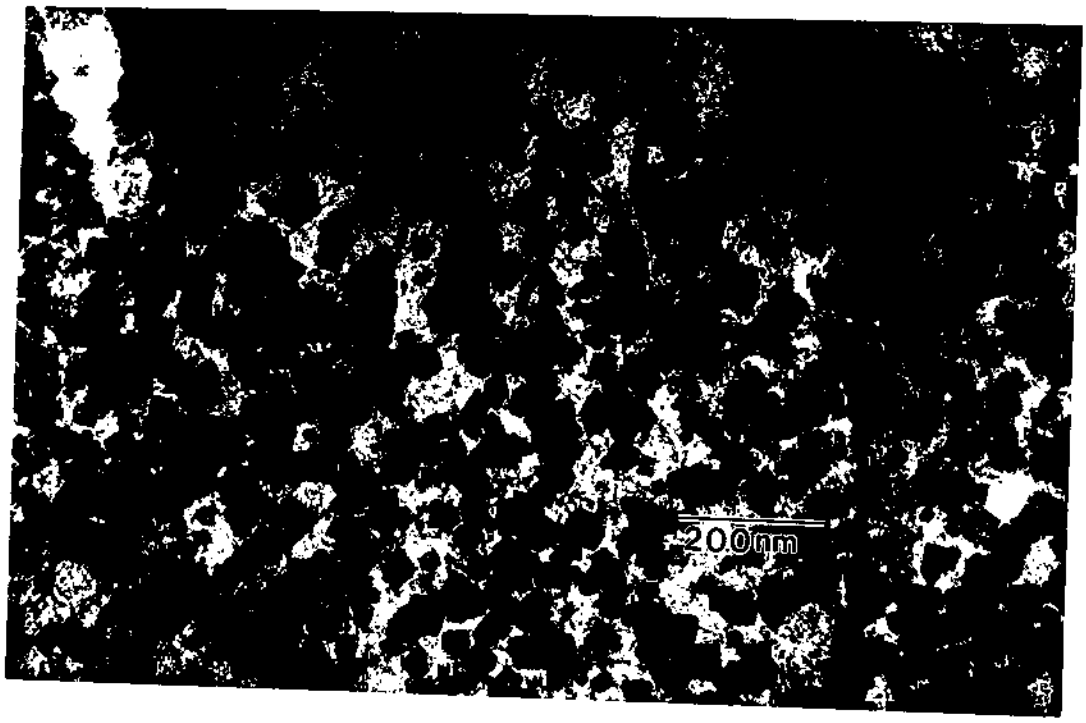

(a)

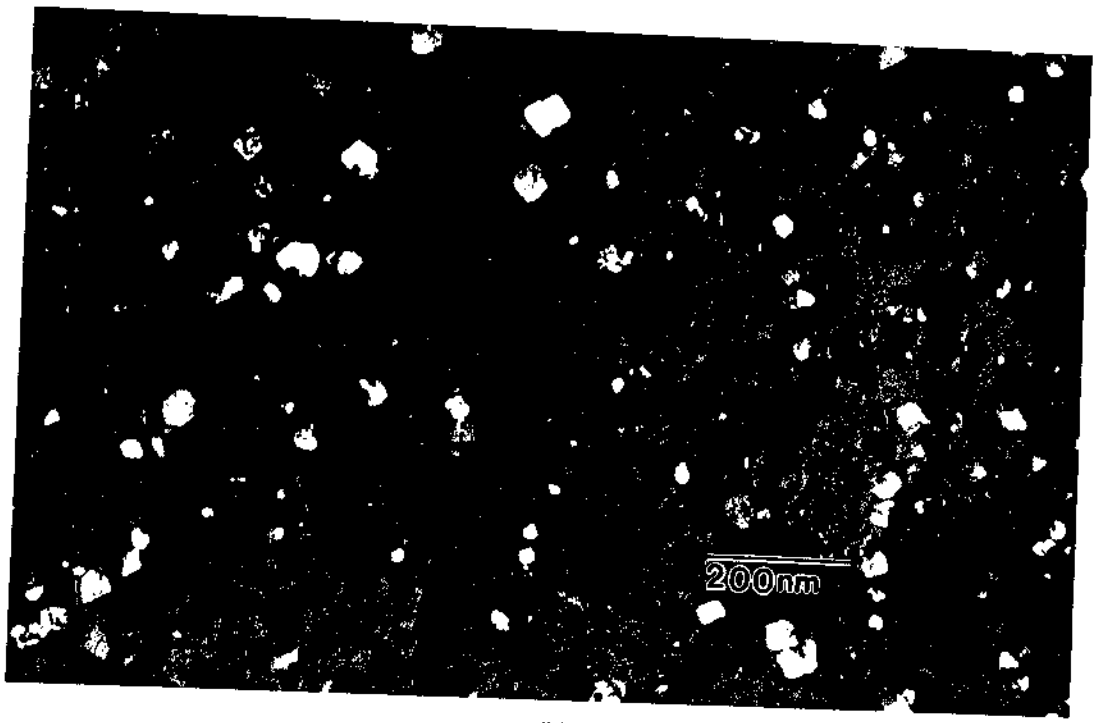

(b)

Figure 6.3 Typical microstructure the hexagonal (wurtzite) CdS particles of the 4 mM cadmium sample fabricated on a carbon substrate by the dropping deposition method. (a) bright field, and (b) dark field.

Figure 6.4 A typical selected area diffraction pattern of hexagonal CdS particles obtained from the same area shown in Figure 6.3. The measured d-spacings match of hexagonal close packed CdS.

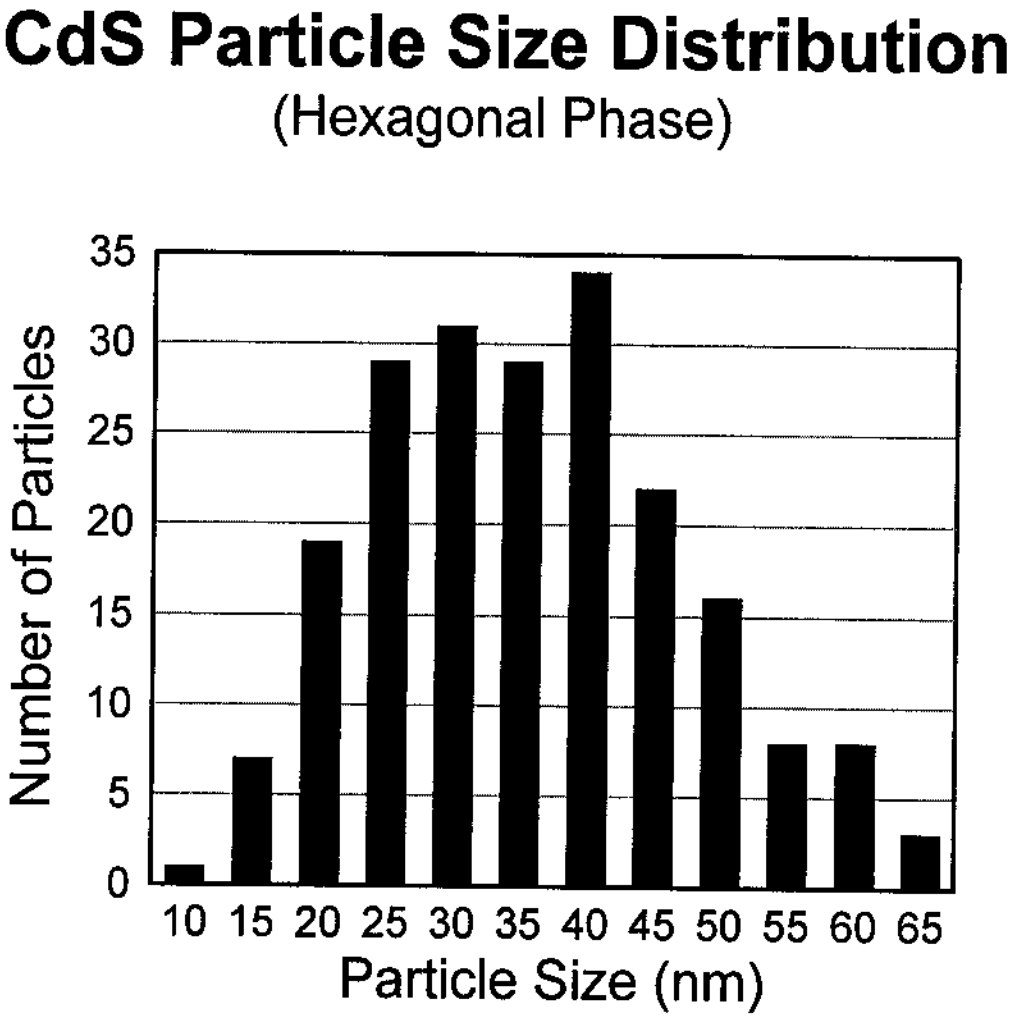

Figure 6.5 Particle size distribution for hexagonal CdS. The average size is 38.4 nm.

(a)

Figure 6.6 HREM images of (a) cubic CdS nanoparticles synthesized on pUCLeu4 circular DNA/carbon film and (b) hexagonal CdS nanoparticles synthesized on pUCLeu4 circular DNA/glass slide.

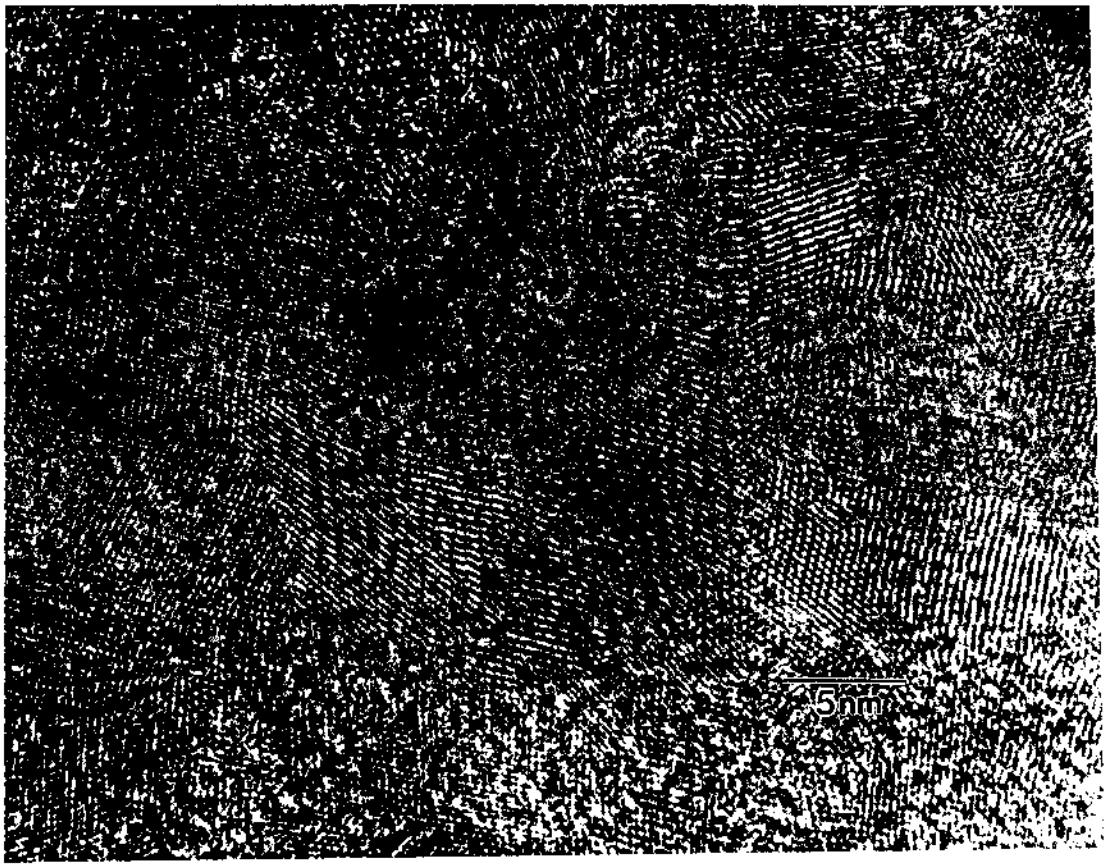

(b)

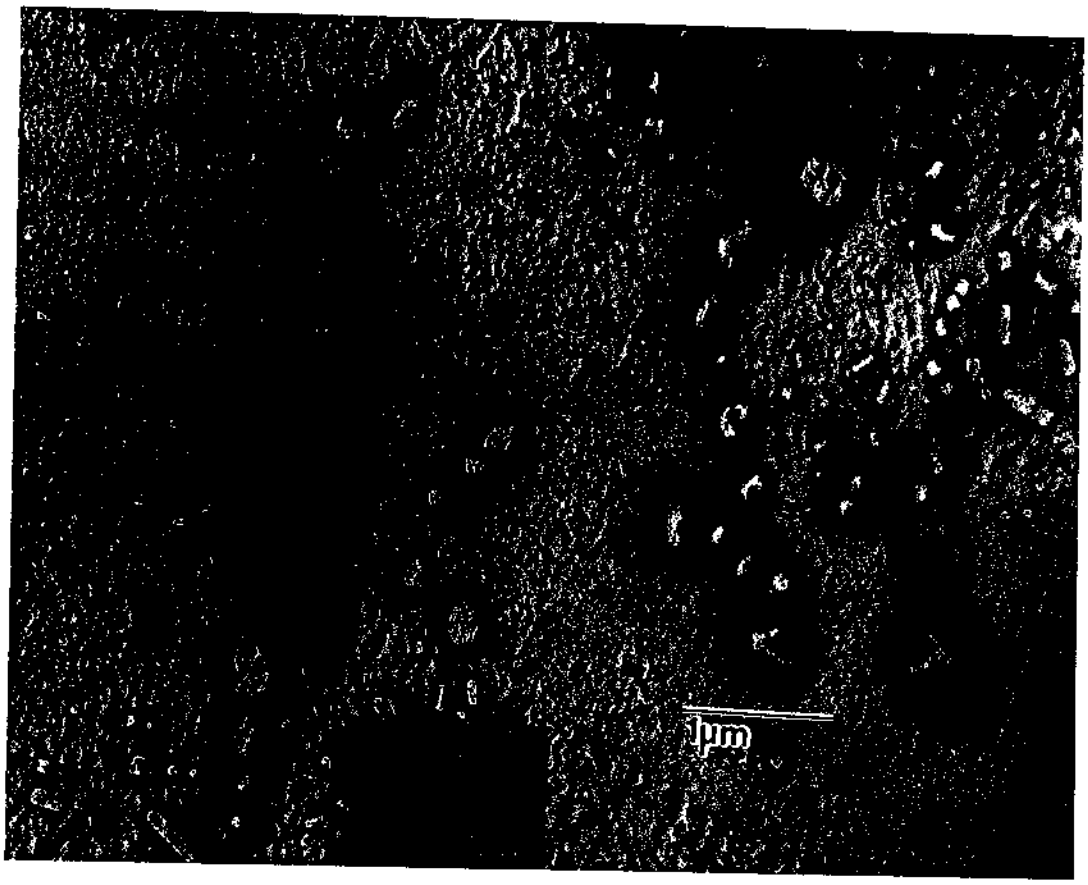

(a)

Figure 6.7 Sizes and shapes of various microbubbles found in the 4 mM CdS only sample. (a) low magnification bright field TEM and (b) high magnification image of one of the circular microbubbles.

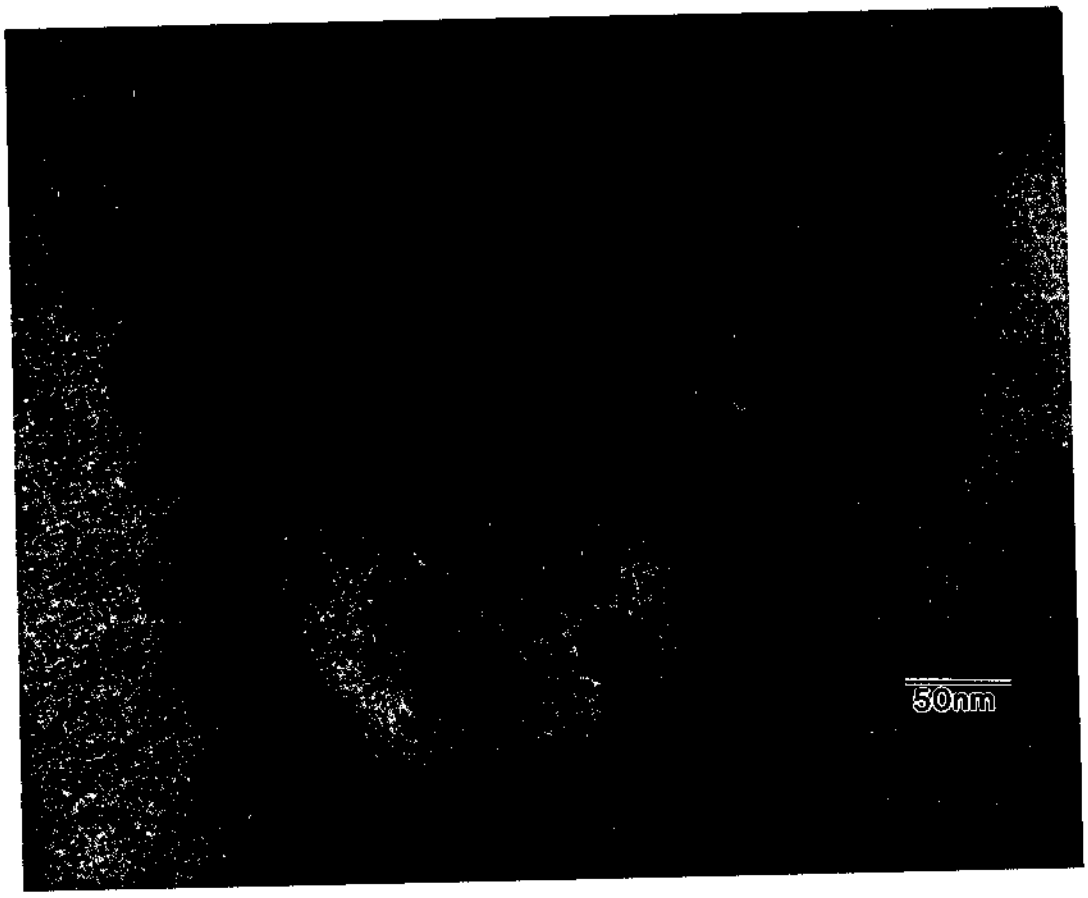

(b)

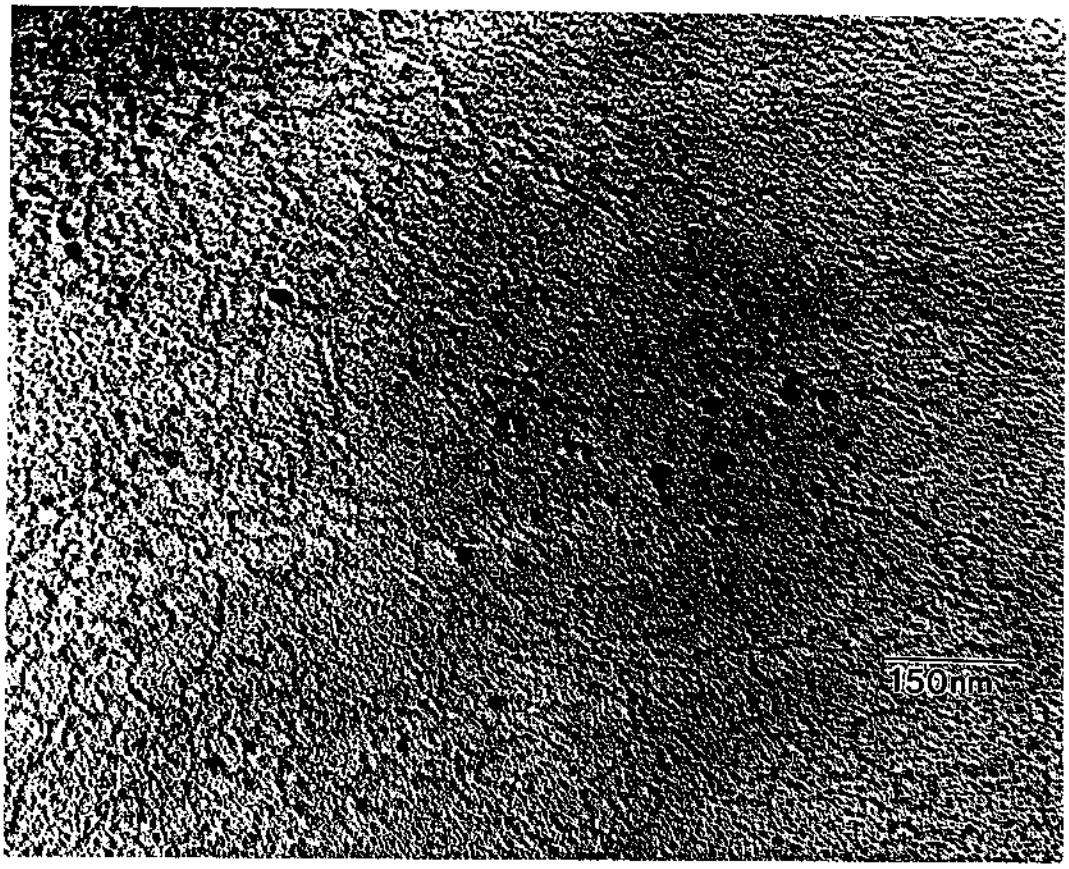

(a)

Figure 6.8 High concentration of DNA microstructures without Q-CdS particles observed after metal shadowing. (a) low-cadmium/circular DNA and (b) low-cadmium/ϕX 174 RF II DNA.

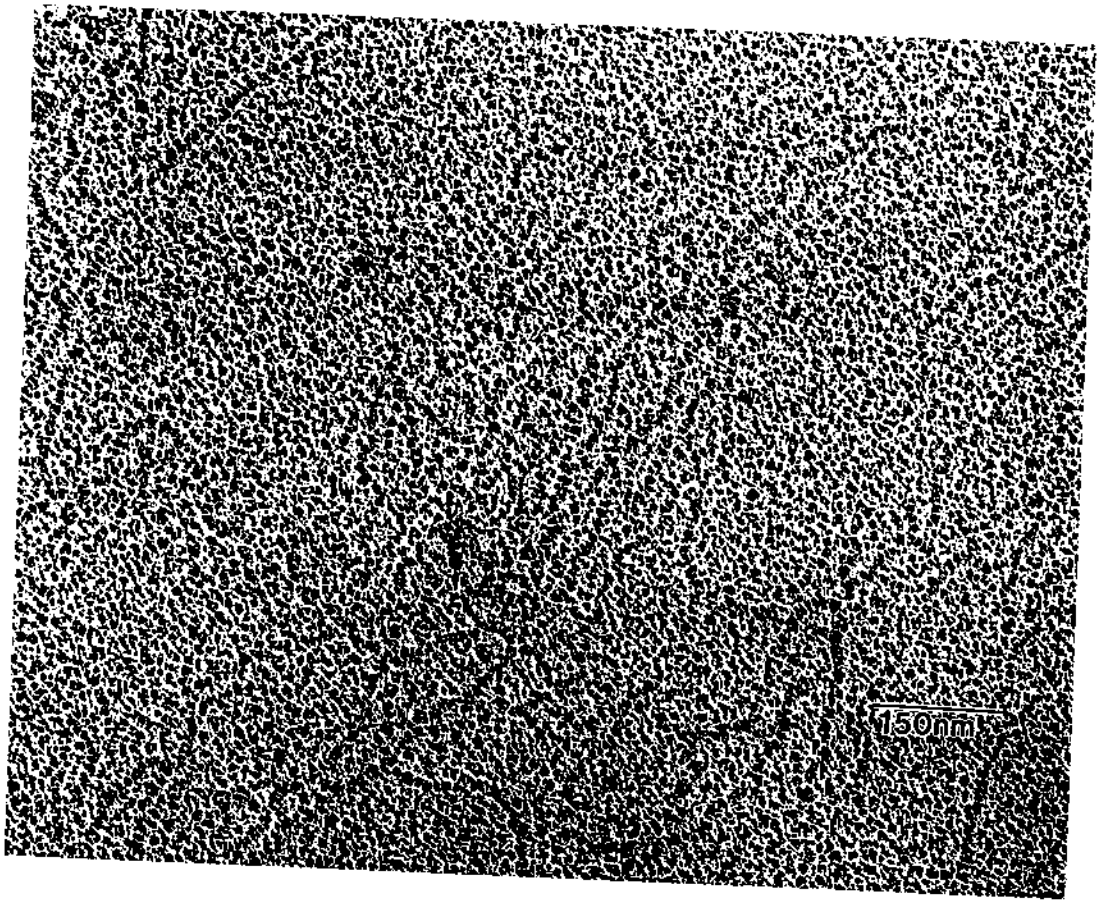

(b)

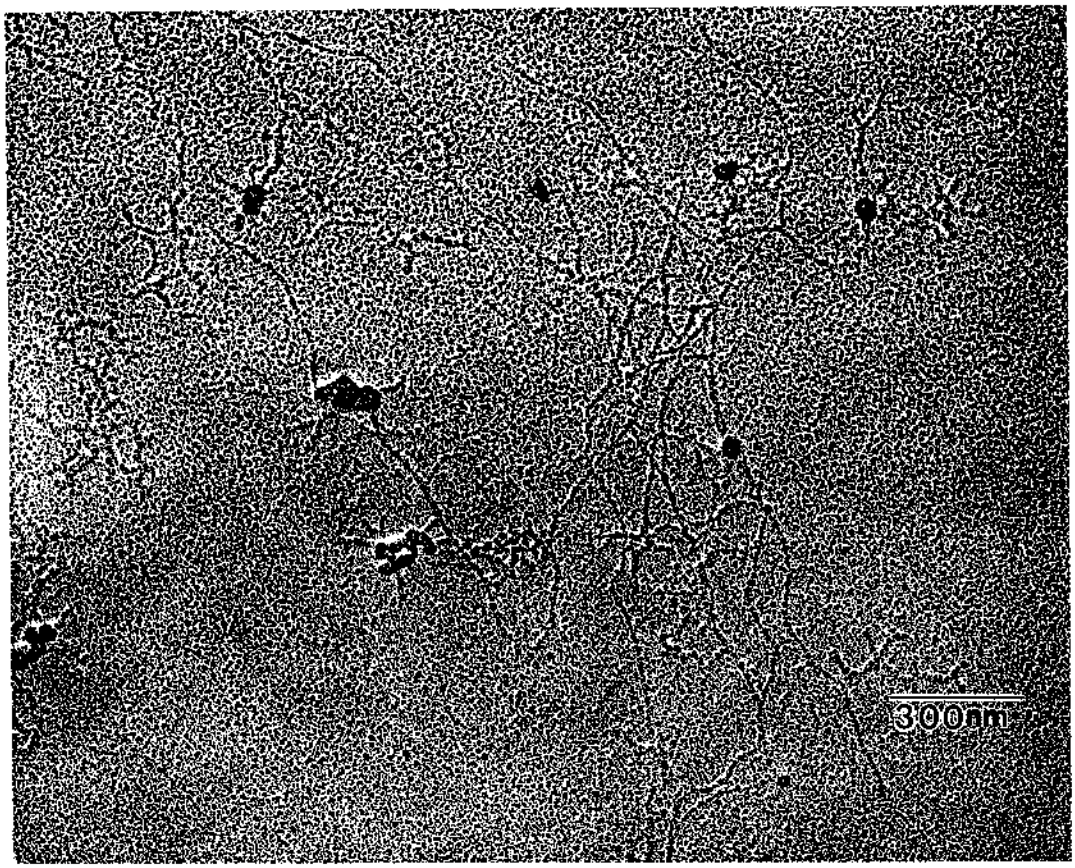

Figure 6.9 Net-like DNA microstructure of the high-cadmium/circular DNA. Q-CdS particles were not detected using SADP.

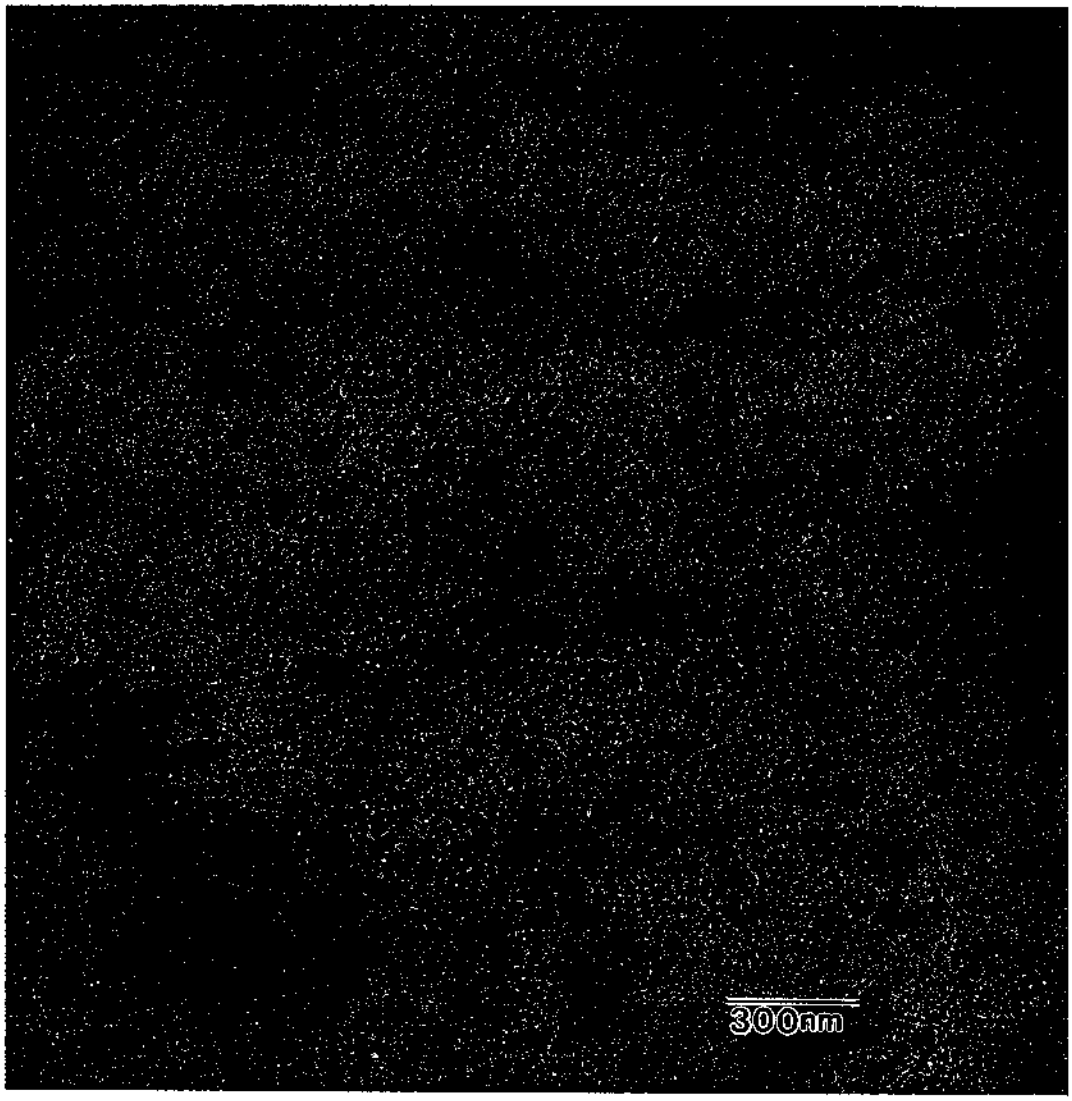

Figure 6.10 Typical bundled CdS/DNA microstructures of samples prepared by floating the grids on the Cd^{2+}/DNA complex solution. (a) BF of the 2 mM cadmium/5 μg/ml circular DNA, (b) DF of the 2 mM cadmium/5 μg/ml linear DNA and (c) DF of the 2 mM cadmium/1 μg/ml ϕX 174 RF II DNA.

(b)

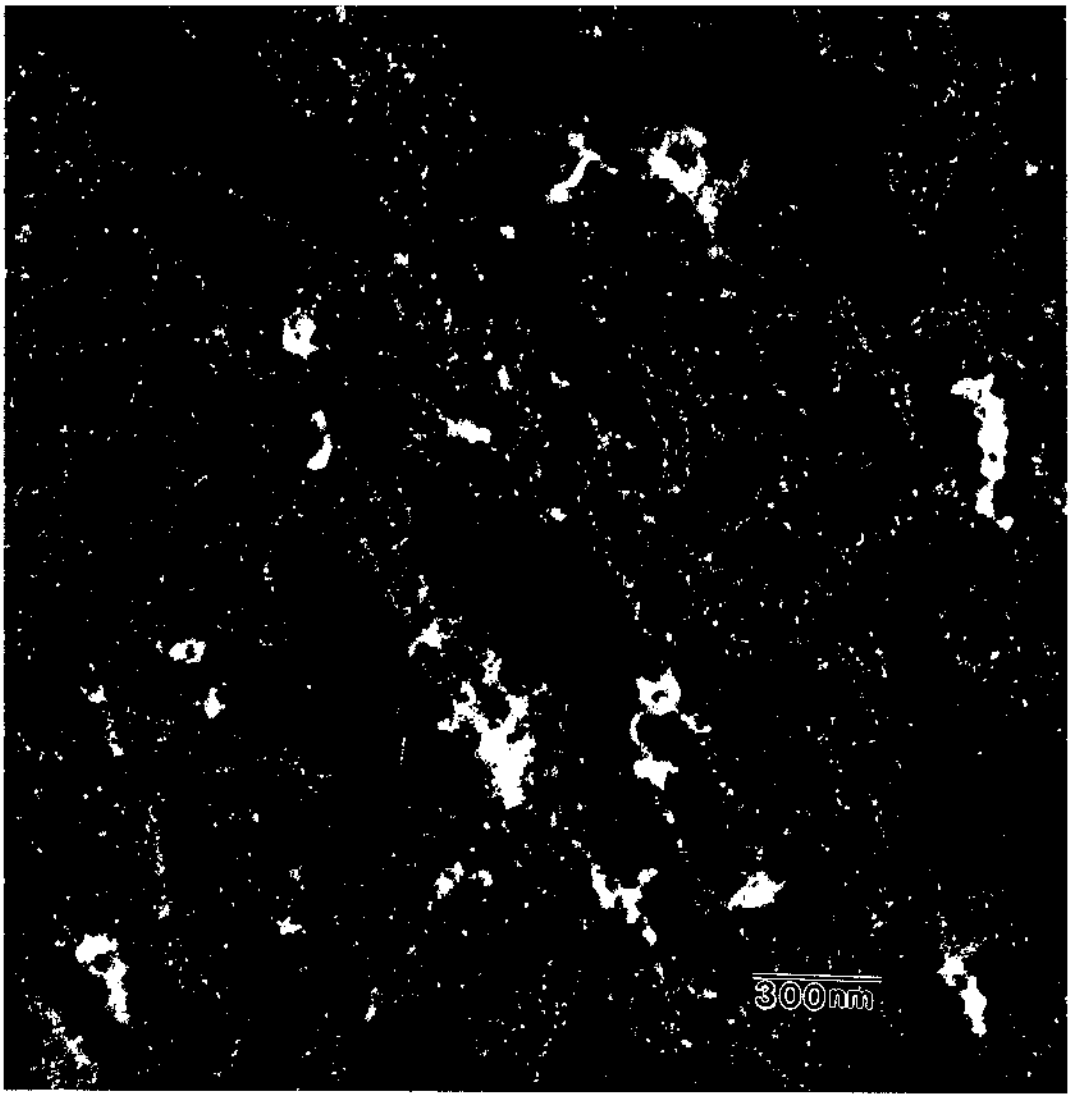

(c)

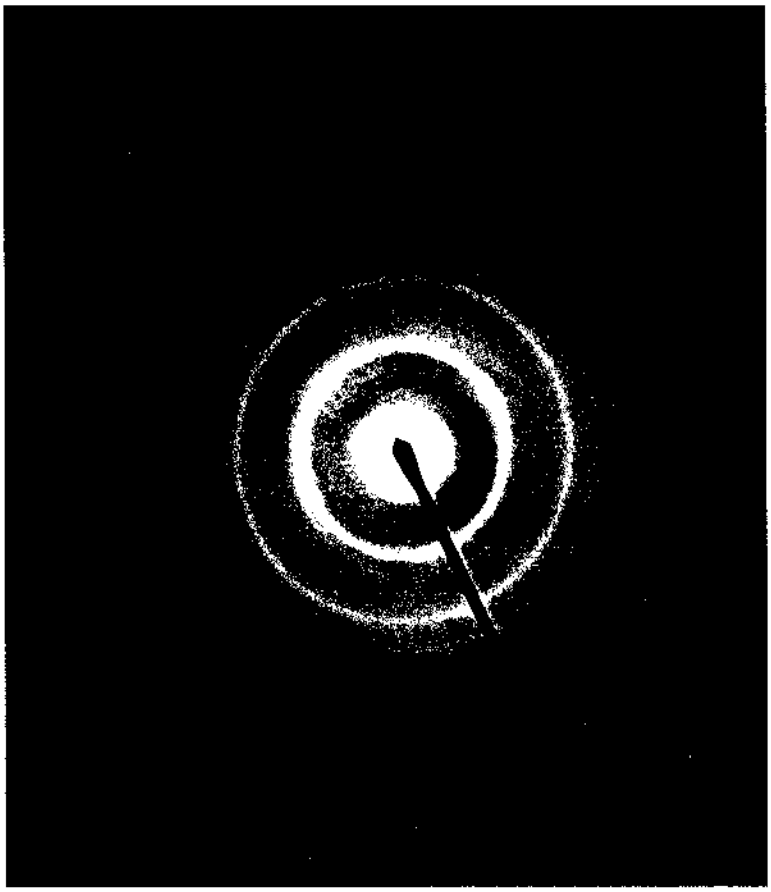

Figure 6.11 Typical SADP of bundled CdS/DNA shown in Figure 6.10. The lattice spacings match cubic CdS.

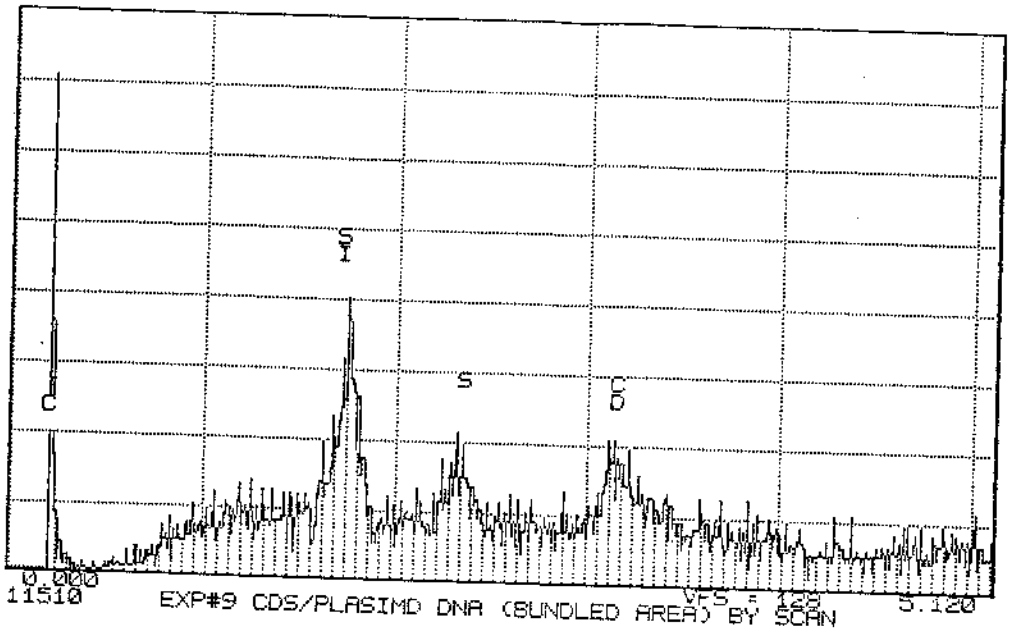

(a)

(b)

Figure 6.12 (a) XEDS spectrum of the nanoparticles in the bundled DNA. (b) STEM micrograph of the area from which the XEDS spectrum was obtained.

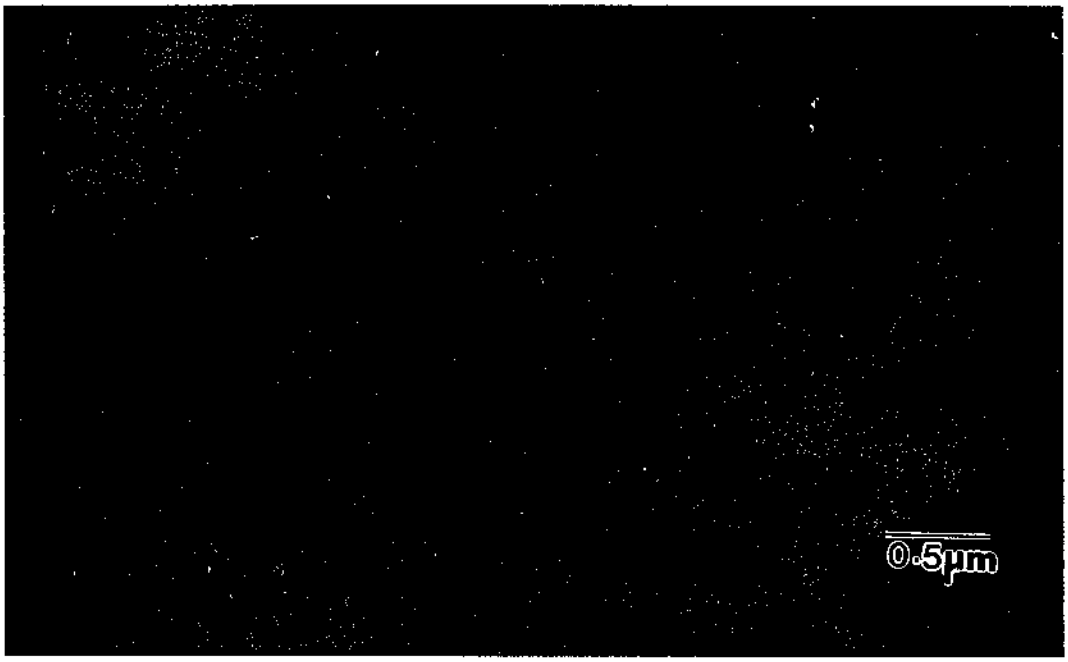

(a)

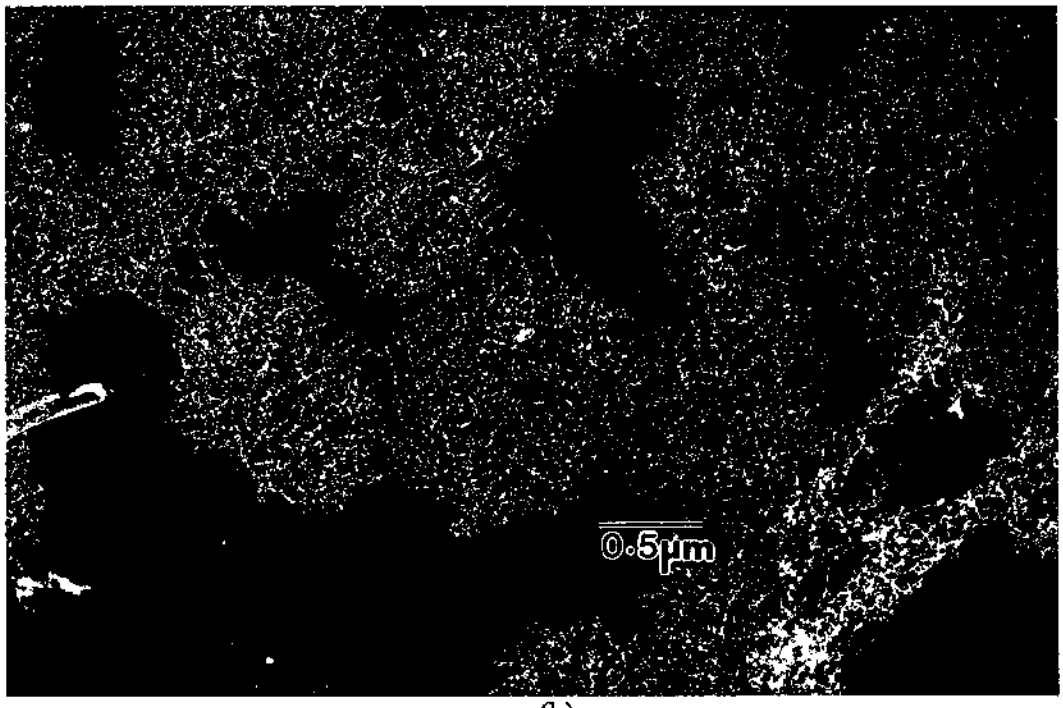

(b)

Figure 6.13 (a) BF and (b) DF low magnification images of the bundled CdS/DNA structures in the 5 μg/ml circular DNA sample. These micrographs show that the contrast of the bright field image varies with the number of Q-CdS particles. They also show that 5 μg/ml DNA is still too concentrated to fabricate individual CdS/DNA semiconductor nanostructures.

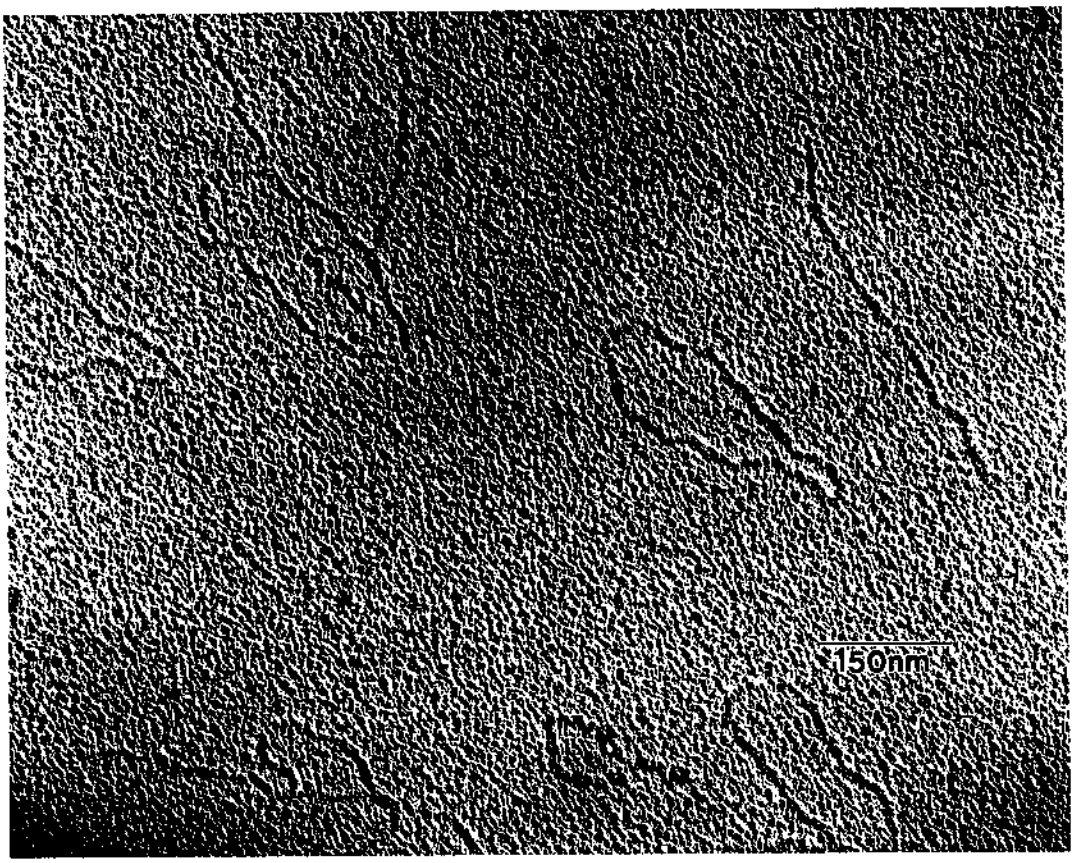

(a)

Figure 6.14 Typical microstructures of DNA only samples deposited by floating the grid on the DNA solution. (a) circular, (b) linear, and (c) ϕX 174 RF II DNA.

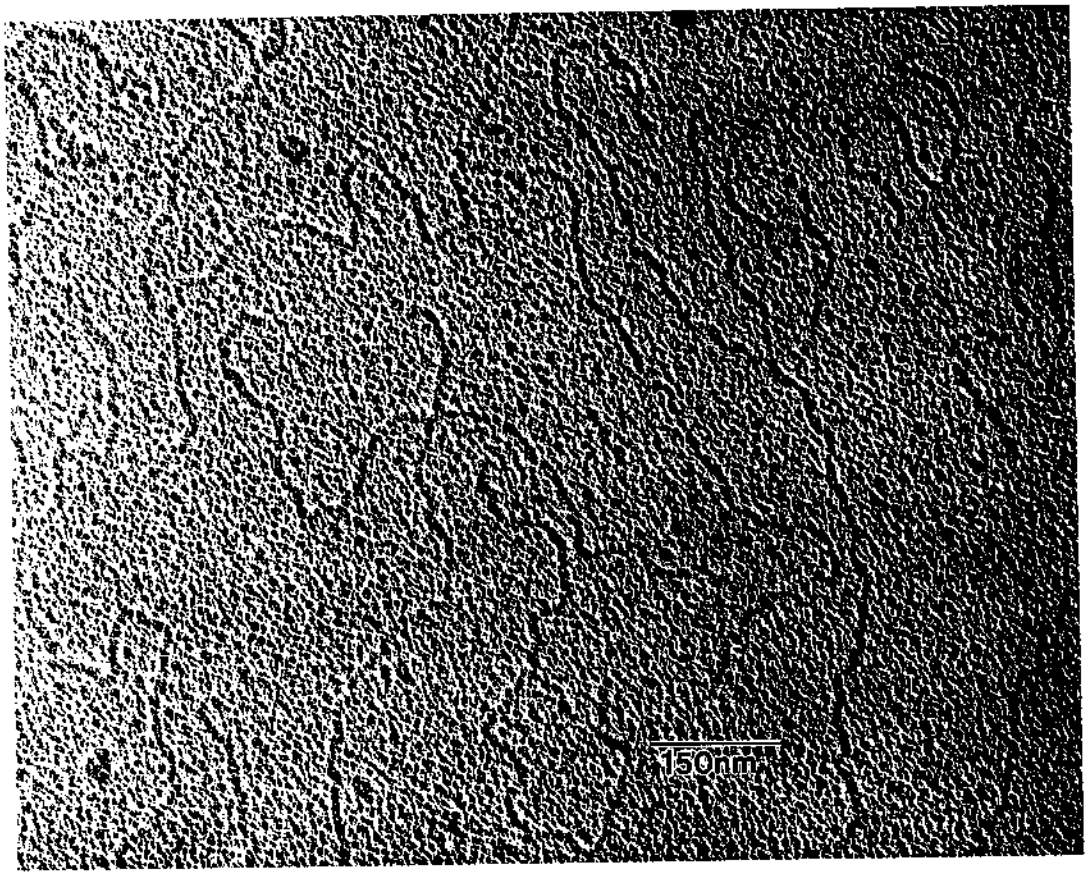

(b)

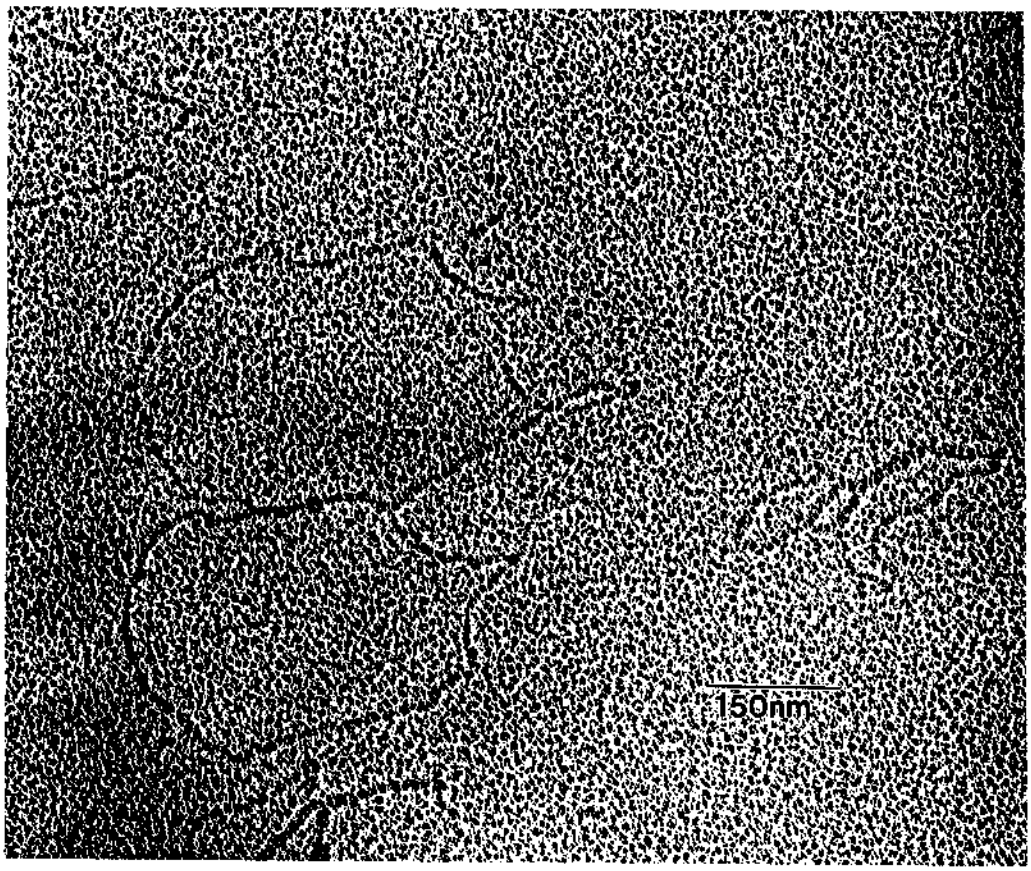

(c)

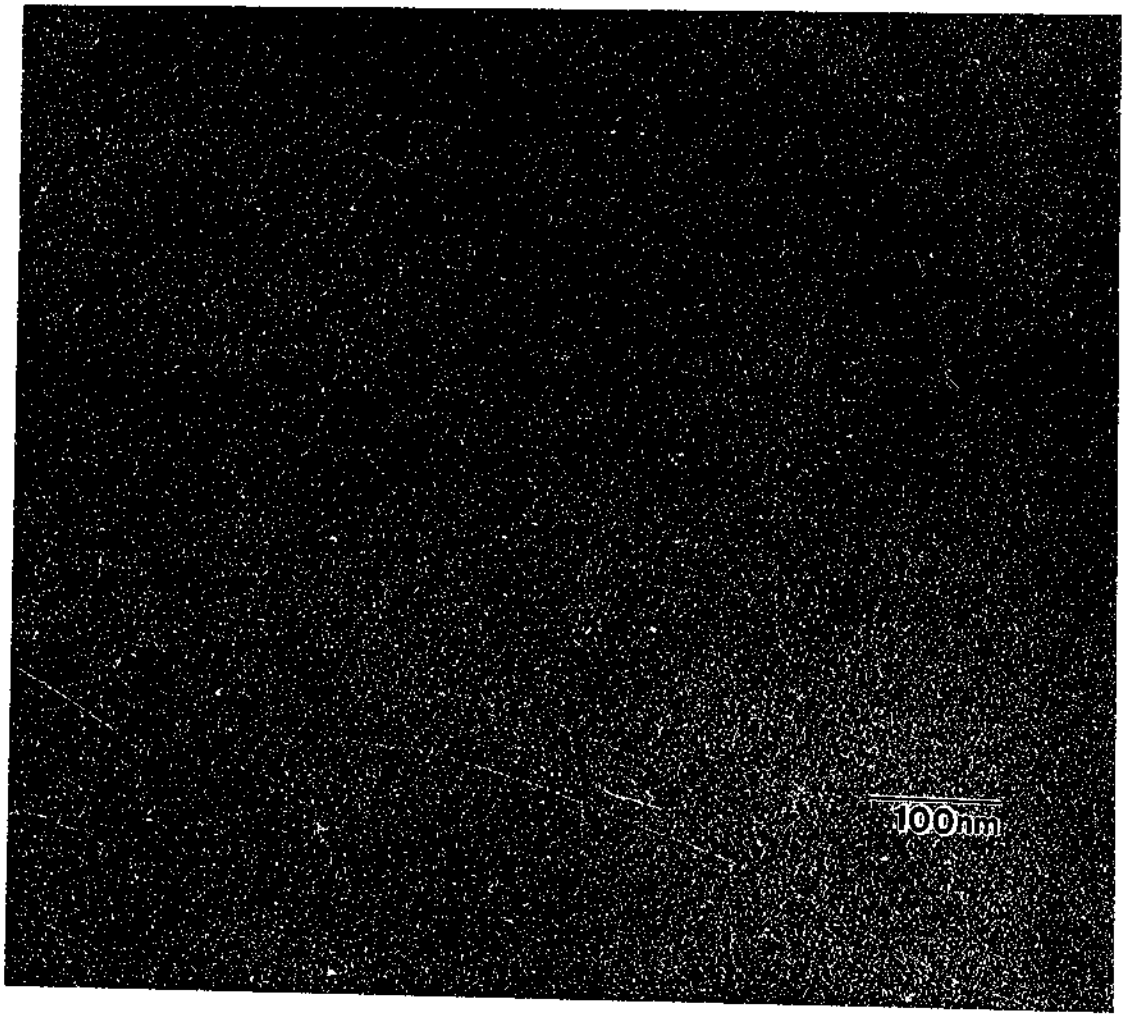

(a)

Figure 6.15 Typical CdS/DNA microstructures for 5 μg/ml circular DNA fabricated by dipping the grid with the attached DNA into 2 mM cadmium solution.

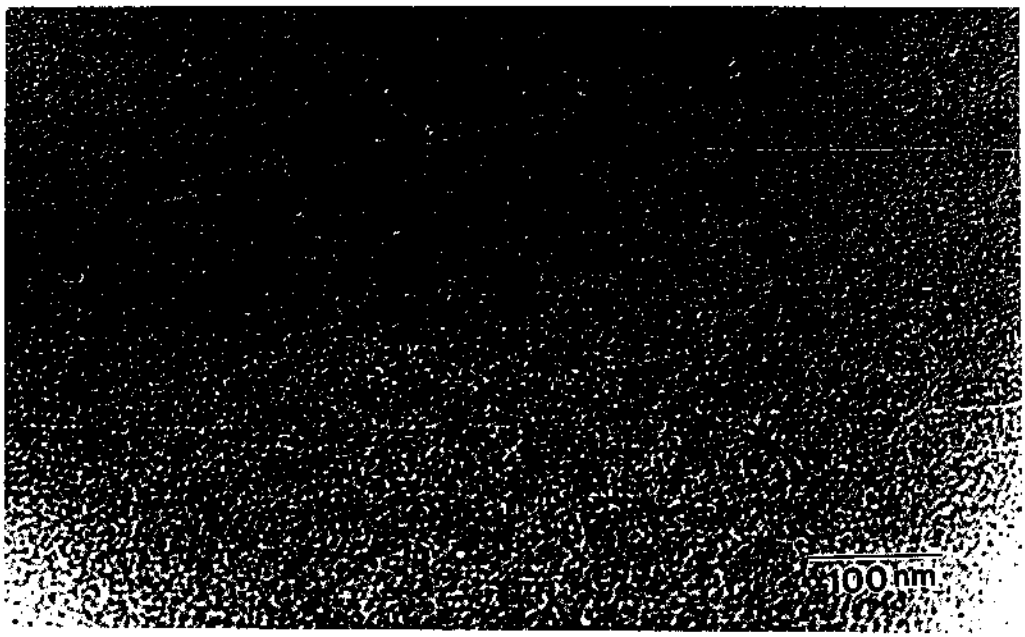

(b)

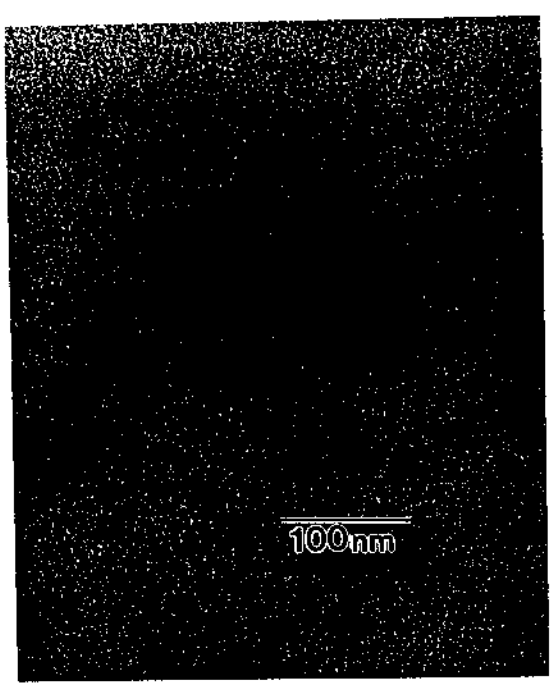

(c)

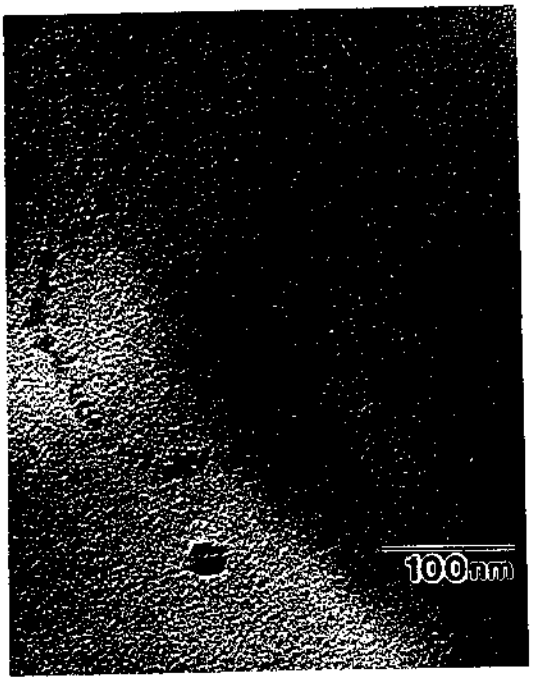

(d)

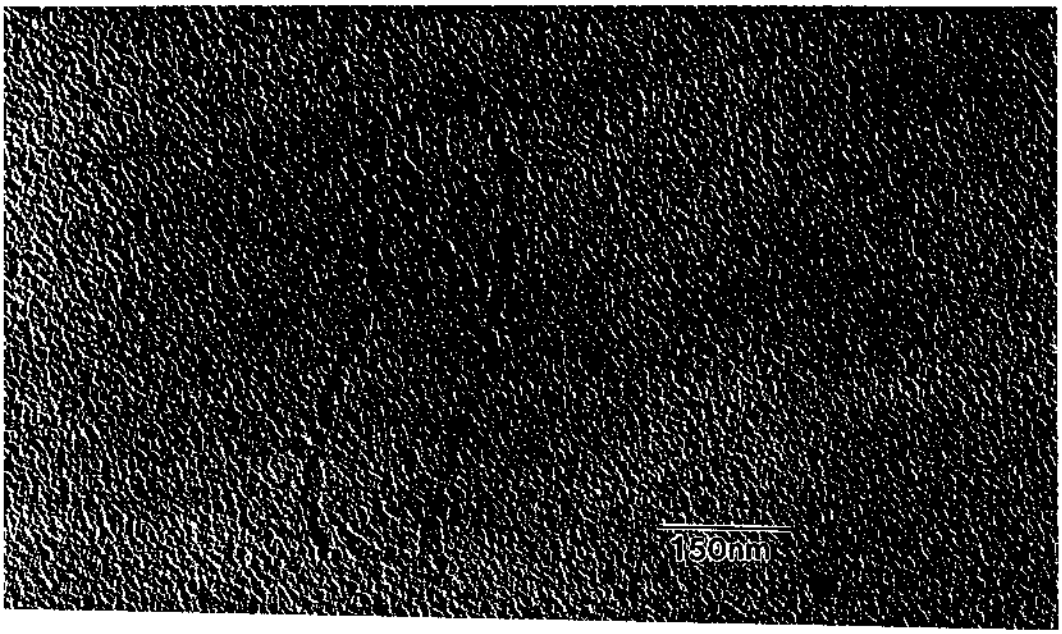

(a)

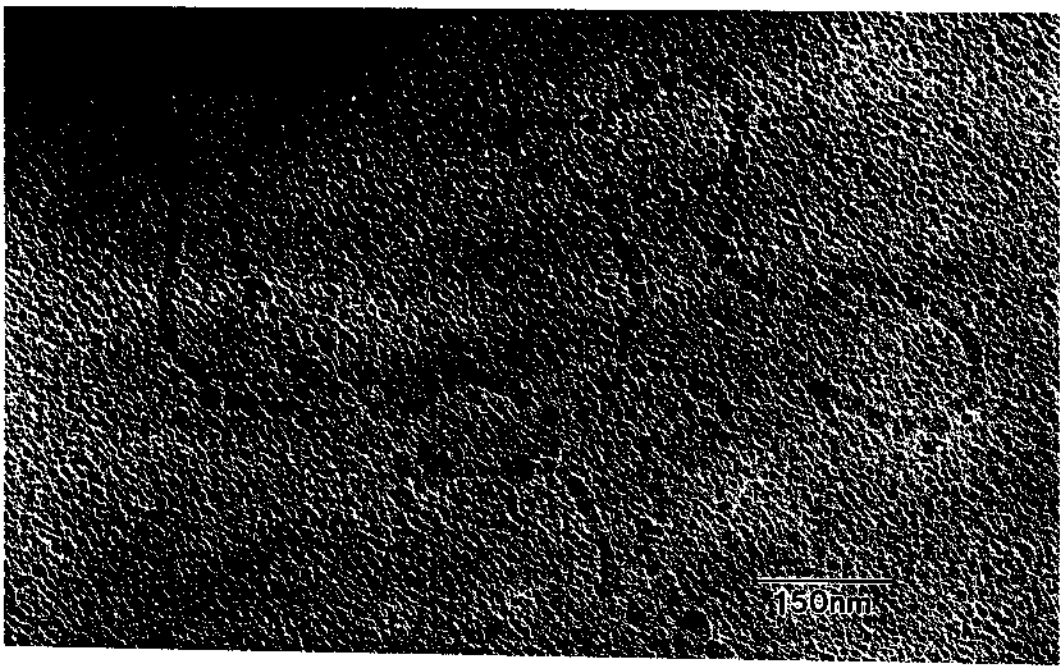

(b)

Figure 6.16 Typical microstructures of CdS/DNA after carbon shadowing of (a) CdS/5 μg/ml circular DNA and (b) CdS/0.5 μg/ml linear DNA.

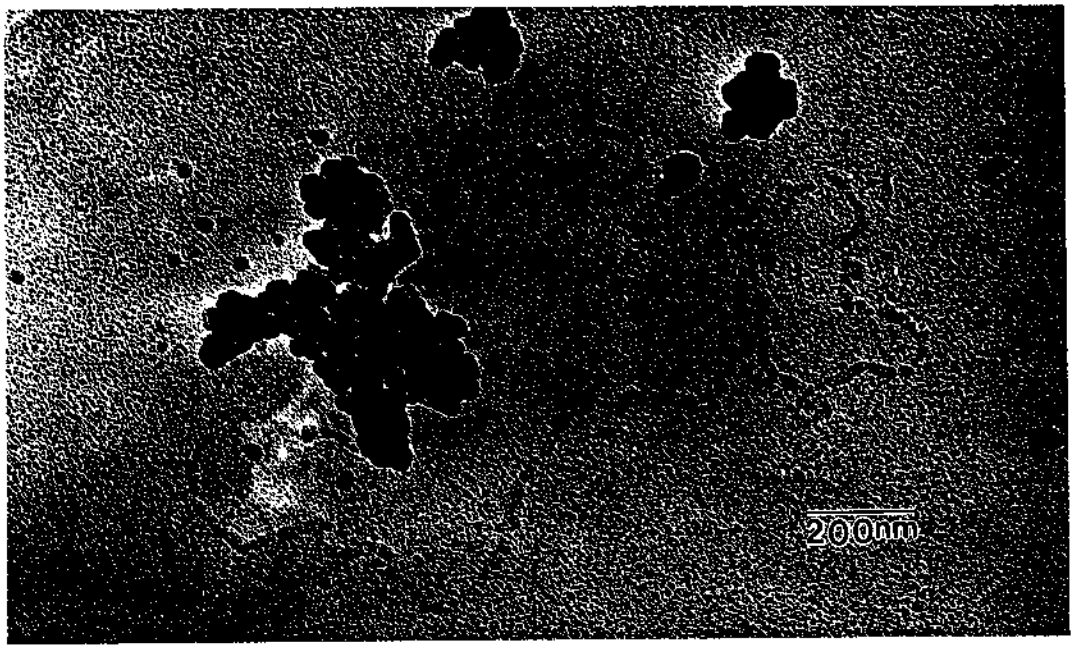

(a)

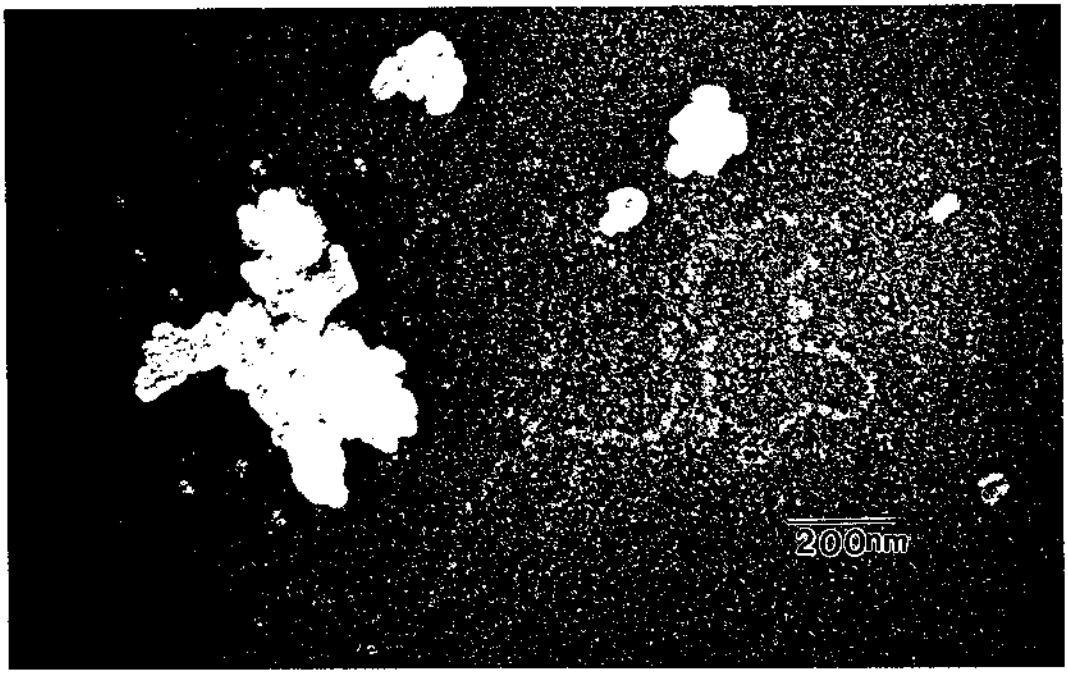

(b)

Figure 6.17 (a) BF and (b) DF images of CdS/DNA bundles of supercoiled DNA molecules. (c) SADP from the microstructure shown in (a).

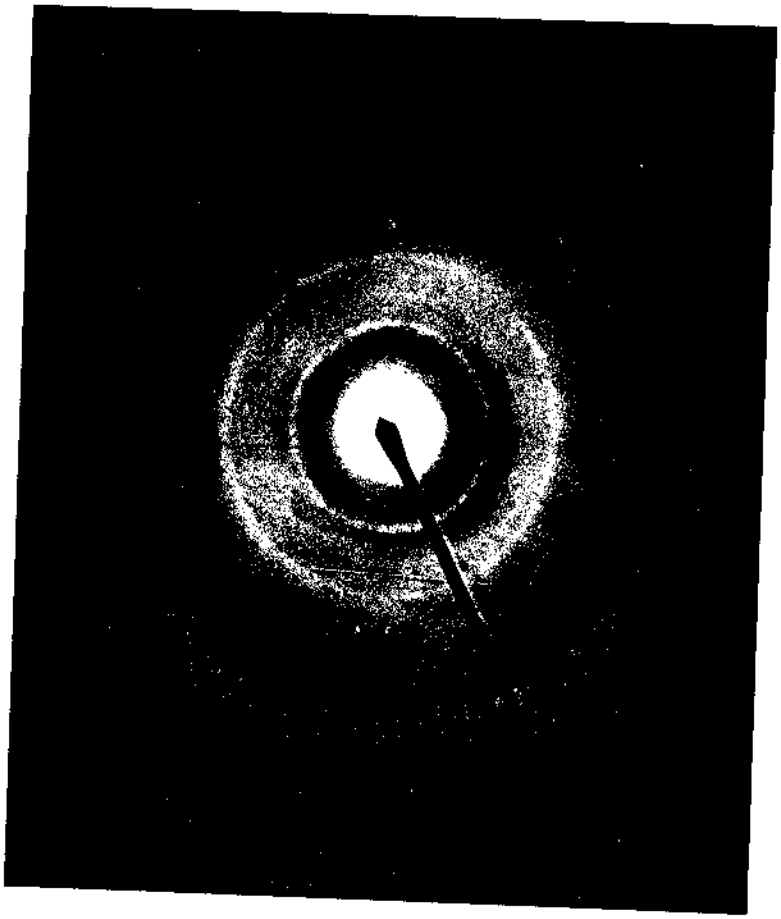

(c)

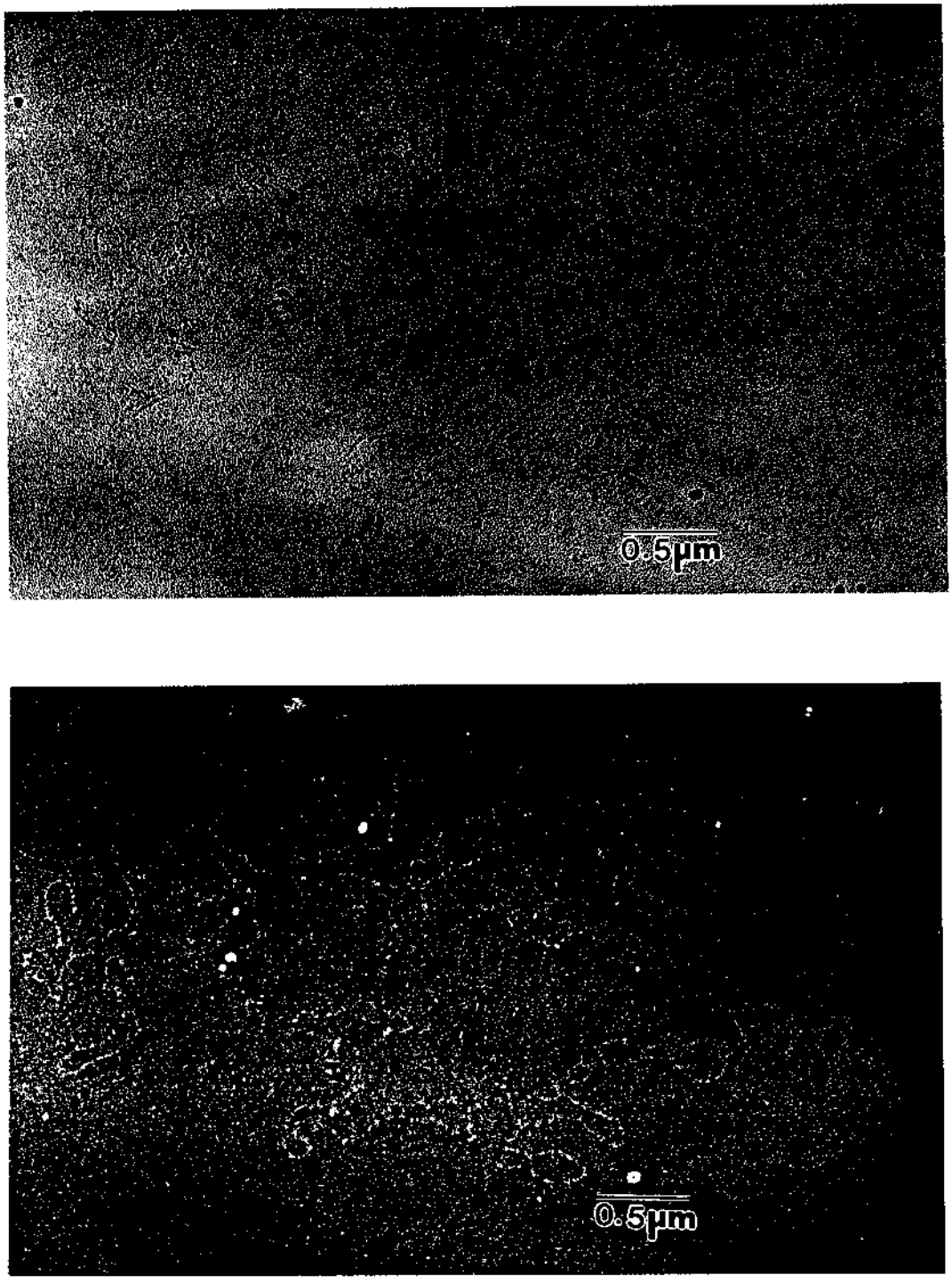

(a)

Figure 6.18 Pairs of BF and DF images of CdS/DNA microstructures from (a) linear DNA and (b) CdS/ϕX 174 RF II DNA. After carbon shadowing.

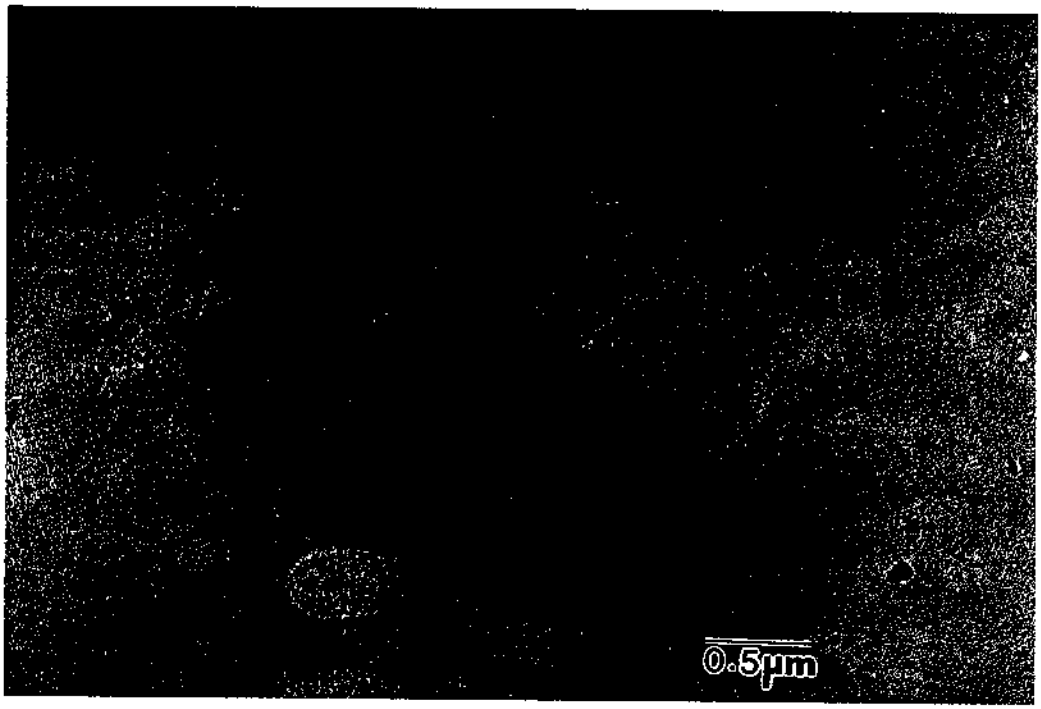

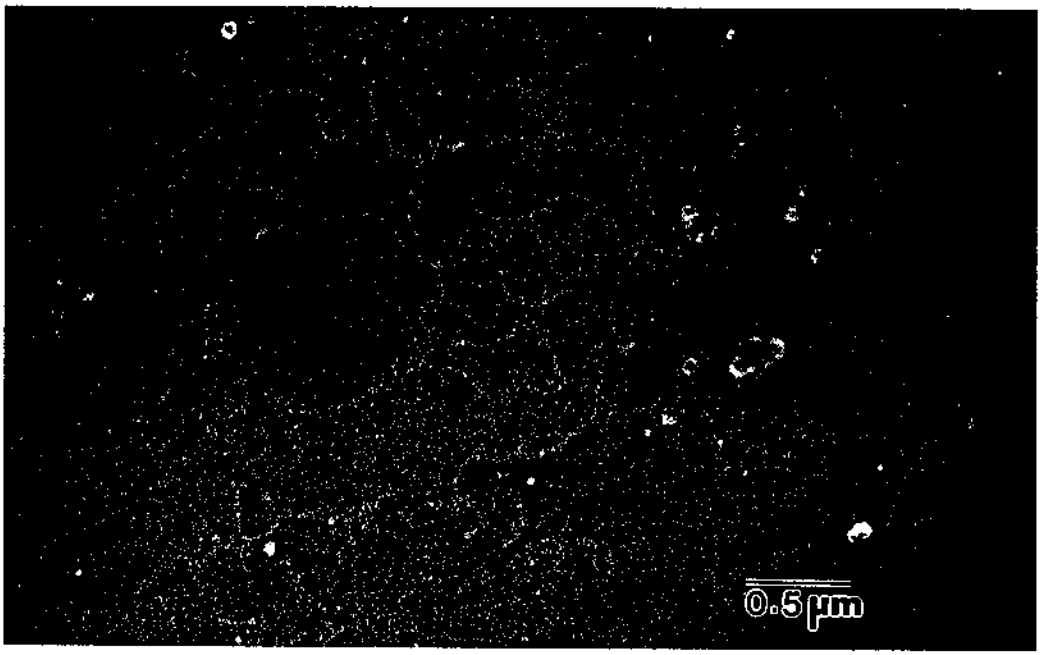

(b)

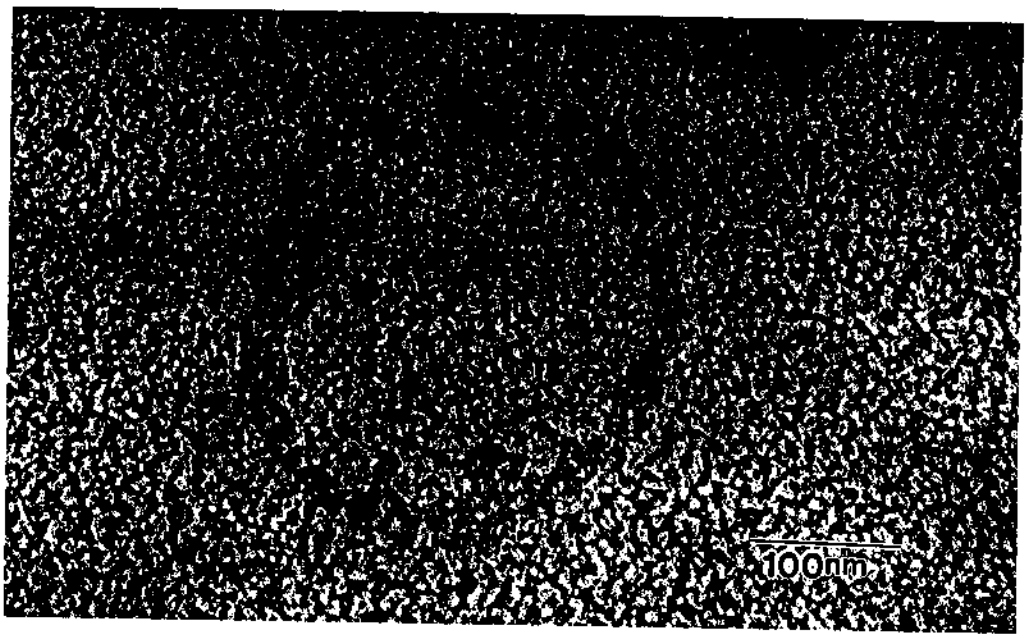

(a)

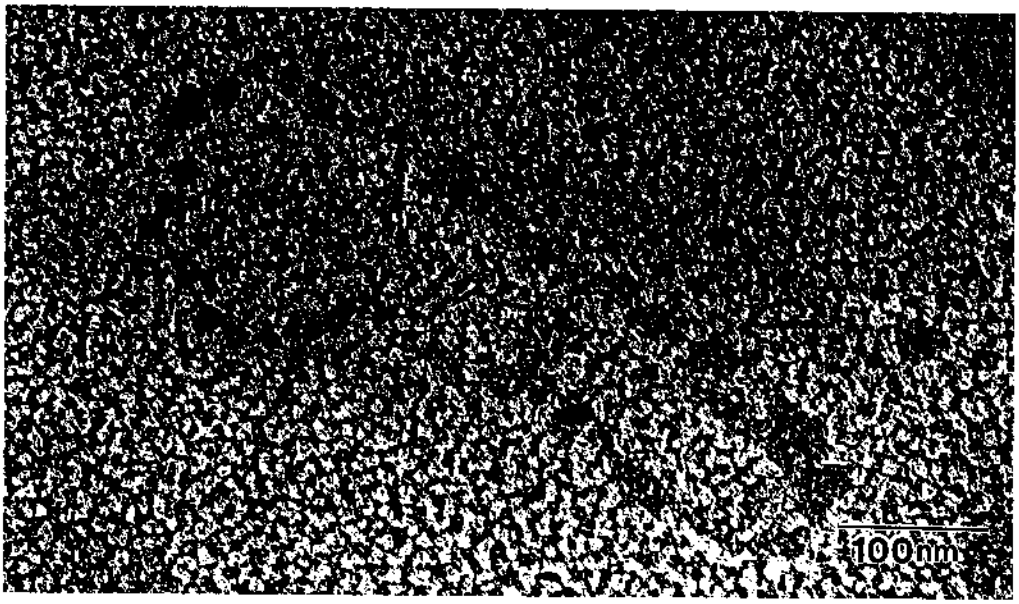

(b)

Figure 6.19 CdS/DNA microstructures from the 5 μg/ml circular DNA after metal shadowing.

REFERENCES

1. Noran Instruments, 2551 W. Beltline Highway, Middleton, WI.

2. H. Weller, Angew. Chem. Interact. Ed. Engl. **32**, 41-53 (1993).

3. D. B. Williams and C. B. Carter, *Transmission Electron Microscopy Vol. IV* (Plenum Press, New York, 1996), p. 32.

4. L. G. Marzilli, T. J. Kistenmacher and G. L. Eichhorn, "Nucleid Acid-Metal Ion Interactions" in *Metal Ions in Biology Vol. 1*, edited by T. G. Spiro, (John Wiley & Sons Inc., New York, 1980), pp. 181-199, 231.

5. M. Sabat and B. Lippert, *Metal Ions In Biological Systems,* edited by A. Sigel and H. Sigel, (Marcel Dekker, Inc., New York, 1996), pp. 143-168.

6. L. Stryer, *Biochemistry*, 3rd ed. (W. H Freeman and Company, New York, 1987), p. 655.

7. International Center for Diffraction Data (12 Campus Blvd., Newtown Square, PA), Power Diffraction File PDF # 41-1049, 10-0454.

CHAPTER 7

SUMMARY

Self-assembled mesoscale semiconductor structures of II-VI nanocrystalline materials are an especially exciting subject because of their controllable band gap and unique photophysical properties. We have developed an innovative method to fabricate diverse nanostructures which relies on the size and a shape of a deoxyribonucleic acid (DNA) template. DNA has anionic sites which bind transition metal ions such as Zn^{2+}, Cd^{2+} and Hg^{2+}. The DNA can thus control the location of nanoparticle synthesis. Therefore, diverse mesoscale structures composed of an array of quantum-confined nanocrystallites can be fabricated on DNA fixed to solid substrates eliminating complicated, expensive photolithography.

Mesoscale arrays of Q-CdS nanoparticles were fabricated on pUCLeu4 plasmid and ϕX 174 RF II DNA. These DNAs are double-stranded and in A-form they are 2.55 nm in diameter, and 0.85 μm and 1.32 μm long, respectively. pUCLeu4 plasmid and ϕX 174 RF II DNA were selected because of their known sizes so that they could be readily detected and unambiguously identified using TEM.

The samples were prepared either by dropping Cd^{2+}/DNA solution on carbon-coated TEM grids or by floating the grids on Cd^{2+}/DNA or DNA only solutions. The grids with DNA only were reacted with Cd^{2+} by dipping them into a cadmium solution. All grids were exposed to H_2S gas to form Q-CdS nanoparticle arrays.

In Chapter 3, Q-CdS nanoparticles were synthesized on calf thymus DNA in solution.

In Chapter 4, CdS/pUCLeu4 plasmid DNA samples prepared using the dropping deposition method were studied. The surface structures of thin carbon films, the primary substrates for the TEM samples, were examined using TEM.

In Chapter 5, the microstructures of the DNA alone samples were examined after sample preparation by the Kleinschmidt method.

In Chapter 6, samples made with various ratios of cadmium to DNA and by different deposition methods were studied. CdS nanocrystallite samples, without DNA, were also examined.

Conventional transmission electron microscopy (CTEM, BF and DF), analytical electron microscopy (AEM), and high resolution electron microscopy (HREM) were used to characterize the Q-CdS nanostructures and the chemical composition of the Q-CdS nanoparticles. Absorption and photoluminescence spectroscopies were used for optical characterization.

The TEM samples were characterized without and with metal shadowing. Carbon shadowing was also sometimes performed to enhance the contrast of the CdS/DNA microstructures.

SUMMARY OF RESULTS

- **CdS/Calf Thymus DNA (Chapter 3)**

  1. The average size of the Q-CdS nanoparticles synthesized on calf thymus DNA was 5.6 nm.
  2. SADP data confirms that the Q-CdS nanoparticles stabilized by calf thymus DNA have the zincblende cubic structure.
  3. The absorption threshold of Q-CdS/calf thymus DNA is approximately 480 nm, blue-shifted from the bulk CdS value (515 nm).
  4. The PL emission spectrum has a maximum near 620 nm.
  5. Q-CdS nanoparticles stabilized on calf thymus DNA are very stable from flocculation when stored in closed vials at 5 °C.
  6. **These results demonstrate that DNA can be used to stabilize Q-SC nanoparticle formation.**

- **CdS/pUCLeu4 Plasmid DNA by Dropping Deposition (Chapter 4)**

  1. BF and DF images show circular structures composed of an assembly of CdS nanocrystallites.
  2. HREM shows diverse sizes of CdS nanoparticles packed onto the DNA without any particular crystallographic orientation relationships among the Q-CdS crystallites, the DNA, or the substrate.
  3. The average diameter of the Q-CdS is approximately 5 nm.
  4. The lattice spacings measured by electron diffraction match zincblende

cubic of CdS.

5. Chemical analysis by XEDS indicates that the nanocrystallites contain only Cd and S.
6. The CdS/DNA nanostructure sizes observed by TEM varied from approximately 0.7 μm to 1.2 μm.
7. After metal shadowing, large numbers of supercoiled DNA structures were found in the undigested CdS/plasmid DNA samples.
8. Highly concentrated network-like structures were frequently found. Most did not contain CdS nanoparticles.
9. Low density DNA-like and other unidentified microstructures were also found.
10. **These results demonstrate that self-assembled mesoscale semiconductor structures can be fabricated on DNA templates.**

- **DNA Only Prepared by the Kleinschmidt Method (Chapter 5)**

1. The DNA microstructures observed were irregular chain-like shapes or sometimes "twisted rubber band" shapes.
2. For the pUCLeu4 plasmid DNA, approximately 20% of the undigested circular DNA and approximately 10% of the linearized DNA were observed as closed and relaxed DNA circles. Approximately 5% of the undigested circular DNA and approximately 30% of the linear DNA were observed as open and unwound DNA. The remainder of the samples,

approximately 75% of the undigested circular DNA and 60% of the linear DNA, were observed in supercoiled form.

3. For the ϕX 174 RF II DNA, approximately 90% was open and less than 5% was closed and relaxed, and only a few percent was supercoiled.
4. From observations of highly concentrated DNA, there are no ionic interactions between the DNA molecules which may induce tangles.
5. The average sizes of the circular, linear and ϕX 174 RF II DNA are 0.89 μm, 0.84 μm, and 1.25 μm respectively, close to lengths expected for the A-form.
6. **Therefore, when DNA is used as a structural template for assembling a mesoscale semiconductor structure, the A-form DNA length should be assumed.**

- **Various Ratio of Cadmium to DNA by Different Deposition Method (Chapter 6)**

1. CdS Only
   a) Both zincblend diamond cubic phase and the hexagonal close-packed phase were found in the CdS only samples. The average crystal size of hexagonal CdS was 38.4 nm, approximately 7 times larger than the cubic phase fabricated on calf thymus DNA in solution (Chapter 3).
   b) The hexagonal CdS particles were cubic or rectangular, while the cubic CdS nanoparticles were nearly spherical.

c) Large numbers of microbubbles were found in the 4 mM CdS only samples. The bubbles were clearly distinguishable from CdS/DNA.

2. 2 μM and 2 mM Cd to 5 μg/ml (pUCLeu4) and 1 μg/ml (ϕX 174 RF II) DNA

a) CdS/DNA structures and CdS nanoparticles were not observed before metal shadowing for samples prepared by the dropping method.

b) After metal shadowing, DNA structures without CdS nanoparticles were observed in most of the samples.

3. Cd^{2+}/DNA Deposited by Floating Deposition

a) Bundled DNA structures with cubic phase CdS nanoparticles were found in all the three 2 mM cadmium to 5 μg/ml plasmid and 1 μg/ml ϕX 174 RF II DNA samples.

b) The aggregated DNA structures were formed due to cadmium ion interactions when the aqueous cadmium solution was mixed with the DNA solution.

c) Neither CdS/DNA nor Q-CdS microstructures were observed for three low cadmium concentration samples, 2 μM Cd^{2+} to 5 μg/ml plasmid and 1 μg/ml ϕX 174 RF II DNA, respectively.

4. DNA Only Deposited by Floating Deposition

   a) Many isolated CdS/DNA microstructures were found after depositing the DNA alone followed by dipping the samples in cadmium solution followed by exposure to H_2S gas.

   b) The CdS nanocrystallites formed on DNA by this method are fewer and smaller than those found in previous experiments.

   c) The CdS/DNA microstructures are approximately 5 nm thick, about twice as thick as DNA only structures. The thickness of the CdS/DNA varies, while it is uniform for the DNA only structures.

   d) DNA anchored by this method remained on the carbon film when the grids were dipped into cadmium solution.

   e) 0.5 μg/ml DNA is still too concentrated for the formation of individual CdS/DNA structures.

   f) In the DNA only deposition experiments, the inhibition of aggregation of DNA induced by Cd^{2+}-binding was demonstrated.

   g) **Freshly mixed Cd^{2+} solution is an absolute requirement.**

The results reported in this dissertation prove that Q-CdS semiconductor nanoparticles are formed on DNA templates, and demonstrate the possibility of fabricating various sizes and shapes of mesoscale semiconductor structures using different sizes and shapes of DNA templates.

BIBLIOGRAPHY

ACF - Metals, 2239 E. Kleindale Road Tucson, AZ.

"Advances in Microcrystalline and Nanocrystalline Semiconductors" in *Materials Research Society Symposium Proceeding,* Vol. 452, edited by R. W. Collins, P. M. Fauchet, I. Shimizu, J. C. Vial, T. Shimada and A. P. Alivisatos, (Pittsburgh, Pennsylvania, 1997).

Alivisatos, A. P. Johnson, K. P. X. Peng, Wilson, T. E. Loweth, C. J. Bruchez, Jr. M. P. and Schultz, P. G. Nature **382**, 6592 (1996).

Alivisatos, A. P., Science **27**, 933 (1996).

Arfken, G., *Mathematical Methods for Physicists,* 3rd ed. (Academic Press, Harcourt Brace Jovanovich Publishers, New York, 1985), pp. 622-630.

Barton, J. K. and Lippard, S. J. "Nucleid Acid-Metal Ion Interactions" in *Metal Ions in Biology,* edited by Thomas G. Spiro, (John Wiley & Sons, Inc., New York, 1980), Vol. I, Chap. 2, pp. 33-81.

Bawendi, M. G., M. L. Steigerwald and L. E. Brus, Ann. Rev. of Phys. Chem. **41**, 477-96 (1990).

Berry, C. R., Phys. Riv. **161**, 3, 848 (1967).

Bigham, S. R. and J. L. Coffer, Colloids Surfaces A: Physicochem. Eng. Aspects **95**, 211-219 (1995).

Biochemicals and Reagents for Life Science Research, Cat. # D 1501 (Product Catalog, Sigma, Louis, MO., 1997), pp. 348.

Bloomfield, V. A., D. M. Crothers and I. Tinooco, Jr. *Physical Chemistry of Nucleic Acids* (Harper & Row, Publishers, New York, Evanston and San Francisco, 1974), pp. 10-19 and 420-727.

Borrelli, N. F., D. W. Hall, H. J. Holland, D. W. Smith, J. Appl. Phys. **61,** 12 (1987).

Bregadze, V. G., J. G. Chkhaberidze and I. G. Khutsishvili, in *Metal Ions In Biological Systems,* edited by A. Sigel and H. Sigel, (Marcel Dekker, Inc., New York, 1996), Vol. 33, pp. 253-265.

Broda, P., *Plasmids* (W. H. Freeman and Company, Oxford and San Francisco, 1979), precipitate.1-15.

Brus, L., Advanced Materials **5**, 4 (1983).

Brus, L. E., Ann. Rev. of Phys. Chem. **41**, 477-496 (1990).

Brus, L., Appl. Phys. A **53**, 465-474 (1991).

Brus, L., IEEE Journal of Quantum Electronic **QE-22**, 9 (1986).

Brus, L. E., J. Chem. Phys. Vol. **80**, 9 (1984).

Brus, L., J. of Phys. Chem. **90**, 2555-2560 (1986).

Canham, L. T., Appl. Phys. Lett. **57**, 1046 (1990).

Catalog Handbook of Fine Chemicals, Cat. # 20804-3 (Product Catalog, Aldrich Chemical Company, Inc., Milwaukee, WI., 1994), p. 1273.

Chandler, R. R., S. R. Bigham and J. L. Coffer, J. of Chem. Ed. **70**, A7 (1993).

Chandler, R. R. and J. L. Coffer, J. of Phys. Chem. **95**, 4 (1991).

Chang, Y. N., I. L. Pirtle and R. M. Pirtle, Gene **48**, 165 (1996). Chang, Y. N., I. L. Pirtle and R. M. Pirtle, Gene **48**, 165-174 (1986).

Chestnoy, N., T. D. Harris, R. Hull and L. E. Brus, The J. of Phys. Chem. **90**, 15 (1986).

Chow, L. T. and T. R. Broker, "Mapping RNA : DNA Heteroduplexes By Electron Microscopy" in *Electron Microscopy in Biology Vol. I,* edited by Jack D. Griffith, (John Wiley and Sons, A Wiley-Intersciences Publication, New York, 1981), pp. 141-156

Clausen, E. M., H. G. Craighead, J. M. Worlock, J. P. Harbison and L. M. Schiavone, Appl. Phys. Lett. **55**, 1427 (1989).

Coffer, J. L, S. R. Bigham, R. F. Pinizzotto, Y. G. Rho, R. M. Pirtle and I. L. Pirtle, Appl. Phys. Lett. **69**,3851 (1996).

Coffer, J. L., R. R. Chandler, C. D. Gutsche, I. Alam, R. F. Pinizzotto and H. Yang, The J. of Phys. Chem. **97, 3** (1993).

Coffer, J. L. and R. R. Chandler, Mat. Res. Soc. Symp. Proc. **206** (1991).

Coffer, J. L., S. R. Bigham, R. F. Pinizzotto and H. Yang, Nanotechnology **3**, 69, (1992).

Coggins, L W., "Preparation of Nucleic Acids for Electron Microscopy" in *Electron Microscopy in Molecular Biology*, edited by J. Sommerville and U. Scheer (IRL Press, Oxford, England, 1987), pp. 1-14.

Cohen-Tannoudji, Claude, Bernard Diu and Franck Laloë, *Quantum Mechanics* Vol II (Chongno Book Center, South Korea, 1977), pp. 924-931.

CRC Handbook of Biochemistry and Molecular Biology Vol. I, Nucleic Acids 3rd edn., edited by G. D. Fasman, (Chemical Rubber Company, Cleveland, OH, 1975) pp. 589-90.

Crick, F. H. C., in *Nucleic Acid Research Future Development,* edited by K. Mizobuchi, I. Watanabe and J. D. Watson (Academic Press, New York, 1983), Chap. 1, pp.11-13; R. E. Dickerson, B. N. Conner, M. L. Kopka and H. R. Drew, Chap. 2, pp.35-40

Cullis, A. G., P. W. Smith, P. J. Parbrookm B. Cockayne, P. J. Wright and G. M. Williams, Appl. Phys. Lett. **55**, 20 (1989).

Dabbousi, B. O., M. G. Bawendi, O. Onitsuka and M. F. Rubner, Appl. Phys. Lett. **66,** 11 (1995).

Efros, A. L. and A. L. Efros, Sov. Phys. Semicond.**16**, 7 (1982).

Ekimov, A. I. and A. A. Onushchenko, JETP Lett. **34**, 345 (1982).

Ekimov, A. I. and A. A. Onushchenko *JETP Lett.* **40**, 1136, 1984.

Elemental and Interplanar Spacing Index (U.S. Department of Commerce, National Institute of Standards and Technology, JCPDS-International Centre for Diffraction Data, 1601 Park Lane, Swarthmore, Pennsylvania 19081, 1989), CDF # 102622 and 02910, PDF # 34-0567. pp. 250.

Empedocles, S. A., D. J. Norris and M. G. Bawendi, Phys. Rev. Lett. **77**, 18 (1996).

Esaki, L., IBM J. Res. **14**, 61 (1970).

Fendler, J. H., "Membrane-Mimetic Approach to Advanced Materials", in *Advances in Polymer Science*, (Springer-Verlag, Heidelberg, New York, 1994), pp. 27-29.

Fischer, C. H. and A. Henglein, The J. of Phys. Chem. **93**, 14 (1989).

Flegler, S. L. *Scanning and Transmission Electron Microscopy*, (W. H. Freeman and Company, New York, 1993), pp. 53.

Fojtik, A., H. Weller, U. Koch and A. Henglein, Ber. Bunsengers. Phys. Chem. **88**, 969-977 (1984).

Freifelder, David, *Molecular Biology*, 2 nd ed., (Jones and Bartlett Publishers, Inc.1987).

Fritsch, T. M., *Molecular Cloning A Laboratory Manual,* 2nd ed. (Cold Spring Harbor Laboratory Press, New York, 1989), pp. 1.2 and 1.13-1.24.

Glass, R. E., *Gene Function, E, coli and its heritable elements* (University of California Press, Berkeley and Los Angeles, 1982), pp. 14, and 159-163.

Goldstein, A. N., C. M. Echer and A. P. Alivisatos, Science **256**, 5 (1992).

Goodgame, D. M. L., I. Jeeves, C. D. Reynolds and A. C. Skapski, Nucleic Acids Research **2**, 8 (1975).

Guschlbauer, W., *Nucleic Acid Structure* (Springer-Verlag, New York, 1976), pp.15-18.

Guzelian, A. A., U. Banin, A. V. Kadavanich, X. Peng, and A. P. Alivisatos Appl. Phys. Lett. **69**, 10 (1996).

Haug, H. and Stephan W. Koch, *Quantum Theory of the Optical and Electronic Properties of Semiconductors* (World Scientific, New Jersey,1990), pp. 324-332, 27-44, and 333-338.

Hayat, M. A., *Principles and Techniques of Electron Microscopy: Biological Applications Vol. 1* (Van Nostrand Feinhold Company, New York, 1970), pp. 324.

Herron, N., J. C. Calabrese, W. E. Farneth and Y. Wang, Science **259** (1993).

Herron, N., Y. Wang, and H. Eckert J. Am. Chem. Soc.**112**, 4 (1990).

Hooghan, T. K., Ph.D. Dissertation, University of North Texas, Denton, TX (1997). Hu, Y. Z., M. Lindberg and S. W. Koch, Phys. Rev. B **42**, 3 (1990).

Hu, Y. Z. M. Lindberg and S. W. Koch, Phys. Rev. B **42**, 3 (1990).

Hu, Y. Z., S. W. Koch, M. Lindberg, N. Peyghambarian, E. L. Pollock and F. F. Abraham, Phys. Rev. Lett. **64**, 15 (1990).

Hummel, R. E. Electronic Properties Materials (Springer-Verlag, New York, 1985), p. 60.

International Centre for Diffraction Data (12 Campus Blvd., Newtown Square, PA. 19073) Powder Diffraction File PDF # 10-0454 and 41-1049.

Jervis and, L., N. M. Pettit, J. Chromatogr. **97**, 33 (1974).

Jovanoviach, Publisher, New York, 1983), pp.11-13; R. E. Dickerosn, B. N. Conner, M. L. Kopka and H. R. Drew, pp.35-40.

Kayanuma, Y., Phys. Rev. B **38**, 9797 (1988).

Kayanuma, Y., Solid State Comm. **59**, 405 (1986).

Kayanuma, Y. and H. Momiji, Phys. Rev. B **41**, 14 (1990).

Kleinschmidt, A. K. and R. K. Zahn, "Über Desoxyribonucleinsäure-Molekeln" in Pritein-Mischfilmen. Z. Naturforsch. B **14**, 770-775 (1959).

Kleinschmidt, A. K., Methods Enzymol. **12** (B), 361 (1968).

Kozelka, J., in *Metal Ions In Biological Systens,* edited by A. Sigel and H. Sigel, (Marcel Dekker, Inc., New York, 1996), Vol. 33, pp.1-23.

Kuczynski, J. and K. Thomas, J. of Phys. Chem. **89**, 2720-2722, (1985).

Lewin, B., *Genes VI,* 4th ed. (Oxford University Press and Cell Press, New York, 1990), pp. 451-456.

Lewin, B., *Gene Expression Volume 3 Plasmids and Phages* (John Wiley & Sons, New York, 1977), pp. 97, 160-168, 261-268.

Lippens, P. E. and M. Lannoo, Phys. Rev. B **39**, 15 (1989).

Littau, K. A., P. J. Szajowski, A. J. Muller, A. R. Krotan and L. E. Brus, J. of Phys. Chem. **97**, 1224-1230 (1993).

Llanos, P. and J. K. Thomas, Chem. Phys. Latt. **123**, 299 (1986).

Loweth, Marcel P. Bruchez Jr & Peter G. Schultz, Nature Vol. **382,** 15 Aug. 1996.

Marzilli, L. G. T. J. Kistenmacher and G. L. Eichhorn, "Nucleid Acid-Metal Ion Interactions" in *Metal Ions in Biology Vol. 1*, edited by T. G. Spiro, (John Wiley & Sons Inc., New York, 1980), pp. 181-199, 231.

Merion, M. and W. Warren, BioTechniques **7**, 1, 60 (1989).

Murray, C. B., C. R. Kagan, M. G. Bawendi, Science **262**, 218 (1995).

Noran Instruments, 2551 W. Beltline Highway, Middleton, WI.

Norden, B., P. Lincoln, B. Akerman and E. Tuite, in *Metal Ions In Biological Systems*, edited by A. Sigel and H. Sigel, (Marcel Dekker, Inc., New York, 1996), Vol. 33, pp. 177-208.

Nozik, A. J., Ferd Williams, M. T. Nenadovic, T. Rajh and O. I. Micic, J. of Phys. Chem. **89**, 397-399 (1985).

O'Neil, M., J. Marohn and G. McLendon, J. of Phys. Chem. **94**, 4356-4363 (1990).

Perkowitz, S., *Optical Characterization of Semiconductors*: *Infrared, Raman, and Photoluminescence Spectroscopy* (Academic Press Limited, University Printing House, Cambridge, 1993), p 27.

Petit, C. and M. P. Pileni, J. of Phys. Chem. **92**, 2282-2286 (1988).

Peyghambarian, N., S. W. Kzoch and A. Mysyrowicz, *Introduction to Semiconductor optics* (Prentice Hall, Englewood Cliffs, New Jersey, 1993), pp. 1, 253, 23-36, 110-114 and 245-249.

Pinizzotto, R. F., Y. G. Rho, Y. Chen, R. M. Pirtle, I. L. Pirtle, J. L. Coffer and X. Li, Mater. Res. Soc. Symp. Proc. **452** 591 (1997).

Product Catalog and Reference Guide, Cat. # 302-2s (New England Biolabs, Inc., 1996), p. 80, 206.

Ramsden, J. J., S. E. Webber and M. Grätzel, J. of Phys. Chem. **89**, 2740-2743 1985).

Rawn, J. David, *Biochemistry* (Carolina Biological Supply Company, Neil Patterson Publishers, 1989), pp. 665-673.

Research Chemicals, Metals and Materials, Cat. # 12936 (Product Catalog, Alfa Aesar, A Johnson-Matthey Company, Ward Hill, MA., 1997), p. 119.

Rhodes, D. and A. Klug, Nature **286**, 573 (1980).

Deegan, R. D. and S. R. Nagel, Science News 152, 298 (1997).

Rosenberg, B. "Nucleid Acid-Metal Ion Interactions" in *Metal Ions in Biology,* edited by T. G. Spiro, (John Wiley & Sons, Inc., New York, 1980), Vol. I, Chap. 1, pp.3-13; J. K. Barton and S. J. Lippard, Chap. 2, pp. 33-81; L. G. Marzilli, T. J. Kistenmacher and G. L. Eichhorn, Chap. 5, pp. 181-199 and 227-236.

Rossetti, R., S. Nakahara and L. E. Brus, J of Chem. Phys. **79**, 2 (1983).

Sabat, M. and B. Lippert, in *Metal Ions In Biological Systems*, edited by A. Sigel and H. Sigel, (Marcel Dekker, Inc., New York, 1996), Vol. 33, pp. 143-168.

Saenger, W., *Principles of nucleic acid structure* (Springer-Verlag, New York, 1984), pp. 105-114 and 201-211.

Schleif, R., *Genetics and Molecuoar Biology,* 2nd ed. (Addison-Wesley Publishing Company, The Johns Hopkins University Press, London Ltd., 1993), pp.265-274.

Smotkin, E. S., C. Lee, A. J. Bard, A. Campion, M. A. Fox, T. E. Mallouk, S. E. Webber and J. M. Whitl, *Chem. Phys. Lett.* Vol. **152,** 3 (1988).

Smotkin, E. S., R. M. Brown, Jr., L. K. Rabenberg, K. Salomon, A. J. Bard, A. Campion, M. Anne Fox, T. E. Mallouk, S. E. Webber and J. M. White, The J. of Phys. Chem. **94**, 19 (1990).

Smotkin, E. S., C. Lee, A. J. Bard, A. Campion and M. A. Fox, Chem. Phys. Lett. **152**, 2, 3 (1988).

Sobiesierski, Z., "Linear and Nonlinear Optical Spectroscopy of Surfaces and Interfaces" in *Epioptics,* edited by J. F. McGilp, D. Weaire and C. H. Patterson, (Springer, New York, 1995), pp. 138-140.

Spanhel, L., M. Haase, H. Weller and A. Henglein J. Am. Chem. Soc. **109**, 5649 (1987).

Steigerwald, M. and L. E. Brus, Acc. Chem. Res. **23**, 183 (1990).

Stemp, E. D. A. and J. K. Barton, in *Metal Ions In Biological Systens*, edited by A. Sigel and H. Sigel, (Marcel Dekker, Inc., New York, 1996), Vol. 33, pp. 325-452.

Strickberger, M. W., *Genetics* (Macmillan Publishing Co., Inc., New York, 1976), pp. 90-92.

Stryer, L., *Biochemistry* (W. H. Freeman and Company, New York, 1988), pp. 649-656.

UV spectrometry group, "Techniques in visible and ultraviolet spectrometry" *Standards in Absorption Spectroscopy Vol. I*, edited by C. Burgess and A. Knowles, (Chapman and Hall, London; New York, 1981), p. 3.

Video-based image Analysis System, MCID M4, Imaging Research, Inc. (St. Catherines, Ontario, Canada, 1992).

Wang, Y., and N. Herron, J. of Phys. Chem. **91**, 257 (1987).

Wang, Y.and N. Herrin, J. of Phys. Chem. **92**, 4988-4994 (1988).

Wang, Y. and N. Herron, J. of Phys. Chem. **95**, 525 (1991).

Wang, Y. and N. Herron, Phys. Rev. B **42**, 11 (1990).

Wang, Y. and W. Mahler, Optics Commun. **61**, 233 (1987).

Wang, Y., A. Suna, W. Mahler and R. Kasowski, J. Chem. Phys. **87**, 12 (1987).

Wang, Y., N. Herron, W. Mahler, and A. Suna, J. Opt. Soc. Am. B **6**, 808 (1989).

Watson, J. D., *Molecular Biology of the gene,* 3rd ed. (W. A.Benjamin, Inc. Menlo Park, California, 1976), pp. 52.

Watson, J. D., *Molecular Biology of the gene,* 4rd ed. (The Benjamin/Cummings Publishing Company, Inc., Menlo Park, California, 1987), pp. 302-334.

Weller, H., Angew. Chem. International Ed. Engl. **32**, 41-53 (1993).

Weller, H., U. Koch, M. Gutierrez and A. Henglein, Ber. Bunsengers. Phys. Chem. **88**, 649-656 (1984).

Williams, D. B. and C. B. Carter, *Transmission Electron Microscopy Vol. IV* (Plenum Press, New York, 1996), pp. 32.

Yang, H., Ph.D. Dissertation, University of North Texas, Denton, TX (1993).

Yoffe, A. D., in *Advances in Phsics*, edited by D. Sherrington (Taylor & Francis, London and Washington DC., 1993), Vol. 42, 2, pp. 173-266.